# The relationship between connectome structure and cognition

Christopher James Hayward

Thesis submitted for the degree of

Doctor of Philosophy

School of Computing

Newcastle University

April 2021

*For my nana, Maureen King.*

# Abstract

Cognition consists of many abilities, designed to allow the animal to interact effectively with the environment. In this thesis, we explore the relationship between cognition and the network of connections within the brain, known as the connectome.

Firstly, we assess the spatial organisation of the macaque monkey connectome. We ask whether regions are arranged so as to minimise the total wiring length, a theory known as component placement optimisation. We find that the total wiring length of the connectome can be reduced by repositioning brain regions, suggesting the presence of alternative constraints on brain connectivity. We subsequently construct a model of neural dynamics to obtain a mechanistic understanding for why the brain is sub-optimally arranged with respect to its wiring configuration.

Next, we explore spatial optimisation in the human connectome. We find that the human connectome can be spatially rearranged to reduce the total length of all connections, and that regions differ in their contribution towards this reduction. We find evidence to suggest that this sub-optimal spatial arrangement of brain regions supports healthy dynamics by encouraging greater fluctuations in global synchrony throughout the brain. We also explore connectome structure in the context of impaired cognition, specifically in subjects with schizophrenia, where we identify a link between symptom severity and the spatial organisation of the frontal lobe.

Lastly, we investigate the relationship between connectome structure and intelligence, performing numerous spatial and topological analyses on the human connectome alongside measures of fluid and crystallised ability. We find evidence suggesting that fluid ability, rather than crystallised, is linked to spatial features of the connectome, and, in particular, with connectivity that is closer to being spatially optimised.

Our work contributes towards an understanding of the spatial and topological features of the connectome, and offers novel insights into the mechanisms that underpin cognition.

# Acknowledgements

I would like to thank my supervisor Prof. Marcus Kaiser for his knowledge, guidance and patience throughout the Ph.D. I would also like to thank Xue Chen for helping me with building the connectomes, and teaching me about image analysis and tractography procedures. My gratitude also goes to Dr. Frances Hutchings and Dr. Chris Thornton for their suggestions, support and kindness. This thesis relies on data provided by the Human Connectome Project (Van Essen, Ugurbil, et al. 2012) and the NKI-Rockland dataset (Nooner et al. 2012). Connectome data was processed by Dr. Micheal Ortiz-Rios (Institute of Neuroscience, Newcastle University); Dr. Cheol Han (Korea University, Sejong); and Dr. Chao Yan and Dr. Xuan Wang (School of Psychology and Cognitive Science, East China Normal University), to whom I am grateful. I am thankful to everyone in the Interdisciplinary Computing and Complex BioSystems (ICOS) research group for providing a supportive environment and to Newcastle University for funding my studies through the Doctoral Training Award. I would also like to thank the Student Wellbeing service at Newcastle University for supporting me during my studies, and Sarah Brown in particular for her kind words. And finally, none of this would have been possible without the love and kindness from my family.

# Contents

# List of Tables

# List of Figures

# Chapter 1. Introduction

Brain regions are positioned in three-dimensional space, connected by a mixture of short- and long-range connections. Longer connections imbue a larger spatial and metabolic cost on the neural system, influencing communication delays between brain regions. Early views of brain connectivity suggested that neural populations are positioned so as to minimise the total connection length to other areas of the brain, a theory termed component placement optimisation (CPO) (Cherniak 1990). Recent findings suggest that such a theory does not hold for the nematode *Caenorhabditis elegans*, nor for the much larger neural system found in the rhesus macaque monkey (Kaiser and Hilgetag 2006). However, the extent to which this theory applies to the human connectome, or if it continues to apply to the macaque connectome using more recent tractography techniques, remains unexplored. And perhaps, crucially, the reason as to why a sub-optimal spatial layout of regions might exist (as suggested by previous studies) remains to be understood. Further questions remain concerning the link between intelligence and connectome structure, as well as the possible spatial changes that might influence some disorders of cognition.

In this thesis, we attempt determine whether CPO exists in the macaque and human connectome, making use of brain imaging data from several sources. Additionally, we attempt to explain the link between the spatial layout of regions in the brain and neural dynamics, using a computational simulation of neural oscillations to do so. A new link between spatial structure and the symptom severity of a selected disorder of cognition (schizophrenia) provides an exciting insight into a mechanistic underpinning for the disorder. We also make headway in identifying new structural correlates of intelligence, comparing spatial and topological connectome features against measures of fluid and crystallised intelligence. Findings highlight an association between spatial connectome features and performance in tasks requiring fluid ability. Taken together, the objective of this thesis is to further our understanding of the relationship between the spatial structure of the connectome and cognition, making use of several datasets and computational techniques to do so.

## 1.1 Summary of Outcomes

Our first analysis focused on wiring optimisation in the macaque connectome, applied to four macaque monkey subjects. In this analysis, we looked at the spatial arrangement of brain regions in the connectome, applying computational search techniques to assess the extent to which the spatial layout of components in the connectome are more or less optimised with respect to minimising the wiring length. Here we test the hypothesis that, given their connections, brain regions are positioned to minimise the total wiring length, an analysis that involves computational search techniques to identify optimised spatial arrangements of the connectome. We find that regions were not positioned to minimise their wiring length, given their connections to other regions. Upon identifying the most costly connections, a large proportion existed along the anterior-posterior axis of the brain. As a result, we provide evidence for a sub-optimal spatial arrangement of brain regions in the macaque, highlighting the variation across regions with respect to their contribution towards such an arrangement. Using as a premise the theory that brain regions communicate based on the phase of their oscillatory dynamics, we attempt to explain the reason for why a sub-optimal arrangement exists, comparing differences in the dynamics — predicted by a computational model — between the originally-arranged connectomes and the rearranged versions which reduce the total wiring length.

Having analysed the macaque connectome, we next applied similar techniques to a much larger dataset of human connectome data (n=280) from the Human Connectome Project (Van Essen, Ugurbil, et al. 2012). From this, we find that the human connectome, as found for the rhesus monkey, shows non-optimal component placement, insofar as a reduction in total wiring length is possible by swapping the positions of regions from their original placements. Moreover, regions varied in their contribution towards the reduction in total wiring length; regions in the frontal, occipital and parietal lobes could be relocated to significantly reduce their connection lengths, while connections from sub-cortical regions and the insular cortex showed fewer changes during optimisation. Long-distance connections between the frontal and occipital/parietal lobes within each hemisphere were found to deviate strongly from an optimal wiring configuration, similar to the macaque connectomes.

Alongside identifying similarly sub-optimal spatial arrangements, for this same dataset

we used a computational model to assess changes in dynamics between original and minimised arrangements of the connectome. We asked the question, "Could a sub-optimal arrangement of brain regions affect global neural dynamics in a beneficial way?". By simulating neural communication between regions for the different spatial arrangements, we observed significant changes in oscillatory behaviour within the sample, specifically in the extent to which the model exhibited metastability — variation in global synchronisation between regions, a suggested crucial ingredient for cognition and communication amongst brain regions (Deco, Jirsa, et al. 2009; Deco and Kringelbach 2016). We suggest that the increased metastability observed within a connectome that is not spatially optimised to minimise wiring length, manifests from the increased heterogeneity of communication delays between areas due a mixture of long- and short-range connections, enabling a greater spatial and temporal distribution of information within the connectome at any given moment. Altogether, this prompts the view that the spatial organisation of the human connectome is shaped by multiple constraints: balancing the spatial and metabolic costs of white matter connections between regions, whilst maintaining dynamics which are necessary for effective cognition. Thus, in addition to providing direct information transmission between distant regions (Kaiser and Hilgetag 2006), we argue that a sub-optimal arrangement of the connectome as a whole supports dynamics which are associated with optimal network performance (Friston 1997); the model supports the claim that a sub-optimal spatial arrangement increases fluctuations in global activity, a feature hypothesised to coincide with healthy brain dynamics.

Next, we analysed the spatial arrangement of brain regions in the case where cognition is impaired, specifically in the connectomes of subjects with schizophrenia. We found that the extent of component placement optimisation in the frontal lobe of schizophrenia patients correlates with symptom severity, uncovering a novel insight into the relationship between spatial features of the connectome and disorders of cognition. From this finding, we hypothesise that a sub-optimal placement within the frontal lobe may disrupt integration with the rest of the brain, and that for healthy brain dynamics to emerge, a requirement of connectome structure may be to support similar metastable dynamics across segregated parts of the network.

Finally, we explored the relationship between the spatial layout of the human connectome and intelligence. We provide an overview of the current research on structural

and functional features of neural activity in the context of IQ, followed by an assessment of the spatial and topological features of the human connectome from the Nathan Kline Institute-Rockland dataset (Nooner et al. 2012). In this final analysis, find an association between spatial features of the connectome and some components of fluid intelligence. In particular, we find that spatial features of the connectome are more closely linked to fluid intelligence than are topological features, and that the extent to which the spatial arrangement of regions is closer to optimal — with respect to minimising the total wiring length — may differ with fluid ability. Our work also highlights the importance of separating fluid and crystallised measures of intelligence when assessing brain structure, and makes a case for spatial factors influencing fluid intelligence.

As with any study of the brain that relies on imaging data to construct a less-than-perfect connectome (as is currently the case for any creature apart from *C. elegans*), our results are dependent on several parameters including the quality of the imaging data, and the choice of parcellation determining the resolution of regions and the density of connectivity within the network. Future work, using different datasets with different parcellations will help to clarify our findings.

Four different collections of connectome data (one macaque, three human datasets) were used in this thesis: the macaque dataset consists of four subjects, the connectomes for which were processed by Dr. Micheal Ortiz-Rios (Institute of Neuroscience, Newcastle University — Ortiz-Rios et al. 2018); 280 subjects from the Human Connectome Project (Van Essen, Ugurbil, et al. 2012); 88 human subjects consisting of healthy controls and patients with schizophrenia, processed by Dr. Chao Yan and Dr. Xuan Wang (East China Normal University); and 98 human subjects from the Nathan Kline Institute-Rockland project (Nooner et al. 2012), processed by Dr. Cheol Han (Korea University, Sejong). The subjects from the Human Connectome Project were pre-processed by the HCP pipeline, with tractography performed by Christopher James Hayward and Xue Chen whilst at Newcastle University.

### 1.2 Thesis Structure

The remainder of the thesis is organised as follows: Chapter 2 (Background) provides an overview of the key concepts which form the basis for the work, including structural

features of the brain, the spatial constraints imposed on neural communication, and an exploration of the definitions of cognition. Chapter 3 (Methods and Datasets) lists the details for the four datasets used in the thesis, and the computational methods used to analyse these datasets. Chapter 4 (Results) provides the outcomes of analysing the spatial and topological properties on the connectomes within the datasets, in addition to the dynamical simulations used to explore the impact of the spatial arrangement of regions on neural communication. Finally, in Chapter 6 (Conclusion) we conclude by highlighting the relationship between the spatial features of the connectome and cognition, discussing the importance of using dynamical models to understand how the brain works and the potential for spatial analysis of connectome structure in understanding brain disorders.

# Chapter 2. Background

Here, we provide an overview of the concepts used in this thesis. This will involve an explanation of the structure of the brain; a definition of cognition; an exploration of the dynamical principles underpinning brain function; descriptions of techniques used to analyse the brain's wiring configuration; and the computational methods used to efficiently explore vast search spaces for combinatorial problems. These topics will lay the foundation for future chapters.

## 2.1 The Brain and its Connectome

The brain is an organ encased within the skull, positioned towards the leading end of the moving body (Braitenberg 2007). Composed of anatomically and functionally distinct regions, the brain is responsible for many processes, enabling the animal to interact with its environment, maintain homeostasis and enable cognitive processes such as planning and reasoning. Communication within the brain, and with the rest of the body, takes the form of sending action potentials along neurons (Fries 2005, 2015; Sporns, Tononi, et al. 2005), and releasing hormones into the bloodstream (Tortora et al. 2018, pp. 315–316, 475, 657–658). In mammals, communication between brain regions partly relies on axons situated in the white matter, underneath the grey matter of the cerebral cortex (Braitenberg and Schüz 2013, pp. 7–14). To speed up the transmission of action potentials, myelin sheaths encase the axons of neurons, giving the white matter is paler appearance compared to that of the cortex (Waxman 1977). Transmission speed is also dependent on the diameter of the conducting axon, with wider diameters supporting faster transmission at the cost of increased volume (Swadlow et al. 2012). Conduction delays — the time delay for an action potential to travel between regions — varies throughout the mammalian brain, ranging from 100 microseconds for short connections, to more than 100 milliseconds for longer and unmyelinated connections (Waxman 1977). In the human brain, physiologically realistic conduction speeds of axons range approximately from 5 to 20 m/s (Waxman 2006), with larger brains across species typically compensating for the

greater distances between regions by increasing conduction speeds (Swadlow et al. 2012).

Connections within the white matter consist of bundles of axons, grouped together to form fibre tracts. The shape and trajectory of such tracts can be delineated with techniques such as Diffusion Weighted Imaging (DWI), techniques that infer fibre direction from the constrained diffusion of water molecules within fibres (Bammer 2003). These tracts connect areas of the cortex together and to other regions such as subcortical areas. Fibre bundles vary in their shape, with some being extensively curved, such as the arcuate fasciculus, connecting temporal and frontal regions (Felten et al. 2015, pp. 342–344). Fibres also vary in their lengths, with a notably long example being the inferior fronto-occipital fasciculus connecting distant posterior and anterior regions of the brain together (specifically regions in the occipital and frontal lobes — see Figure 2.1). The primary route of communication between hemispheres involves the corpus callosum, situated relatively close to the centre of the brain. Other routes between hemispheres include the anterior commissure, the function of which may have been replaced by the corpus callosum (Winter et al. 2014).

The comprehensive map of connections within the brain is referred to as the connectome (Hagmann 2005; Sporns, Tononi, et al. 2005), which has yet to be obtained at is fullest level of detail for any creature apart for the nematode *Caenorhabditis elegans* (White et al. 1986), consisting of 302 neurons in total. Due to the intrinsic relationship between brain structure and function (Honey et al. 2007), by analysing the structure of the connectome it is possible to gain an insight into how regions communicate, as well as the topological and spatial constraints imposed on connections in three-dimensional space. The study of connectome has broadened over the last several years, becoming its own field in neuroscience under the title connectomics (Kaiser 2013).

### 2.1.1 Non-invasive observation of structural connectivity

Using non-invasive methods, it is possible to observe both the internal structure and function of the brain. The structure of white matter fibre tracts can be inferred by measuring the diffusion properties of water within the fibres (Bammer 2003), a collection of techniques known under the heading of diffusion weighted imaging (DWI). DWI is widely used as an alternative to invasive techniques like tract-tracing which rely on the injection of tracer molecules into the brain tissue (Purves et al. 2004). In addition to T1-

weighted magnetic resonance imaging, diffusion images have been used to complement the process of identifying cortical and subcortical areas of the brain, a process known as segmentation (Cheng et al. 2020).

The white matter consists mainly of myelinated axons (tracts) of different lengths, with local connectivity managed by U-fibres which hug the underside of the cortex and connectivity between spatially distant regions handled by commissural and association fibres, connecting regions between and within hemispheres, respectively (Schmahmann et al. 2009, pp. 81–87). Using three-dimensional data obtained from magnetic resonance imaging, white matter fibre tracts can be virtually reconstructed by generating 'streamlines' which follow the direction of the diffusion of water within each voxel of the brain image. By following the start and end of these streamlines, connections between regions can be identified. Within such a process, several parameters can be defined to control the number, length and direction of generated streamlines, amongst other properties, all of which influence the structure of the generated connectome. Regarding the streamlines themselves, it is important to note that such streamlines do not always correspond to real fibre tracts, and that caution should be used when interpreting streamline counts (Jones et al. 2013). The development of reconstruction methods is an ongoing area of research, with the aim to improve the accuracy of the tractography procedure in ambiguous situations where fibres cross, branch and kiss (Jbabdi et al. 2011).

Several software packages exist for the downstream processing of brain images. Tools such as Freesurfer (Fischl 2012) are able to automatically parcellate (divide) the brain into grey and white matter, and to identify boundaries between cortical and subcortical regions using the Desikan-Killiany atlas (Desikan et al. 2006). To perform the streamline reconstruction, several software solutions exist, one example being DSI-Studio (Yeh, Wedeen, et al. 2010). The segmented output from Freesurfer can be used by DSI-Studio to track the streamlines representing the connectome. Constructed connectomes are macroscopic representations of brain connectivity, and can be used as input into dynamical models which simulate changes in neural activity across the entire brain (Haimovici et al. 2013; Kinouchi et al. 2006; Váša et al. 2015). Imaging processing tools, including Freesurfer and DSI-Studio, are used in our forthcoming analysis of the mammalian brain, allowing us to analyse the relationship between connectivity and cognition.

### 2.1.2 Parcellating the brain

Areas of the brain differ in terms of the types and quantities of neurons present, including differences in the distribution of neuron types within cortical layers and across the cortex (Brodmann 1909, Braitenberg and Schüz 2013, pp. 7–14). The cerebral cortex represents around 84% of the total mass of the human brain (Hofman 1988), containing approximately 19 to 23 billion neurons (on average, for females, and males respectively — Pakkenberg and Gundersen 1997; Pakkenberg, Pelvig, et al. 2003; Songthawornpong et al. 2021) of the 86±8.1 billion total brain neurons (Azevedo et al. 2009). A substantial number of neurons are contained in the cerebellum, containing approximately 3.6 neurons to every neuron found in the cortex (Herculano-Houzel 2010). To enable downstream analysis and the comparison of region properties between subjects or species, various kinds of parcellations/atlases exist which group together and label neighbouring brain structures, rooted in the seminal work by Brodmann (1909) and Penfield (1950). This effort paved the way for a range of boundary definitions based on cytoarchitecture and/or functional features of the subcortex and surrounding cortex. More recently, these atlases enable a down-sampling of structural and functional detail which provides a basis for network analysis, enabling brain connectivity and shape to be treated as a collection of edges and vertices (Kaiser 2011), and the subsequent use by *in-silico* models to simulate brain dynamics at a computationally tractable resolution (for an example simulation of global neuronal dynamics, one which inspired some of the simulations used in this thesis, see Váša et al. 2015).

Parcellations of the brain vary in the number of regions they delineate, using anatomical and/or functional features to do so, relying on the identification of boundaries using local features or clustering similar regions at a global scale (Eickhoff et al. 2018). Typically, parcellations range in size from single-digit counts (brain lobes) to hundreds of regions (for example, including the various nuclei of the thalamus, as found in Fan et al. 2016). Some of these atlases parcellate cortical areas only, such as the anatomically-derived Desikan-Killiany atlas, which consists of 34 cortical regions per hemisphere (Desikan et al. 2006). Figures 2.1A and 2.1B provide a visual example of a partial cortical parcellation and some of the underlying streamlines generated using DSI-Studio. Additional parcellations also separate subcortical areas (for example: Fischl, Salat, et al. 2002). Variation in areal topography between individuals is one aspect which makes challenging the process

of defining a parcellation which can be robustly applied to a population (Gordon et al. 2017), prompting the ongoing development of new atlases (Eickhoff et al. 2018).

In addition to structural features, some parcellations also rely on functional properties of regions when grouping and applying labels to areas. The brain consists of functionally distinct areas, evidence for which can be obtained from task-based functional MRI scans (Vakhtin et al. 2014; van den Heuvel and Pol 2010), and studies assessing the impact of localised lesions (Aharonov et al. 2003; Barbey et al. 2014; Duncan et al. 1995). Localisation of function is often a consequence of the point of entry of the fibre tracts associated with a particular sensory modality, resulting in, for example, defined areas which process visual signals and those which handle auditory input (Braitenberg 2007). Some regions of the brain appear to be crucial in maintaining a state of awareness, in particular subcortical areas and the brainstem (Negrao et al. 2009; Ward 2011), and potentially the claustrum (Crick et al. 2005), while other areas can be removed without substantially impacting the day-to-day life of the individual (as is often performed in cases of intractable epilepsy – Kovanda et al. 2014). Interestingly, a considerable portion of the cortex can be resected or disconnected from the brain stem whilst maintaining continued awareness and/or interaction with the environment (Whishaw 1990). These studies and surgical experiments shed light on the distribution of functional responsibilities of brain regions, informing the construction of functional-derived parcellations.

The size and shape of regions often differ depending on the choice of parcellation, informed by functional and/or structural features. For the previously mentioned Desikan-Killiany atlas (containing a total of 68 cortical regions) regions were delineated based on the boundaries traced by sulci and the position of the corpus callosum, averaged over 40 subjects (Desikan et al. 2006). In humans, studies measuring the combined cortical pial surface area of both hemispheres have provided values in the region of 1,600 $cm^2$ (Barta et al. 2003) to 1,800 $cm^2$ (Kang et al. 2015). Using these values, this equates to a mean surface area of approximately 23.5 $cm^2$ to 26.5 $cm^2$ per Desikan-defined cortical region, each consisting of 280–340 million neurons on average. These values will depend on differences in neuron density across the cortex (Pakkenberg and Gundersen 1997). As an example finer-grained parcellation, the Brainnetome atlas consists of 210 cortical regions and 36 subcortical regions in total, defined using connectivity data obtained from diffusion tensor imaging and probabilistic tractography (Fan et al. 2016; Maier-Hein et al. 2017). Natu-

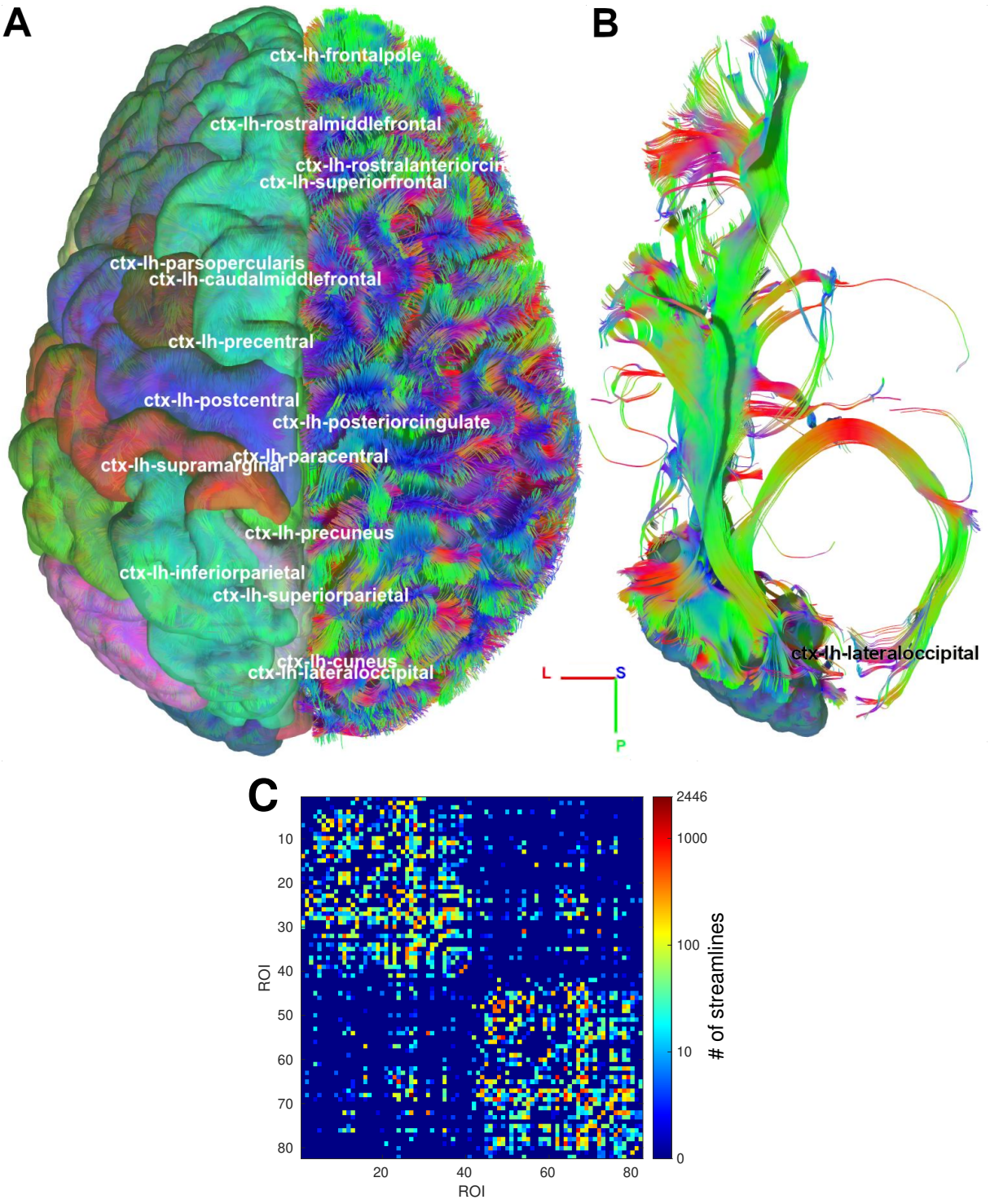


Figure 2.1: Example output of the tractography procedure on a single subject from the Human Connectome Project (Van Essen, Ugurbil, et al. 2012) using DSI-Studio (Yeh, Wedeen, et al. 2010). **A:** Axial view of the human brain, showing regions for the left hemisphere using the Desikan-Killiany atlas (Desikan et al. 2006) combined with a subcortical parcellation (Fischl, Salat, et al. 2002) (from a total of 82 regions), and the underlying one million streamlines representing the white matter connections (red, green, blue streamlines denote direction: left/right, anterior/posterior, inferior/superior, respectively). **B:** For the same subject, streamlines seeded from the left hemisphere lateral occipital region. Using such streamlines, one can infer the shape of real fibre tracts between regions, e.g. the fronto-occipital fasciculus (Standring et al. 2005). **C:** The 82×82 adjacency matrix containing the number of streamlines between pairs of regions (numbered 1–41 and 42–82 for the left and right hemisphere).

rally, the regions specified by this more granular parcellation would include fewer neurons on average, compared with those that define larger regions. For the Brainnetome atlas, regions contain approximately 90–110 million neurons, each with a mean surface area of approximately 7.6 $cm^2$ to 8.6 $cm^2$. Another popular schema is the automated anatomical labelling (AAL) atlas, parcellating the entire brain into 166 regions, including subcortical areas and the cerebellum, the most recent version being AAL version three (Rolls et al. 2020). Using a more detailed parcellation may improve the spatial accuracy, but for computational algorithms which represent brain regions and their connections as a graph, computational complexity often scales non-linearly with the number of nodes, especially in cases where the algorithm relies on exploring permutations of nodes (for instance, when finding the shortest path that visits all regions (Christofides 1976), or rearranging graph nodes to minimise the total connection length (Cherniak 1994)). For large networks, it is often too time consuming to find a provable global minimum when the task involves exploring different permutations (Knuth 1974). For human subjects, our study makes use of the relatively low-resolution Desikan-Killiany atlas, which eases the computational burden when it comes to assessing spatial optimisation by rearranging regions. This atlas also helps by reducing the total number of pre-processing steps needed to generate connectome from the diffusion images — this atlas is the default atlas outputted by the popular image analysis tool Freesurfer (Fischl 2012). The Desikan-Killiany atlas has been adopted by many other studies which make use of the Freesurfer tool, such as in the study by Hutchings et al. (2015).

Parcellations also exist for non-human brains, including for the rhesus macaque monkey. An earlier atlas for the macaque by Saleem and Logothetis (2012) consisted of a 2D histological demarcation of region boundaries across several 1mm–spaced slices, taken from a single macaque subject. This work has since been enhanced to create a 3D higher resolution atlas — the D99 atlas — including a parcellation of cortical and sub-cortical areas, and the cerebellum (Reveley, Gruslys, et al. 2017). This atlas consists of 83 cortical areas per hemisphere, resulting in 15.6 million to 20.5 million neurons per region on average (with a notably greater density of neurons present in visual areas) (Turner et al. 2016). Many other parcellations exist for other non-human primates, as well as for other mammals including dogs, cats and rodents (Hess et al. 2018; Van Essen 2002).

### 2.1.3 The network representation of the connectome

Brain connectivity may refer to either structural or functional relationships between brain regions. At the macroscopic level, the former represents the physical fibre tracts between regions (Hagmann et al. 2008), whereas the latter is based on correlating patterns of activation between regions (van den Heuvel and Pol 2010), often derived from resting state functional magnetic resonance imaging (MRI), where changes in the fluctuations in the blood-oxygen-level-dependent (BOLD) signal — a proxy measurement for changes neural activation — are compared between pairs of regions (D. Zhang et al. 2010). These definitions of connectivity can be used to construct networks of relationships between pairs of regions, a format amenable to analysis using graph theory. Connectomes can be represented in this network format.

Informally, networks refer to a collection of elements and the interactions between those elements (Brandes 2005, p. 7). Brain connections comprising the connectome can be represented as a network, or graph, consisting of edges (functional relationships or physical fibres) and nodes (cortical and subcortical regions). The topology of a network refers the arrangement of connections between regions. Nodes may vary in the number of their connections (the degree), as well as the total number of edges in the network, represented by the edge density. These networks can be succinctly described by data structures known as adjacency matrices, which capture the presence of connections between regions in the network, and other features such as the strength of the connections (Figure 2.2). Using a network representation of the brain, it becomes possible to assess the pathways of communication between brain regions (Bullmore et al. 2009; Sporns, Chialvo, et al. 2004) and to infer how directly or indirectly connected regions might interact. Studies often make use of both structural and functional networks of the brain, and both can be combined as a way to inform and validate connectivity between regions in computational models of neural dynamics (Cabral et al. 2011; Hellyer, Scott, et al. 2015; Kuramoto 1975; Váša et al. 2015; Wildie et al. 2012).

A network description of the brain at a global level requires a specification of how different areas should be separated, making use of a particular atlas or parcellation to do so. Connections (network edges) between these brain areas (network vertices) define relationships between regions, such as whether an axon links the two, or whether a strong functional correlation exists, possibly emerging from temporally correlated activa-

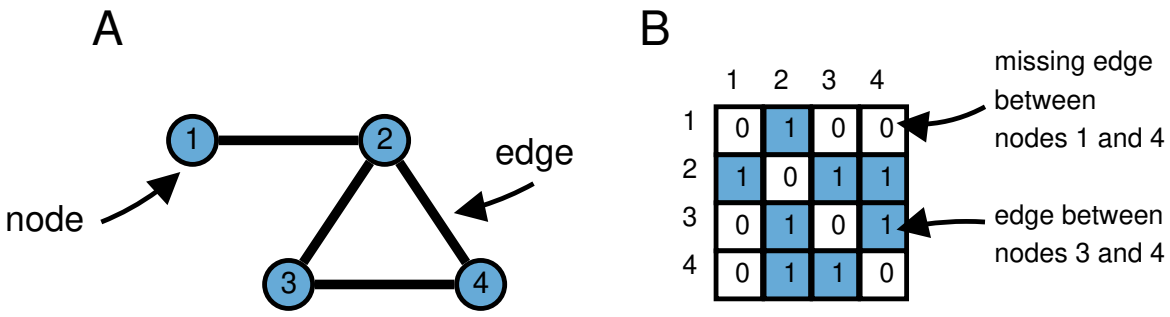


Figure 2.2: An example network and adjacency matrix, showing **A:** the nodes and edges in the network, and **B:** the network's binary adjacency matrix.

tion (D. Zhang et al. 2010). Networks can also be used to model interactions between components in a great deal of natural phenomena, including animal behaviour in social networks (Wasserman et al. 1994, pp. 8–10, 17–20), their shape being amenable to many forms of analysis (Kaiser 2011; Rubinov and Sporns 2010).

One such approach of investigating brain region communication involves forming an association between the 'ease' with which a pair of regions can communicate, and a quantity such as the number of connections joining the two. At a global level between all pairs in the connectome, this distance between nodes in a network can be measured using the characteristic path length: the mean path length between all pairs of nodes in the network (Rubinov and Sporns 2010). Shorter path lengths correspond to a measure of global integration of information, where information becomes accessible to many regions. Formally, the characteristic path length, $L$, is the average length of paths between any two nodes in the network:

$$L = \frac{1}{n(n-1)} \sum_{i,j=1}^{n} d(i,j), \tag{2.1}$$

where $d(i,j)$ is the distance along the shortest path between nodes $i$ and $j$, and $n$ is the number of nodes in the graph. In the case of the binary characteristic path length, this becomes the mean number of edges to be traversed before reaching a destination region. Alternatively, the connection length — based on a chosen metric — can be used to calculate $d(i,j)$. In addition to measuring the ease of communication between any two regions, the extent to which region connectivity is clustered provides an insight into segregated communication (Hilgetag et al. 2004); the clustering coefficient $C$ is the fraction of neighbouring nodes who are also neighbours (connected via an edge):

$$C = \frac{\sum_{i,j,k=1}^{n} a_{ij}a_{ik}a_{jk}}{\sum_{i,j,k=1}^{n} a_{ij}a_{ik}}, \tag{2.2}$$

where $a_{ij}$ are the entries of the adjacency matrix. Using a binary or weighted adjacency matrix computes the binary and weighted versions of $C$, respectively. The term 'neighbour' refers to a node connected to another node by an edge in the network. Small world networks are those which have a relatively high clustering coefficient and a relatively short path length (Humphries et al. 2008; Watts et al. 1998), quantified by $\sigma$:

$$\sigma = \frac{\frac{C}{C_r}}{\frac{L}{L_r}} \tag{2.3}$$

where $C_r$ and $L_r$ are the mean clustering coefficient and characteristic path length of several randomly rewired networks (Maslov et al. 2002). Small world networks support efficient information transmission along with clustered connectivity, helping to enable both global information integration and segregated processing. Many networks in the real world display small world properties, including the brain (Hilgetag et al. 2004; Sporns, Chialvo, et al. 2004).

Structural features of brain networks consist of short path lengths between regions and a high clustering coefficient, both of which are suggested to support information processing within regions and transmission between regions (Hagmann et al. 2008; Hilgetag et al. 2004; Watts et al. 1998). A combination of integrated and segregated neural activity is thought to mediate effective cognition and behaviour (Sporns 2013), with long-range connectivity supporting global integration, and short, modular connectivity enabling efficient processing locally, giving rise to small-world topologies (Humphries et al. 2008; Watts et al. 1998). These features exist alongside a hierarchical structure consisting of a modular organisation at multiple spatial scales (Felleman et al. 1991; Kaiser, Hilgetag, and Kötter 2010; Meunier et al. 2009).

In this thesis, we make use of both structural and functional connectivity and their corresponding network representations. The aforementioned network analysis methods are also used, in combination with a spatial description of brain regions and their connections. In order to obtain connectivity information, we need a method of extracting the real connectivity within the brain, using information obtained from MRI.

### 2.1.4 Spatial organisation of the connectome

The brain consists of numerous spatially distributed, functionally distinct regions/components. The set of structural connections between brain regions — the human connectome (Sporns, Tononi, et al. 2005) — encompasses long-range links between distant regions, supporting integration, and short-range links mainly within network modules supporting local processing (Watts et al. 1998). Alongside lowering the total wiring length in the connectome, the presence of these long-distance connections is thought to reduce the transmission time in terms of the number of intermediate regions on pathways between regions (Bassett and Bullmore 2006; Bullmore et al. 2009; Hagmann et al. 2008; Hilgetag et al. 2004; Sporns, Chialvo, et al. 2004), an organisation thought to facilitate effective cognition (Sporns 2013). Concerning the network's spatial organisation, a suggested trade-off exists between the physical and metabolic costs of long-range connections and their benefits for distribution, robustness after network perturbations, and modular/segregated processing (Bullmore et al. 2012). Indeed, there are more long-distance connections than would be expected in the case where wiring is strictly minimised (Kaiser and Hilgetag 2006).

Communication in the brain takes place between spatially distributed regions, using axons of various lengths. Early observations of the structure of the brain by Cajal (1909) suggested that neural circuits are under pressure to minimise the time delay of signal transmission between regions. Early hypotheses suggested that the spatial arrangement of brain regions minimises the total wiring length (Cherniak 1994), reducing conduction delays, and lowering space and metabolic costs. These suggestions arose from a detailed analysis of the nervous system of the nematode *Caenorhabditis elegans*, based on the observation that the majority of neurons were positioned in the head region, with very few long-range projections to other areas. Comparisons made with the structure of the human brain lead to the conclusion that all neural systems minimise the lengths of their connections, implying that any spatial rearrangement of the components within the neural system would lead to an increase in the total connection length, a theory known as component placement optimisation (CPO) (Cherniak 1990). For this alternative perspective, the brain is thought to minimise the total wiring length by optimising the spatial positioning of brain regions, rather than constraining connectivity. Indeed, similarities in organisational principles of the connectome have been observed across mammalian species (Horvát et al. 2016).

CPO would predict that any rearrangement of the spatial position of brain regions, e.g. swapping around the position of two regions, would always result in a longer total wiring length. In other words, it would be impossible to reduce the total wiring length by rearranging positions (Cherniak 1994; Cherniak et al. 2004). Recent studies, however, have suggested that the wiring length of connectomes of several species could be reduced whilst still retaining the topology and adhering to spatial constraints, identified in *C. elegans* and the macaque monkey (Kaiser and Hilgetag 2006), and in humans (Raj et al. 2011). In these cases, the original connectomes did appear to keep the wiring lengths low, but not minimal. Methods which moved the spatial location of regions *in silico* enabled this kind of analysis, combined with global search heuristics to identify spatial arrangements with a shorter total wiring length (Kirkpatrick et al. 1983; Metropolis et al. 1953). These recent findings related to CPO in neural networks rely on swapping the position of nodes within a connectome network, trying many possible permutations in an attempt to find the best arrangement. In the study by Kaiser and Hilgetag (2006), long connections were found to contribute to a spatially sub-optimal placement, the inclusion of which are thought to reduce the time needed for information to move throughout the system by limiting the number of intermediate processing steps. These results suggest that the brain supports integration among distant brain regions at the expense of driving up the metabolic and spatial costs of the network beyond those derived from a strict minimisation of the wiring length (Laughlin et al. 2003). Interestingly, this sub-optimal spatial organisation has also been seen in smaller structures in the brain, with the morphology of dendritic arbors being governed by similar wiring principles (Budd and Kisvárday 2012; Budd, Kovács, et al. 2010).

The spatial analysis of connectomes can also take place without swapping the positions of regions, instead comparing them with other networks that share similar properties. The creation of 'baseline' networks is common practice in computational neuroscience, connectivity for which is derived from the network (or connectome) of interest, and augmented in some way so as to provide a point of reference (Fornito, Zalesky, and Breakspear 2013; Kaiser 2011). Baseline networks often take the form of networks with the same number of nodes and edges, but the connections are reorganised randomly, sometimes preserving features such as the degree distribution or the strength of each region. Comparisons can be made between the originally-wired connectome of an individual's brain and these reference networks, highlighting the prevalence of spatial pressures in the connectome,

or other biological phenomena not present in the synthetically generated graphs. For instance, such analyses have shown that the wiring costs of connectomes are lower than that expected in a random network (Bassett, Greenfield, et al. 2010), prefrontal areas are predisposed to disconnection in cases of cost-preserving rewiring (Gollo et al. 2018), and that the connectomes across species display segregated connectivity and direct long-distance connections, the presence of which is suggested to enable integration between neural populations despite the increased spatial and metabolic costs (Samu et al. 2014).

The search methods used to explore the spatial optimisation of the connectome are widely used in many other research areas. Variants of the rearrangement technique used to find optimal arrangements of system components have been applied to the field of operations research to maximise throughout in factories through optimal floor planning, providing a solution to what is known as the 'facility layout problem' (Meller et al. 1996). These methods are also reminiscent of the process of 'compaction' of electrical circuits, where components are positioned to minimise the length of copper tracks, reducing construction costs whilst preserving circuit-board function (Kedem et al. 1984).

In addition to applying techniques such as shuffling the positions of nodes within a network, other measures exist for quantifying the shape/complexity of graphs. One method to assess the complexity of a three dimensional structure is to measure the difficulty with which the structure can be embedded into a lower dimensional space. The Rentian exponent can be used to measure the spatial complexity of a network in N-dimensional space, quantifying the scaling relationship between the number of nodes and edges within partitions/3D-subspaces of a network (Landman et al. 1971). Partitions are 3D-'boxes' arranged randomly in the space of the network, of a random size, overlapping some number of nodes and edges from the network. A greater Rentian exponent corresponds to a greater spatial complexity of the network — as the number of nodes within a growing partition of the network increases, a substantial increase in the number of edges implies a greater complexity, and subsequently an increased difficulty in describing that network in a lower dimensional space. A network's Rentian exponent was originally developed in the context of microprocessor connectivity, used to assess the spatial efficiency of wiring between components (Christie et al. 2000; Lanzerotti et al. 2005). The measurement has been used to assess the complexity of other artificial (Bassett, Greenfield, et al. 2010; Sperry et al. 2016) and biological networks (Klimm et al. 2014; Papadopoulos

et al. 2016).

While sub-optimal component placement has been identified in the connectomes of several species including human (Kaiser and Hilgetag 2006; Raj et al. 2011), there remains scope for further spatial analysis of the connectome; replication is an important component of good scientific research, and the field would benefit from further exploration into the relationship between connectome connectivity and the spatial placement of regions, and how this relates to cognition. Limited understanding exists on the contribution of individual regions which defy this minimisation protocol, and the specific connections which contribute towards a sub-optimal arrangement. Evolution has designed the brain, but the impact of spatial arrangement on neuronal dynamics and whether spatial properties of the connectome are correlated with neurological disorders, remains unclear. We attempt to explore these areas in this thesis, and, by making use of computational models of brain activation, offer an exciting insight into relationship between spatial features of the connectome and cognition.

## 2.2 Cognition

Alongside maintaining homeostasis, the brain's raison d'être is to enable positive interaction with the environment. The way in which cognition should be defined remains a topic of debate (Allen 2017). For animals, one abstract definition might state that cognition is the ability of the brain to bring to bear its resources to solve problems derived from the environment (Shanahan 2012). Some of these resources might include the capacity to plan for the future, a skill not limited to humans (Raby et al. 2007). Moreover, some argue that cognition is present in simpler organisms, such as bacteria (Macnab et al. 1972) and even plants (Calvo Garzón et al. 2011). For this thesis, we concern ourselves with capacities of the mammalian brain, specifically in humans and the rhesus macaque monkey.

One suggested hallmark of cognition is the capability to form a unique combination of learned behaviours to resolve ambiguity and novelty, making use of skills such as memory, attention and planning to do so (Pessoa 2009). Planning, for instance, may involve predicting an outcome of a behaviour based on forming an internal representation of the action (Shanahan 2010a, pp. 159–165). Cognition is not limited to humans, with many

non-human animals demonstrating great feats of ingenuity and comprehension of complex problems; Bird and Emery (2009) demonstrate the extraordinary abilities of rooks (*Corvus frugilegus*) in obtaining food by controlling the level of water using pebbles. Earlier studies by Fiorito et al. (1990) show that the common octopus (*Octopus vulgaris*) can become more efficient over time at opening sealed jars to obtain food. The building blocks of cognition, such as vision and motor control, manifest from communication between brain regions using a complex tapestry of local and global physical projections. Damage to these regions and connections brought about by disease and/or trauma can disrupt these components of cognition, the effect of which can be quantified by comparing performances on a number of tests used to assess abilities such as planning (Creed et al. 2011; Rocca et al. 2019). Localised lesions also provide an insight into the functional responsibilities of different areas of the brain (2014; 1939b).

Structural connections within the brain are reminiscent of artificial networks displaying clustered connectivity alongside long distance 'short-cut'connections, features suggested to enable segregated processing and to reduce the time needed for information to move between regions, the definition of a small-world architecture (Hagmann et al. 2008; Hilgetag et al. 2004; Humphries et al. 2008; Watts et al. 1998). A connective core is hypothesised to underpin the communication between neural processes (Shanahan 2012), forming a backbone which may enable the formation of novel coalitions of processes, broadcasting information between regions and acting as an arena for competition, giving rise to a 'global workspace' (Blackmore 2017, p. 36; Baars 2007; Dehaene, Kerszberg, et al. 1998; Dehaene and Naccache 2001; Mashour et al. 2020). A proposed neural substrate for this workspace supporting broadcast and competition are the recurrent thalamo-cortical connections between the thalamus and the rest of the cortex (Stratton et al. 2015; Ward 2011). In this hypothesised framework, the brain is represented as a spatially distributed set of dynamical processes, exerting influence on one another, ebbing and flowing between bouts of global integration and localised segregation (Tononi, Sporns, et al. 1994). As a problem is being addressed, these processes individually contribute their resources and expertise to finding a solution, alongside competing for control over the workspace in a 'winner-takes-all' scenario. The thalamo-cortical loop has been attributed to maintaining distant segregation between areas of the brain, supported by the use of computational modelling (Stratton et al. 2015). This communication between neural processes is suggested to rely on differences in phase synchronisation (Fries 2015), enabling the binding

of percepts from different sensory modalities (Hummel et al. 1992; von der Malsburg 1995). This global workspace architecture is thought to allow the brain to utilise its vast parallel processing capabilities, whilst ensuring that a timely solution is found (restricting the propagation of information from the winning coalition of processes) (Shanahan 2012). This theory is a prominent idea serving as a high-level description of how the brain operates, utilising its resources to overcome problems (Deco, Vidaurre, et al. 2021).

The level of proficiency of cognitive features differs among humans. Indeed, many of the abilities which support effective cognition are also measured when assessing a subject's fluid intelligence — the ability to solve novel problems using a unique combination of acquired knowledge. Fluid intelligence sits alongside crystallised intelligence — the depth and breadth of accumulated knowledge. Effective cognition taps into both fluid and crystallised processes. Cognition can be measured using a variety of techniques, often through an observation of a behavioural response to carefully designed verbal and visual cues. For humans, the battery of tests included in the Wechsler Abbreviated Scale of Intelligence (WASI) covers both fluid and crystallised aspects of intelligence (Wechsler et al. 1999). Other tests include the Stroop test, assessing the ability of the subject to suppress responses which do not satisfy a particular goal (Stroop 1935) — a component of cognition referred to as executive function. Another common test is the N-Back test, which assesses the capacity to retain and utilise information in working memory (Kirchner 1958; Richard J. Haier 2016, pp. 145–146) — memory which is limited in capacity, whose temporary contents can be manipulated and utilised by other cognitive processes. By comparing the scores for these assessments between individuals, and correlating brain structural markers, insight can be gained into the underlying structural features of the nervous system that support the components of problem solving.

### 2.2.1 Communication within the brain

Regions in the brain communicate with the use of action potentials — all-or-nothing binary pulses — sent over axons of various lengths, linked together with chemical synapses, propagating signals between neurons. At a high-level, activity in the brain consists of neurons undergoing excitation or inhibition, either free or restricted to propagate action potentials to other neural populations, respectively. This change in activation, specifically, where regions coincide between moments excitation and inhibition, is thought to

underpin communication between spatially distant regions through near zero-phase synchronisation, a theory named communication through coherence (Fries 2005, 2015). In this theory, the increase and decrease in activation of one population of neurons mirrors that of another, allowing for epochs where populations are receptive to information encoded by action potentials. Empirical evidence supporting this theory consists of gamma- and beta-band synchronisation between near and distant regions of the cortex (Bastos et al. 2015). Additional evidence found that attended stimuli, when compared to unattended stimuli, resulted in greater synchronisation between regions V1 and V4 of the visual cortex (Bosman et al. 2012). The process of forming a 'tag' that binds together of features associated with a perceptual object has also been hypothesised to rely on phase differences among neuronal groups, a theory known as binding by synchronisation (Singer and C. M. Gray 1995).

Instead of relying on phase synchronisation between regions, an alternative theory namely, gating by inhibition, relies on changes in alpha-band power of oscillations (9-13Hz) enabling the release of inhibition within communicating regions (Jensen et al. 2010). Empirical data supporting this theory include observations of alpha activity suppressing dorsal visual streams during a working memory task (Jokisch et al. 2007). Some suggest a possible coexistence with this theory and communication through coherence (Bonnefond et al. 2017).

Communication between distant regions relies on myelinated axons within the white matter, with myelin helping to speed up the transmission of signals (Felten et al. 2015, p. 25). In addition to myelination and other axonal properties such as diameter (Felten et al. 2015, pp. 26–29), the length of a connections also affects the time taken for action potentials to reach a target neuron. Abnormal wiring lengths are thought to underlie some brain disorders, likely affecting region communication. For instance, subjects with autism present a lack of long connections and an excess of short connections (Barttfeld et al. 2011), possibly explaining the difficulty in seeing the 'bigger picture' in stories.

For the brain to operate effectively, optimal dynamics are thought to exist somewhere between complete stability and maximum flexibility, operating in a state that is capable of processing information both globally (integrated) and locally (segregated) (Senden et al. 2017; Tononi, Sporns, et al. 1994). Maximisation of these key ingredients is thought to take place near, or close to, a state of criticality (Atasoy et al. 2019; Massobrio et al.

2015; Tagliazucchi 2017), the definition of which has multiple components, not limited to the divergence of the correlation length across space and time (Haimovici et al. 2013). Criticality is not limited to the brain; groups of animal have been observed to display critical dynamics, with susceptibility to external stimuli possibly serving as a significant evolutionary advantage (Cavagna et al. 2010).

Non-invasive methods are able to explore the shifts between integrated and segregated states within the brain. Using methods such as functional magnetic resonance imaging (fMRI), it is possible to observe neuron activity in a non-invasive manner, collecting data on activation when the brain is at rest or when processing information during a task. The brain exhibits different dynamics depending on whether it is at rest (giving rise to the so-called resting state functional network) (Greicius et al. 2003), involved in a cognitive task (Shine, Bissett, et al. 2016) or sleeping (Tagliazucchi, M. Behrens, et al. 2013). For example, using fMRI, Cohen et al. (2016) noticed that the change in the level of segregation and integration between regions was dependent on the task being performed, with motor tasks emphasising segregated activity, whilst tasks requiring working memory entailed greater integration. Moreover, disruptions to activity akin to those seen during sleep have been linked to seizures (Englot et al. 2009). Studies tasked with understanding the mechanisms of phenomenological consciousness, and even going as far as defining a measurement for the level of consciousness in *any* system, suggest that integration between system components is a critical ingredient of a conscious state (Tononi 2005; Tononi, Boly, et al. 2016). This integrated information theory of consciousness proposed by Tononi et al. (2016) boldly claims that consciousness *is* integrated information, a theory that has been the target of criticism given in part by the lack of supporting empirical evidence (Cerullo 2015). In the brain, integration between brain regions reduces in minimally-conscious patients (Casarotto et al. 2016) and during sleep (Tagliazucchi, M. Behrens, et al. 2013). Additionally, several studies have pointed towards differences in oscillations (Singer 2000) and structural connectivity (Boly et al. 2011) as crucial components that underpin a wakeful state. Of course, much work remains in understanding the biological components that give rise to awareness, and how the brain produces rich, diverse and sequential experiences of one's internal and external environment.

When problem solving, one suggested mechanism which allows the brain to make use of its resources is thought to involve the formation of unique combinations of functionally

integrated neural processes (Shanahan 2012). In this model, these processes — consisting of coalitions of neural populations — compete to influence the selected response when presented with uncertainty in the environment; bouts of parallel processing — communication and competition between these neural coalitions (processes) — are punctuated with the selection of a behaviour, the consequence of a search over a vast space of possible choices. The parallel processing among regions enabling an exploration of this 'choice-space' requires communication between and within neural groups, evidenced by experimental observations of functional segregation and integration within and between brain regions (Fries 2015; Shine, Breakspear, et al. 2019; Tagliazucchi, Chialvo, et al. 2016; Tononi, Sporns, et al. 1994; Varela et al. 2001). This functional integration between regions — where the processing undertaken by a neural population is dependent on the processing by, and subsequent communication with, other populations — may rely on bouts of oscillatory synchronisation as the mechanism of communication between distributed brain areas (Fries 2015). From an experimental standpoint, the strength of a functional connection between region pairs — measured for example by correlating the BOLD signal in fMRI studies (van den Heuvel and Pol 2010; D. Zhang et al. 2010) — provides and insight into how different regions communicate with the rest of the brain, including the transitions between integrated and segregated system states, and how these states might differ alongside measures of intelligence (Rex E Jung et al. 2007) and in cases of disease (Lynall et al. 2010).

Synchronisation in the firing activity of neural populations is suggested to underpin communication between brain regions (Fries 2015). Bouts of synchronisation between different combinations of neural coalitions are thought to enable flexible coordination between neural processes (Deco, Rolls, et al. 2009; Friston 1997) and task switching (Deco, Kringelbach, et al. 2017). This metastability exhibited by the brain occurs spontaneously, where the brain transitions between attractor-like states, characterised by combinations of synchronised regions (Tognoli et al. 2014). These states manifest as combinations of regions becoming functionally integrated with, and segregated from, other areas of the brain over time. Resting state dynamics — that which emerge while the brain is at 'rest', i.e., not undertaking a task — also encompass metastable features, activity which enables timely responses to external stimuli and the consolidation of past events (Buckner et al. 2007; Deco, Jirsa, et al. 2009). Moreover, Deco et al. (2016) suggest that communication through coherence — one suggested mechanism of communication between groups of

neurons (Fries 2015) — requires metastable dynamics between components, emphasising the dependence between the ability for brain regions to communicate, with an overall heightened exploration of the space of possible bindings between regions.

Computational modelling is a key method to understand the dynamics of complex systems such as the brain, and where such systems are thought to transition between states in a non-deterministic manner. For example, computational models which simulate the interaction between neural populations have been used to explore the nature of consciousness (Dehaene, Kerszberg, et al. 1998; Sergent et al. 2004; Shanahan 2006, 2008), as well as the presence of criticality in the brain (Chialvo 2010; Haimovici et al. 2013; Hellyer, Shanahan, et al. 2014; Hopfield 1982; Tagliazucchi, Chialvo, et al. 2016). Computer models are also capable of modelling the dynamics of individual neurons, with such techniques often finding a balance between replicating action potentials with a high level of accuracy (e.g. Hodgkin et al. 1952), or sacrificing detail for decreased computational load (e.g. Izhikevich et al. 2003).

Other mathematical entities can be used to simulate oscillatory activity within the brain, which may be interpreted as communication between regions (Fries 2015). Models consisting of Kuramoto oscillators (Kuramoto 1975) have been used to explore metastable dynamics (Shanahan 2010b), where each Kuramoto oscillator mimics the oscillatory behaviour of individual brain regions, influenced by the phase of other regions within the connectome via their connections. Such models enable one to draw conclusions on connectome structure and its impact on dynamics, tasked with simulating changes in oscillation frequency within regions whilst they interact using the connectome as the structural backbone. These models are useful to explore changes in synchronisation and metastability between regions concurrently with and without perturbing the underlying structure (Hellyer, Scott, et al. 2015; Váša et al. 2015). The brain is thought to operate at peak levels of metastability (Friston 1997), enabling behaviours such task switching (Deco, Kringelbach, et al. 2017). By measuring the differences in the phase of the oscillators, the mean global synchrony in the system, and subsequently the extent to which dynamics are metastable (showing fluctuations in the level of global synchrony in the system) can be calculated. Changes in metastable dynamics exhibited by the model caused by structural changes in the network may highlight structural features which are important for maintaining fluctuations in global synchrony in the system.

### 2.2.2 Defining intelligence

Within the repertoire of cognition lies intelligence. While much debate continues to revolve around how intelligence should be defined (Braaten et al. 2006; Neisser 1979), intelligence is broadly thought to reflect an individual's ability to solve problems, adapt to the environment and learn from past experiences (Richard J. Haier 2016, pp. 5–9). Gottfredson (1997) defines intelligence as the "[...] capability for comprehending our surroundings – 'catching on', 'making sense' of things, or 'figuring out' what to do". An alternative take on the issue of might state that "intelligence is what is measured by intelligence tests" (Boring 1923). Early work by Charles Spearman on the observation of positive correlations among these aforementioned abilities lead to the hypothesis that intelligence consists of one general factor, $g$, a value which could be measured and compared between individuals (Spearman 1904). An alternative view — one which explores the possibility of distinct abilities which are not attributed to a single latent variable such as $g$ — states that intelligence is comprised of two subgroups of similar abilities, namely fluid and crystallised intelligence (Cattell 1943, 1963; Horn 1965). Fluid intelligence assesses the ability to solve novel problems and identify complex relationships, while crystallised intelligence refers to a capacity to use past experience (recalling facts, for example) to solve problems. McGrew (2009) defines fluid intelligence as "the use of deliberate and controlled mental operations to solve novel problems that cannot be performed automatically", and crystallised intelligence as "the knowledge of the culture that is incorporated by individuals through a process of acculturation. [...] typically described as a person's breadth and depth of acquired knowledge of the language, information and concepts of a specific culture". Work by Carroll (1993, Chapter 16) which describes three levels of intellectual ability (narrow, broad and general, with the latter referring to $g$) has since been combined with the fluid/crystallised model, resulting in the Cattell-Horn-Carroll theory of intelligence. Broad categories of ability described by this model include: processing speed; reading and writing ability; fluid reasoning; and comprehension-knowledge, the latter encompassing the depth of knowledge and the capacity to communicate this knowledge.

Cattell (1943) provides evidence for the existence of fluid and crystallised components of intelligence, describing how test scores corresponding to either category were influenced by age and also following brain injury. In the context of assessing intellectual ability in

subjects with cortical lesions, concurrent contributions by Hebb (1939b) highlighted the importance of using a range of tests to measure individual abilities, rather than relying on the outcome of a single assessment as some subjects showed no change in ability following cortical resection when measured using the tests that were defined at the time (Hebb 1939a, pp. 444–445). Further work supporting the distinction of fluid and crystallised factors follows from the prediction of reasoning ability based on working memory even when crystallised intelligence is controlled for (Buehner et al. 2006).

An operational definition, i.e., "[...] a procedure agreed upon for translation of a concept into measurement of some kind." (Deming 1993, p. 105), of crystallised and fluid intelligence may be formed by using tests which measure individual abilities within these two categories. More recent work by Cattell and Horn (1978) focused on formulating an operational definition primarily for fluid intelligence, developing over 30 tests, emphasising that measurements should be independent of cultural upbringing. Since reasoning and knowledge are seen as crucial components of fluid and crystallised intelligence, respectively (Beauducel et al. 2002), tests are designed to tap into these abilities. Many of these tests involved identifying a pattern from a given set of symbols, and selecting the next item from a list of possibilities. Tests for crystallised ability typically measure the depth and breadth of knowledge by means of vocabulary and other verbal tasks (naming unlabelled images for example).

Arguably, the involvement of prior experience is common to a certain degree in tests measuring fluid and crystallised ability, contributing towards fluid performance in the case where finding a solution to a 'novel' problem involves going through a learned set of steps or using knowledge to look for previously encountered patterns. For instance in Raven's Matrices (Carpenter et al. 1990), one may be experienced at looking for particular shapes that have arisen in previous instances of the test. At its core, an operational definition of fluid intelligence could incorporate the question: "Is it possible to perform well on the task without making use of previously acquired knowledge?". Interestingly, some studies suggest that fluid intelligence can be improved separately from the effect caused by practise (Jaeggi et al. 2008).

Operational definitions of intelligence may be derived from the claims made by Carpenter et al. (1990), who suggested that the individual differences in tasks measuring fluid intelligence are explained by the ability to construct abstract relations and to main-

tain a large set of candidate goals in working memory during tasks, with the capacity of working memory being the measurement of choice in this case. More recent findings have found a strong link between short-term storage processes and fluid intelligence (Martínez et al. 2011). Work is ongoing in categorising human ability, meaning that a precise, operational definition of intelligence, one which can be applied in a reliable and consistent manner across experiments, remains elusive. Efforts by Carroll (1993), Cattell (1963) and Horn (1965) continue to act as a foundation for modern day studies on intelligence.

Regarding the effect of age, both fluid and crystallised become more distinct across development, aligning to the general reduction in fluid and increase in crystallised ability as one grows older (Cattell 1943; Simpson-Kent et al. 2020). Causal influences between crystallised and fluid intelligence have been suggested by both Cattell (1987) and Ackerman (2001), stating that greater fluid intelligence results in faster accumulation of crystallised ability. An additional group of abilities constitutes spatial intelligence, involving the construction, retention and manipulation of mental shapes and images (Lohman 2000), which, alongside fluid and crystallised components, makes up the trio of intellectual skills (Hunt 2000).

### 2.2.3 The functional and structural correlates of intelligence

With regards to experimental observations of brain function and structure, an array of studies have provided evidence linking functional and structural features of the brain with changes in scores from tests which measure intelligence. Modern day assessment of intelligence involves undertaking a range of tests which assess these fluid and crystallised abilities, followed by amalgamating these into a single score called the intelligence quotient (IQ) (Braaten et al. 2006). On the relationship between intelligence and brain function, brains with higher IQ are thought to be more efficient at recruiting and managing neural resources during cognitively demanding tasks (Y. Li et al. 2009; Micheloyannis et al. 2006).

Is higher intelligence linked to widespread topological and spatial network changes or are changes more localised? Studies of brain activity, have indicated that fluid intelligence involves the frontal cortex (Duncan et al. 1995; J. R. Gray et al. 2003; Isingrini et al. 1997; Roca et al. 2009) suggesting its role as a hub region (Cole, Ito, et al. 2015; Cole, Yarkoni, et al. 2012) while lesion studies suggest a primary role of the right hemisphere (Barbey

et al. 2014) with differences in degree centrality in frontal and parietal regions (Langer et al. 2012). Cortical gyrification in distributed regions has shown positive correlations with fluid and crystallised intelligence, while their associations with cortical surface area and thickness are thought to be more localised (Tadayon et al. 2020). In this analysis of surface area and thickness, crystallised intelligence was associated with language areas, while fluid intelligence was linked with areas related to working memory, attention and visuo-spatial processing. Genome-wide association studies have linked fluid intellect with genes affecting neuron quantity, and subsequently neuronal efficiency (Christoforou et al. 2014). Candidates for mediating fluid intelligence include the lateral prefrontal cortex; anterior cingulate cortex/pre-supplementary motor area; and the intraparietal sulcus (Bishop et al. 2008).

Several studies have explored differences in brain activity with that of intelligence, with inconsistent results. Studies assessing functional connectivity have reported that intelligent individuals are more efficient at transmitting information globally throughout the connectome (Y. Li et al. 2009; van den Heuvel, Stam, et al. 2009). However, studies with larger cohorts were unable to confirm the correlation with network efficiency (Kruschwitz et al. 2018). A prominent theory of intelligence is that of the parieto-frontal integration theory, which highlights the correlation between intelligence and distributed neural activation in regions within the parietal and frontal lobes (Rex E Jung et al. 2007). Nonetheless, individual differences in intelligence, and in the structural and functional features of the brain make it difficult to predict intelligence from imaging data and the corresponding connectomes generated from them (Richard J. Haier and Rex E. Jung 2018, p. 222).

Efforts have been made to elucidate the relationship between intelligence and brain connectivity (Garrett et al. 2011; Thatcher et al. 2008; van den Heuvel, Stam, et al. 2009), but we still lack a clear understanding of why some brains are smarter than others. In this thesis, we explore the relationship between connectome structure and intelligence. We apply a number of techniques — primarily those derived from graph theory — to elucidate this relationship. We examine the spatial and topological structure of human brain connectivity against differences in intelligence, testing the hypothesis that communication efficiency is linked to intellectual ability. In particular, we attempt to find novel structural correlates which explain why some brains are more intelligent than others.

### 2.2.4 Disorders of cognition: Schizophrenia

In addition to exploring the structure of healthy connectomes, we will also look at a number of connectomes diagnosed with schizophrenia as a means to understand some of the associations between spatial structure and abnormalities in cognition. Cognitive disruption is a well documented phenomena of schizophrenia (Heinrichs 2005), a condition with symptoms that consist of misinterpreting reality, and the presence of delusions and hallucinations (Picchioni et al. 2008). Symptoms are categorised into positive symptoms (e.g. visual and auditory hallucinations) and negative symptoms (e.g. withdrawal from society and self neglect). Subjects with schizophrenia also experience cognitive deficits, such decreased processing speed, as well as impaired attention and working memory (Keefe et al. 2012; Matheson et al. 2008).

Structural abnormalities are associated with severe schizophrenia, with smaller whole brain volumes and larger lateral ventricles (Steen et al. 2006), reductions in grey matter volume (Tandon et al. 2008) — particularly in areas with many structural hubs, such as temporal and prefrontal cortices (Takahashi et al. 2009) — and changes to white matter integrity for patients experiencing hallucinations (Hubl et al. 2004). Studies correlating white matter integrity against IQ scores found that reduced coherence of the fronto-temporal tracts explained a substantial portion of the variance in IQ for schizophrenia subjects (Nestor et al. 2004). The disease is thought to be linked to the distribution of structural hubs (Bassett, Bullmore, et al. 2008; Rubinov et al. 2013; Yuanchao Zhang et al. 2012), with some regions becoming more hub-like (anterior cingulate and insula), while other regions functioning less like a hub (fusiform cortex) (Palaniyappan et al. 2019). The connectomes of schizophrenia subjects are sub-optimal with respect to their topological organisation (Yuanchao Zhang et al. 2012), with altered hub regions affecting integration. Changes to hubs are linked with structural abnormalities across a wide range of diseases, not only in schizophrenia (Crossley et al. 2014). In the case of schizophrenia, it is however unclear whether the loss of brain tissue may be exacerbated by anti-psychotic medication, taken to alleviate symptoms, or if the disease itself is the cause (Ho et al. 2011). From a functional perspective, schizophrenia subjects display impaired gamma-band responses to cognitive tasks (Minzenberg et al. 2010), suggesting that cortical oscillatory dysfunction may be a central component of the disease. Lowered functional integration with several resting state networks has also been observed in schizophrenia patients (W. H. Lee,

Doucet, et al. 2018).

In the forthcoming work, we will explore the links between schizophrenia and spatial features of the connectome. We will apply novel techniques in our analysis of the possible structural differences between the connectomes of healthy subjects and those diagnosed with schizophrenia. Moreover, we will compare intra-patient differences alongside a measure of symptom severity, with the goal being to find associations between the severity of the disorder and spatial features of the connectome.

## 2.3 Intractable Problems

Many problems in science and engineering require looking for an optimal answer to problems in which the solution space is too vast to be explored in its entirety, due to limitations in computational resources and time. One such example is the travelling salesman problem (TSP) (Christofides 1976), which involves finding the shortest path (or a path shorter than a given length) needed for a 'salesman' to visit all cities (nodes in a network), and return to the initial city. As the number of cities/nodes grows, the problem quickly becomes computationally intractable. In the instance where the number of cities is larger than say, 30 (corresponding to $2.6\times10^{32}$ possible pathways), the problem becomes too demanding for brute force approaches (where the length of every possible path is calculated, and the minimum obtained). As demonstrated, the time complexity for this brute force approach is $\mathcal{O}(n!)$, an algorithm that runs in factorial time in relation to the size of the problem (number of nodes in the network). These kinds of problems fall into the famous NP-Hard category of problems (Knuth 1974), where the size of the search space (all permutations of visiting all cities) grows beyond the bounds of any polynomial description of the input (the number of cities and the distances between them, in the case of TSP). It remains unknown whether these 'difficult' problems can be solved in polynomial time (Cook 1971), a question which, for the decision variant of the problem, is succinctly stated as *is P equal to NP?*. Attempts at proofs in either direction often rely on techniques that transform one problem into another within a supposed polynomial time bound. Despite this hurdle, and the likelihood that intractable problems are likely to remain intractable for the foreseeable future, various methods exist in finding near-optimal solutions to intractable problems without performing a brute force search over all possible solutions. For TSP, that could involve using techniques which give an upper bound on the time needed to

find an approximated shortest path as a multiple of the actual shortest path (one such technique involves reducing the network of routes between cities to a minimum spanning tree (Christofides 1976; Kruskal 1956)).

### 2.3.1 Simulated annealing

To deal with these kinds of difficult problems, especially those combinatorial in nature, various search methods exist which instead explore the original search space in a more efficient manner, combining methods of exploration and exploitation. By doing so, these search algorithms find solutions which are considered 'good enough' by being close enough to an optimal solution (Garey et al. 1979, pp. 121–148). Simulated annealing is one such technique for efficiently finding solutions to problems with vast solution domains, inspired by the process of slowly cooling metal to achieve a particular physical consistency (Kirkpatrick et al. 1983), the technique being rooted in the work by Metropolis in the 1950's (1953). The search method attempts to find solutions in the search space which are close to an optimal solution by comparing the performance of the current 'best' solution against that of alternative solutions. Constraints on selecting one solution over another are made more restrictive as the search progresses; local minima are avoided by selecting worse solutions with a probability that reduces over time, known as the 'temperature'. Given a current best-so-far solution, $s$, from the set of all solutions $S$, one method of accepting an alternative solution, $s'$, involves comparing the performance of $s$ and $s'$ and introducing a probability of selecting a solution with a poorer performance:

$$f(s, s') = \begin{cases} s', & \text{if } r < \exp\left(\frac{g(s)-g(s')}{t}\right) \\ s, & \text{otherwise} \end{cases} \tag{2.4}$$

where $r$ is a uniformly distributed random number in the interval [0,1]; $g : S \to \mathbb{R}_{\geq 0}$ is the custom performance function for this problem; $t > 0$ is the current 'temperature'. This example preferentially obtains solutions with lower performance values, i.e. where $g(s') < g(s)$. By repeatedly comparing $s'$ with other possible solutions, and updating $s'$ with better solutions, the algorithm converges on an approximated global minimum in $S$. The rate at which $t$ decreases will alter the performance of the best solution identified, with slower rates improving the identification of better solutions at the cost of increasing

the search time. A simple method of reducing the temperature involves multiplying $t$ by a factor less than one. The process of obtaining $s'$ usually involves perturbing the current solution, relying on the assumption that good solutions can be improved upon through a local exploration of the search space. In the case of TSP, this might involve swapping the position of two cities in the path that visits all cities. Local search is combined with a more extensive search by, for a given $t$, repeatedly perturbing the current best solution, before reducing the temperature and continuing. The search can be halted when $f(s, s') = s$ for all repetitions for a given temperature $t$. Searches can be restarted, and attempted several times in the hope of finding an even better solution. However, the process of selecting the number of repetitions and controlling the temperature is non-trivial, impacting the quality of the final solution. Often, the initial temperature is set to a value which is high enough to encourage selection of poorer solutions early on in the search process, avoiding local minima, and a function used that decreases the temperature such that a good enough solution is found in good time.

# Chapter 3. Methods and Datasets

To analyse the structure of the connectome, we make use of several computational techniques and image processing methods. This includes global search optimisation across a vast search space, and ways of modelling neural synchronisation within the brain. Both of these areas make up the bulk of the implemented tools facilitating our analysis. Additionally, we rely on several DTI processing tools such as DSI-Studio to build connectomes. These methods and tools are described in this chapter.

## 3.1 Searching for an Optimal Component Placement In the Connectome

It is useful to have an appreciation of search techniques like simulated annealing when dealing with problems that require searching for an optimal permutation or a combination of components. In this analysis, we apply simulated annealing in an attempt to answer questions concerning the spatial arrangement of the connectome. While many other search methods exist, including algorithms inspired by evolution (Fraser 1957; Sastry et al. 2005, Chapter 4), simulated annealing can be applied to a great variety of problems and is arguably one of the simplest stochastic search methods to implement, requiring few parameters (the starting temperature, the temperature reduction, number of trials for each temperature value and threshold for termination).

With regards to component placement optimisation, one way to assess whether the spatial arrangement of brain regions minimises the total wiring length involves interchanging the spatial positions of regions with the aim of finding one which reduces the total wiring length (Figure 3.1). The process of identifying a spatial arrangement which decreases the total wiring length involves navigating a vast combinatorial space of possible arrangements, a space which is too large to explore in its entirety. Search heuristics such as simulated annealing can be used to navigate this space, and to find solutions which are close to the global optimum; because of the size and complex topography of the search space, finding component placements with the least possible total wiring length is

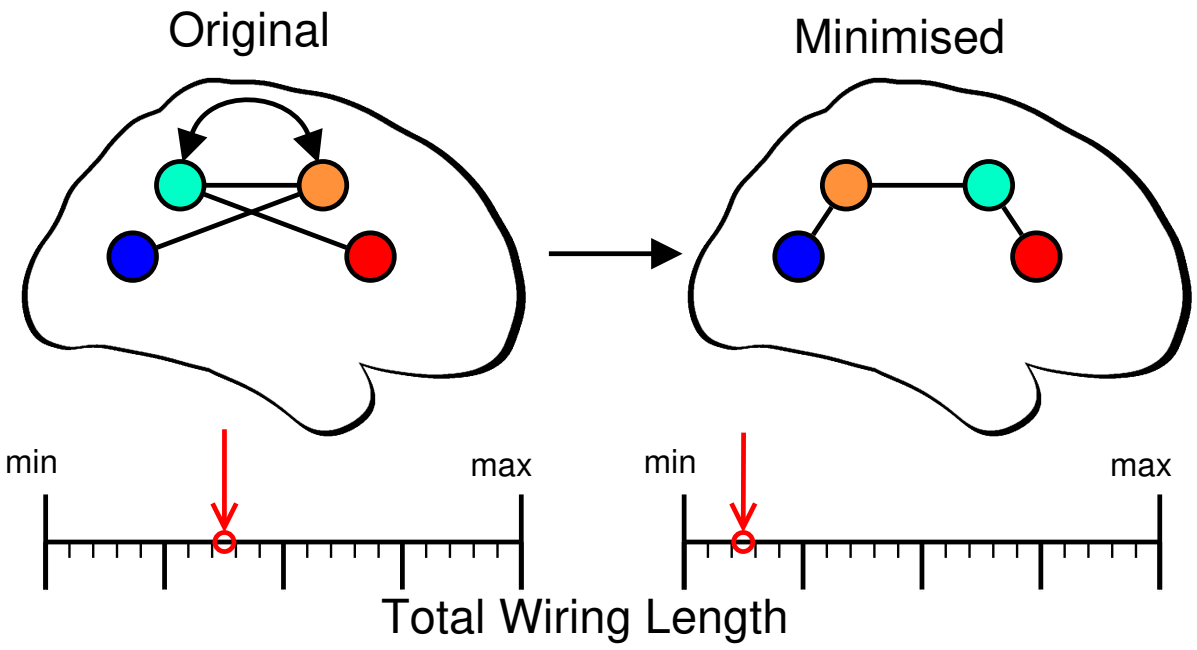


Figure 3.1: Overview of region-swapping procedure. Spatial positions of regions are swapped to reduce the connectome's total wiring length while maintaining the topology. We use simulated annealing to estimate the minimal arrangement by exploring the vast number of possible spatial arrangements (a total of $n!$ possible arrangements for $n$ regions).

a challenging task. As such, in our subsequent analyses, we settle for approximating the real global minimum, as is often the case when dealing with large search spaces (Garey et al. 1979, pp. 121–148).

Regarding our problem of finding an arrangement that reduces the wiring length of the network, Algorithm 1 lists the pseudo-code for the main portion of the simulated annealing algorithm used to find minimal component placements. The implemented code is adapted from that used in Kaiser et al. (2006), which is based on the Metropolis search algorithm (Metropolis et al. 1953) and the numerical recipe found in Press et al. (1988, pp. 444–455). The algorithm was adapted by Christopher Hayward to decrease the running time. Specifically, when updating the total wiring length, only the change in wiring length for the pair of regions which are swapped is recalculated, rather than that of the entire connectome (most of the wiring lengths will not change when swapping two regions at each step). This saved a substantial amount of running time, particularly when optimising larger connectomes. Part of our study involves comparing the original total wiring length of the connectome relative to the minimum and maximum possible wiring lengths after spatial rearrangement (termed the *relative* wiring length). Thus, for

finding a component placement which instead maximises the total wiring length, line 13 is altered: $s$ and $s'$ are swapped.

**Algorithm 1** Simulated annealing procedure (based on Metropolis et al. 1953) for obtaining a component placement which minimises the total wiring length of the network. Note, for finding the component placement which instead *maximises* the total wiring length, line 13 is altered: $s$ and $s'$ are swapped.

1: $t \leftarrow initialTemperature$
2: $s \leftarrow [1, \ldots, n]$ ▷ initialise current arrangement of $n$ regions
3: **do**
4: $minLength \leftarrow \infty$ ▷ keep track of min/max wiring lengths
5: $maxLength \leftarrow 0$
6: $trialNum \leftarrow 0$ ▷ several iterations for each temperature value
7: $acceptedNum \leftarrow 0$
8: **while** $trialNum < trialLimit$ & $acceptedNum < acceptedLimit$ **do**
9: $s' \leftarrow s$ ▷ initialise altered arrangement
10: $[i, j] \leftarrow randomNodePair([1, \ldots, n])$ ▷ select pair to swap
11: $s'(i) \leftarrow s(j)$
12: $s'(j) \leftarrow s(i)$
13: **if** $rand(0,1) < \exp\big((wiringLength(s) - wiringLength(s'))/t\big)$ **then**
14: $s \leftarrow s'$ ▷ $s'$ is accepted
15: $minLength \leftarrow \min(minLength, wiringLength(s))$
16: $maxLength \leftarrow \max(maxLength, wiringLength(s))$
17: $acceptedNum \leftarrow acceptedNum + 1$
18: $trialNum \leftarrow trialNum + 1$
19: $t \leftarrow reduceTemperature(t)$
20: **while** $\big((maxLength - minLength)/(maxLength + 1)\big) > stopLimit$
21: **return** $s$ ▷ return the minimised arrangement

In Algorithm 1 we use the following parameters for all subsequent analyses involving component arrangement: The initial temperature (*initialTemperature*) is calculated by randomly swapping the positions of a pair of regions, and multiplying the typical change in length by a factor of 10. For $n$ nodes in the network, the temperature $t$ is decreased to 90% of the previous iteration's temperature, after either $n\times1000$ swap attempts (*trialLimit*=$n\times1000$) or $n\times100$ accepted swaps (*acceptedLimit*=$n\times100$), whichever occurs first. This continues until the change in total wiring length falls below a predefined threshold of 0.5% (*stopLimit*=0.005, i.e. a maximum and minimum wiring length difference of less than 0.5% at a given temperature). The choice of selecting an alternative arrangement $s'$ with a given wiring length depends on the that of the best-so-far spatial arrangement $s$ and a decaying probability $t$ of selecting an arrangement that increases the wiring length. By occasionally accepting arrangements that increase the wiring length, the search can 'jump' out of local minima early on in the search.

Figure 3.2 provides a visual example of a random network before and after rearrangement. Because of the random element of the simulated annealing algorithm (selecting the next $s'$), it is possible for separate runs of the algorithm to converge on different spatial arrangements for the same initial arrangement, as shown in Figure 3.3. This prompts the use of repeated runs on the same network to find different spatial arrangements with a reduced wiring length. By repeating the search, this also helps to avoid local minima.

The extent to which the wiring length can be reduced depends on the number of nodes in the network and the edge density (the fraction of edges which are present in the network out of all possible edges which could be present). These dependencies are shown in Figure 3.4 for a simple toy network: assessing random networks with different numbers of nodes — all with the same edge density — showed that fewer nodes affords a greater reduction in wiring length in this simple example. The same can be said for a reduced edge density, when the number of nodes remains fixed.

### 3.1.1 Correcting inter-hemispheric connections

Algorithm 1 treats connections as straight edges in the network, and their lengths based on this. Approximating connections as straight lines is physically unrealistic, as real white matter connectivity deviates from being perfectly straight (Braitenberg and Schüz 2013, pp. 7–14). This is especially prominent for connections between hemispheres which primarily pass through the corpus callosum. To mimic the presence of inter-hemispheric constraints on the directions of connections and thus improve our approximation of the change in total wiring length following rearrangement, the lengths of inter-hemispheric connections are set to the combined length of two straight edges which both connect to the centre of mass of the network (the mean 3D-position of all nodes/regions). Thus connections are lengthened in a similar way as if they were constrained similarly to those routing through the corpus callosum. This simple correction method is applied to all datasets in this study.

In addition to this, Algorithm 1 also ensures that regions cannot move between hemispheres, keeping arrangements more biologically-plausible (the total volume of all regions in each hemisphere remains the same for before and after spatial rearrangement, and inter-hemispheric connections are neither created nor removed). As with the inter-hemispheric correction method, this additional constraint is applied to all datasets in this study.

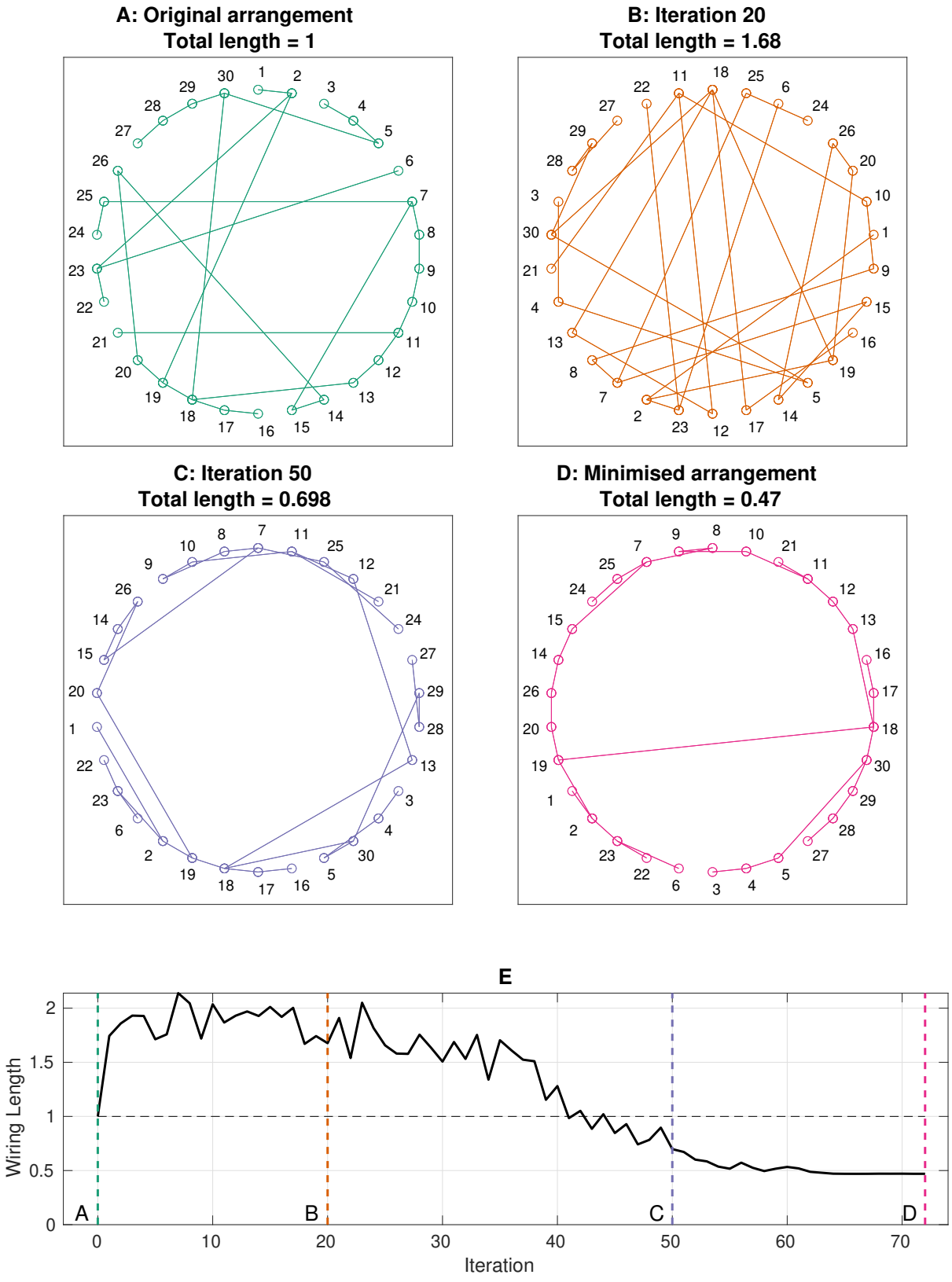


Figure 3.2: Minimising the total wiring length using simulated annealing, for a randomly wired network consisting of 30 nodes. **A:** The initial spatial arrangement of nodes. **B/C:** Arrangements part-way through the simulated annealing search. **D:** The final arrangement of nodes providing the best reduction in wiring length identified by this single application of the simulated annealing algorithm. **E:** The change in wiring length over the course of the simulated annealing search (normalised against the length of the initial spatial arrangement). The iterations corresponding to **A/B/C/D** are denoted by vertical dashed lines.

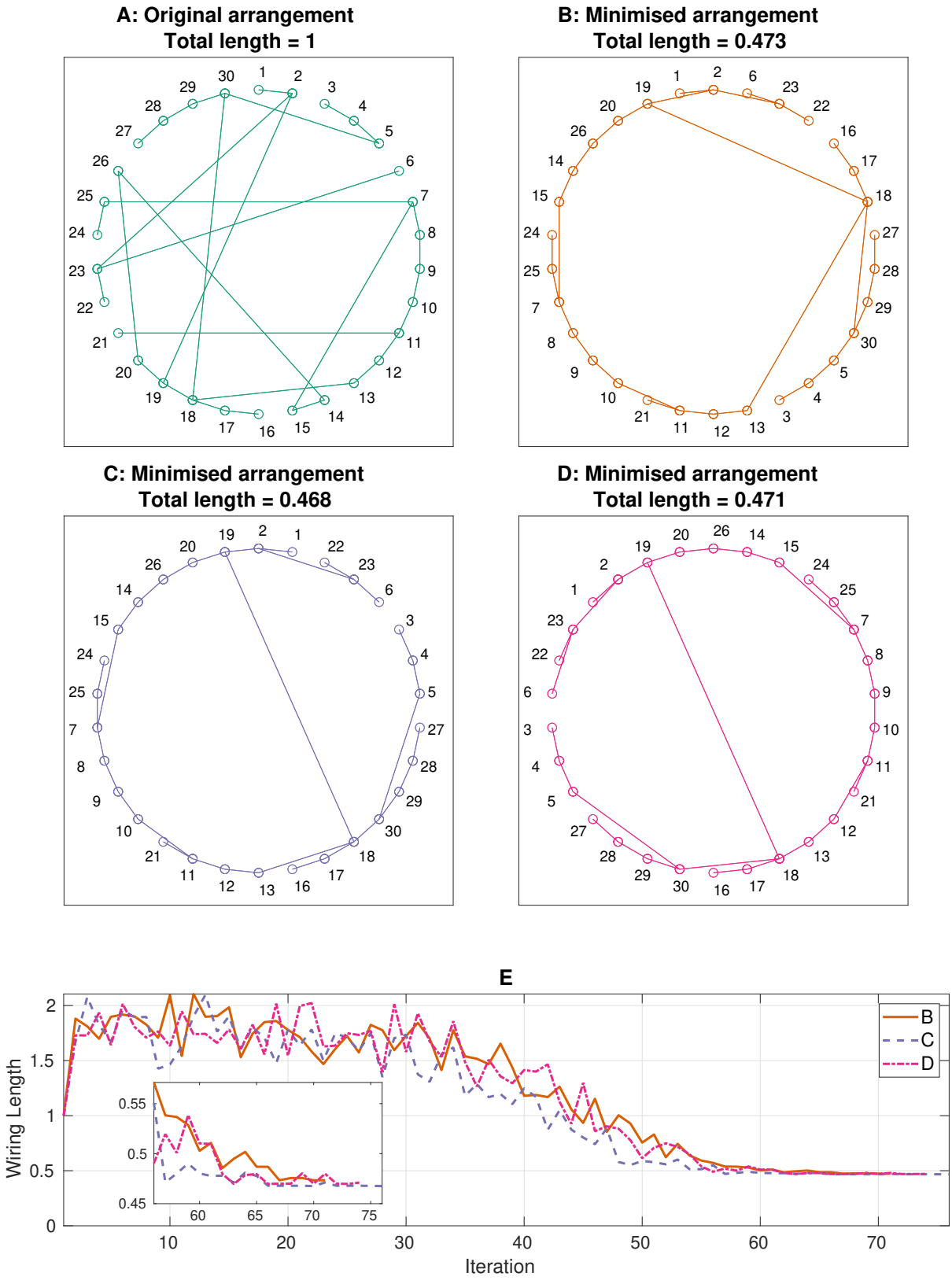


Figure 3.3: Separate executions of the simulated annealing algorithm may result in different minimised arrangements. **A:** The initial spatial arrangement of 30 randomly connected nodes. **B/C/D:** The final arrangements from three separate runs of the simulated annealing search, each with different total wiring lengths and different spatial placement of regions. **E:** For each run, the change in wiring length over the course of the simulated annealing search (normalised against the length of the initial spatial arrangement). **Inset:** The change in wiring length for the last several iterations of each search.

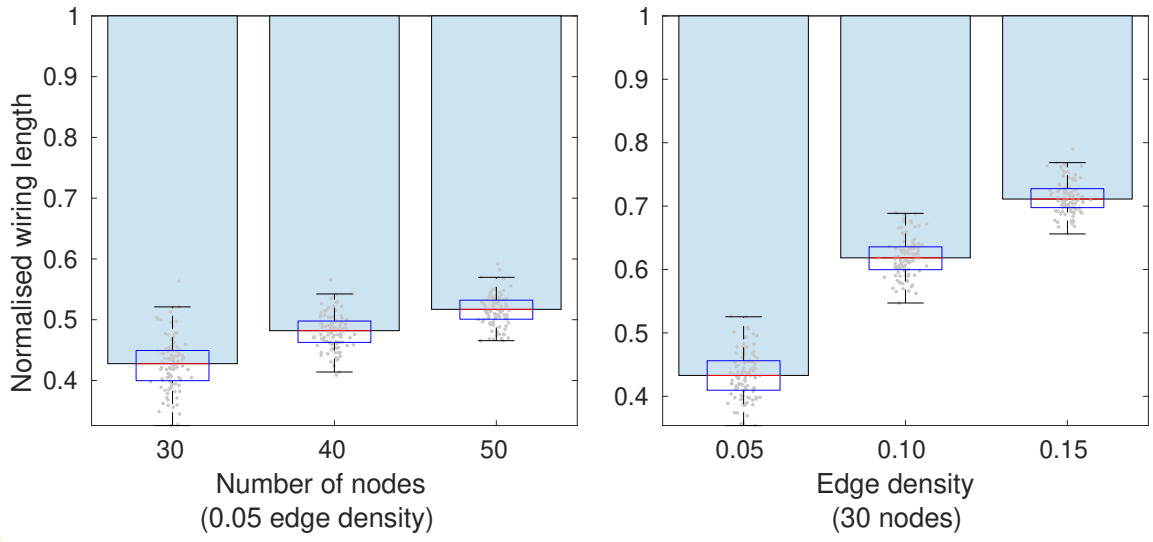


Figure 3.4: For a random network, the effect of the number of nodes and edge density on the total connection length of the minimised arrangement, normalised against the length of the initial arrangement (the length of the original arrangement is equal to one). Here, we swap the positions of regions positioned in a circular arrangement, wired randomly, repeating this 100 times for each condition. The same search parameters (temperature reduction, etc) were used for all cases. For a fixed edge density, a greater number of nodes impedes the reduction in wiring length. For a fixed number of nodes, mores edges also makes it more difficult for the search to reduce the wiring length.

## 3.2 Simulating Oscillating Dynamics of Neural Populations

As part of understanding why connectomes are structured the way they are, our methods involve assessing the impact of spatial factors on global neural dynamics. Kuramoto oscillators (Kuramoto 1975) provides a good estimation of global dynamics (W. H. Lee, Bullmore, et al. 2017) whilst minimising the computational burden associated with more detailed models of neural activity (e.g. H. R. Wilson et al. 1972).

The Kuramoto model consists of three important parameters: the coupling strength (K), the conduction velocity (V) and the oscillation frequency of each region. K refers to the strength of the connections between regions, with higher values meaning regions have a stronger influence over others (defined in arbitrary units). V refers to the speed at which signals (phase information from other regions) travel along connectome fibres (defined here in metres per second). Additionally, each region is assigned a default oscillation frequency which is realised by the individual regions in the case where connectivity to that region is removed. Additional parameters can also be included, such as noise perturbing this default frequency, increasing the complexity of the model but incorporating aspects which may

be central to inter-region communication (Deco, Jirsa, et al. 2009).

The theory that groups of neurons communicate through differences in the phase of their oscillations (Fries 2005, 2015) informs our assumption of the mechanism of communication in this computational model. In our following computational experiments, near zero-phase lag synchronisation between two oscillators represents ongoing communication between those two oscillators (regarded as brain regions, in the context of connectivity defined by the connectome). Thus, by measuring synchronisation, we estimate the extent to which neural populations are engaging in communication.

Validation of these models can take place by performing a parameter sweep over K and V, and correlating model activity with the functional connectivity produced by correlating the BOLD signals from empirical data between all pairs of regions. In this regard, the inclusion of empirically-derived functional data is crucial insofar as it validates the computational model, helping to ensure that the results are biologically-plausible and that dynamics resulting from perturbations to the model reflect to a greater extent what might occur *in-vivo*.

Synchronisation is measured as the difference in phase between oscillators, with zero representing opposite phase and zero synchronisation, and one representing identical phase and full synchronisation. For each oscillator, the phase $\theta$ of oscillator $i$ at time $t+1$ is determined by the equation:

$$\frac{d\theta_i}{dt} = \omega_i + \sum_{j=1}^{n} K A_{ij} sin(\theta_j(t - \tau_{ij}) - \theta_i(t)), \tag{3.1}$$

where $\omega_i$ (selected from the gamma-band range: 40Hz, 60Hz or 80Hz) is the natural frequency for oscillator $i$, $K$ is the global coupling strength, $A_{ij}$ is the binary connection between oscillators $i$ and $j$, $\theta_i(t)$ is the phase of oscillator $i$ at time $t$, and $\tau_{ij}$ is the conduction delay between oscillators $i$ and $j$. The delay $\tau_{ij}$ is defined by $\tau_{ij} = d_{ij}/V$. Where $d_{ij}$ is the Euclidean distance of the connection between the two regions and $V$ is the global conduction velocity (in metres per second). For the natural frequency, frequencies from the gamma-band range are often used as this range is associated with functional activation of the cortex (Fries 2015), observed across mammalian species. Simulations are usually run for a fixed length of time, after ignoring an initial time period to allow the

effects of initial conditions to dissipate.

To calculate mean synchrony and metastability within the model, we use the instantaneous synchronisation $\phi$ at time $t$, defined as (Shanahan 2010b):

$$\phi(t) = |\langle e^{i\theta_k(t)} \rangle_k|, \tag{3.2}$$

where $i = \sqrt{-1}$, $k$ is an oscillator, and $\langle \rangle_k$ denotes the mean over all oscillators. Mean global synchrony (abbreviated to just 'synchrony') is calculated as the mean of $\phi$ over the duration of the simulation, and metastability as the standard deviation of $\phi$ over the duration of the simulation. The standard deviation of the instantaneous synchronisation of the system of oscillators over the duration of the simulation reflects the tendency for the system to transition between synchronised (greater values of $\phi$) and desynchronised states (lower values of $\phi$), measuring the variability in the states of phase configurations over time. Using the standard deviation of $\phi$ to quantify metastability in the context of Kuramoto oscillators is an approach which has been used by other studies (Deco and Kringelbach 2016; Shanahan 2010b; Váša et al. 2015), and we use this value to estimate the fluctuations in synchronisation within our *in-silico* model.

### 3.3 Additional Software Tools

We use a number of tools throughout this thesis. MATLAB version 9.7.0 (R2019b update 2) was used for performing analyses and running dynamical simulations. Newcastle University's Rocket computing cluster, the School of Computing's High Performance Computing cluster, and the SAgE Faculty TOPSY cluster were used to run models of neural dynamics and other compute-intensive analyses. MATLAB MEX functions were used to speed up compute-intensive functions. We used the Brain Connectivity Toolbox to compute various graph theory measurements (Rubinov and Sporns 2010). Where appropriate, P-values are corrected for multiple comparisons using the Benjamini-Hochberg procedure (Benjamini et al. 1995). FSL (Smith, Bannister, et al. 2001), Freesurfer (Fischl 2012) and DSI-Studio (Yeh, Wedeen, et al. 2010) were used to reconstruct connectomes and extract functional connectivity from resting-state functional MRI, structural MRI and diffusion MRI brain images. To visualise the networks, we used the BrainNet Viewer (Xia et al. 2013) and BrainStorm (Tadel et al. 2011) MATLAB packages. GIMP (gimp.org),

DIA (dia-installer.de) and Inkscape (inkscape.org) were used to create and manipulate figures. GNU Emacs (www.gnu.org/software/emacs) and LaTeX (www.latex-project.org) were used for document construction.

### 3.4 Rhesus Macaca Dataset

Using a collection of connectome data for rhesus monkeys (*Macaca mulatta*) — a nonhuman primate commonly used in studies of the connectome — we will analyse the spatial arrangement of brain regions and their connections (vertices and edges within the connectome 'network', respectively). Algorithm 1 will be used to assess the spatial arrangement and whether the macaque connectome exhibits CPO. See Figure 3.1 (Chapter 2) for a visual guide for this procedure.

Several connectivity datasets of macaque connectomes exist, including CoCoMac (Kötter 2004) (used in Kaiser and Hilgetag 2006), comprising aggregated connectivity of the macaque connectome obtained from over 300 tract-tracing experiments (where axonal tracers are injected into the brain to identify the presence of fibre tracts — Heimer et al. 2013, Section 1.2). Here, we analyse the connectome of the macaque using more recent DWI approaches compared with those used in CoCoMac database. Previous comparisons between tract-tracing and DWI suggest that DWI is a reliable method of identifying fibre tracts in a non-invasive manner (van den Heuvel, Reus, et al. 2015). We attempt to replicate the findings of other studies, claiming that the macaque connectome is spatially sub-optimal with regards to the minimisation of the total wiring length (Kaiser and Hilgetag 2006).

The dataset consists of four connectomes from four female macaques, named VL and DP (both 6 years of age); and FL and AL (4–5 years of age). Data is provided by Ortiz-Rios et al. 2018. For each subject, we were provided with the structural connectivity matrices consisting of 184 regions, resulting from a parcellation of cortical and subcortical structures using the D99 atlas (Reveley, Gruslys, et al. 2017; Saleem et al. 2012). Figure 3.5 displays the connectome and adjacency matrix for subject AL.

Additionally, we were provided with the functional connectivity matrices for the four subjects, computed by correlating BOLD signals between regions while the subjects were tasked with free viewing a selection of movies. Using movies allows for obtaining "reliable

and consistent visual activation across all monkeys" (Ortiz-Rios et al. 2018). A single FC matrix was obtained for each subject, the mean across several matrices each corresponding to the activity within an 18 second time window (12 sample points at TR=1.5 seconds). Twenty-five movies were shown to each subject, each 30 seconds long. The method for calculating the time-varying functional matrix is based on (Shine, Bissett, et al. 2016).

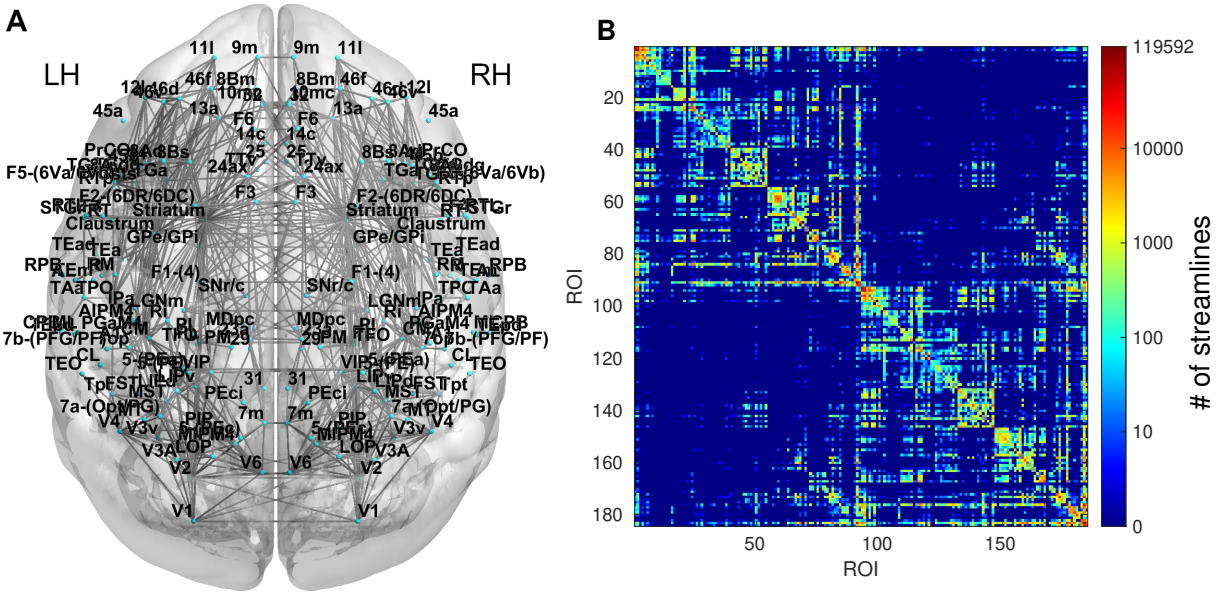


Figure 3.5: Connectome for macaque subject AL. **A:** Axial view of the connectivity between 184 regions. For improved clarity, we only show the connections with streamlines greater than that of 95% of connections in the network. LH/RH=Left/Right Hemisphere. See Tables A.1 and A.2 for the full region names and lobe mappings. **B:** The corresponding adjacency matrix showing all connections and their number of streamlines. Regions 1–92 are in the left hemisphere, 93–184 are in the right.

Algorithm 1 will be used to obtain the spatial arrangements of the regions which minimises the total wiring length of the macaque connectomes. For the original arrangements, each region is in its original position whereas in the minimised arrangements, the regions are spatially swapped so as to minimise the total length of the connections. Connections lengths are calculated as the Euclidean distance between the connected regions (connections are treated as straight edges). The simulated annealing algorithm is repeated 1000 times per subject, and the arrangements corresponding to the greatest reduction in wiring length are used for subsequent analysis. The lengths of connections which pass between hemispheres are corrected using the previously described method of 'routing' the connections through the centre of mass of the network. For example, connections such as the visually 'short' ones between regions 9m in Figure 3.5 are substantially lengthened

following this correction. Figure 3.6A illustrates the change in connection length for an example inter-hemispheric connection in the macaque connectome. Figures 3.6B and 3.6C provide the adjacency matrices for before and after correction, respectively.

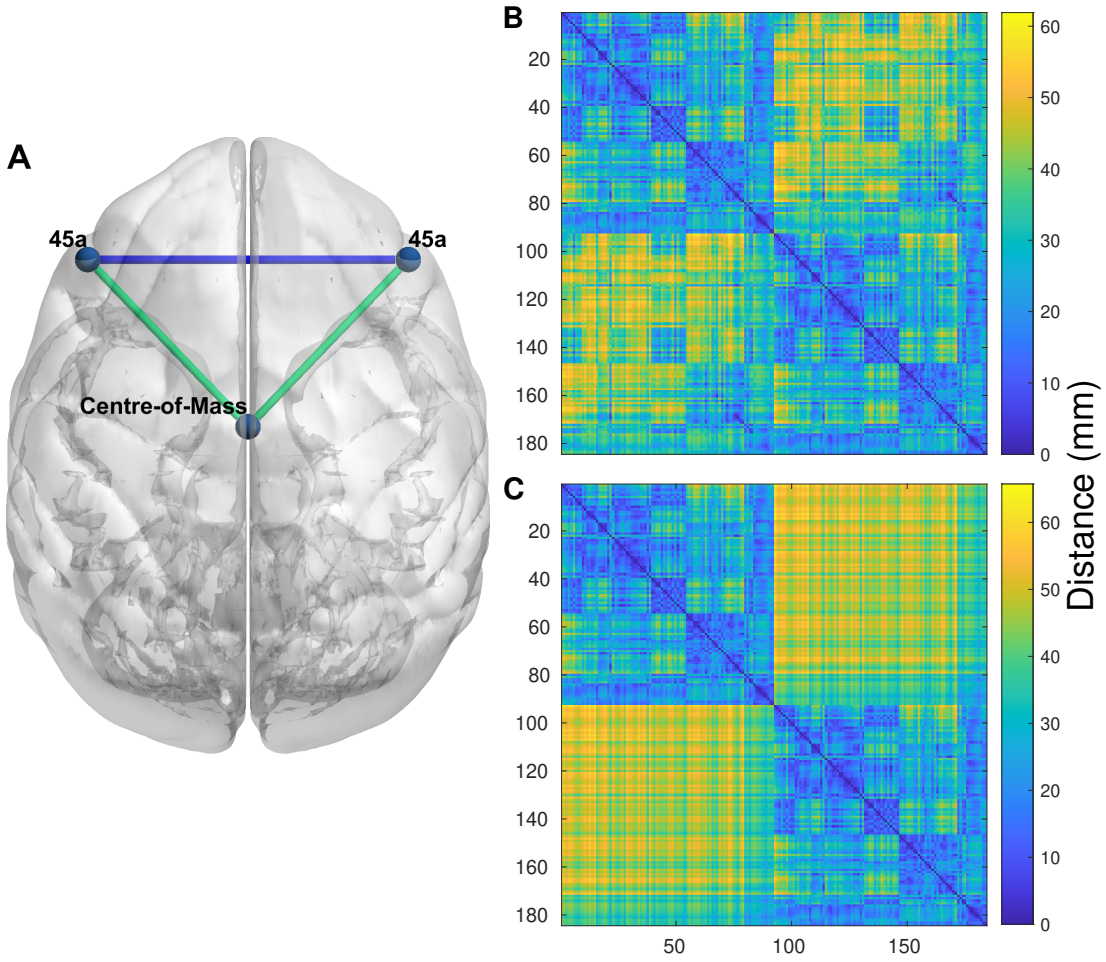


Figure 3.6: Visual demonstration of correcting the inter-hemispheric connections. **A:** For inter-hemispheric connections, their lengths reflect the sum of the two edges connecting each region to the centre-of-mass of the network. The length of the blue (top) edge is the distance between area 45a (premotor) across hemispheres without correction. The summed length of both green edges reflects the adjusted length. The centre-of-mass is the mean position of all regions in the connectome. **B:** The Euclidean distance matrix before the adjustment, and **C:** after the adjustment, showing lengthened inter-hemispheric connections in the corrected version (between regions 1–92 and 93–184).

## 3.5 Human Connectome Project Dataset

We will also test for component placement optimisation (CPO) by swapping the positions of regions in the human connectome, using data from 280 subjects from the Human Connectome Project (HCP) (Van Essen, Ugurbil, et al. 2012). We test the hypothesis that,

like *C. elegans*, the human connectome also displays sub-optimal component placement with regards to the minimisation of the total wiring length (Raj et al. 2011). The macaque connectome shares many structural similarities with that of the human, including similarly positioned hub regions (L. Li et al. 2013). However, the evolutionary lines leading to the modern macaque and human diverged around 25 million years ago (Kumar et al. 1998), making it possible that the level of spatial optimisation in the connectome differs between the species.

The HCP dataset consists of 280 healthy adults aged between 22 and 30, 138 of which are female. Structural, diffusion and functional data for these subjects was obtained from the Human Connectome Project (Van Essen, Ugurbil, et al. 2012) (HCP — www.humanconnectome.org, S1200 release). The subjects were pre-processed by the HCP pipeline (Glasser et al. 2013), before being further processed (streamline tractography) by Christopher James Hayward and Xue Chen. For structural and diffusion data, we used T1-weighted 3T MRI and diffusion imaging pre-processed data. Pre-processed data included a Freesurfer parcellation of each subject's T1 image into 34 cortical and 7 subcortical regions per hemisphere (amygdala, caudate, hippocampus, nucleus accumbens, pallidum, putamen, and thalamus) (Fischl, Salat, et al. 2002). Cortical segmentation makes use of the Desikan-Killiany atlas (Desikan et al. 2006) (Figure 4.12). Further imaging parameters and details are found in Section B.1.

Following the same methods as for the macaque, we use this data to assess the spatial arrangement of brain regions in the context of their connections, and the extent to which CPO occurs in the human brain. In the event of finding that the human connectome is sub-optimal with respect to the spatial arrangements of regions, we attempt to identify a reason for a possible sub-optimal component placement in the brain by simulating changes in dynamics using the Kuramoto model — whether functional dynamics differ for a sub-optimal component placement versus one that minimises the wiring length.

## 3.6 Schizophrenia Dataset

In addition to healthy connectomes, we will also explore whether spatial differences exist in the connectomes of healthy controls and subjects diagnosed with schizophrenia. We use schizophrenia as an example of where cognition has been impaired, and we attempt to

find a link between this impairment and the spatial arrangement of regions in the context of their connections, potentially uncovering new insights into structural differences that may be driving some aspects of the disorder.

Connectome data for subjects with and without schizophrenia diagnoses were obtained from the School of Psychology and Cognitive Science, East China Normal University (processed by Dr. Chao Yan and Dr. Xuan Wang). The data consists of 88 subjects in total (Table 3.1): 43 healthy controls and 45 schizophrenia patients. Forty-one of the 45 schizophrenia subjects were known to be taking anti-psychotic medication at the time of scanning. Symptom severity was measured using the Positive and Negative Syndrome Scale (PANSS) (Kay et al. 1987), with higher scores indicating more severe symptoms. PANSS consists of a positive, negative and general score for each subject, corresponding to non-overlapping categories of symptoms associated with the disease. Each of the three scores is a summary statistic across a number of specific symptoms, seven symptoms for positive and negative categories, 16 for general. Each symptom is rated from one (not present) to seven (severe).

Connectomes are composed of 78 regions, based on the Desikan-Killiany atlas (Desikan et al. 2006) alongside a subcortical partitioning (Fischl, Salat, et al. 2002). The insula and thalamus regions were excluded from the connectomes due to inadequate segmentation output from Freesurfer, reducing the total number of regions from 82 to 78; Freesurfer can fail to identify regions for a number of reasons, such as movement artefacts or poor image quality causing an inability to identify boundaries between white and grey matter, and around sub-cortical areas. Processing the data involved registering the T1 structural images (resolution: 1×1×1mm) to the b0 DTI images (resolution: 1.9×1.9×2.5mm). Attempts were made at segmenting structural T1-weighted images into 82 regions in total, including cortical and subcortical regions by running the 'recon-all' command from Freesurfer (Fischl 2012). Eighty-two regions were selected based on aparc+aseg.mgz, generating 82 '.nii' mask files using the 'mri_binarize' command from Freesurfer. These masks were used as regions in the tractography procedure, performed using FSL (Smith, Bannister, et al. 2001), using an angular threshold of 65 degrees. Functional data was not available for this dataset.

Table 3.1: Demographics for healthy controls and schizophrenia patients

| | Healthy controls (N=43) | Schizophrenia patients (N=45) |
|---|---|---|
| Age (years) | 21.6±3.5 | 23.4±5.3 |
| Males/Females | 28/15 | 29/16 |
| PANSS General score (min/max=16/112) | n/a | 30.8±8.5 (N=43) |
| PANSS Positive score (min/max=7/49) | n/a | 14.2±6.4 (N=43) |
| PANSS Negative score (min/max=7/49) | n/a | 18.5±6.7 (N=43) |

*Note.* PANSS scores were unknown for two schizophrenia subjects. Positive and negative scores have a lower/upper limit of 7/49, and general scores have a lower/upper limit of 16/112. Values are mean±SD. Patients had more severe negative than positive symptoms. Significant positive correlations existed between all three scores — positive versus negative: $\rho$=0.31, $P$=0.039; positive versus general: $\rho$=0.5, $P$ <0.001; negative versus general: $\rho$=0.58, $P$ <=0.001.

### 3.7 Data From the Nathan Kline Institute

Here, we list the dataset used to investigate the relationship between connectome structure and intelligence. Our goal for this dataset is to explore the link between the spatial/topological structure of the brain, and intellectual ability, making use of our simulated annealing algorithm as well as other methods. The corresponding results include the outcome from an analysis of the spatial and topological features of the human connectome in relation to estimations of fluid and crystallised intelligence.

This dataset consists of 98 healthy adults, ranging from 18 to 85 years of age (49 female, mean age 43±21) (Table 3.2), processed by Dr. Cheol Han (Korea University, Sejong). We used T1-weighted MRI and DTI (diffusion) data from the Nathan Kline Institute (NKI, part of the FCP/INDI sharing initiative — http://fcon_1000.projects.nitrc.org — Nooner et al. 2012). Using the Desikan-Killiany atlas (Desikan et al. 2006) and a subcortical partitioning (Fischl, Salat, et al. 2002), we considered the structural connectivity between 82 brain regions — provided by Freesurfer — consisting of 34 cortical and seven subcortical regions per hemisphere. Subcortical regions consisted of the amygdala, caudate, hippocampus, nucleus accumbens, pallidum, putamen, and thalamus. For further details of the image processing methods, see (Lim et al. 2013). This sample was age-matched across genders, where subjects were grouped into bins, each spanning 10 years.

In this dataset, fluid and crystallised intelligence were estimated using four tests (Wechsler et al. 1999), combined into composite scores (performance IQ, and verbal IQ) and

Table 3.2: Subject IQ scores (WASI) and age

| Data | Mean±SD | Min – Max | Population mean±SD |
|---|---|---|---|
| Age, years | 43±21 | 18 – 85 | – |
| Full Scale IQ (FSIQ) | 111±14 | 74 – 138 | 100±15 |
| ⌊— Performance IQ (PIQ) | 109±15 | 62 – 143 | 100±15 |
| ⌊— Block Design (BD) | 55±10 | 29 – 72 | 50±10 |
| ⌊— Matrix Reasoning (MAT) | 56±10 | 20 – 78 | 50±10 |
| ⌊— Verbal IQ (VIQ) | 110±12 | 67 – 135 | 100±15 |
| ⌊— Similarities (SIM) | 56±8 | 22 – 69 | 50±10 |
| ⌊— Vocabulary (VOC) | 55±9 | 31 – 75 | 50±10 |

*Note.* WASI scores are age-adjusted.

a final overall score (full scale IQ). Approaches to measuring intelligence often rely on the individual performing a battery of tests, with each test probing a subset of intellectual abilities. By performing these tests, the aim is to link individual differences in test scores with individual differences in intelligence, whilst being aware of the shortcomings associated with each test (Ackerman and Hambrick 2020). It is important to emphasise that these tests only approximate a subset of the full range of intellectual ability, with no single test providing a perfect assessment of fluid or crystallised abilities (Gignac 2015); the definition of intelligence used for this dataset refers to the ability to identify and extrapolate patterns by using non-verbal reasoning and planning — undertaken by the fluid component of intelligence — as well as the ability to recall facts and to place objects within abstract object classes — handled by crystallised intelligence.

### 3.7.1 IQ scores

For this sample, the Wechsler Abbreviated Scale of Intelligence (WASI-II, simplified here as 'WASI') battery of tests was used to assess intelligence (Wechsler et al. 1999), and serves as an abbreviated version of the more comprehensive Wechsler Adult Intelligence Scale (WAIS) (Wechsler 2008). WASI includes four 'subtests', assessing both fluid and crystallised intelligence. Block design (BD) and matrix reasoning (MAT) assess fluid intelligence, while similarities (SIM) and vocabulary (VOC) subtests probe crystallised intelligence.

Block design, a measure of fluid intelligence, involves physically arranging blocks on a table to match a predefined pattern in as little time as possible, testing visual perception,

visual-motor coordination and problem solving. Performance in block design — an assessment devised by Kohs (1920) in the early twentieth century — is superior among autistic individuals, thought to be caused by an improved ability to segment a whole (the block pattern) into its constituent parts (E. L. Hill et al. 2003; Shah et al. 1993). Alongside visual-motor coordination, this ability to decompose a gestalt — something that when experienced as a whole, has qualities which are more than the sum of its parts (Wertheimer 1938) — appears to be a central component for performance for BD, and may correspond to a measurement of local processing capacity (Stewart et al. 2009).

Additionally measuring fluid intelligence, matrix reasoning requires selecting — from five options — a single item that best fits a pattern, and measures inductive reasoning (see Richard J. Haier 2016, pp. 15–16 for a typical matrix reasoning problem). Modelled on the Raven's Standard Progressive Matrices (Carpenter et al. 1990) — a test which may be regarded as the most general single assessment of intelligence (Neisser 1998) — MAT was added to the WAIS and WASI battery of tests to enhance the assessment of non-verbal fluid reasoning (Wechsler 1997, p. 6). Inductive reasoning, traditionally seen as the most important component of intellectual ability (Spearman 1923, p. 295), refers to the ability to build conclusions based on an open-ended mixture of information presented in, and inferred from, the premises, an ability which is distinct from deductive reasoning which leads to definitive conclusions from information found in the premises alone (Johnson-Laird 1999).

To measure crystallised intelligence, WASI includes two verbal tests that assess the structure of semantic memory (facts and concepts which have been stored in memory). The similarities test involves asking the examinee to pair together matching pictures, and to explain how two words or concepts are alike, assessing abstract reasoning skills. The vocabulary test asks the examinee to define words and provide names of items presented in pictures, assessing range of vocabulary and verbal skills. Derivations of these tests have been used to assess memory degradation in cases of traumatic brain injury (Spencer et al. 2016), and stronger connectivity has been linked to brain regions associated with language processing for subjects with greater vocabulary skills (N. R. Lee et al. 2014).

In the WASI framework, these four subtests (BD, MAT, SIM and VOC) use age-adjusted $T$-scores with a population mean of 50 and a standard deviation of 10. The results of the subtests are used to calculate the three composite scores: BD and MAT

combine to form a perceptual reasoning score (performance IQ, or PIQ) approximating fluid intelligence; SIM and VOC combine to form a verbal comprehension score (verbal IQ, or VIQ) approximating crystallised intelligence; and all four subtests combine to form a full IQ score (FSIQ) estimating general intelligence. Here we use FSIQ-4 (abbreviated to FSIQ) in contrast to the FSIQ-2 score which is calculated from MAT and VOC alone. In the WASI framework, composite scores (PIQ, VIQ, FSIQ) have a population mean of 100 and a standard deviation of 15. Across all measures, higher scores indicate greater levels of intelligence. The scores for our sample are displayed in Table 3.2. The intelligence scores used in this thesis consists of the age-adjusted $T$-scores for the four subtests, and the corresponding composite scores calculated from these subtests. It is important to emphasise that the collection of tests used here are partial estimations of intelligence, and as with any test, do not represent perfect measures of fluid and non-fluid skills. Taken together, however, they do provide a more comprehensive assessment when compared with studies that focus on one particular test only, or in the case where only MAT and VOC are used (for the FSIQ-2 version).

Using this data, we compare spatial and topological features of the structural connectome of the subjects with their scores from the aforementioned intelligence tests. We make the assumption that intelligence has a structural correlate in the brain, driven by findings between intelligence scores and connectome differences observed in previous studies (Garrett et al. 2011; Thatcher et al. 2008), including suggestions of differences in the length of paths between regions (van den Heuvel, Stam, et al. 2009). Moreover, observations of functional changes across the spectrum of intellectual ability (Colom et al. 2009; Rex E Jung et al. 2007), combined with the observed correlation between structural and functional connectivity (Honey et al. 2007), strongly suggests a structural correlate for intelligence, and cognition more generally (Heinrichs 2005). Furthermore, lesion studies suggest that distributed regions across parietal and frontal cortices contribute towards general intelligence (Gläscher et al. 2010). Because of the spatially distributed significant correlations between region activation and IQ scores (Colom et al. 2009), and the varied range of skills that intelligence is often defined against (Braaten et al. 2006; Neisser 1979), it is likely that structural correlates of IQ are spatially distributed throughout the brain; much in the same way that the concept of a single 'seat of consciousness' existing within the brain is unlikely to exist (Baars 2005; Tononi 2005) — although some neuroscientists such as Crick and Koch (2005) suggest that the claustrum could function as such — in-

telligence too is unlikely to be mediated by a single region. In this study, we examine the spatial and topological characteristics of the connectome in an attempt to understand the neural correlates of intelligence.

### 3.7.2 Connectome wiring angles

Information moves throughout the brain between regions which are positioned in three dimensional space. The way in which regions project their connections to other regions in the network affects information transmission throughout the connectome. While our data does not include directed connectivity (adjacency matrices are undirected), it is possible to infer this level of information distribution by measuring the angles between connections. Wide angles could imply a greater capacity for regions to concurrently broadcast information to, and integrate information from, spatially distributed areas of the brain (Baars 2007). Despite the connections being approximated by straight lines, the angles capture the distances between connection end–points, rather than the physical trajectory of fibre tracts. Here, the wiring angles of connections offers another perspective on information flow throughout the network. We test the hypothesis that angles differ alongside brain processes that rely on inter-region communication, specifically, intelligence (Rex E Jung et al. 2007; Vakhtin et al. 2014).

Calculated wiring angles takes place between pairs of edges connected to the same region, calculating the cosine of the angle between two edges (Figure 3.7). In this case, connections are treated as straight edges between regions. By calculating the angles between region connections, we can assess the capacity of the network to integrate information between spatially distributed regions; regions that are positioned further apart, both connected to the same node, may support integration across distant regions of the brain. The angle $\theta$, between two vectors (connections), $A$ and $B$, is defined as:

$$\theta_{AB} = \cos^{-1}\left(\frac{A \cdot B}{\parallel A \parallel \parallel B \parallel}\right) \tag{3.3}$$

with $\theta_{AB}$=0 when $A$ and $B$ are parallel, and $\theta_{AB}$=180°when the pair of vectors 'leave' the region in opposite directions (again, connectivity is undirected so the true movement of signals is unknown). For a single subject, we define the wiring angle as the mean across all regions of the mean angles between all pairs of edges connected to a

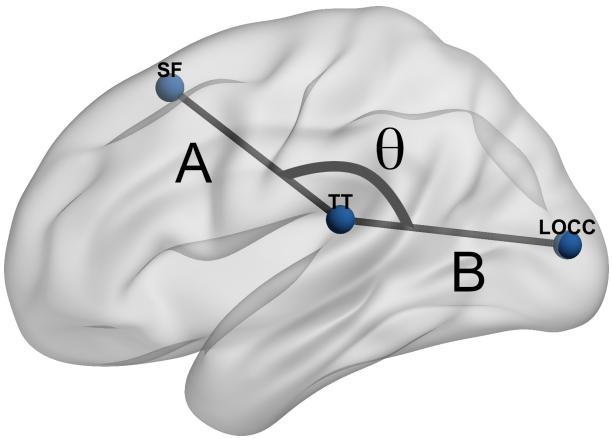


Figure 3.7: Visual representation of wiring angles between connections in the brain. Angles correspond to those between connections, such as that formed between the superiorfrontal (SF) / lateral occipital (LOCC) and the transverse temporal (TT) regions (connections A and B). In addition to the angle between A and B, the mean wiring angle associated with region TT consists of the mean angle between all combinations of pairs of connections connected to region TT.

region.

### 3.7.3 Rentian exponent calculation

For our analysis of the connectomes, we calculated the Rentian exponent for each subject, and correlated these with IQ scores to assess whether the spatial complexity of connectomes differed alongside intellectual ability. Connectomes consisting of straight edges between regions are used to calculate the Rentian exponent, using code in the Brain Connectivity Toolbox (Rubinov and Sporns 2010). To determine whether a network exhibits Rentian scaling, boxes of random sizes are placed at random locations over the network. The number of nodes within a box, and the number of edges crossing the boundary of a box are counted for each box. Rentian scaling is the tendency for these two quantities (number of nodes $n$ and number of edges $e$) to follow a linear relationship in log-space. A Rentian exponent can be approximated by fitting a linear model to these quantities in log-space (robust multilinear regression in MATLAB is used). Coinciding with other studies (Sperry et al. 2016), 5000 boxes are generated for each connectome. To avoid boundary effects (where boxes straddle the edge of the connectome envelope), only boxes containing 1 to $x - 1$ nodes for each network are used in the calculation, where $x$ is the minimum number of nodes for which fewer than 50 boxes (less than 1% of the total number of boxes) containing $x$ nodes were found (this restricts the number of nodes in boxes to at most ten nodes for most subjects in the NKI dataset).

# Chapter 4. Results

In this chapter, we provide the results from a spatial analysis of the connectomes across the various previously mentioned datasets. We attempt to understand the constraints placed on connectome structure, applying simulated annealing to rearrange brain regions, comparing changes in total connectome connection length before and after rearrangement. Moreover, we explore the influence of the spatial layout of the connectome on neuronal dynamics by comparing phase synchronisation across regions before and after rearrangement. Regarding the disorders of cognition, we provide a novel analysis into spatial differences between healthy connectomes and those diagnosed with schizophrenia, again relying on our simulated annealing algorithm. Finally, we investigate the structural correlates of fluid and crystallised ability, using spatial and topological analyses of the human connectome.

## 4.1 Assessing the Spatial Layout of the Macaque Connectome

The first dataset consists of four macaque monkeys, for which we have the structural and functional data between 184 regions covering cortical and subcortical areas. In these results, we list the outcome from applying the spatial rearrangement algorithm to determine the extent to which component placement optimisation (CPO) occurs in the macaque connectome. Using a computational model of neural communication, relying on differences in phase influencing communication (Fries 2015), we also explore the influence that the spatial arrangement of regions has on functional dynamics in the macaque brain.

### 4.1.1 Comparing connectome structure with the CoCoMac data

We first computed several network properties of the connectomes, displayed in Table 4.1. Our four subjects had similar characteristic path lengths and clustering coefficients to that of the CoCoMac data. The mean wiring length and the total wiring length were lower in the tract-tracing aggregated CoCoMac data compared with the four individual DWI

Table 4.1: Connectome properties for the macaque subjects

| Subject | # of regions | TW (mm) | Mean wiring length (mm) | L (mm) (metric) | L (binary) | C | Edge density |
|---|---|---|---|---|---|---|---|
| AL | 184 | 229310 | 24.2 | 36.15 | 1.8 | 0.719 | 0.281 |
| DP | 184 | 204170 | 24.5 | 36.13 | 1.8 | 0.7 | 0.247 |
| FL | 184 | 247490 | 25.0 | 34.9 | 1.7 | 0.711 | 0.294 |
| VL | 184 | 256770 | 26.1 | 36.31 | 1.7 | 0.691 | 0.292 |
| CoCoMac | 95 | 50455 | 21.0 | 35.0 | 1.9 | 0.643 | 0.269 |

*Note.* TW = total wiring length (Euclidean). L (metric/binary) is the metric/binary version of the characteristic path length; the metric form uses the Euclidean distance of connections along paths. C is the binary clustering coefficient. Properties for the CoCoMac data were obtained from (Kaiser and Hilgetag 2006).

connectomes, while the edge density of the CoCoMac connectomes remained comparable to the mean edge density of the four macaque subjects (0.279±0.02).

### 4.1.2 Assessing component placement of connectome regions

Upon running the simulated annealing algorithm (Algorithm 1), swapping the spatial positions of regions, we were able to reduce the total wiring length for all four subjects, with a mean reduction of 15±1% SD (Figure 4.1A). A greater reduction was previously reported for the CoCoMac data, with a wiring length reduction of 32% (Kaiser and Hilgetag 2006). Differences in the number of regions likely contributed to this difference in percentage reduction, with the CoCoMac data consisting of fewer cortical areas. As was highlighted in our spatial analysis of random networks (Figure 3.4 in Chapter 2), reducing the number of regions can affect the reduction in wiring length following rearrangement.

While searching for a reduced wiring length would be the best-case scenario of saving wiring, we also looked at the worst-case scenario of increasing the total wiring length as much as possible (Kaiser and Hilgetag 2006). Using these 'maximum' networks, we can calculate the relative total wiring length of the original network where a value of zero would represent the best-case (minimal wiring length) and a value of one would represent the worst-case (maximal wiring length). In the case where the wiring length of the connectome is closer to that of the minimised arrangement, this implies that the spatial placement of components in the original connectome is better suited to reduce the total wiring length. Using this approach, we can normalise the wiring length of the original connectome, allowing us to assess spatial optimisation across the different subjects, each

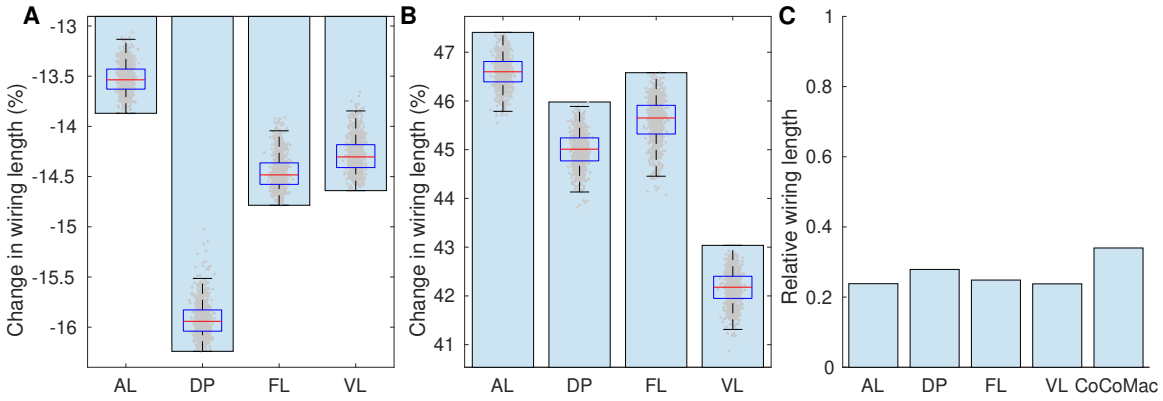


Figure 4.1: The change in wiring length following **A:** minimisation and **B:** maximisation of the total wiring length for the macaque subjects (bars correspond to the greatest change over 1000 repetitions, the distributions of which are displayed as box-plots). Significant differences in the median of the repetitions existed between all pairs of subjects (Mann-Whitney U, P<0.001). **C:** The relative wiring length of each connectome, calculated as the total wiring length of the original spatial arrangement relative to the minimum and maximum total wiring length obtained by rearrangement (mean 0.25±0.02). Also shown is the relative wiring length of the macaque from the CoCoMac data (0.34), presented in (Kaiser and Hilgetag 2006).

with their own topology. Using the same simulated annealing approach as was used for finding the minimum wiring length arrangements, we altered Algorithm 1 to converge on longer wiring lengths, resulting in a mean increase in total wiring length of 46±2% over the four subjects (Figure 4.1B). By comparing the minimum and maximum possible wiring length, we found that the originally arranged connectomes had a wiring length which was closer to the minimum possible wiring length, with a mean relative wiring length of 0.25±0.02 (Figure 4.1C). Our results coincide with the findings of the CoCoMac data, which also showed that the total wiring length can be reduced and that the original spatial arrangement resulted in a wiring length which was closer to the minimal length (with a CoCoMac relative wiring length of 0.34).

Each subject displayed similar variance when comparing the range of wiring length reductions over the 1000 repetitions (width of boxplots in Figures 4.1A and 4.1B). However, we observed differences in the extent to which the wiring length reduced following rearrangement between subjects — significant differences in the median of the repetitions existed between all pairs of subjects for both minimisation and maximisation (Mann-Whitney U, P<0.001). Subject DP displayed the greatest percentage reduction (-16.2%), and also the greatest relative wiring length out of the four subjects (0.28), implying that the original component placement was the most sub-optimal for DP. The original com-

ponent placement for subject AL on the other hand was closest to optimal out of the four subjects (-13.9%), showing the least percentage reduction in wiring length following rearrangement and a low relative wiring length (0.24). A likely cause for the variance are the differing edge densities across the subjects. Edge density is lowest for DP (0.247), showing the greatest difference from the mean edge density (0.279±0.02) across the four subjects. In random networks positioned in a circular arrangement, a reduced edge density contributed to a greater percentage reduction in wiring length, demonstrated earlier in Figure 3.4 (Chapter 2); edges acts as constraints on the search algorithm, with fewer edges likely increasing the number of degrees of freedom within the swapping procedure. Perhaps more interestingly, subject AL displayed the least reduction in wiring length, but did not have the greatest edge density in the sample (both FL and VL had more edges). AL did however display a lower initial total wiring length and mean wiring length compared to FL and VL, which may have influenced its component placement that is closer to optimal, with fewer long-distance connections to shorten.

Another interesting observation is that the maximal arrangement for subject DP was regarded by MATLAB an outlier amongst the distribution of maximised wiring lengths. In this case, outliers are values with a distance greater than 1.5 × IQR from the $25^{th}$ or the $75^{th}$ percentile of the distribution of wiring length changes across the rearrangement repetitions. This observation emphasises the importance of repeating the search many times for the same subject in order to find optimal solutions, as the simulated annealing algorithm moves between local minima. It is of course computationally intractable to confirm whether this outlier is the global minimum (or one of several minima with equivalent wiring length) over the entire search space of possible spatial arrangements. Nonetheless, this highlights the difficulty of traversing the search space, often faced by search algorithms.

The reduction in total wiring length was made possible by reducing the number of long-range connections in the minimised arrangements (Figure 4.2). Most regions (63%) experienced a decrease in their wiring lengths following minimisation of the total wiring length (Figure 4.3). In particular, in the original connectome, connections from the visual areas could be reduced the most, with changes in wiring length being broadly consistent across hemispheres for this limited sample size. For the following distances, values are normalised against the maximum distance between any pair of regions in the inter-

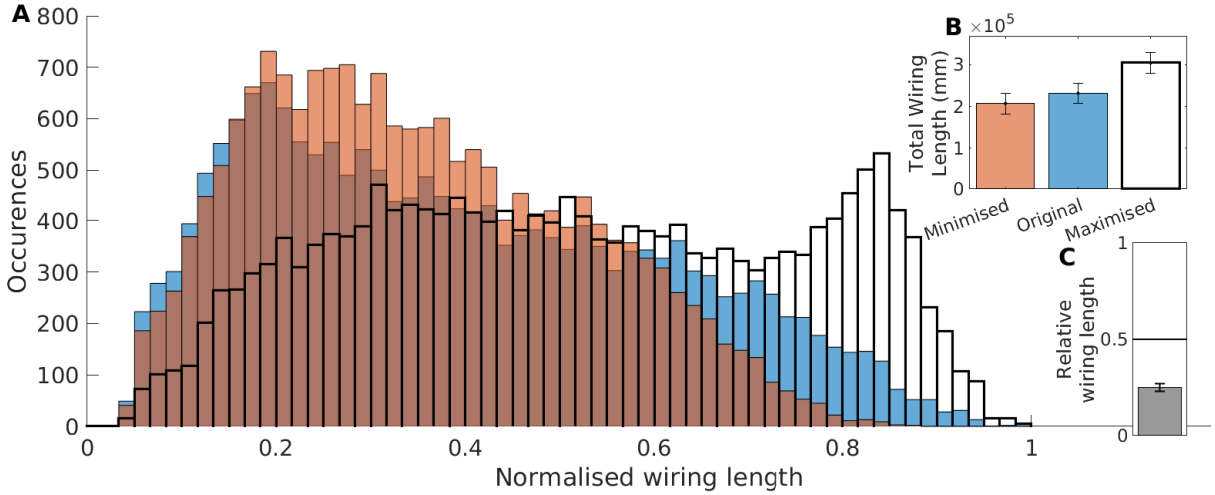


Figure 4.2: Wiring length changes across spatial arrangements. **A:** For all four subjects: distribution of wiring lengths, for original (blue), minimised (orange) and maximised (transparent/bold) networks following spatial arrangement. Compared with the original arrangements, fewer long-distance connections existed in the minimised arrangements. Whereas, many more long-distance connections were generated in the maximised arrangements. **B:** The mean total wiring length across all four networks for spatial arrangements which minimised (orange), and maximised (transparent/bold) the total wiring length, alongside the wiring length of the original arrangement (blue). **C:** The mean relative wiring length, across of all four networks (0.25±0.02). Error bars are ±1 SD.

hemispheric corrected connectomes (equal to one). Several regions in the visual cortex experienced substantial reductions in the lengths of their connections, in particular V2 (-22±1.8) and V1 (-20±2.9). In the prefrontal lobe, connection lengths for region 9m (dorso-medial prefrontal area) also greatly reduced (-16±4.3). Connections from auditory, subcortical and motor lobes displayed minimal change in the lengths of their connections following rearrangement; several regions increased the length of their connections in the minimised arrangements (37%), including regions PM (medial pulvinar — subcortical — increased by 3.6±3.0), 23a (area 23a in posterior cingulate cortex — prefrontal lobe — increased by 1.8±2.1) and MDpc (mediodorsal nucleus, parvicellular division — subcortical — increased by 2.6±1.4). Region PM, part of the thalamus, showed the greatest mean increase in wiring length following minimisation. The insula cortices also experienced an increase in wiring length following rearrangement, with Ri (retroinsula, auditory lobe) and PI (parainsular area, subcortical) increasing by 2.0±2.4 and 2.4±0.9, respectively.

For an example subject (subject FL), the original and the spatial arrangement minimising the total wiring length are shown in Figure 4.4. Connectomes before and after arrangement for the other subjects (AL, DP and VL) can been seen in Figures A.1, A.2, A.3.

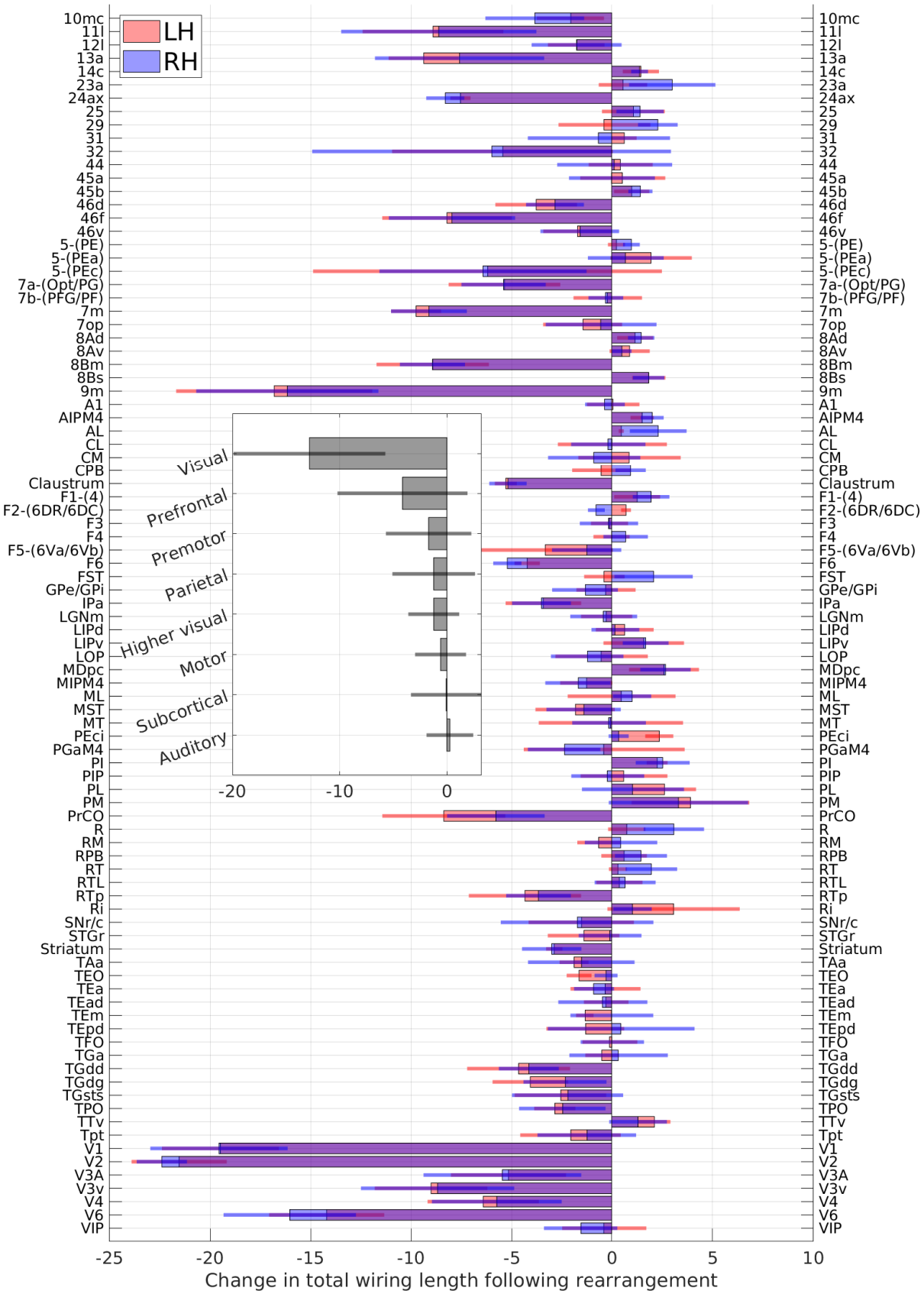


Figure 4.3: For all four subjects: the change in wiring length for each region following minimisation of the total wiring length of the network. Wiring lengths are normalised against the maximum distance between regions in the connectome (equal to one). **Inset:** The mean change in total wiring length, per functional area. Most regions, especially visual areas, experienced a decrease in wiring length following minimisation. Error bars are ±1 SD. See Tables A.1 and A.2 for the full region names and lobe mappings (Saleem et al. 2012).

Generally, across subjects, connectivity between anterior and posterior spatial positions, as well as inter-hemispheric connections connecting bilateral anterior and posterior regions, decreased in quantity in the minimised arrangement (as shown in white in the adjacency matrices in Figure 4.4A). Regions with many inter-hemispheric connections moved closer to the centre of mass (COM) of the network (4.4B), constrained by the routing of connections through the COM (as explained previously, connections between hemisphere are lengthened to mimic the spatial constraints of the corpus callosum). For subjects AL and FL, when comparing the connectomes before and after rearrangement, originally-positioned anterior regions often remained within the anterior part of the connectome (Figure 4.4B/C). A similar effect was observed for the posterior regions, remaining in place towards the posterior end of the brain.

To assess which connections were most affected by repositioning the regions, we identified the connections which were no longer present between spatial positions after rearrangement. For the 30 spatial locations with the greatest reduction in wiring length, missing connections existed between anterior and posterior regions, particularly between the occipital lobe and prefrontal areas (Figure 4.5). When considering all regions, connections from the spatial location V4 (visual region) in both hemispheres showed the greatest number of missing connections following rearrangement; many such missing connections were linked to visual areas. When examining the rate of disappearance of connections which were only present in all four subjects, and comparing the disappearance of connections within and between hemispheres, 41±33% of intra-hemispheric connections and 62±35% of inter-hemispheric connections were no longer present in the rearranged connectomes — rearranged connectomes caused a greater percentage of connections between hemispheres to disappear, implying that such connections contribute towards the sub-optimal placement of brain components.

We next assessed whether changes in region wiring length between arrangements were influenced by the initial wiring length of a region's connections, and its original positioning in the connectome. We found that regions which had a greater initial wiring length, and which were further from the COM of the network displayed greater reductions in wiring length following rearrangement (Figure 4.6). While for most functional areas a significant relationship existed between total initial wiring length and the reduction in wiring length, the results were more mixed for the distance from the COM — regions in the premotor

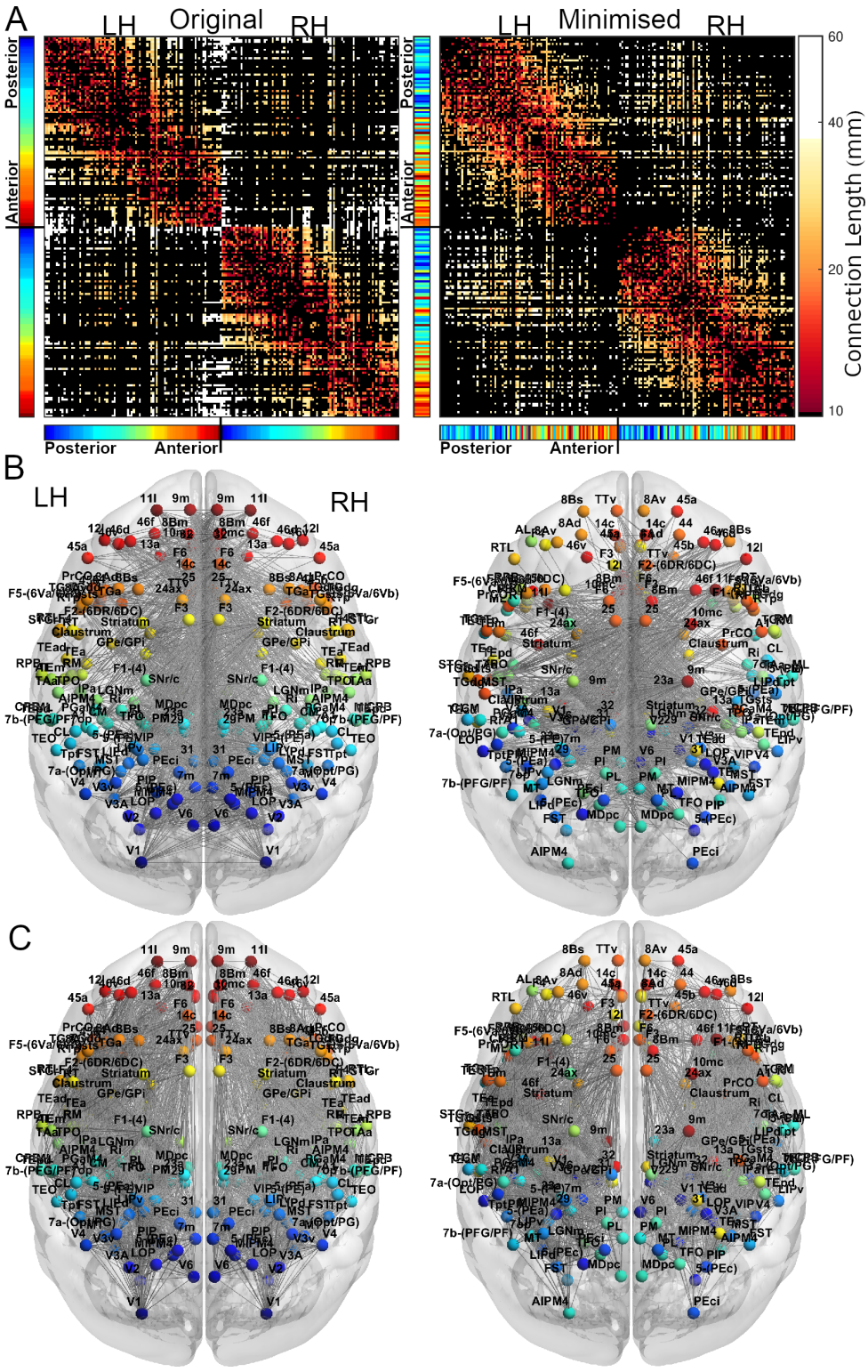


Figure 4.4: For subject FL: Changes in connectome structure before and after rearrangement. **A:** Example adjacency matrices showing the connections between spatial locations for original and minimised spatial arrangements. Regions are coloured based on their anterior-posterior position in the original arrangement, displayed in the colour bars next to the adjacency matrices (red = anterior, blue = posterior). The topology of the connectome is preserved in both arrangements, but the positions of regions often differ. White connections in the adjacency matrices are those with lengths greater than 80% of connections in the original arrangement. **B/C:** Connections between hemispheres for connectomes, for the original arrangement **(left)** and the arrangement that minimises the total wiring length of the network **(right)**. For additional clarity, connectome connections are displayed separately for between and within hemispheres.

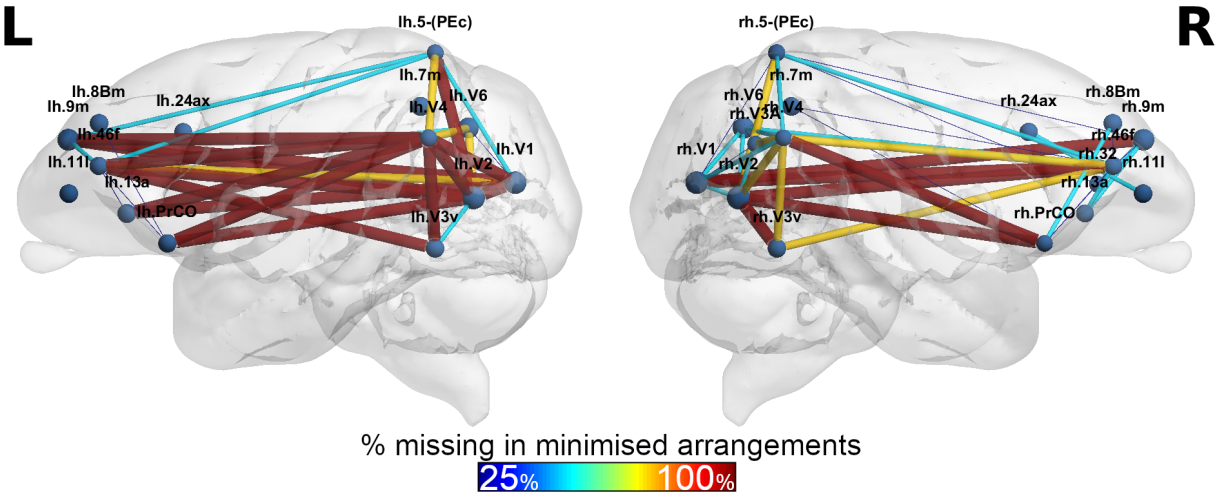


Figure 4.5: Lateral view of the macaque brain, showing the connections which were no longer present in the minimised arrangements. Shown are the missing connections for the spatial locations of the 30 regions showing the greatest reduction in wiring length in the minimised arrangements. Connections are coloured based on the rate of disappearance. 100% = connection disappeared between spatial locations for *all* subjects in the minimised arrangements. Connections between anterior and posterior spatial positions most frequently disappeared. **L/R**=Left/Right Hemisphere.

and prefrontal areas further from the COM experienced a greater change in wiring length.

### 4.1.3 Simulating functional differences between original and minimised spatial arrangements

We next tested the hypothesis that a spatially sub-optimal arrangement (one that does not minimise the total wiring length) benefits the global dynamics of the connectome. To answer the question of whether a sub-optimal spatial arrangement of regions maintains metastability, we used computational techniques to analyse the dynamics supported by the original and minimised spatial arrangements of regions. Similar to other approaches which simulating activity in the macaque connectome at a global level (e.g. K. Shen et al. 2019) we constructed a model of brain dynamics using a network of Kuramoto phase oscillators (Kuramoto 1975) to study specifically the spatial influence on dynamics. We measured synchronisation between regions as a means of quantifying communication, with elevated synchrony reflecting elevated levels of communication between regions (Fries 2015). Mean global synchronisation and metastability were calculated for the original spatial arrangements and those that minimise the total wiring length. An example output of the simulation is displayed in Figure 4.7.

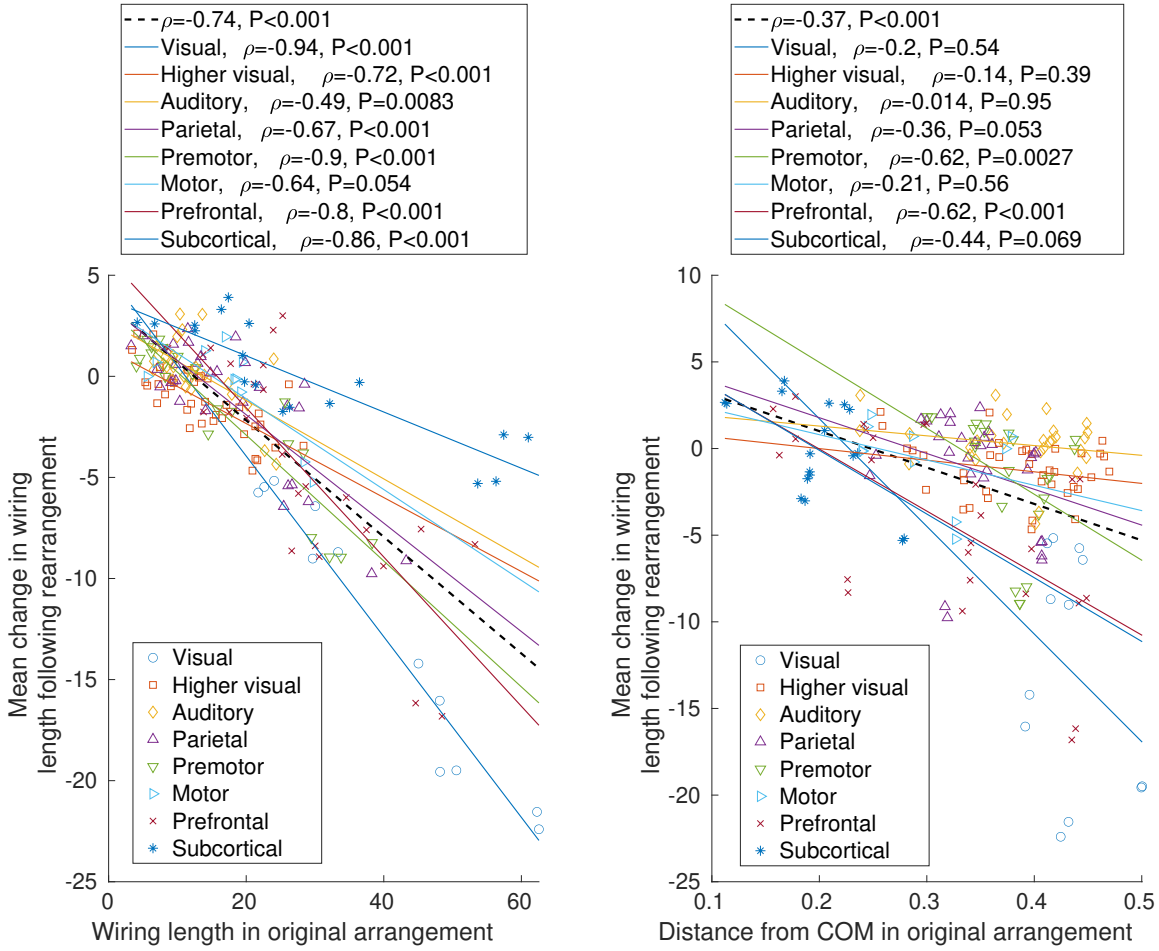


Figure 4.6: The change in region wiring length between original and minimised arrangements correlated with wiring length in the original arrangement, and the distance from the centre of mass of the network. Generally, regions with longer connections and those situated further from the COM in the original arrangements displayed greater reductions in the minimised arrangements. The dashed lines represent the correlation over all regions ($\rho$ = Spearman rank correlation).

The two parameters (coupling strength K and the conduction velocity V) were chosen through a validation process comparing the activity of the model with that of empirical functional connectivity obtained from the BOLD signals for each monkey. A model which is validated against real world data helps ensure that the dynamics produced by the model reflect reality. Validation of the model involved computing the Spearman rank correlation coefficient between the upper right triangles of the simulated functional connectivity and the BOLD empirical functional connectivity matrices over a range of conduction velocities, V (0.5 to 15 m/s, in steps of 0.5) and coupling strengths, K (0.025 to 3 in steps of 0.025). The third parameter, the natural oscillation frequency of each oscillator, is set to a frequency in the gamma band range (defined as 30–80Hz). Specifically, we simulated the model at frequencies of 40Hz and 60Hz. See Figure A.4 for empirical matrices and the corresponding validated simulated functional connectivity matrices for both 40Hz and 60Hz. At 40Hz (60Hz) the maximum Spearman rank correlation coefficients between empirical and simulated correlation matrices were 0.11 (0.12), 0.17 (0.19), 0.29 (0.28) and 0.16 (0.14), for AL, DP, FL and VL, respectively. Empirically validated K and V values were 0.33±0.12 and 10±1.6m/s for 40Hz; and 0.43±0.06 and 11.9±0.7m/s for 60Hz.

Kuramoto model simulations were run for 90 seconds of biological time (ignoring activity in the first nine seconds of the simulation to allow the influence of the initial conditions to dissipate). We used Euler integration (Euler 1845) to obtain the time series of each oscillator, using a step size of 0.2 ms. The selected conduction velocity was applied equally to all connections. Binary adjacency matrices were used as connection weights, multiplied by the selected coupling strength.

Changes in the correlation between the empirical and simulated functional connectivity (FC) matrices, as well as the synchrony and metastability across over the parameter space, are shown in Figures 4.8, 4.9 and 4.10 for 40Hz, and in Figures A.5, A.6 and A.7 for 60Hz. At points of maximum correlation between empirical and simulated FC, subjects experienced metastability which was lower than the maximum metastability in the parameter space, generally showing stronger correlations for parameters producing higher mean synchrony. At 40Hz (60Hz), validated metastability for the four subjects were 0.07 (0.07), 0.11 (0.06), 0.02 (0.04) and 0.08 (0.06) — 29±16% (22±4%) of the maximum metastability in the parameter space. And for synchrony: 0.79 (0.72), 0.66 (0.59), 0.77 (0.58) and 0.78 (0.55) – 83±7% (72±8%) of the maximum synchrony in the

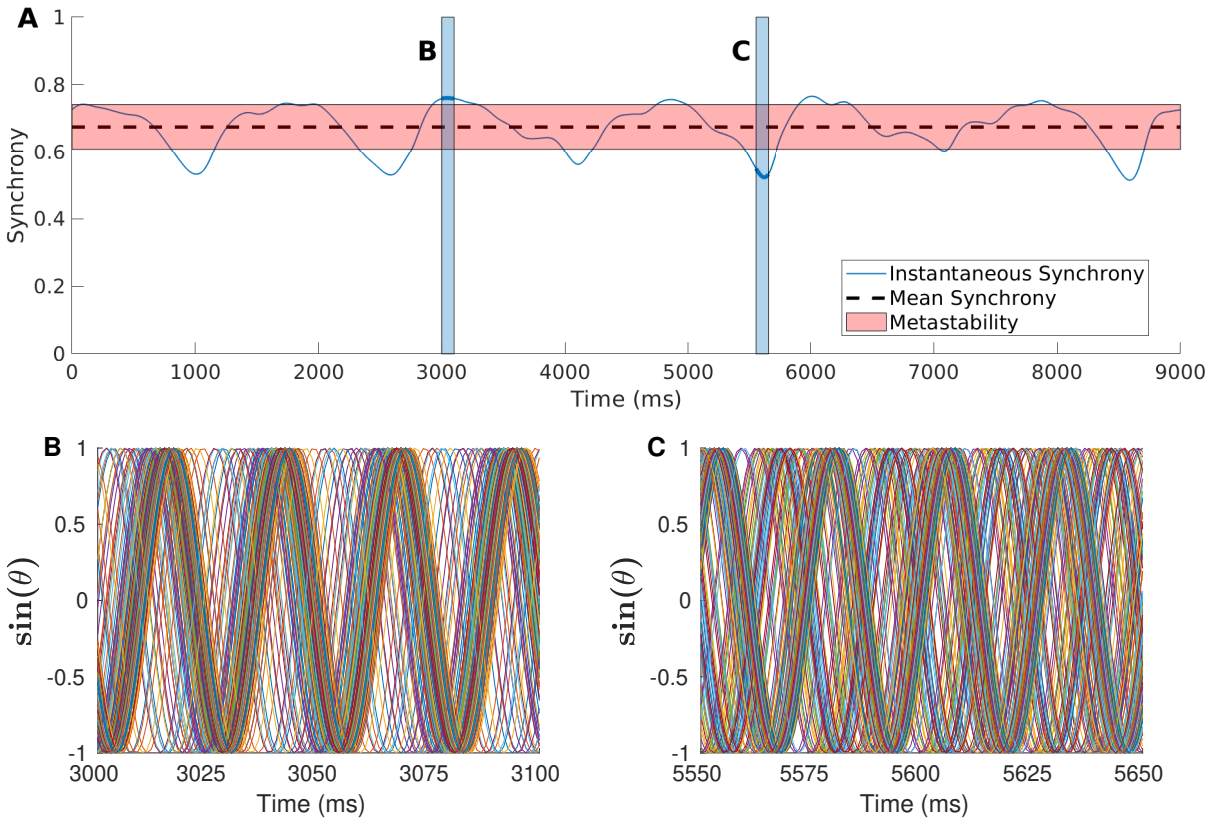


Figure 4.7: An example simulation showing the change in mean synchrony across all regions in the macaque connectome. **A:** For subject VL (using the empirically-derived conduction velocity and coupling strength of 10m/s and 0.33, respectively, with a default frequency of 40Hz), nine seconds of simulated activity showing the instantaneous synchronisation between regions (phase similarity at a point in time between all regions), the mean synchronisation (mean of the instantaneous synchronisation over all time points) and metastability (standard deviation of the instantaneous synchronisation, indicated by the height of the shaded red area — above and below the black dashed line). **B:** Sine of the angle, $\theta$, of all oscillators between t=3000ms and t=3100ms (highlighted on the top plot). Within this time window, synchrony is high, as seen by the similar phases between many of the regions. **C:** $\theta$ for a period of lower synchrony between regions, between t=5550ms and t=5650ms (also highlighted in the top plot).

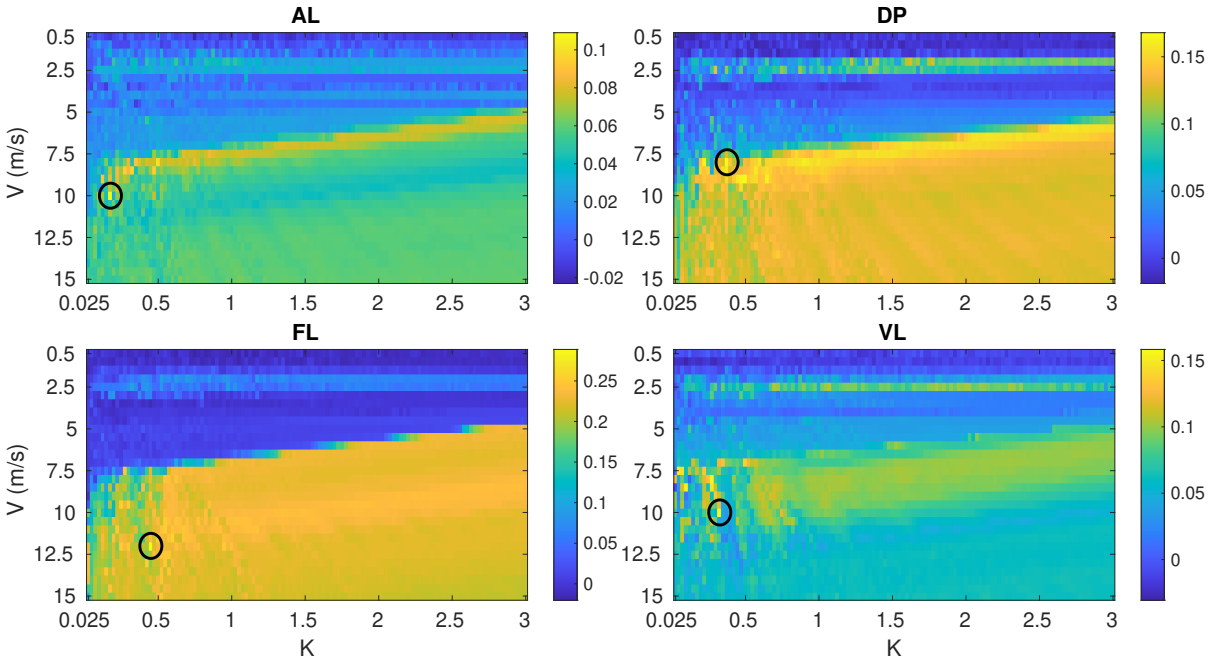


Figure 4.8: For 40Hz: For the four subjects (AL, DP, FL, VL), the Spearman rank correlation coefficients between the empirical and simulated functional connectivity matrices over the parameter space of coupling strengths (K) and conduction velocities (V). Circled is the pair of parameters which maximise the correlation with the empirical functional connectivity.

parameter space.

Having validated the models, we then compared synchrony and metastability in the original and minimised spatial arrangements, hypothesising that a spatial arrangement which reduces the wiring length decreases metastability in the brain. Parameter spaces differed between original and minimised arrangements; for minimised arrangements, peaks in metastability were found at lower values of K and V. Where synchrony began to substantially decrease in the original arrangements, synchrony remained high for minimised arrangements, beginning to reduce for smaller values of K and V. We used the same choice of K and V values to simulate activity in both the original and minimised spatial arrangements.

To allow us to compare the simulated metastability between original and minimised arrangements, for each subject we identified the free parameters (K and V) for the spatially minimised arrangement which minimised the difference in synchrony from that produced by the empirically-validated model of the original arrangement (a similar approach of matching synchrony between networks was used (Fukushima et al. 2020)). By closely matching synchrony between the arrangements, we evaluated the contribution of the

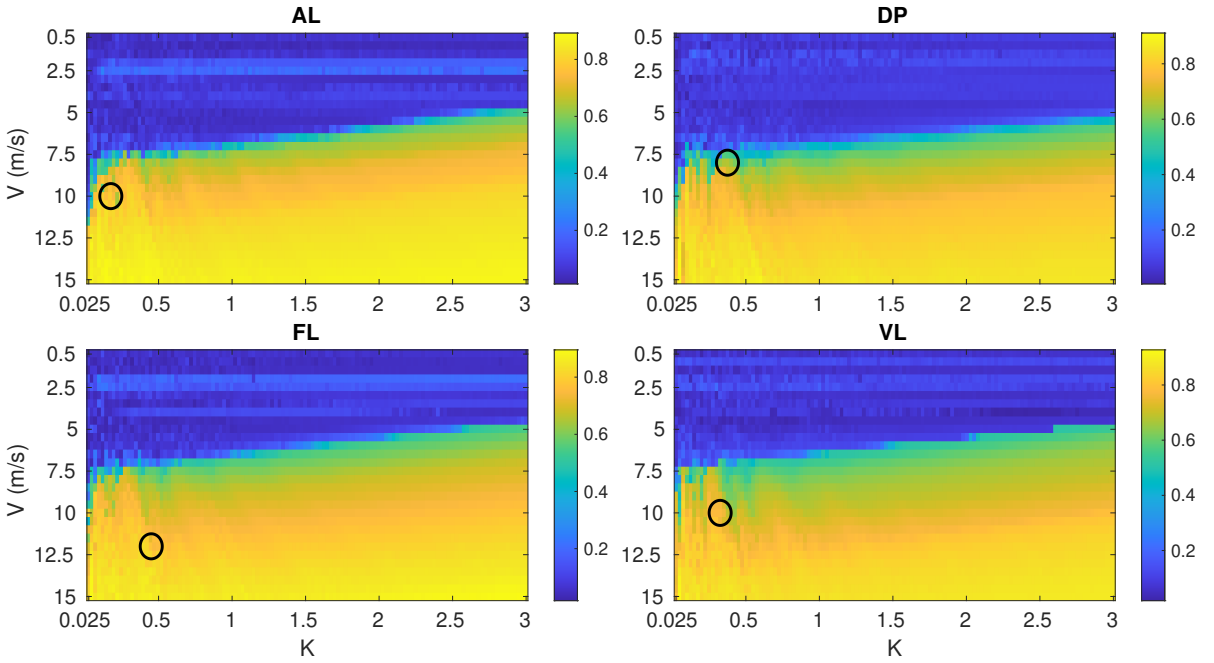


Figure 4.9: For 40Hz: For the four subjects (AL, DP, FL, VL), the mean global synchrony between regions from the simulated neural activity over the parameter space of coupling strengths (K) and conduction velocities (V). Circled is the pair of parameters which maximise the correlation with the empirical functional connectivity.

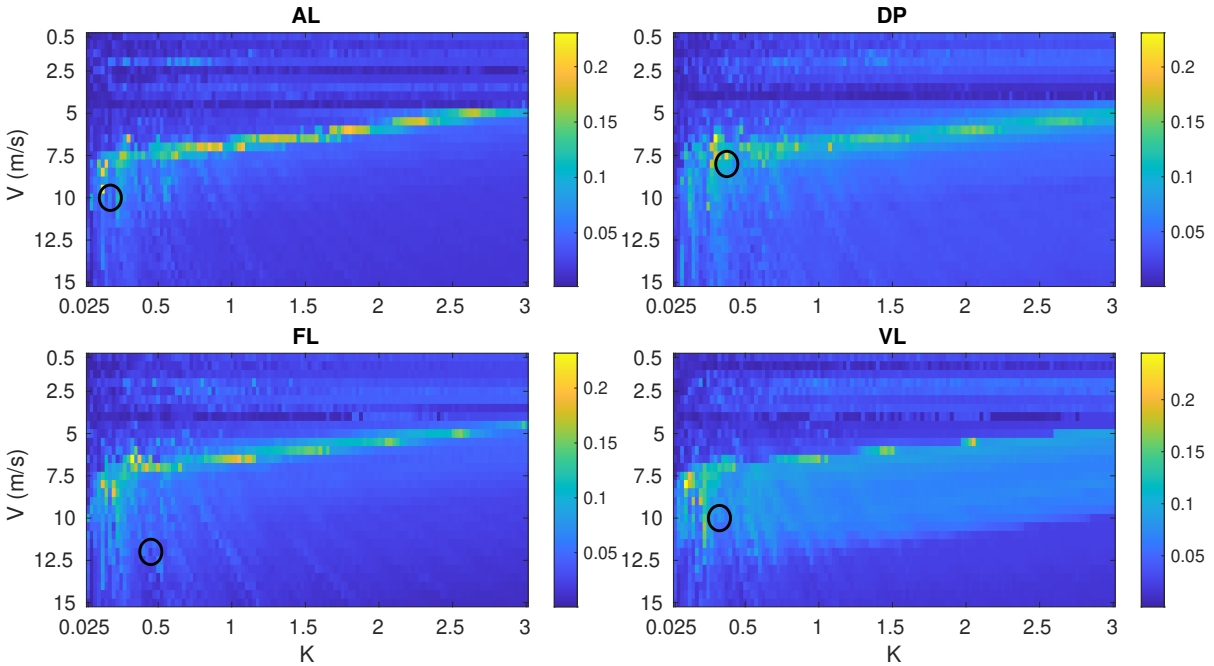


Figure 4.10: For 40Hz: For the four subjects (AL, DP, FL, VL), the metastability from the simulated neural activity over the parameter space of coupling strengths (K) and conduction velocities (V). Circled is the pair of parameters which maximise the correlation with the empirical functional connectivity.

spatial arrangement of the connectome to the dynamic fluctuations between segregation and integration (measured by metastability). By maintaining synchrony across the two spatial arrangements, we attempt to observe changes in dynamic fluctuations when the mechanisms which are thought to underpin communication were comparable (Fries 2015; von der Malsburg 1995). We conducted two separate searches over the conduction velocity and the coupling strength (each time fixing one of the empirically-validated parameters whilst changing the other). The resulting metastability for the minimised arrangement corresponded to the mean metastability produced by these two fixations, providing two pairs of parameters. Fixing one of the two parameters helped to constrain the parameter selection to those which are more biologically plausible, as informed by the empirical data.

Changes in metastability are displayed in Figure 4.11. At 40Hz, we observed a general decrease in metastability in the minimised arrangements. AL, DP and VL experienced a decrease in metastability in the minimised arrangements compared with the original. At 60Hz, three out of four subjects (DP, FL and VL) experienced an *increase* in metastability in the minimised arrangements. For both frequencies, similar levels of synchrony were observed between arrangements as expected, by our attempts to match synchrony between arrangements.

To see whether our method of matching the synchrony between arrangements influenced these changes in metastability, we matched synchrony by changing the coupling strength K and conduction velocity V *simultaneously* (i.e. without the aforementioned single dimension search across K and V separately). This involved a search for a similar level of synchrony across the entire parameter space, varying K and V together and allowing for uninhibited deviation from the empirically-validated parameters of the original arrangements. Compared with the more restrictive approach of matching synchrony, changes in metastability were largely consistent (Figure A.8): At 40Hz, the same three subjects experienced a decrease in metastability (AL, DP and VL). At 60Hz, except for subject DP (whose metastability instead decreased), all subjects experienced the same change in metastability following minimisation.

As a whole, across the two oscillation frequencies, we did not observe a consistent change in metastability between the original and minimised arrangements. Nonetheless, the effect of spatial arrangement on metastability requires further study, as the small sample size used here limits the possibility of finding conclusive results.

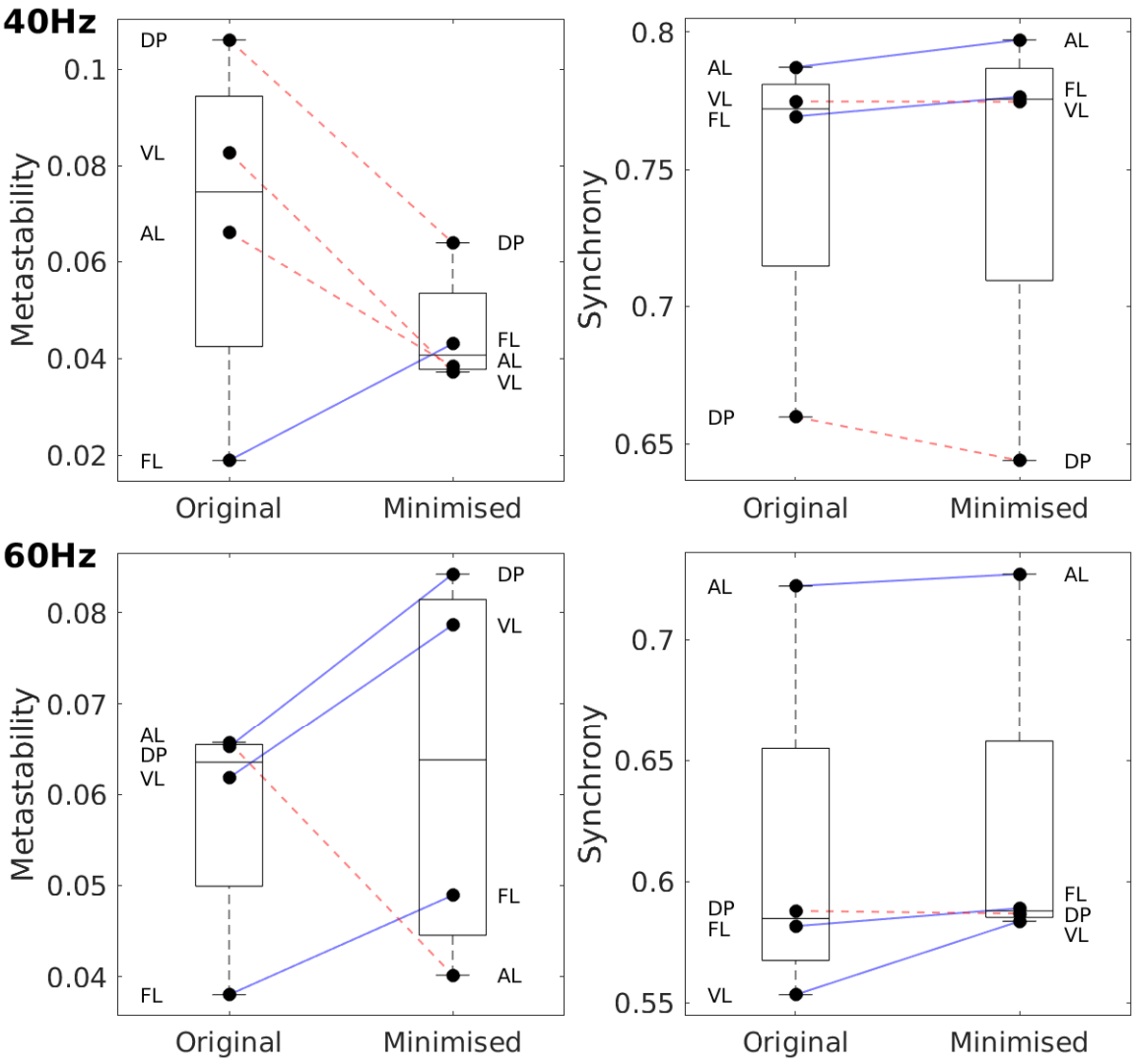


Figure 4.11: Changes in metastability and synchrony between original and minimised arrangements (subjects are labelled: AL, DP, FL, VL). Here we minimise the difference in synchrony between original and minimised arrangements. At 40Hz, three subjects (AL, DP, and VL) showed reductions in metastability in the minimised spatial arrangement (denoted by dashed red lines). At 60Hz, three subjects (DP, FL and VL) showed an *increase* in metastability in the minimised spatial arrangement (denoted by solid blue lines).

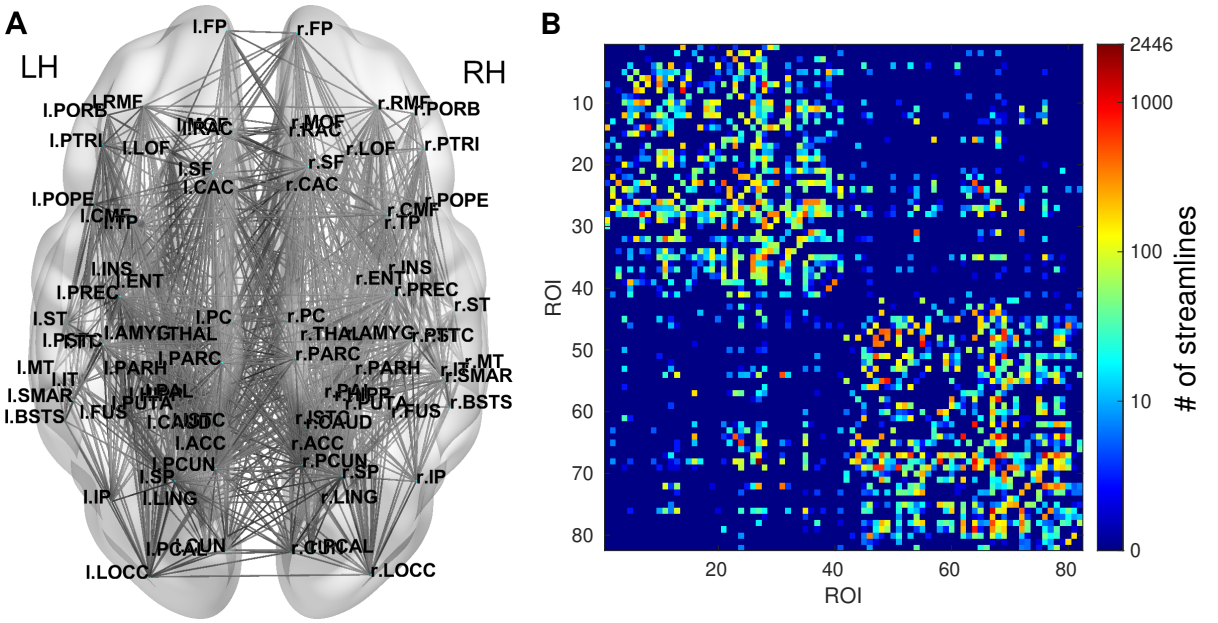


Figure 4.12: The connectome for an example human subject from the HCP data. **A:** Axial view of the connectivity between 82 regions. All connections are shown. LH/RH=Left/Right Hemisphere. See Table B.1 for the full region names. **B:** The corresponding adjacency matrix showing all connections and their number of streamlines, showing dense intra-hemispheric connectivity (regions 1–41 are in the left hemisphere, 42–82 are in the right).

## 4.2 Spatial Analysis of Healthy Subjects From the Human Connectome Project

We next assessed wiring length optimisation in the human connectome dataset (from the Human Connectome Project). This involved rearranging the spatial locations of brain regions and testing whether the total length of all connections — estimated by the Euclidean distance between connected regions in the connectome — changes during optimisation. As used previously in component placement optimisation (CPO) analysis (Kaiser and Hilgetag 2006), we used simulated annealing to identify spatial arrangements which were as close as possible to an optimal placement (Algorithm 1, Chapter 2). We also corrected the length of inter-hemispheric connections by lengthening such connections as if they had passed through the centre of the network (as was done for the previous macaque analysis). A comparison between connectomes with and without this correction, alongside the streamline lengths of the connections is shown in Figure 4.13; performing this correction reduced the error between the distribution of straight line lengths and the curved lengths of connections.

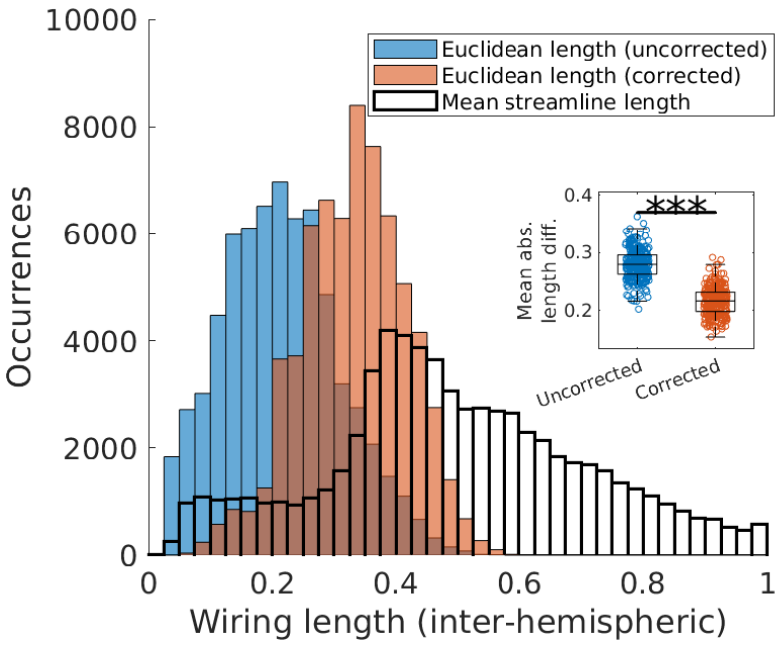


Figure 4.13: Wiring length distributions of inter-hemispheric connections, for the uncorrected, corrected and streamline distances, over all subjects (normalised by the longest streamline per subject). Inset: The absolute different in wiring length between the normalised mean streamline length and the Euclidean distance (mean over all inter- hemispheric connections per subject). Compared with the uncorrected Euclidean wiring length, the corrected Euclidean wiring length generally displays an improved overlap with the real connection length distribution.

### 4.2.1 Structural differences alongside age and sex

Before performing spatial optimisation, we first assessed differences in the original wiring between age groups and sex (Table 4.2). To compare differences in network features across sex and age groups, we conducted non-parametric permutation testing. We computed the selected network property for all subjects, followed by interchanging subjects between either sex or age groups based on a random permutation, preserving the original sizes of the groups. We then compared the mean difference between the original groups with that of one million permutations, and computed the proportion of permuted mean differences exceeding the original mean difference. We rejected the null hypothesis — a random sampling explains the differences in the two groups — at the 5% significance level if this ratio was less than 0.05 (two-sided $P$-value). Females had a greater edge density and a longer mean wiring length (normalised against the maximum Euclidean in each subject's network). Significant differences between age groups for edge density and mean wiring length were not observed.

Table 4.2: Connectome properties for age groups and sex

| | Age 22–25 (N=91) | Age 26–30 (N=189) | $P_{\text{age}}$ |
|---|---|---|---|
| Edge density | 0.308±0.021 | 0.304±0.02 | 0.104 |
| Mean wiring length (norm.) | 0.409±0.015 | 0.408±0.013 | 0.605 |
| Relative wiring length | 0.451±0.034 | 0.449±0.03 | 0.582 |
| | Males (N=142) | Females (N=138) | $P_{\text{sex}}$ |
| Edge density | **0.302±0.02** | **0.308±0.02** | **0.009** |
| Mean wiring length (norm.) | **0.406±0.013** | **0.411±0.014** | **0.002** |
| Relative wiring length | 0.443±0.033 | 0.456±0.029 | 0.46 |

*Note.* Network measures for both age groups and the corresponding $P$-value using a two-tailed permutation test (one million permutations). The mean wiring length is the mean Euclidean distance between all directly connected regions in each connectome, normalised against the maximum Euclidean distance between regions (equal to one). $P$-values for the relative wiring length are calculated after regressing out the differences in edge density between groups. Values are mean±SD.

### 4.2.2 Reduction in total wiring length by component rearrangement

We next used simulated annealing (Algorithm 1) to obtain the minimised spatial arrangements of the regions for all 280 human connectomes. Beginning with the original spatial arrangement of regions, this involved swapping the positions of regions so as to reduce the total wiring length of the connectome (calculated as the sum of the Euclidean distance between connected regions). We repeated the search 100 times for each subject, with the greatest reduction in wiring length used in the subsequent analysis. By swapping the spatial positions of regions, the simulated annealing algorithm was able to reduce the total wiring length of the connectome for all subjects, with a mean reduction in total wiring length of 21.6±1.4% SD (Figure 4.14A), i.e. the original arrangement was sub-optimal for all subjects. Compared against the distribution of wiring lengths in the original networks, these 'minimised' arrangements displayed fewer long-distance connections (Figure 4.14B).

As well as minimising the total wiring length, we also swapped the positions of regions to *maximise* the total wiring length, using the same approach as for the macaque data. This allowed us to determine the relative wiring lengths for each subject, where the wiring length of the spatial arrangement providing the minimum wiring length is used as the lower bound, and that of the maximum arrangement is set as the upper bound (Kaiser and Hilgetag 2006) (Figure 4.14C). The relative wiring length adopts a value between zero (the lower bound) and one (the upper bound). A relative wiring length of less than

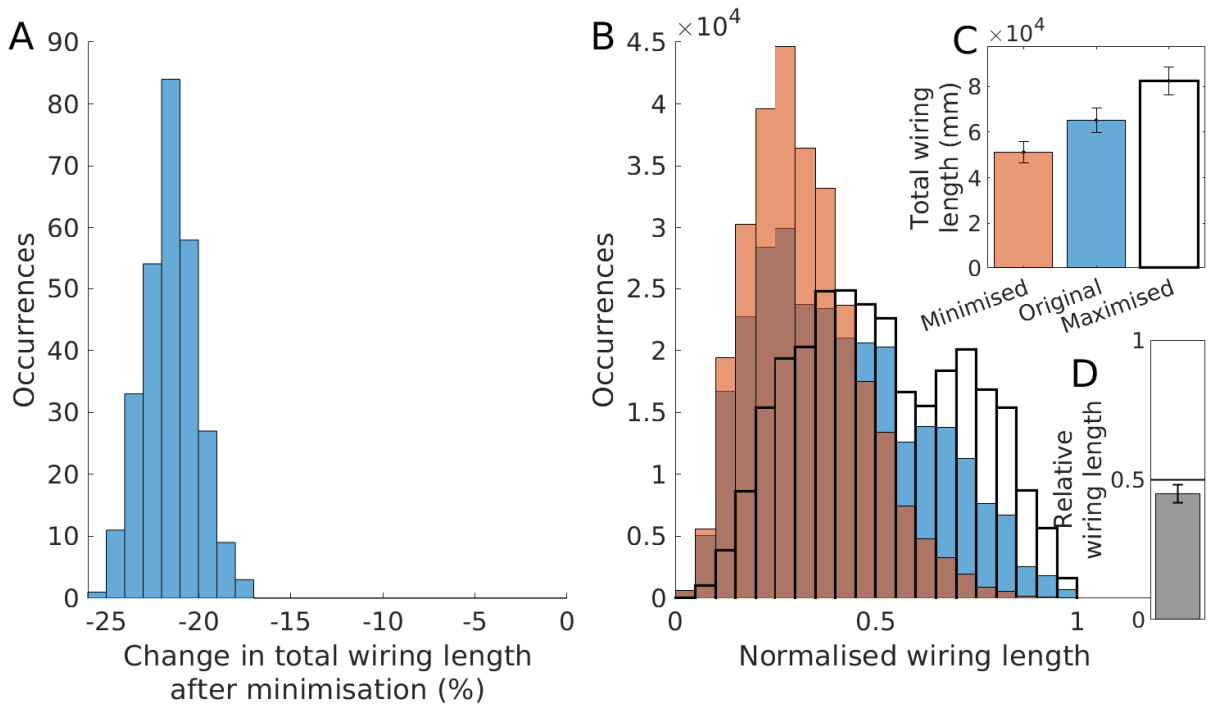


Figure 4.14: For the HCP dataset — changes in wiring length distributions for the original, minimised and maximised spatial arrangements. **A:** The percentage difference in wiring length between the original connectomes and the spatial arrangements which minimise the total wiring length (mean -21.6±1.4%). **B**: The distribution of wiring lengths for the original (orange), minimised (blue) and maximised (transparent, bold) spatial arrangements. **C:** The mean wiring lengths for the minimised, original and maximised arrangements. **D:** The mean relative wiring length across all subjects (0.45±0.03) — original lengths normalised against that of minimised and maximised arrangements (error bars = ±1 SD.).

0.5 indicates that the original spatial arrangement of regions is more suited to keeping the total wiring length low. Following maximisation, the absolute percentage change in wiring length for the spatially maximised arrangements was generally greater than that of the minimised arrangements, with 95% of subjects displaying a relative wiring length less than 0.5, giving a mean relative wiring length of 0.45±0.03; the original spatial arrangements of the connectomes supported a wiring length which was slightly closer to that of the minimised arrangements (Figure 4.14D).

Figure 4.15 shows the original and the minimised arrangements in anatomical space for an example subject, and how this leads to reductions in the length of connections. In particular, connections between anterior and posterior positions disappeared in the minimised arrangement.

We next assessed whether the relative wiring length differed according to age and sex.

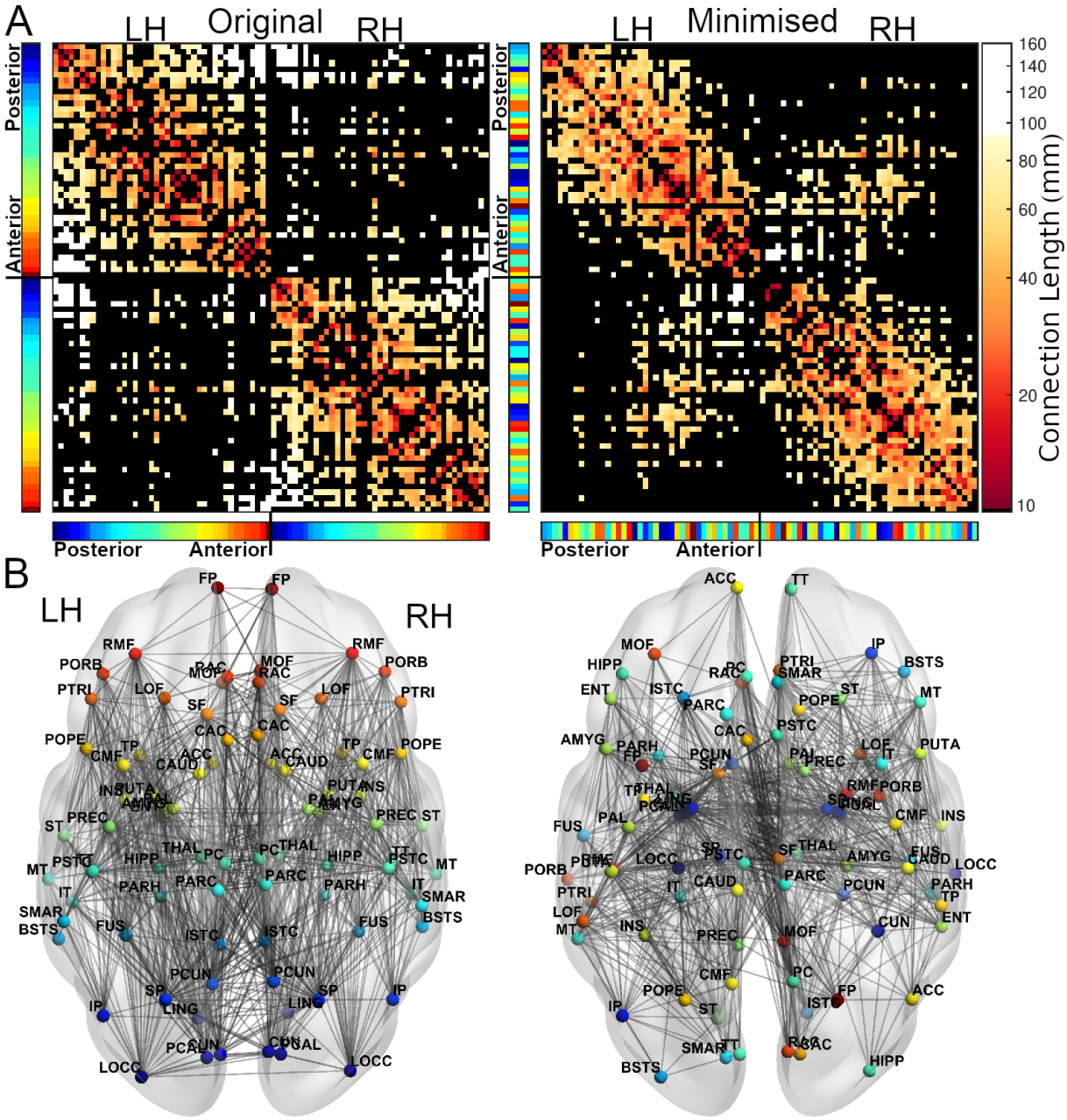


Figure 4.15: For an example subject, the original **(left)** and minimised **(right)** spatial arrangements of connectome components. In the minimised arrangement, the spatial positions of regions are swapped so as to reduce the total wiring length. Regions are coloured based on their anterior-posterior position in the original arrangement, displayed in the colour bars next to the adjacency matrices (red = anterior, blue = posterior). The topology of the connectome is preserved in both arrangements, but the positions of regions often differ. White connections in the adjacency matrices are those with lengths greater than 80% of connections in the original arrangement. LH/RH = Left/Right hemisphere. See Table B.1 for full region names.

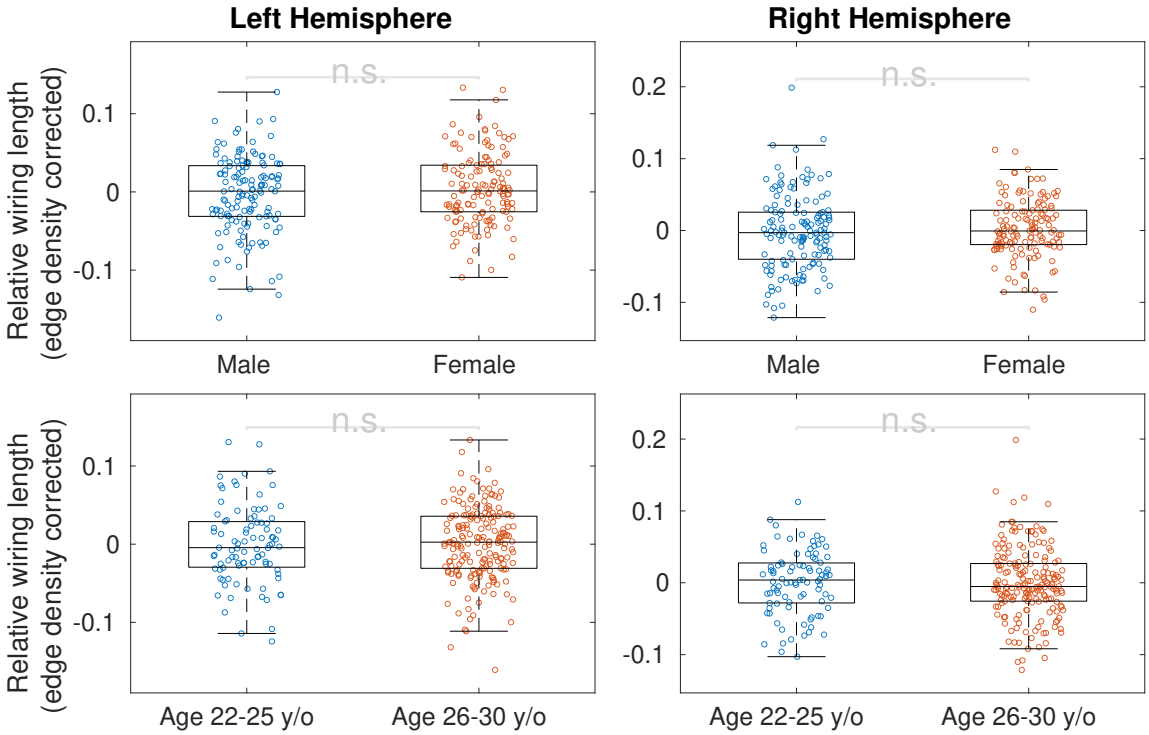


Figure 4.16: Comparing the relative wiring length of hemispheres between age groups and sex. Corrected relative wiring lengths refer to the residuals from a linear regression between edge density and the relative wiring length. No significant differences were observed for the left hemisphere or the right hemisphere across groups (Mann-Whitney U, n.s. $= P > 0.05$).

Because of the differences in edge densities in our sample between sexes (Table 4.2) and the significant positive correlation between edge density and relative wiring length (Figure B.1), we adjusted the relative wiring length by linearly regressing out the effect of edge density. No difference in the corrected relative wiring length was observed between age groups or sexes (Table 4.2). Investigating the hypothesis that individual hemispheres may be differ in their arrangements between groups, we calculated the relative wiring length of individual hemispheres and found no difference between sex or age groups (Figure 4.16).

Whilst the topology does not change between original and minimised arrangements, connections between spatial locations will often differ between arrangements. To assess which edges often disappeared and thus the most costly connections, we compared the connectivity for each originally positioned region with the connectivity of the region replacing it in the minimised arrangement. Considering connections which were present in all subjects (resulting in an edge density of 0.05), Figure 4.17 shows the fraction of connections which were no longer present between spatial positions after rearrangement. Longer connections most often disappeared in the minimised arrangements (Figure 4.18).

Many of the frequently missing connections were connecting distant anterior and posterior regions, primarily connected to the lateral occipital (LOCC), superior parietal (SP) and rostral middle frontal (RMF) cortices (Tables B.2 and B.3). Shorter connections, particularly from subcortical and anterior temporal regions, on the other hand, were less likely to be affected, persisting before and after rearrangement.

Inter-hemispheric connections were more likely to disappear in the minimised arrangements, with a mean percentage of disappearance of 77±18% for inter-hemispheric and 29±25% for intra-hemispheric connections. For connections which existed in the majority of subjects before rearrangement (edge density = 0.23±0.01), a similar pattern was also observed (78±23% and 45±33% for inter- and intra-hemispheric connections, respectively). This trend is similar to that of the macaque subjects, which also displayed a greater number of missing connections between hemispheres rather than within.

Our results assumed that any region could be swapped with any other, irrespective of volume differences. In reality, swapping regions with different volumes may alter the positions of neighbouring regions, subsequently changing their wiring lengths to other regions. To assess whether we were still able to observe reductions when taking into account region volume, we tested the effect of an additional constraint on the swapping procedure: only regions with a similar size were allowed to swap positions. We performed this over several thresholds, where regions were only allowed to swap positions with another if their volumes differed no more than a percentage threshold (constrained by the larger of the two regions). The results are shown in Figure 4.19. As the volume constraint is relaxed, we were able to obtain a greater reduction in wiring length, roughly plateauing at a threshold of ±50%. Crucially, even when two regions could only swap position if the volume of the larger region differed by no more than ±5%, we still observed a wiring length reduction for *all* subjects (a reduction of 3.4±1.2%). This suggests that our results are robust when taking into account differences in region size.

Alterations in the tractography parameters used to construct the connectomes will influence the structure of the connectome (e.g. decreasing the turning angle threshold of streamlines would likely reduce the total wiring length, with fewer streamlines reaching distant areas). We assessed the impact of such changes on the percentage wiring length possible by rearrangement. Rather than re-process all images and form a new collection of connectomes, we instead followed the simpler route of simulating stricter tractography

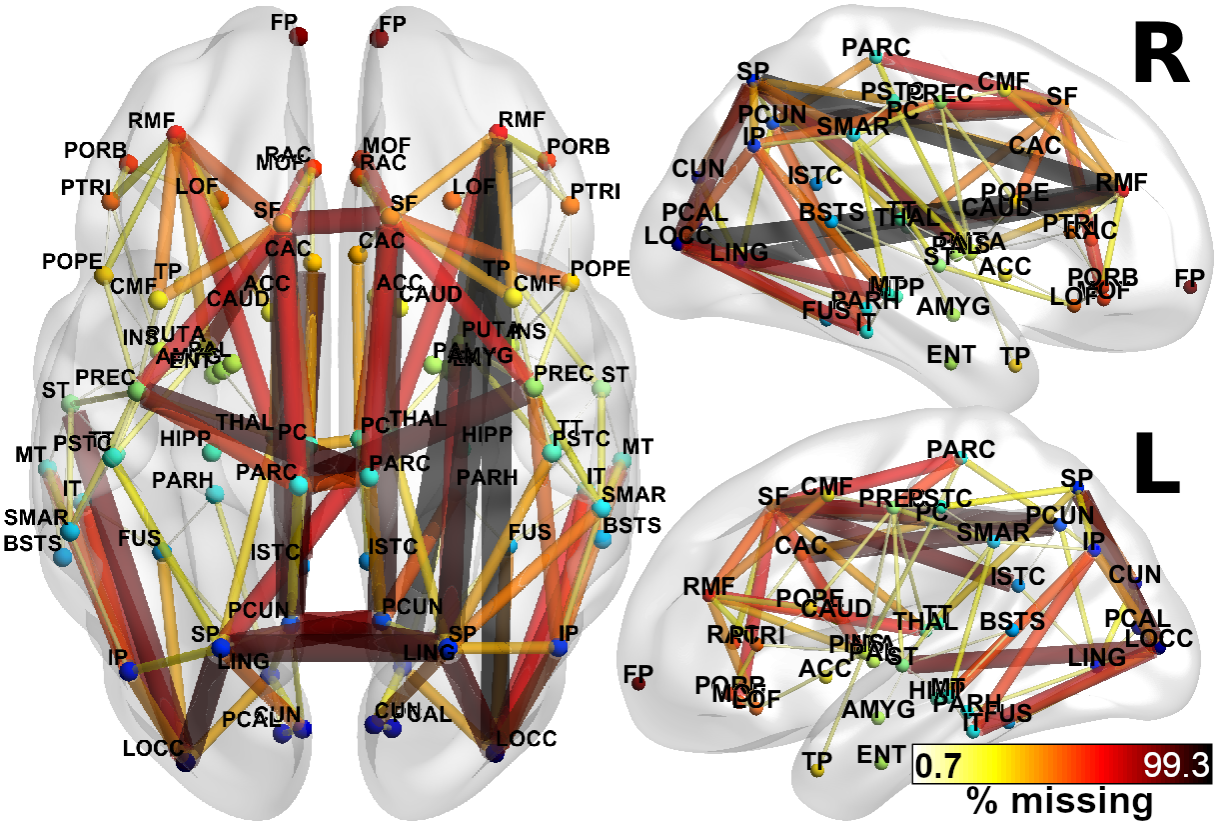


Figure 4.17: Connections which are no longer present between spatial locations in minimised arrangements: axial (left) and lateral (right) views (L/R = left/right hemispheres). Connections are coloured according to percentage of subjects without that connection in the minimised arrangements. Only the connections between regions which were present in *all* subjects are considered (edge density = 0.05). A notable change in the minimised arrangements is the reduced number of intra-hemispheric connections between anterior and posterior regions, particularly between occipital/parietal and frontal lobes. See Table B.2 for the list of connections which disappeared in at least 80% of subjects.

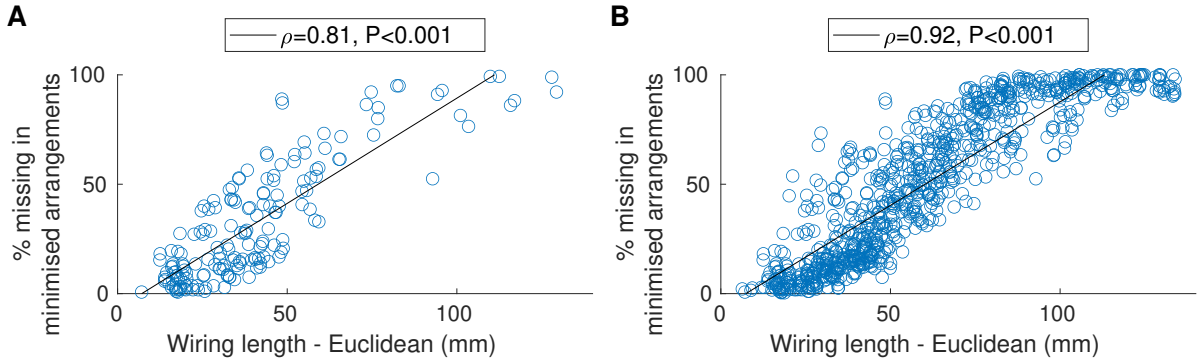


Figure 4.18: Connection length versus the percentage of subjects where the connection was no longer present between spatial positions in the minimised arrangements. **A:** Only considering connections which existed in all subjects prior to rearrangement (edge density = 0.05). **B:** Only considering connections which existed in at least 50% of subjects prior to rearrangement (edge density = 0.23±0.01). Longer connections were more likely to disappear in the minimised arrangements. See Tables B.2 and B.3 for the connections which disappeared most frequently.

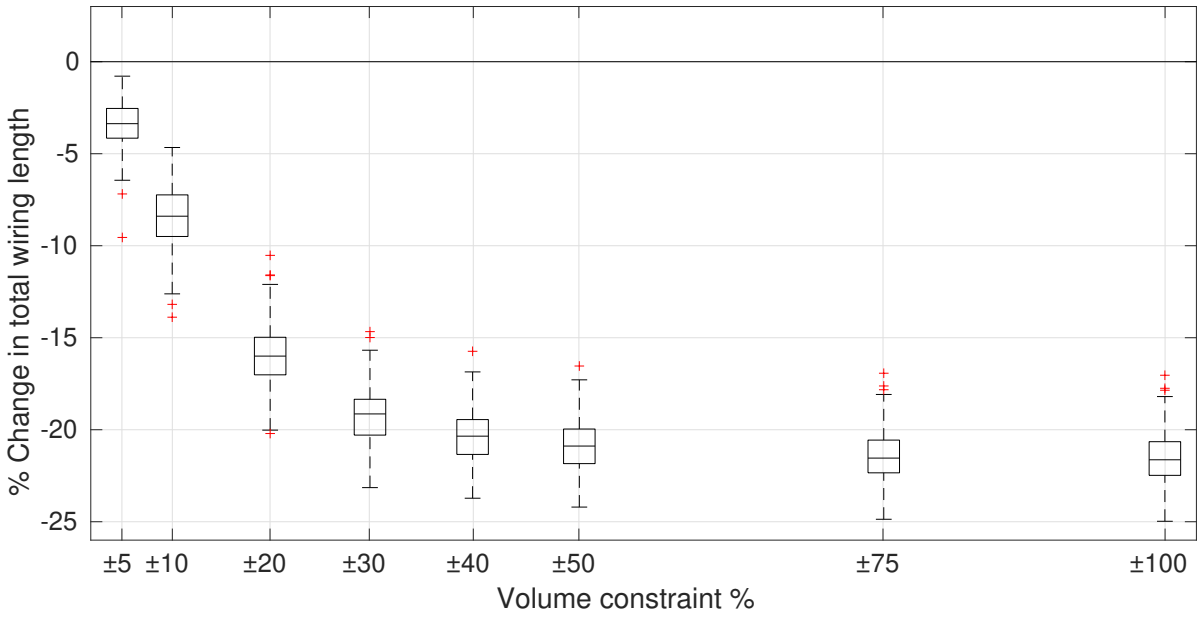


Figure 4.19: Constraining spatial rearrangement based on region volume. We ran the minimisation algorithm over various volume constraints (i.e. regions can only swap with other regions if they have similar volumes, defined by a percentage tolerance). For less restrictive volume constraints, a greater reduction in wiring length was possible. Moreover, reductions in wiring length were still possible even for very restrictive constraints (where regions could only swap with other regions ±5% of their volume, a reduction in wiring length 3.4±1.2% was still possible).

parameters by pruning connections with few streamlines. This tests whether weak connections — those with few streamlines — had an effect on our CPO results. Since many connections consisted of just a single streamline, we used an initial threshold of 20% — the weakest 20% of connections are removed from the connectome — as well as 30% and 40%. It was not always possible to remove an exact percentage of connections as many had the same number of streamlines. Instead, the percentage was used as an upper bound on the number of connections removed. After removing weaker connections and re-running the spatial swapping procedure, a reduction in total wiring length was still possible (Figure 4.20). In fact, as more connections were removed and the rearrangement procedure became less constrained, a greater reduction in total wiring length was observed, suggesting that stronger connections are particularly costly in the connectome. Whilst removing connections, we ensured that the network remained fully connected by preserving the edges which formed part of the network skeleton (the minimum spanning tree (Boruvka 1926; Kruskal 1956) of connections which minimised the inverse total streamline count of the connectome).

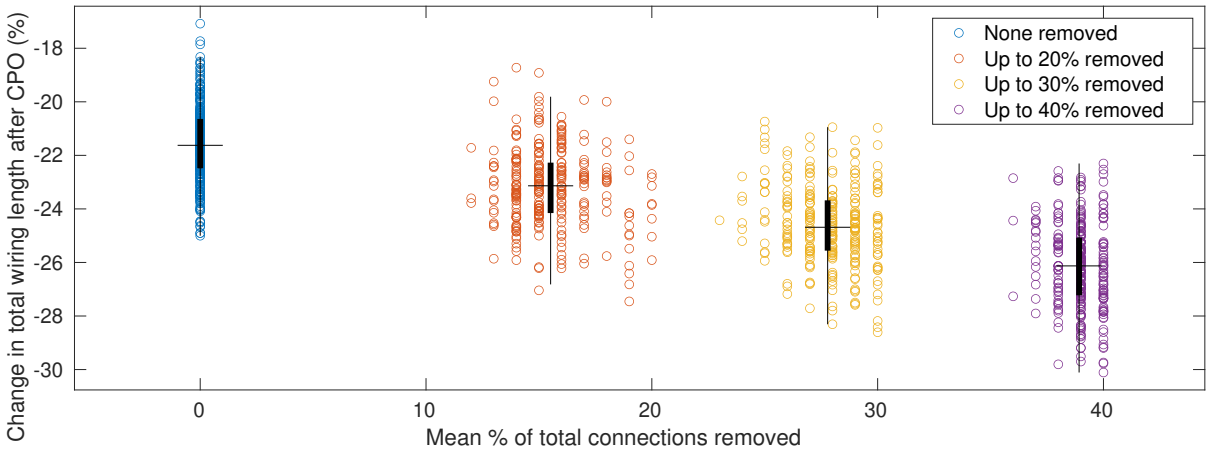


Figure 4.20: Performing the spatial arrangement procedure on connectomes with weaker edges removed (those with few streamlines). Connectomes with weaker edges removed supported a greater reduction in total wiring length following rearrangement.

### 4.2.3 Changes in wiring length for individual regions

As a next step in our analysis, we measured how much each region contributed towards the reduction in wiring length in the minimised spatial arrangements. The goal of this analysis was to assess whether regions differed in their level of spatial optimisation, given their connections to other regions. Figure 4.21 shows the change in wiring length over the 82 regions, calculated as the change in length of all connections attached to a region between the original and minimised placements. Wiring lengths were normalised against the maximum distance between regions, per subject. Almost all regions displayed reduced wiring lengths in the minimised arrangements, with changes broadly consistent across hemispheres. Components in the anterior and posterior spatial locations experienced the greatest reduction in wiring length, particularly the lateral occipital and superior parietal regions. Comparing the lobes, the occipital lobe experienced the greatest reduction in wiring length, while insular and subcortical regions contributed the least towards changes in the wiring length (Figure 4.21, inset). Some regions had a mean *increase* in their connection lengths: nucleus accumbens, caudate, hippocampus, paracentral cortex, bank of the SSTS and transverse temporal regions often moved to positions which increased the total wiring length, likely replaced by regions which made more efficient use of their original spatial positions.

Comparing the wiring lengths between the original and minimised arrangements, a greater reduction in wiring length was observed for regions which had a greater initial

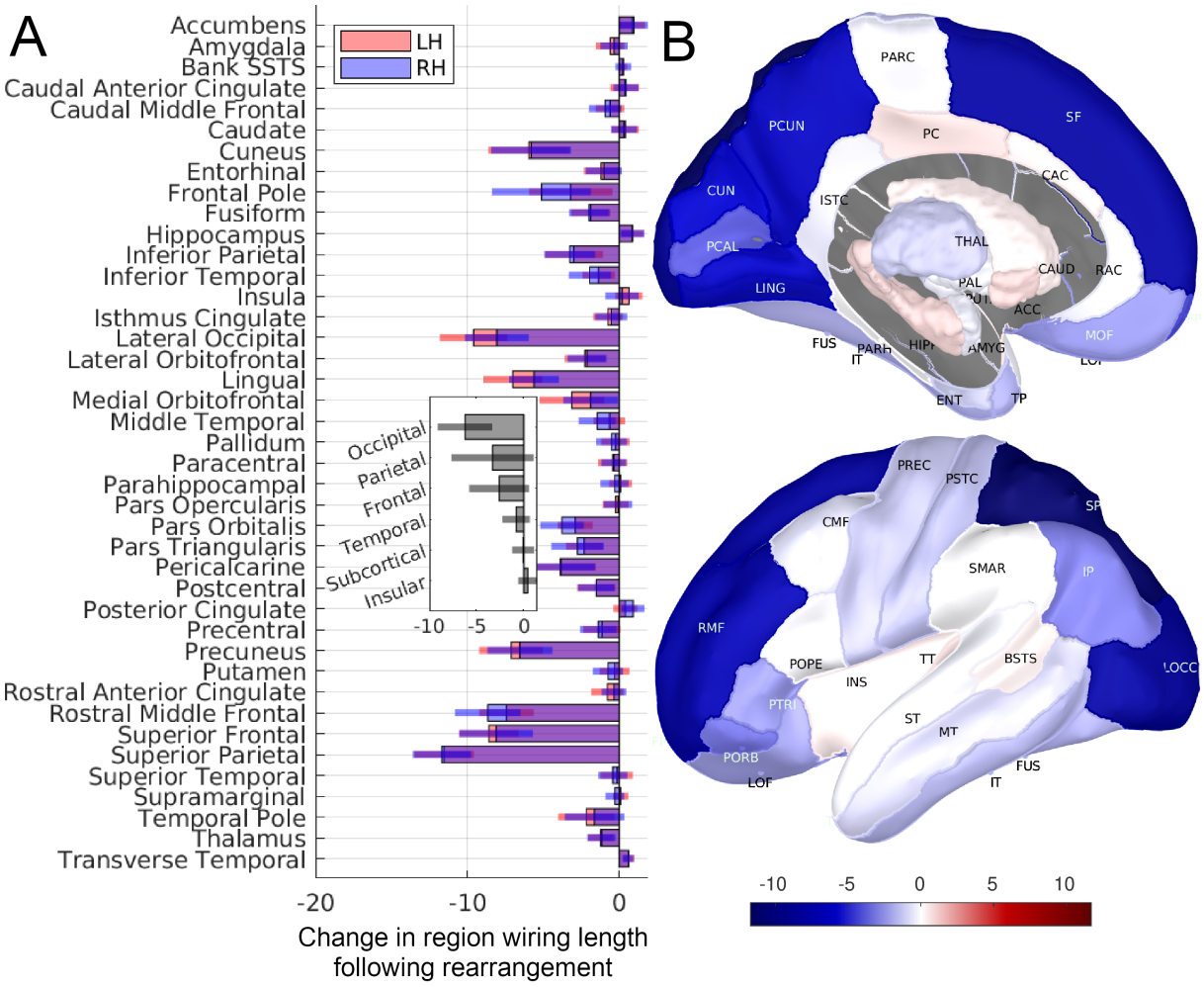


Figure 4.21: The change in the connection length for each region, comparing its position in the original and minimised spatial arrangements. **A:** Changes in the summed wiring length per region for both hemispheres. **Inset:** The mean change in wiring length with regions grouped into lobes. **B:** Medial and lateral views of regions coloured according to their change in wiring length (blue = decrease, red = increase; mean across hemispheres). Regions in the occipital lobe experienced the greatest decrease in total wiring length, while subcortical and insular regions experienced a reduced change (error bars = ±1 SD). Region abbreviations and names are listed in Table B.1.

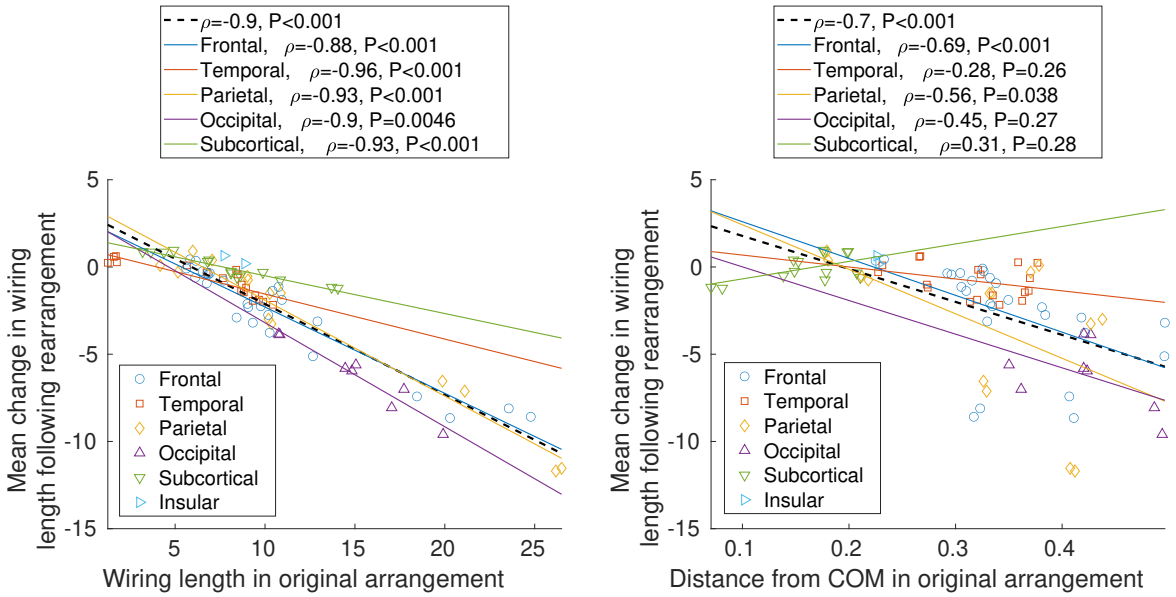


Figure 4.22: Comparing the initial wiring length of each region and its distance from centre of mass (COM) with its change in wiring length across spatial arrangements. Regions with a greater initial wiring length experienced a greater reduction following rearrangement. Also, generally, spatially peripheral regions (those far from the COM) experienced a greater reduction in wiring length. The dashed lines represent the correlation over all regions ($\rho$ = Spearman rank correlation).

wiring length in the original arrangement (Figure 4.22). This correlation was significant for all lobes — excluding the insular lobe — when analysed individually (occipital: $P$ <0.01; all other lobes: $P$ <0.001, uncorrected). Generally, regions which were further from the centre of mass (COM) of the network also displayed a greater reduction in wiring length. Again, the COM was computed as the mean of the spatial coordinates of all regions in each connectome. This correlation was observed as significant for the frontal ($P$ <0.001, uncorrected) and parietal lobes ($P$ <0.05, uncorrected). The insular lobe was excluded from this analysis as it consists of only one region in each hemisphere.

### 4.2.4 Comparison with the macaque connectome

Our previous analyses of the effect of edge density and the number of nodes on wiring length reductions suggested that a greater number of regions, for the same edge density, resulted in a lesser reduction in wiring length following spatial rearrangement (Figure 3.4 in Chapter 2). This coincides with our results for the human and the macaque, with a greater reduction observed in the coarser parcellation of the human (15.0±1.0% for macaque and 21.6±1.4% for human connectomes). However, unlike the random networks, biological connectomes are not randomly wired, with a tendency to connect to

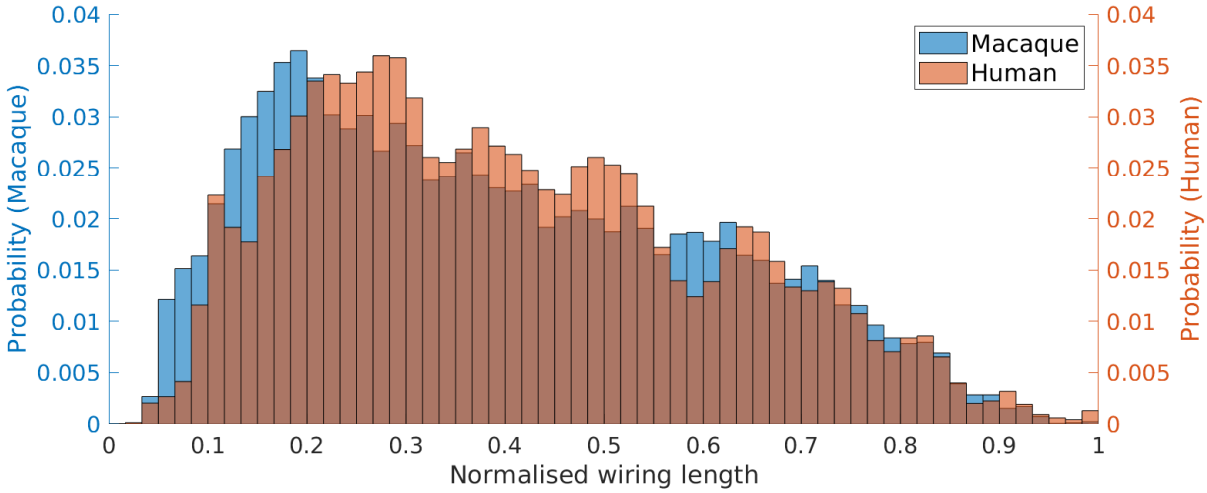


Figure 4.23: Probability density function (PDF) of the wiring length distributions of the original spatial arrangements, for the macaque and human connectomes. Shown is the PDF of connection lengths for all four macaque subjects, and all 280 human subjects. Lengths are normalised against the maximum Euclidean distance over all pairs of regions. In our samples, macaque subjects displayed a greater number of shorter connections compared with human subjects.

nearby regions (Braitenberg and Schüz 2013, pp. 83–87, 129–134). Moreover, the positions of the brain regions are not uniformly distributed in space, as was the case in our 'toy' network analysis in Chapter 2. Comparing the wiring length distribution for the human and macaque data (Figure 4.23), the macaque connectomes displayed a greater number of short connections, which likely constrained the simulated annealing search, limiting the reductions in total wiring length. This difference may reflect a structural difference between species, but much more likely reflects differences in the tractography methods used, such as streamline turning angle thresholds.

### 4.2.5 Functional implications of sub-optimal arrangements

Having identified that optimal component placement (with respect to minimising the wiring length) does not occur in the human connectome, we explored the reasons for this sub-optimal arrangement by hypothesising that a sub-optimal arrangement benefits communication between regions in some way. As with the macaque study, we used the same underlying model of neural oscillations to compare differences in segregated and integrated activity between original and minimised arrangements. Between all regions, we measured synchronisation — whether bouts of neural activation occur at a similar time — as well as metastability — the variance in synchronisation over time to investigate the

effect of spatial factors.

We used a model composed of 82 Kuramoto coupled oscillators, with each oscillator representing the neural dynamics of each human brain region (Kuramoto 1975). The parameters for this dynamical model are altered in several ways, compared with those used for the previous macaque study. To reduce the computational burden caused by the larger sample size, we changed the simulation to represent 30 seconds (rather than 90 seconds) of biological time (ignoring the first three seconds of activity). We also used a coarser range of conduction velocities and coupling strengths when validating the model. We used the same Euler integration method, with a step size of 0.2ms. For an example subject, Figure 4.24 displays the change in mean simulated synchrony across all regions ($\phi$) for a variety of coupling strengths and conduction velocities.

To validate the Kuramoto models, we made use of resting state fMRI BOLD data from the Human Connectome Project, specifically from the S1200 resting state FIX-denoised release, consisting of 15 minutes of BOLD signal activity per subject. Using FSL fnirt (Smith, Bannister, et al. 2001), we performed a non-linear registration of each subject's structural parcellation (Freesurfer's aparc+aseg file) into the MNI space. For each region, we obtained a mask which consisted of the associated segmented cortical region and white matter (also included in the Freesurfer parcellation data). Using this combined mask, we used FSL fslmeants to extract the 1200 BOLD signal time points, repeating this for the 68 cortical and 14 sub-cortical regions across both hemispheres. Sub-cortical regions did not have an associated white matter parcellation. The global mean BOLD signal, calculated as the mean signal across all regions over time, was regressed out from the signal of each region. We applied a bandpass filter of between 0.01Hz and 0.2Hz to each region's BOLD signal. The simulated functional connectivity (FC) matrix was obtained by computing the Pearson correlation coefficient between all pairs of 82 time-series.

Occasionally, mean global synchronisation within the model becomes stationary. To avoid the complexity of incorporating a noise parameter into the dynamical model, and to avoid these situations from interfering with our analysis, we detected stationary synchronisation for each pair of coupling strength and conduction velocity parameters. This check was performed across all simulations used in the analysis. We identified stationary activity by measuring the change in standard deviation in the level of global synchroni-

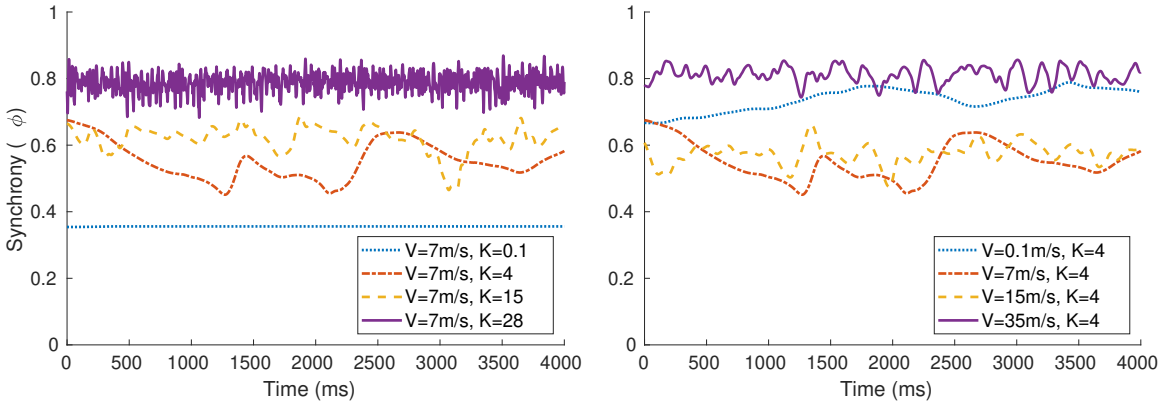


Figure 4.24: Change in mean simulated synchrony ($\phi$) over a range of coupling strengths (K) and conduction velocities (V) for an example subject. For this subject, the maximum correlation between the simulated and empirical BOLD functional connectivity data corresponds to K=4, V=7m/s. Extreme K and V values leads to a reduced correlation with the empirical data; stronger weights and increased speeds produce faster dynamics in the simulation.

sation, using a sliding window of width one second and a standard deviation threshold of $10^{-7}$. Figure B.4 shows the frequency of occurrences of stationary synchronisation across the K/V parameter space, aggregated over all subjects. When comparing dynamics produced by original and minimised arrangements, we analysed changes with and without detecting stationary activity in the model.

As with the macaque study, the model was simulated at different oscillating frequencies from the gamma-band range (defined as 30–80Hz), frequencies associated with region communication and higher-order cognitive functions (Fries 2015). Gamma-band activation is thought to be a general feature of top-down modulation, such as attentional selection (Herrmann et al. 2004). We used three frequencies from this range: 40Hz, 60Hz and 80Hz. Connectivity between oscillators is defined by the binary adjacency matrix (connections with at least one streamline were set to one, and zero otherwise) weighted by the coupling strength $K$ (Figure 4.27A). We validated the model by correlating each subject's simulated functional connectivity (based on the original spatial arrangement) with that of the empirical resting state fMRI BOLD signal over a range of coupling strengths, K, (1 to 25, in steps of 1) and conduction velocities, V (1 to 29 m/s, in steps of 2 m/s). This was achieved by performing a Pearson correlation of the upper right triangles of the simulated and empirical functional matrices.

To demonstrate that the Kuramoto model replicates real brain dynamics beyond that

produced by random interactions between components, we compared the model dynamics from the unperturbed connectomes with that derived from a null model using a connectome whose connectivity has changed (Fornito, Zalesky, and Bullmore 2016, section 10.2). This alteration consisted of rewiring the connectome several times for each subject, followed by comparing the empirical functional connectivity with the simulated functional connectivity of each rewired connectome, over the parameter space. Performing this null-model analysis also helps to validate the structural connectivity derived using our tractography pipeline. For both originally-wired (original) and randomly-wired (rewired) connectomes, we selected the maximum Pearson correlation coefficient between the empirical and simulated functional connectivity, chosen from a parameter scan over coupling strengths (1-25, in steps of 2) and conduction velocities (1-29m/s, in steps of 2m/s) — compared with the other parameter scans, we used a smaller parameter space to reduce execution times. We down-sampled the parameter space for the original network, to match that of the rewired networks; identical parameter spaces were used for the original and rewired connectomes, and across all subjects. For the rewired connectomes, the connectivity of each subject was rewired randomly 20 times, with each edge being re-positioned approximately 100 times, whilst preserving the degree distribution of the original wiring. The mean Pearson correlation coefficient with the empirical data is calculated for each of these 20 rewirings and subsequently used when being compared with the originally-wired connectome. For this analysis, the oscillation frequency was set to 40Hz, and simulations were run for 120 seconds of biological time. Compared with the null model, the simulated functional connectivity of the original (non-rewired) connectomes displayed significantly stronger correlations with the empirical data (Figure 4.26). This finding supports the results which follow, helping to justify our use of Kuramoto oscillators in exploring brain dynamics.

Referring to the unperturbed connectomes, the maximum Pearson correlation with empirical functional connectivity equated to 0.13±0.04, 0.13±0.04 and 0.14±0.04 for 40Hz, 60Hz and 80Hz (Figure B.6). At 40Hz, 60Hz and 80Hz, validation resulted in a mean conduction velocity of 8.6±3.5 m/s, 12.4±6.1 m/s and 15.0±5.8 m/s, and a mean coupling strength of 4.2±3.2, 7.3±5.4. and 9.3±6.5, respectively. Using the validated models, we then calculated the global synchrony and metastability in the original arrangement by measuring the mean difference in phase between regions over time (Figure 4.27B). Figures 4.25 (40Hz), B.2 (60Hz) and B.3 (80Hz) display the change in synchrony, metasta-

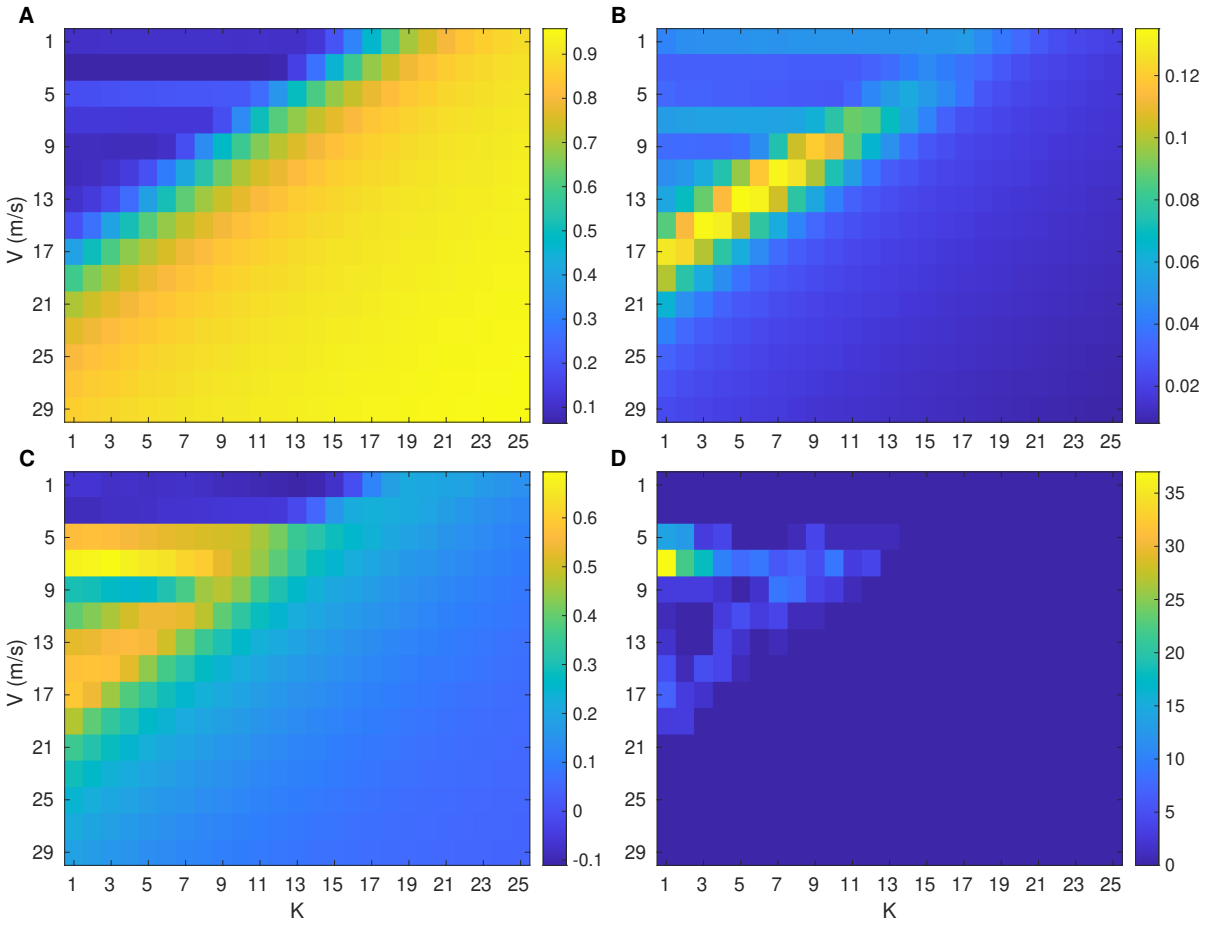


Figure 4.25: For an oscillation frequency of 40Hz, the changes in dynamics over the parameter space of conduction velocities (V) and coupling strengths (K) for all subjects. **A:** Mean synchrony, **B:** mean metastability, **C:** mean normalised Pearson correlation with empirical data (maximum correlation set to one, for each subject), and **D:** the number of occurrences in the parameter space for which a pair of parameters provided the maximum correlation with empirical data.

bility and empirical correlations across the K/V parameter space.

Empirically-validated simulated synchrony and metastability values were broadly consistent across frequencies: At 40Hz, mean values were 0.22±0.13, and 0.08±0.05, respectively (22±13% and 42±26% of the maximum synchrony and metastability). At 60Hz, these were 0.21±0.13 and 0.08±0.05, respectively (23±14% and 40±25% of the maximum values achieved over the parameter space). At 80Hz, mean values were 0.20±0.12 and 0.08±0.05, respectively (23±14% and 39±24% of the maximum values achieved over the parameter space).

Having validated the model against the empirical data, we next compared the change

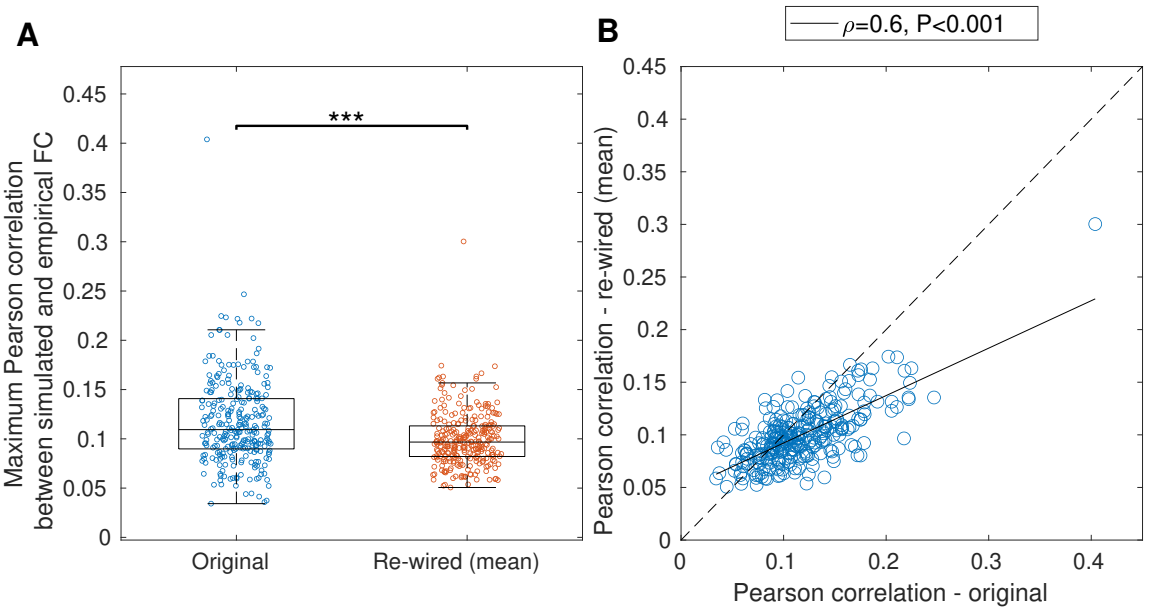


Figure 4.26: Validating the dynamics of the Kuramoto model using a null model. At 40Hz, we compared the maximum Pearson correlation coefficient between the empirical and simulated functional connectivity (FC) across the parameter space, for the original and rewired structural connectomes. **A:** Simulated activity based on the original structural connectomes (those closer to the true connectivity profile) displayed stronger correlations with the empirical data, compared with the rewired connectomes ($P$ <0.001, Wilcoxon signed-rank test). 60% of subjects experienced a stronger correlation with the empirical data when the model used the original structural connectivity. **B:** Correlating the Pearson correlation coefficients between wirings — original connectomes often displayed stronger correlations with the empirical data. Dashed line = diagonal.

in metastability between the original and minimised arrangements, using the same approach as that used for the macaque data — we selected K and V so as to minimise the difference in synchrony between the two arrangements. This was performed separately for K and V, and the mean metastability was obtained from both searches. Subsequently, for all frequencies, both conduction velocities and coupling strengths were reduced for the choice of parameters corresponding to the closest match in synchrony with the original arrangements. Specifically, in the model based on the minimised arrangement, K and V reduced by: 2.6±3.6 m/s and 1.1±3.4 at 40Hz (reduced to 5.9±3.5 m/s and 3.2±2.1); 4.2±5 m/s and 1.4±5.5 at 60Hz (reduced to 8.2±5.9 m/s and 6.0±4.0); 4.3±6.9 m/s and 1.1±7.6 at 80Hz (reduced to 10.7±6.3 m/s and 8.2±5.4). These speeds remain within the biologically plausible range of 5–20m/s (Waxman 2006).

At these new positions in the parameter space, we then assessed the difference in metastability with that of the original arrangements. Compared with the parameters for the original arrangements, metastability was significantly reduced in the minimised arrangements for all three frequencies; for 40Hz the minimised layouts showed significantly reduced metastability compared with the original arrangements (Wilcoxon signed-rank test, $P < 0.001$, Cohen's $d = 0.39$, Figure 4.27C). Reductions in metastability for 60Hz ($P < 0.001$, Cohen's $d = 0.45$) and 80Hz ($P < 0.001$, Cohen's $d = 0.42$) are displayed in Figure 4.28. Most subjects experienced a decrease in metastability in the minimised arrangements (71%, 65% and 69% for 40Hz, 60Hz and 80Hz respectively). Putting these percentages into context, the probability of obtaining at least 182 (65%) heads from 280 coin tosses is approximately 2.92e-07 (assuming a fair coin). Additionally, the magnitude of the change in metastability was greater for subjects which experienced a decrease in metastability in the minimised arrangements — for 40Hz, 60Hz and 80Hz resp., the mean change in metastability for subjects with a decrease (increase) in metastability in the minimized arrangements was -0.034±0.032 (0.023±0.023), -0.041±0.041 (0.018± 0.019) and -0.034±0.040 (0.016±0.014). Reductions in metastability remained significant for the 50% of subjects with the strongest Pearson correlation with the empirical data (Figure 4.29), and in cases where stationary synchronisation was not omitted (Figure B.5).

By using a dynamical model, we have identified a possible mechanistic reason for why brain regions are sub-optimal in their spatial arrangement with respect to minimising the wiring length (by increasing metastable dynamics in the system).

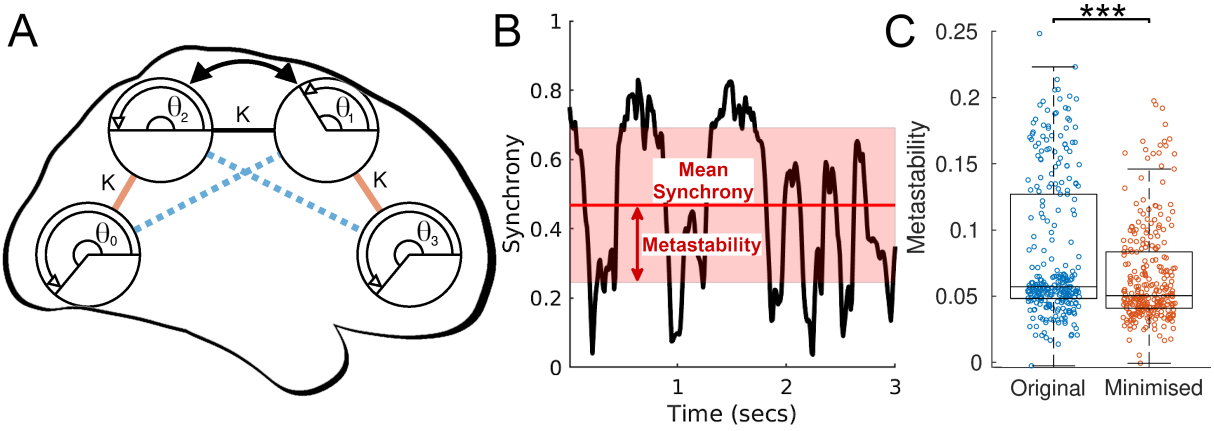


Figure 4.27: Simulating changes in neural activity for original and minimised connectomes. **A:** Regions are Kuramoto oscillators (coupling strength K, phase $\theta$), displayed here in a minimised arrangement (the original arrangement is achieved by swapping regions 1 and 2 — indicated by the arrow and dashed lines). **B:** A snippet of simulated activity showing the change in synchrony over all regions (black line) and the corresponding mean synchrony (red line) and metastability (SD of synchrony, shaded). **C:** For 40Hz, 60Hz and 80Hz (40Hz shown), simulated metastability is significantly reduced in the minimised arrangements compared with the original arrangements (*** = $P < 0.001$, Wilcoxon signed-rank test, Cohen's $d = 0.39$). At 40Hz/60Hz/80Hz, 71%/65%/69% of subjects experienced a reduction in metastability in the minimised arrangements.

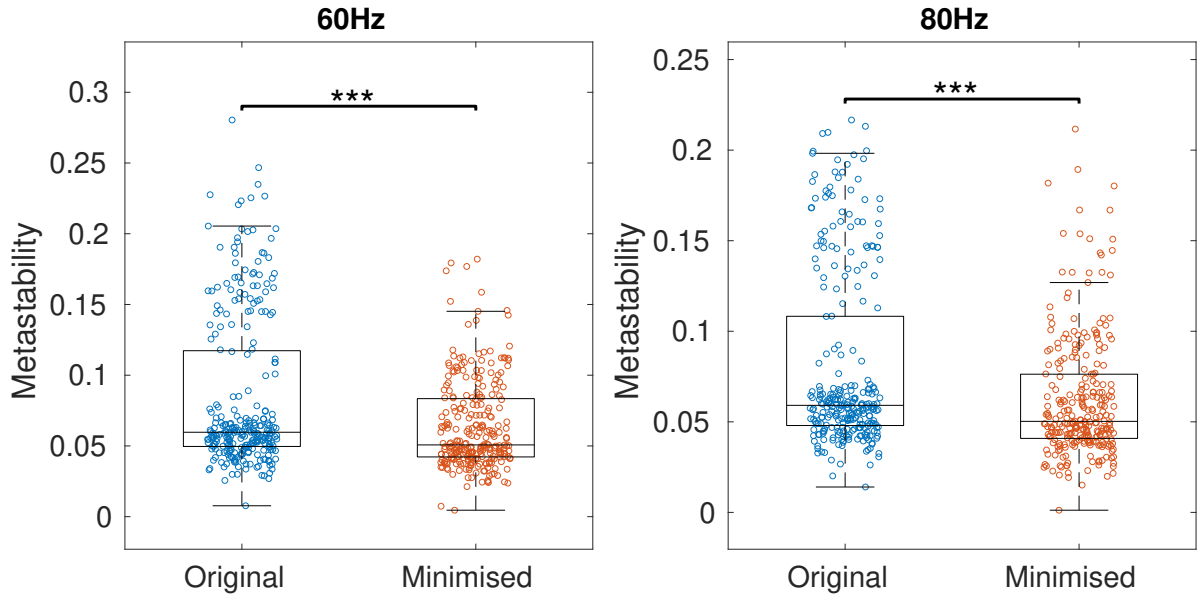


Figure 4.28: For oscillation frequencies of 60Hz and 80Hz, simulated metastability for the original and minimised arrangements, for all subjects. Metastability is significantly reduced in the minimised arrangements compared with the original arrangements (*** = $P < 0.001$, Wilcoxon signed-rank test). Cohen's $d = 0.45$ (60Hz), 0.42 (80Hz). For 60Hz and 80Hz, 65% and 69% of subjects experienced a reduction in metastability in the minimised arrangements, respectively.

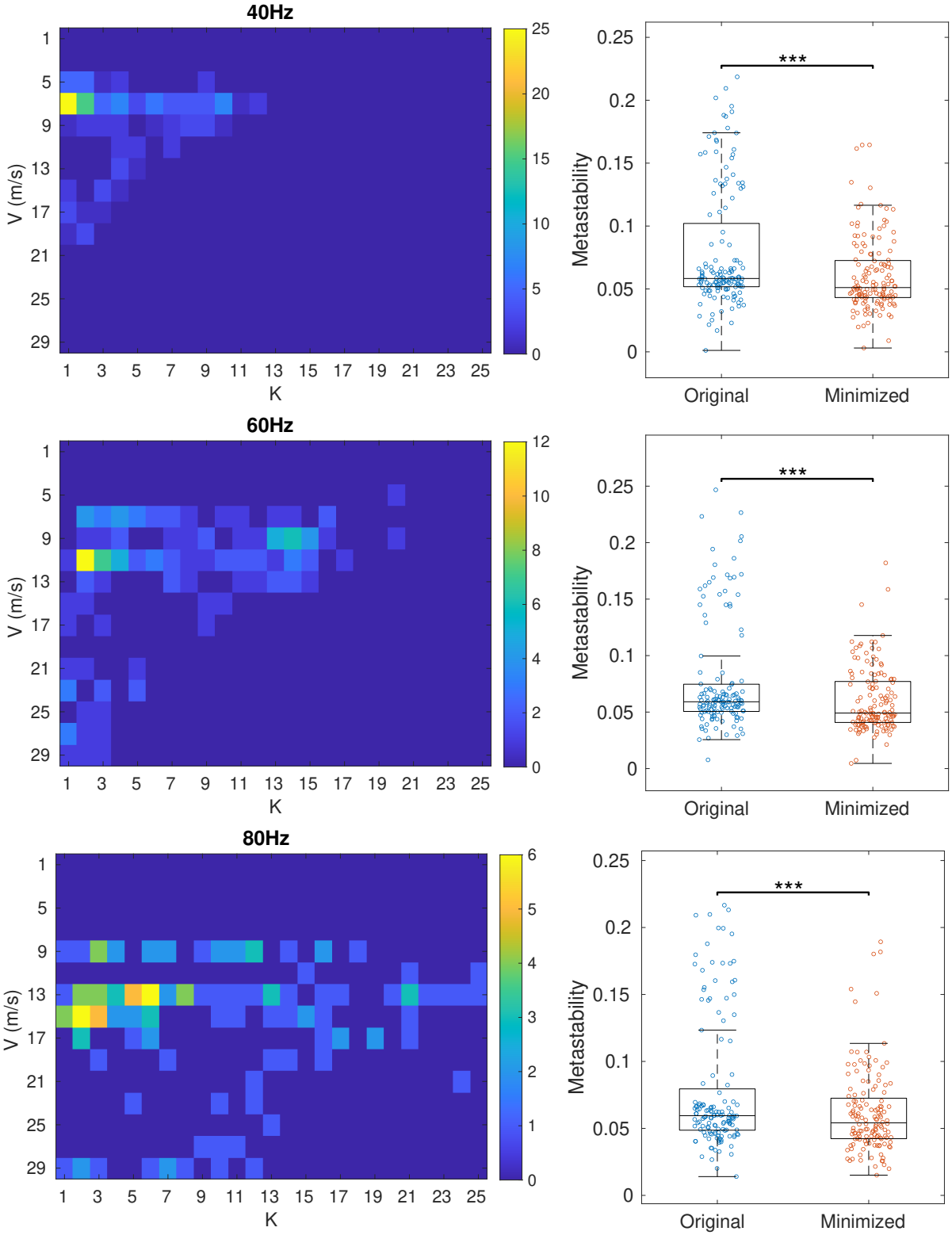


Figure 4.29: Changes in simulated metastability for the 50% of subjects showing the strongest Pearson correlation coefficient between the empirical and simulated functional connectivity (0.16±0.04, 0.17±0.04 and 0.16±0.04 for 40Hz, 60Hz and 80Hz respectively). **Left column:** The number of occurrences in the parameter space for which a pair of parameters provided the maximum correlation with empirical data. **Right column:** The difference in metastability between the original and minimised spatial arrangements, with all frequencies showing significant reductions in metastability (*** = $P < 0.001$, Wilcoxon signed-rank test). Cohen's $d = 0.46$ (40Hz), 0.43 (60Hz), 0.40 (80Hz). Reductions in metastability in the minimised arrangements: 71% (40Hz), 65% (60Hz), 63% (80Hz)

## 4.3 Spatial Analysis of Schizophrenia Subjects

Here, we turn our attention to analysing the spatial arrangement of the connectome in situations where cognition is impaired, specifically in case of schizophrenia. We apply the same simulated annealing rearrangement algorithm to two sets of connectomes — derived using the same imaging parameters — namely, healthy controls and subjects diagnosed with schizophrenia. For this kind of novel analysis, we attempt to link the symptoms associated with schizophrenia with spatial differences between the two groups, and also within the patient group using symptom severity scores.

### 4.3.1 Comparing the connectomes of healthy controls with schizophrenia subjects

As a first step, we compared the differences in connectome connectivity between controls and schizophrenia patients. Table 4.3 lists the results after applying several network properties. For several features, we found significant differences between groups: healthy controls had more connections and a greater number of streamlines per connection on average, when compared with schizophrenia patients. We did not observe a significant difference in the characteristic path length (binary/weighted/metric), clustering (binary/weighted), small-worldness, total wiring length, or the convex hull volume between groups.

Because of the reported changes to hubs within the connectome and observed functional alterations (Bassett, Bullmore, et al. 2008), we tested the hypothesis that the connectomes of subjects with schizophrenia deviate from component placement optimisation to a greater extent than controls. By doing so, we hope to identify whether spatial features can explain some of the symptoms observed in schizophrenia subjects, such as altered cognition. For instance, a particularly sub-optimal component placement in schizophrenia patients may explain symptoms such as reduced processing speed (Keefe et al. 2012; Matheson et al. 2008). Moreover, the reported changes in gamma-band oscillatory activity in patients may be partly driven by a sub-optimal spatial arrangement, as suggested by the link between spatial arrangement and dynamics for the HCP data. Here, we present our findings on analysing the spatial arrangement of connectomes for a sample of healthy controls and subjects with schizophrenia.

We used the simulated annealing algorithm to identify whether a spatial arrangement

Table 4.3: Connectome properties for healthy controls and schizophrenia patients

| Measurement | Healthy controls | Schizophrenia patients | $P$-value |
|---|---|---|---|
| Edge density | **0.0813±0.0035** | **0.0796±0.0038** | **0.035** |
| Streamlines per connection | **14.0±1.5** | **12.3±1.5** | **1.7e-06** |
| $L_u$ | 1.23±0.035 | 1.24±0.031 | 0.44 |
| $L_w$ | 1.27±0.11 | 1.31±0.11 | 0.095 |
| $L_m$ | 0.746±0.025 | 0.733±0.027 | 0.054 |
| $C_u$ | 5.4±0.35 | 5.45±0.48 | 0.73 |
| $C_w$ | 6.18±0.4 | 6.08±0.52 | 0.31 |
| Small-worldness | 4.39±0.24 | 4.41±0.32 | 0.93 |
| TW (mm) | 10,270±836 | 10,040±825 | 0.31 |
| Convex hull volume ($mm^3$) | 681,876±58,731 | 680193±69,261 | 0.8 |
| CPO: Minimum TW % change | -16.0±1.2 | -16.5±1.6 | 0.13 |
| CPO: Maximum TW % change | 97.7±4.2 | 98.6±5.3 | 0.38 |
| Relative TW | 0.141±0.011 | 0.144±0.015 | 0.39 |

*Note.* $L_u$ = unweighted path length. $L_w$ = weighted path length (by streamline count). $L_m$ = metric path length (weighted by the Euclidean distance along edges). $C_u$ = unweighted clustering coefficient. $C_w$ = weighted clustering coefficient (by streamline count). TW = total wiring length. CPO = component placement optimisation (the results from swapping the positions of regions). The total wiring length is the total Euclidean distance between all connected regions. $P$-values are from a Mann Whitney U test. Other values are mean±SD.

of regions that is closer to optimal could be identified by swapping the positions of regions within the connectome (one which reduces the total length of connections). We applied this method to both healthy controls and schizophrenia patients. To reiterate, during the search, the spatial location of regions are swapped whilst the topology is maintained. The rearrangement procedure is applied despite the insula and thalamus regions missing in this data. We repeated the search 100 times for each subject, with the greatest reduction in wiring length used in the subsequent analysis.

Coinciding with the previous findings, we found that all subjects showed sub-optimal component placement (Figure 4.30); for all subjects, we were able to rearrange regions so as to reduce the total wiring length in the connectome (mean reduction: 16±1.4%, relative wiring length: 0.14±0.013). Comparing healthy controls and schizophrenia patients, we found no significant difference in the relative wiring length or the percentage change in wiring length following rearrangement (Table 4.3). The distribution of length changes for separate groups can be found in Figures B.7 and B.8. Comparing the change in wiring length between controls and patients at the level of individual regions also showed no differences, with all $P$-values from a Mann-Whitney U test failing to survive FDR correction ($P > 0.05$) (Figure 4.31).

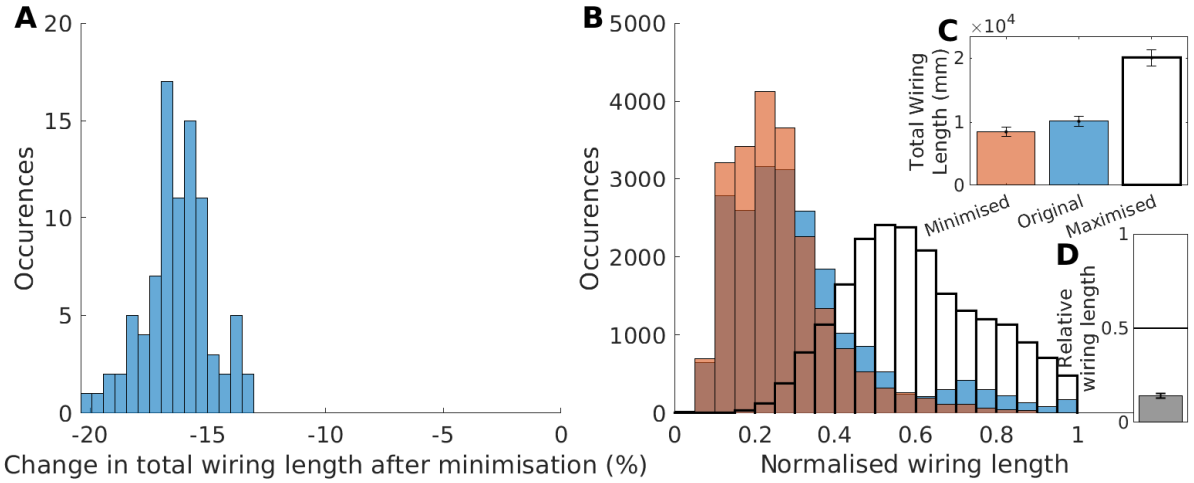


Figure 4.30: For the schizophrenia dataset (both healthy controls, and schizophrenia patients) — changes in wiring length distributions for the original, minimised and maximised spatial arrangements. **A:** The percentage difference in wiring length between the original connectomes and the spatial arrangements which minimise the total wiring length (mean -16.0±1.4%). **B**: The distribution of wiring lengths for the original (orange), minimised (blue) and maximised (transparent, bold) spatial arrangements. **C:** The mean wiring lengths for the minimised, original and maximised arrangements. **D:** The mean relative wiring length across all subjects (0.14±0.013) — original lengths normalised against that of minimised and maximised arrangements (error bars = ±1 SD.).

Informed by findings from other studies regarding differences in hub-nodes within the connectome for schizophrenia subjects (Bassett, Bullmore, et al. 2008; Rubinov et al. 2013; Yuanchao Zhang et al. 2012), we assessed whether hubs differed between controls and patients. We measured both the degree and betweenness centrality to identify hubs in the connectome, with the latter representing the frequency with which a region exists on a shortest path between a pair of regions (Freeman 1977; Rubinov and Sporns 2010). Here, path lengths are summed using the Euclidean distance between connected regions. No single region showed significant differences in hub characteristics between groups ($P$ >0.05, after correcting for multiple comparisons — Figure B.9); regions in both groups displayed similar degree (despite the reduced edge density in patients) and betweenness centrality. Before correction, for degree, the caudate (LH), frontal pole (LH), pars triangularis (LH), superior temporal (LH), transverse temporal (LH) and caudate (RH) all displayed higher degree in controls ($P$ <0.05, uncorrected). Before correction, for betweenness centrality the amygdala (LH), fusiform (LH) and frontal pole (RH) displayed higher centrality in patients ($P$ <0.05, uncorrected); and the pars triangularis (LH), superior temporal (LH) and caudate (RH) displayed higher centrality in controls ($P$ <0.05, uncorrected). Normalising the degree by the edge density also failed to produce significant differences

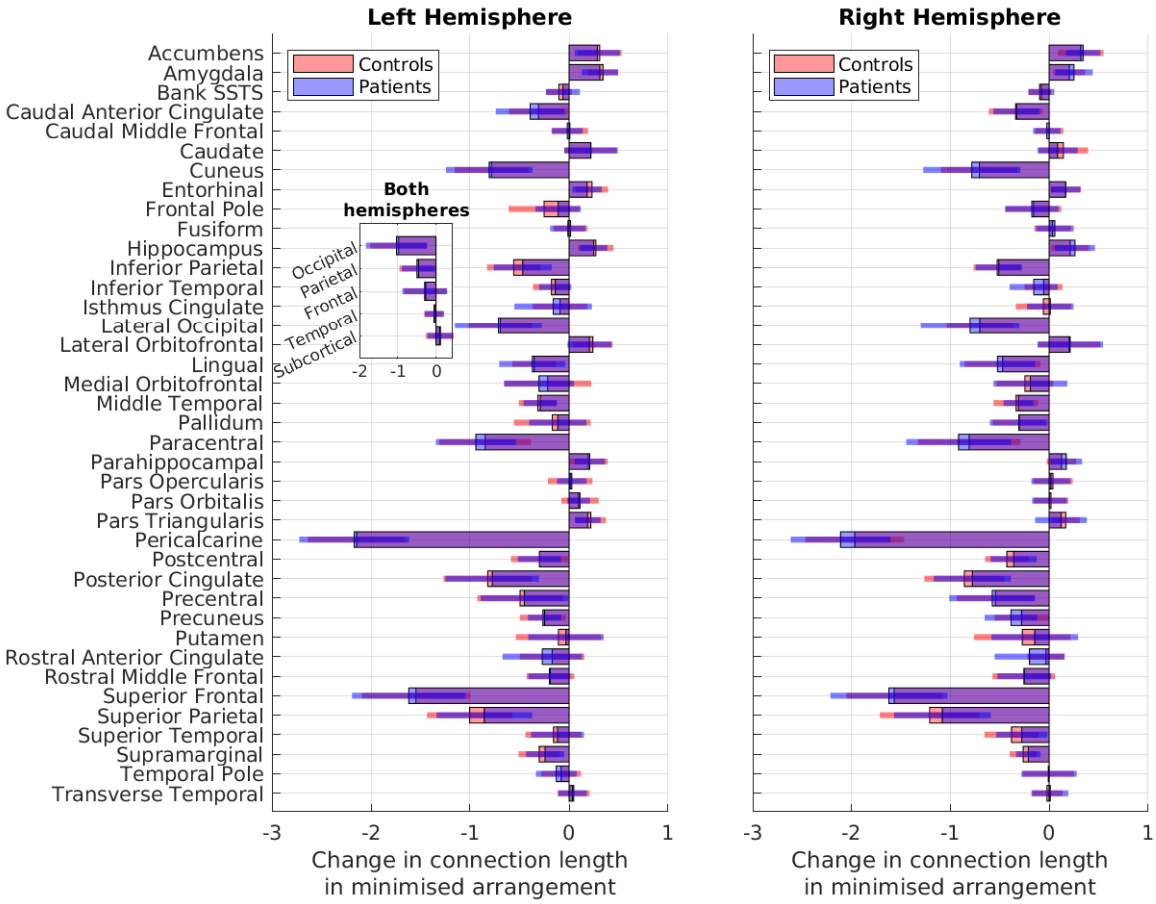


Figure 4.31: For controls and schizophrenia patients, the changes in region wiring length between original and minimised spatial arrangements. Comparing differences at a region-level, no significant difference between groups was observed.

between groups ($P$ >0.05, corrected).

### 4.3.2 Comparing frontal lobe structure

Because of the reported functional and structural alterations in the prefrontal cortices of schizophrenia patients (Minzenberg et al. 2010; Mubarik et al. 2016; Picchioni et al. 2008), we performed a *post-hoc* analysis on the spatial arrangement within the frontal lobe alone. This involved applying our rearrangement method to the isolated frontal lobe network, consisting of 26 regions across both hemispheres. We tested the hypothesis that spatial changes are localised in the frontal networks in schizophrenia patients, as suggested by structural and functional alterations in this area. For all subjects, the wiring length of frontal lobe networks could reduced by 3.97±1.72% (relative wiring length: 0.025±0.013), indicating that this lobe was particularly spatially optimised. Neither the percentage change in wiring length, nor the relative wiring length displayed significant differences between controls and patients ($P$ >0.05); changes in wiring length were 4.02±1.61% for controls and 3.92±1.84% and patients, with a relative wiring length of 0.026±0.012 and 0.025±0.013, respectively. After correcting for multiple comparisons, changes in wiring length at the region-level (Figure B.10) failed to display significant differences between groups ($P$ >0.05, corrected). Uncorrected $P$-values were significant for the RH pars triangularis only ($P$=0.03), displaying a greater wiring cost in patients (wiring lengths in the minimised arrangements displayed a greater increase in controls compared with patients).

Continuing to analyse the frontal lobe, we attempted to predict the severity of positive, negative and general symptoms (PANSS scores) within the patient group (after excluding two subjects for which the PANSS score was unknown). No significant correlation existed ($P$ >0.05, Spearman rank correlation coefficient) between the positive/negative/general PANSS scores and the path length, clustering coefficient or the mean wiring length of the isolated frontal network (Figure B.11). Finally, we correlated the PANSS scores with the relative wiring length of the isolated frontal lobe network, computed using the spatial arrangement procedure to minimise and maximise the total wiring length. We linearly regressed out effect of edge density on the relative wiring length to assess spatial placement independently of the influence of the number of connections. Schizophrenia subjects with more severe positive symptoms (conceptual disorganisation, hallucinations, hostility,

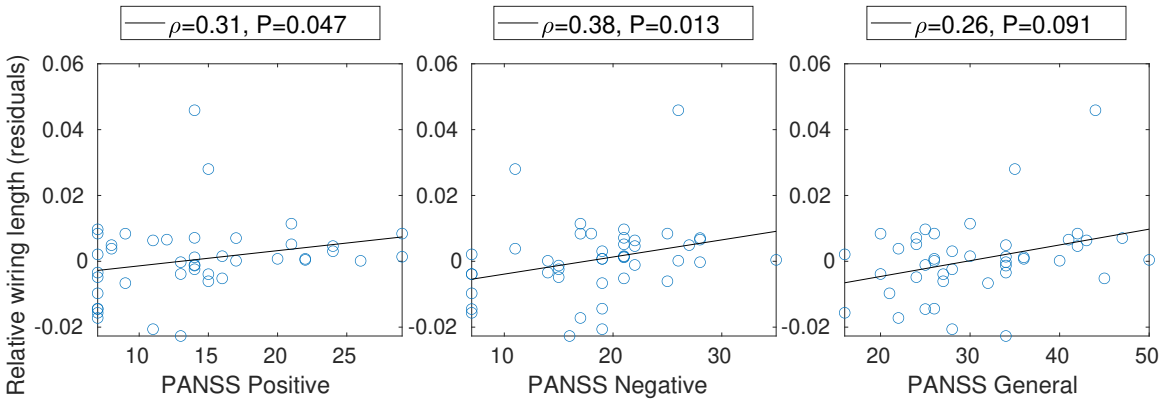


Figure 4.32: Comparing PANSS symptom scores with the relative wiring length of the isolated frontal lobe network in schizophrenia patients. PANSS scores were correlated with the residuals of a linear regression between the relative wiring length and edge density. Schizophrenia subjects with more extreme positive and negative symptoms displayed less spatially optimised frontal networks (greater relative wiring lengths) ($P$ <0.05, Spearman rank correlation coefficient).

etc.) and negative symptoms (emotional withdrawal, difficulty in abstract thinking etc.) showed a greater relative wiring length ($P$ <0.05), indicating less spatially optimised frontal network connectivity in subjects with more severe positive and negative symptoms (Figure 4.32). Correlations coefficients were $\rho$ =0.31 and $\rho$ =0.38 respectively. A trend appeared for the same correlation between the relative wiring length and general scores (poor attention, disorientation, etc.) ($P$ =0.091). These results suggest the presence of a link between the spatial organisation of the frontal lobe and the severity of symptoms in schizophrenia patients.

## 4.4 Spatial Analysis of the Connectome Alongside Intelligence

Analysing the final dataset in this study, the following section provides the results from an investigation into the structural features of the connectome alongside scores obtained from measures of fluid and crystallised intelligence, using data from the Nathan Kline Institute-Rockland (NKI) cohort (Nooner et al. 2012). We make use of the simulated annealing algorithm to assess spatial features alongside intelligence scores, with the aim of identifying structural correlates of intellectual ability within the connectome.

### 4.4.1 Correlations between IQ scores

For our sample of subjects from the NKI dataset, significant positive correlations existed between all WASI scores (Table C.1) — subjects with higher scores in one subtest generally displayed higher scores in other subtests. Between these four subtests, the strongest correlation existed between BD and MAT ($\rho$ =0.65), followed by SIM and VOC ($\rho$ =0.58). Moreover, BD and MAT were marginally more strongly correlated with SIM than with VOC: For BD, $\rho$ =0.4 with VOC and $\rho$ =0.44 with SIM. For MAT $\rho$ =0.45 with VOC and $\rho$ =0.5 with SIM. We did not observe a significant correlation between age and any of the WASI scores (confirming the age-correction of these scores), nor between genders ($P$ >0.05, Mann-Whitney U), aligning with negligible differences between males and females (Dykiert et al. 2009).

### 4.4.2 Topological structure of the connectome

As a first assessment of connectome structure alongside intelligence we investigated the topological features of the brain networks (Figure 4.33, Table C.2). $C$ corresponds to the mean clustering coefficient over all regions in the network, for a given subject. $L$ is the mean path length over all shortest paths between nodes in the network. For the unweighted versions of path length $L_u$ and clustering coefficient $C_u$ each edge has unit length. The metric path length $L_m$ uses the length of edges in millimetres (Euclidean distances of connections). The mean weighted clustering coefficient $C_w$ uses the number of streamlines per edge, while for the weighted path length $L_w$ the inverse of the number of streamlines is used. Small-worldness is computed using $L_u$ and $C_u$. $L_{u/m/w}$, and $C_{u/w}$ were all normalised against 100 randomly rewired networks preserving the degree distribution of the original network. In the rewiring process, each edge is rewired approximately 100 times.

A significant positive correlation was observed between $L_w$ and BD scores meaning that paths between regions incorporated fewer streamlines in subjects with higher BD scores. Also, the mean number of connection streamlines increased with greater BD and PIQ scores. Against WASI scores, there were no significant correlations with the unweighted characteristic path length $L_u$, mean weighted/unweighted clustering coefficient $C_{w/u}$, small-worldness or edge density of the connectome. Older subjects had reduced $L_u$,

edge density and streamline count, compared to younger subjects.

### 4.4.3 Spatial structure of the connectome

Here we ask the question: Does intelligence relate to the level of spatial optimisation of the connectome? A spatial arrangement of regions closer to optimal could reduce the communication delays between regions, coinciding with the reported increases in reaction speed seen in subject with higher intelligence (Penke et al. 2012). Spatial features, in contrast to topological features, showed a much closer link with intelligence (Figure 4.33, Table C.3). Both PIQ and BD had significant positive correlations with the volume of the convex hull enclosing the network. Moreover, the total normalised wiring length (based on the Euclidean distance between regions) was reduced for subjects which scored highly on FSIQ, PIQ, BD and MAT. Total wiring lengths based on streamlines were also reduced in higher PIQ and BD scorers. In contrast, there were no significant correlations for $L_m$, but we did observe a significant reduction in $L_m$ in older subjects.

Next, we investigated the extent to which the spatial positioning of network components supported a shorter total wiring length, again treating the wiring length as the Euclidean distance between regions (with the correction of inter-hemispheric connections). We rearranged the spatial positions of regions to search for an arrangement which minimised the total wiring length of the network (using Algorithm 1). For all subjects, we were able to find a component placement which was closer to optimal with a total wiring length lower than that of the original network (Figure 4.34A), obtaining a mean reduction in wiring length of 10±2.5%. These reductions were possible due to the existence of long-range connections in the original network which were not present in the rearranged networks (Figure 4.34B); regions were positioned so as to shorten the lengths of long range connections. Compared with the maximal arrangement of regions (where the regions are positioned to maximise the wiring length), the wiring lengths of the connectomes were substantially closer to the minimised arrangements (mean relative wiring length = 0.11±0.03) (Figures 4.34C and 4.34D).

Subjects with greater age-adjusted PIQ, BD and MAT scores had lower relative wiring lengths (the original wiring lengths were closer to the minimised arrangements — Figure 4.33, CPO: Relative Wiring Length). The relative wiring length was also strongly negatively correlated with age. To provide an additional perspective of the differences

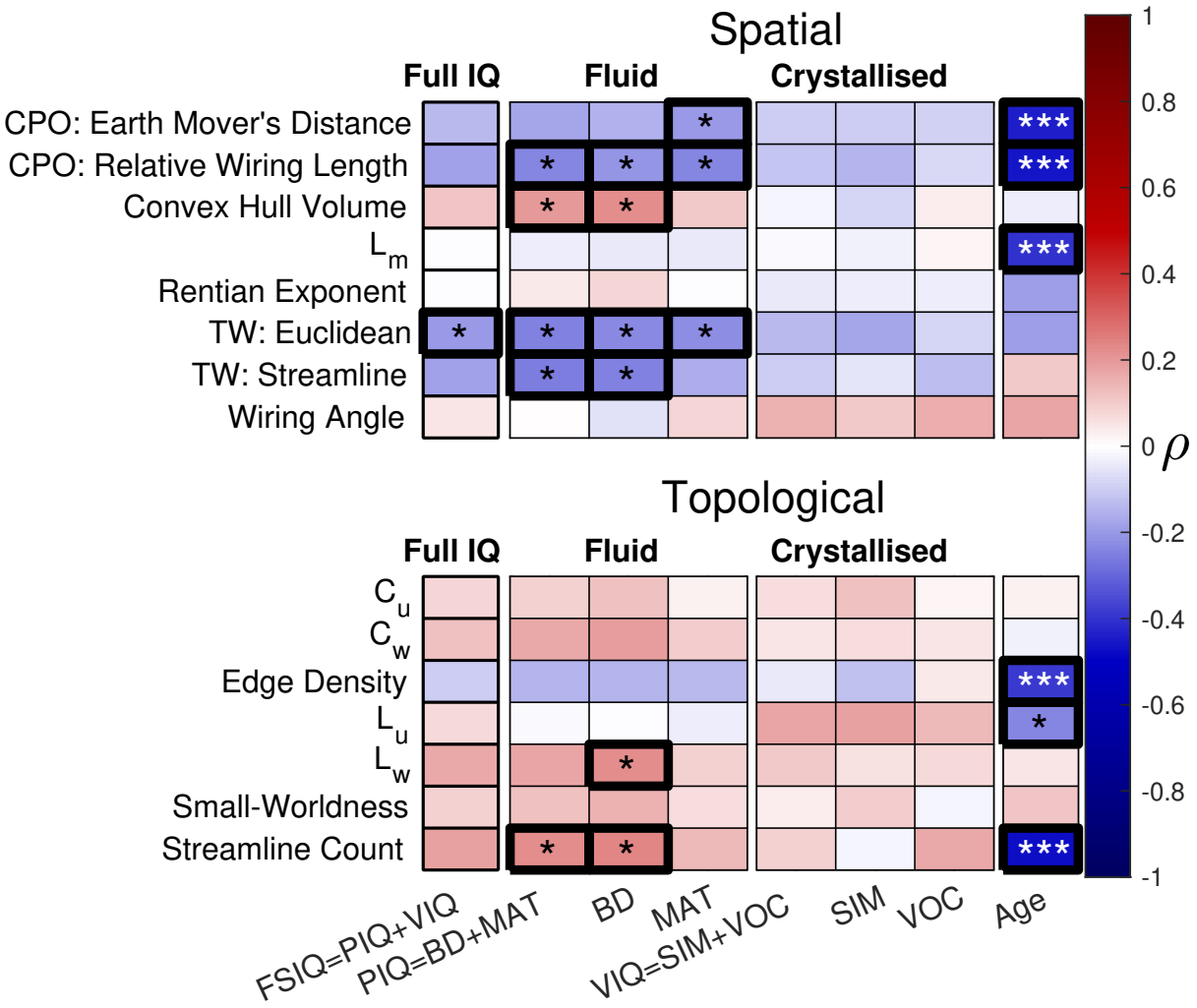


Figure 4.33: Spearman rank correlation ($\rho$) of WASI scores and spatial/topological network measures. Significant correlations are highlighted with bold rectangles and labelled: * = $P < 0.05$, ** = $P < 0.01$, *** = $P < 0.001$. $L$ = Characteristic path length. $C$ = Mean clustering coefficient. Subscripts u/w/m=unweighted/weighted/metric version of measure. TW = Total wiring length ('Euclidean' treats connections as straight, whereas 'Streamline' uses the mean streamline length following tractography). TW is normalised against the maximum Euclidean distance between regions. CPO = component placement optimisation (these measurements rely on comparing connectomes before and after swapping the positions of regions using Algorithm 1). Scatter plots for the significant correlations are shown in Figures C.1 and C.2

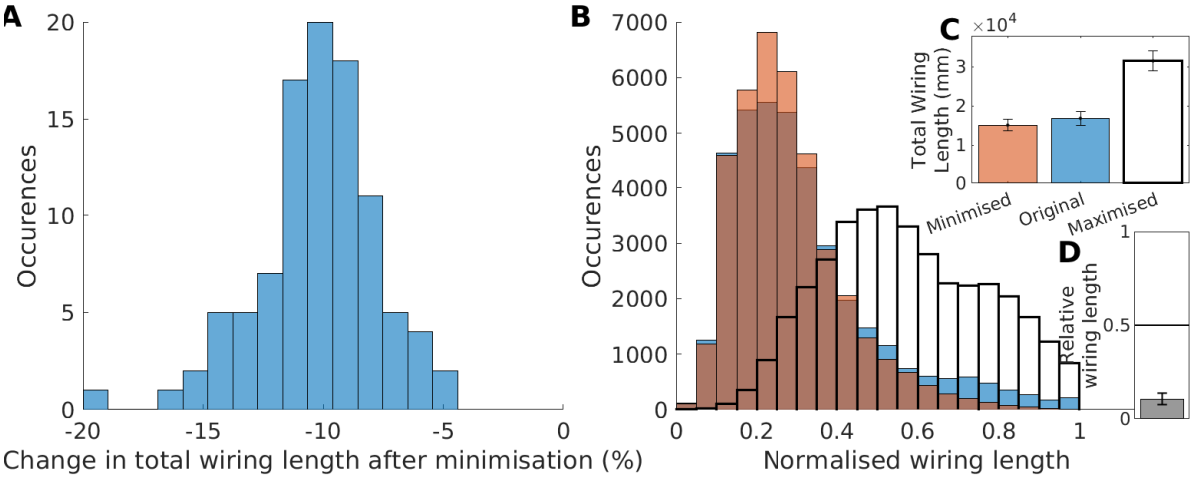


Figure 4.34: For the NKI dataset — Changes in the wiring length distribution before and after spatial arrangement to minimise the total wiring length. **A:** For all subjects, the percentage change in wiring length after arrangement into a minimised spatial layout (greatest reduction from 100 repetitions). For all subjects, we were able to reduce the total wiring length (-10±2.5%). **B:** For all subjects, the distribution of normalised wiring lengths, for the original (blue), minimised (orange) and maximised (transparent, bold) component placements. Long range connections disappeared in the minimised arrangements (wiring lengths are normalised against the maximum Euclidean distance between regions for each subject). **C:** The mean total wiring length for the original, minimised and maximised spatial arrangements. **D:** The mean relative wiring length over all subjects (0.11±0.03). Error bars = ±1 SD.

in the wiring length distributions, we also correlated intelligence scores with the Earth Mover's Distance (EMD) between the wiring length distributions of the original and minimised arrangements (Rubner et al. 2000). To calculate EMD, we used optimised MEX code provided by (Rubner et al. 2000). For the results in Figure 4.33, EMD is calculated as the mean distance over five bin sizes, consisting of normalised lengths from 0.05 to 0.25 in steps of 0.05 (see Table C.4 for the results for individual bin sizes). These lengths are normalised against the maximum Euclidean distance between regions in each individual network. To account for the different bin sizes when computing the mean distance, the cost of moving 'earth' from bin to another is weighted by the width of the bin — the cost of moving earth between wider bins is greater than for narrower bins. Combining both the total wiring length and EMD provides a more comprehensive assessment of the spatial layout of the connectome alongside the relative wiring length.

The EMD between original and minimised wiring length distributions was reduced for subjects with greater age-adjusted MAT scores (Figure 4.33, CPO: Earth Mover's Distance); the shape of the original wiring length distributions more closely resembled that of the minimised arrangements in these subjects. As was the case for the relative wiring length, EMD was also strongly negatively correlated with age. These findings suggest a spatial embedding of the network topology that is closer to optimal in subjects with greater fluid intelligence: a spatial arrangement which is closer to the optimal arrangement given the constraints of the network topology.

### 4.4.4 Angular changes in connectivity

Next, we looked at changes in wiring angles between connections, using this as a possible marker for the capacity for the connectome to broadcast information to spatially distributed regions. Because of the influence that wiring length has on wiring angle (Figure 4.35 — connectomes with longer connections generally displayed narrower angles between edges), and the significant relationship between wiring length and some aspects of IQ, we used the wiring angle residuals from a linear regression between wiring length and wiring angle in our comparison with IQ. Across the different IQ measurements, we did not observe a significant relationship with changes in wiring angle (Figure 4.33, wiring angle).

As the last step in analysing wiring angles, we compared the mean wiring angle against

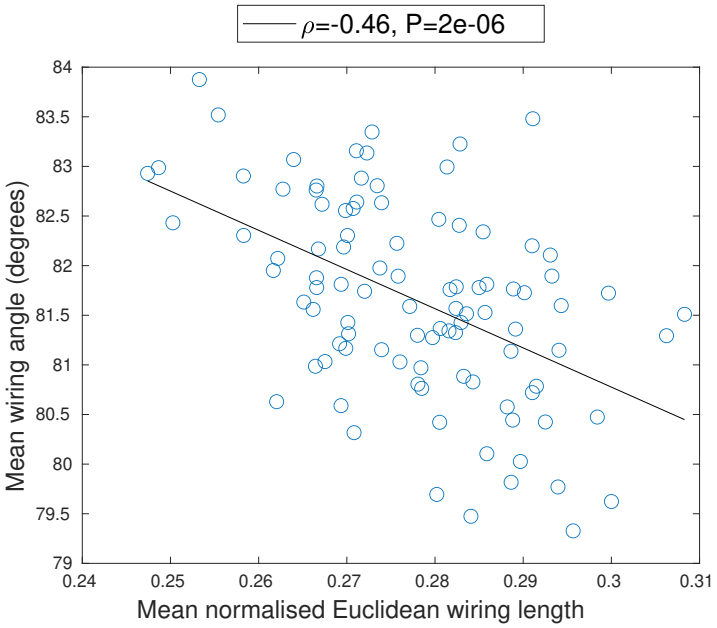


Figure 4.35: Comparing the mean wiring angles of subjects with the mean wiring length across all connections (normalised by the maximum Euclidean distance between regions, per subject). Greater mean wiring lengths were associated with reduced wiring angles ($\rho$ =Spearman rank coefficient correlation).

IQ on a region–by–region basis. For our comparison with IQ scores, we used the wiring angle residuals from a linear regression between the mean wiring angle between pairs of region connections, and the mean wiring length of the connections attached to each region. Across all intelligence scores, we did not observe a significant correlation with this 'node–level' wiring angle, after correcting for multiple comparisons ($P$ >0.05, Spearman rank correlation coefficient). Figure C.3 shows the correlations between wiring angle and PIQ/VIQ. This suggests that intelligence does not rely on changes in wiring angles for any particular region.

### 4.4.5 Spatial complexity of the connectome

We next assessed whether changes in intelligence coincide with the spatial complexity of the connectome, correlating the Rentian exponent with IQ scores. We calculated this Rentian exponent for all subjects. Networks exhibited a Rentian exponent of 0.85±0.06, slightly higher than that identified for previously analysed human connectome data ≈0.78 (Bassett, Greenfield, et al. 2010). When aggregating across all partitions/boxes for all subjects, networks produced a Rentian exponent of ≈0.86 (Figure 4.36). We did not observe a significant correlation between the Rentian exponent and IQ scores

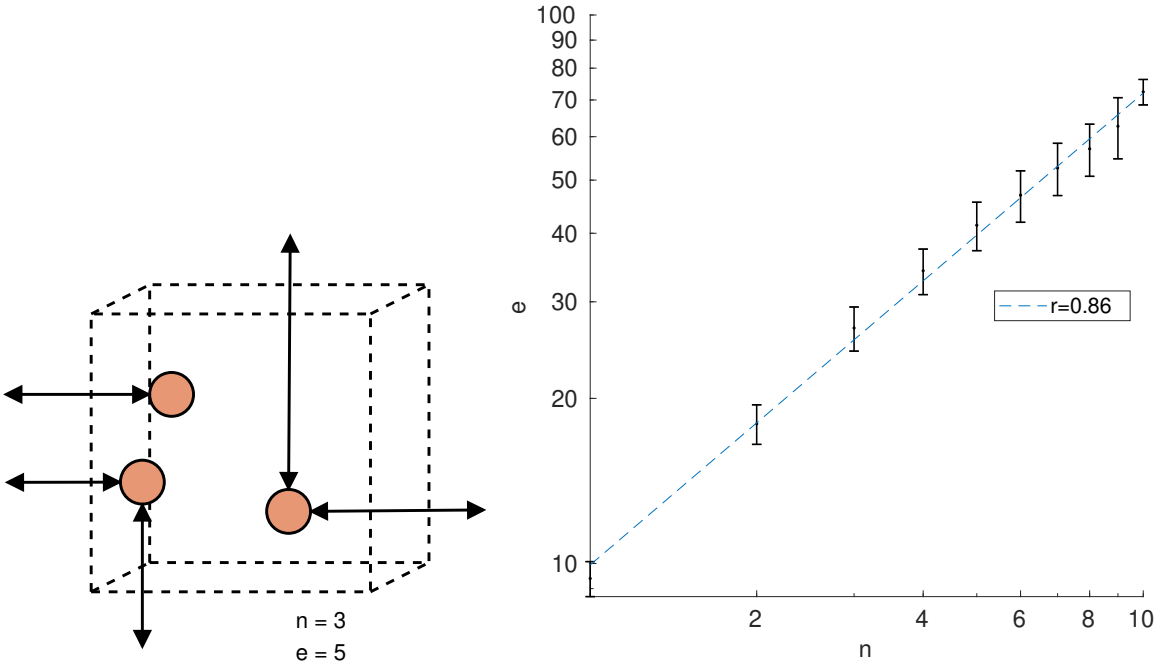


Figure 4.36: Approximating the Rentian exponent of the human connectome (by random arrangement of boxes of various size over the network). Shown is the relationship between the number of nodes/regions $n$ within a box and the number of edges/wires $e$ crossing the box boundary, for all connectomes. After fitting with a linear model, we obtain a mean Rentian exponent $r$ of 0.86. Error bars = $\pm 1$ SD.

($P$ >0.05, Spearman rank correlation coefficient). Additionally, we also calculated a normalised version of the Rentian exponent for each subject, using the Rentian exponents from 100 randomly rewired networks that preserved the degree distribution. Again, we did not observe a significant correlation with IQ scores (Figure 4.33, Rentian Exponent, $P$ >0.05), suggesting that connectome spatial complexity (as approximated by the Rentian exponent) does not vary with intelligence.

### 4.4.6 Comparing the connectome with reference networks

As an aside to looking at intelligence measures, we tested the hypothesis that a spatially sub-optimal arrangement of brain regions reduces the number of intermediate steps across the connectome. This hypothesis is driven by the findings in (Kaiser and Hilgetag 2006), and we extend this by applying similar techniques to the human connectome. We constructed three reference networks for each subject based on their connectomes, rewired to 1) minimise the total wiring length ('compact' networks); 2) maximise the total wiring length ('expanded' networks); 3) randomly reposition connections. By constructing these

networks, and comparing the network properties with the subject's connectomes, we attempt to identify the effect that rewiring has on network properties, and subsequently, whether connection length influences information transmission across the connectome. In these reference networks the edges are moved rather than the components. By doing so, we can test network properties in the extreme cases where connectivity is strictly minimised or maximised.

Compact networks started with a minimum spanning tree which minimised the sum of the Euclidean distance of connections (Boruvka 1926; Kruskal 1956). For the remaining edges, we iterated over each brain region and connected each region to its closest neighbour. For expanded networks, the inverse of the Euclidean distance between regions was used instead. For random networks, the wiring method made use of randomly shuffled Euclidean distances. The edge density for all three networks matched that of the corresponding subject network. These networks however do not maintain the topology of the original subject networks, and serve as extreme cases of wiring. For each reference network, we computed the unweighted clustering coefficient ($C_u$), the metric characteristic path length ($L_m$), the unweighted characteristic path length ($L_u$) and the total wiring length (TW).

The results of this analysis are shown in Table 4.4. Compared to original connectomes, compact networks displayed increases in $L_u$ and $C_u$, and decreases in $L_m$ and TW; rewiring to minimise the wiring length caused a decrease in the metric distance of the shortest paths between regions and increased clustering at the expense of increasing the number of intermediate steps between regions. Expanded and random networks displayed a reduced number of processing steps (approximated by $L_u$), and substantially reduced clustering and increased wiring length.

The observation that the original networks had a reduced number of intermediate steps between regions compared with compact networks suggests that, while the long-range connections in the original connectome increase the total wiring length, they also help to reduce the total number of processing steps between regions. Moreover, compared with expanded and random networks, the original networks showed similarities with the compact networks in terms of the mean unweighted clustering coefficient. From this, we infer that the connectome reduces the number of intermediate steps on shortest paths through long-range connections whilst maintaining clustered connectivity, features which

Table 4.4: Properties for original and rewired reference networks

| | Original | Compact | Expanded | Random |
|---|---|---|---|---|
| $L_u$ | 2.49±0.08 | 2.86±0.11 | 2.18±0.04 | 2.17±0.05 |
| $L_m$ | 83.2±3 | 77.5±3 | 181.4±7.3 | 100.1±3.8 |
| $C_u$ | 0.5±0.02 | 0.53±0.01 | 0.14±0.02 | 0.11±0.01 |
| TW | 28,673±2,735 | 20,970±1,953 | 76,316±6,263 | 47,823±3,940 |

*Note.* Values are mean±1SD. Edge density=0.12±0.01. $L$=Characteristic path length, $C$=Mean clustering coefficient, TW=Total wiring length (Euclidean, mm), $m/u$=metric/unweighted.

define small-world networks (Humphries et al. 2008; Watts et al. 1998). Note, however, that the degree distributions are not maintained in these compact/expanded/random benchmark networks. Instead, these networks served as simple examples of extreme cases of minimal, maximal and unconstrained wiring length.

### 4.4.7 Explaining changes in wiring length alongside metric path length

We found that for higher FSIQ and fluid intelligence scores the total wiring length decreased, yet no significant correlation was found for $L_m$ (metric path length) (Figure 4.33). Moreover, in our reference network analysis $L_m$ decreased for compact networks (metric path length) (Table 4.4). This suggests that 'auxiliary' connections — those which tend not to reside on the shortest paths between regions — are shorter in cases of high fluid intelligence. A *post-hoc* was conducted to test this hypothesis, checking whether edges with low edge betweenness (edges which infrequently appear on shortest paths, Brandes 2005, p. 31) had reduced wiring lengths in higher fluid intelligence subjects. We use the Euclidean distance along edges in the edge betweenness calculation, mirroring the calculation for $L_m$. Individually for each subject, edges were categorised into four groups each containing approximately 25% of the total number of edges in the network: edges with the lowest 25% edge betweenness (Q1), 25%—50% (Q2), 50%—75% (Q3), 75%—100% (Q4). To account for differences in the number of edges between subjects, the total wiring length in each category was normalised against the mean wiring length of the corresponding edge betweenness category (Q1 through to Q4) over 100 randomly rewired networks. Edge betweenness categories were calculated independently for each randomly rewired network. Randomly rewired networks preserved the degree distribution. The Brain Connectivity Toolbox was used to calculate edge betweenness (Rubinov and Sporns 2010).

This analysis revealed shorter wiring lengths only for edges with low edge betweenness (Q1) in subjects with high PIQ/BD/MAT scores (Figure 4.37), supporting our hypothesis that these auxiliary connections are shorter in higher fluid performing individuals. This explains the reduction in wiring length observed in these subjects, despite no difference in $L_m$.

### 4.4.8 Topological and spatial differences between sexes

To examine whether topological and spatial properties of the connectome differ between sexes, we performed the same topological (Tables C.5 and C.6) and spatial (Tables C.7 and C.8) analyses separately for females and males. Scatter plots for the significant correlations are shown in Figures C.4 and C.5 for females, Figures and C.6, C.7 for males. Interestingly, there were no overlapping significant connectome features (topological or spatial) against IQ scores when assessed individually according to sex.

Several topological correlations appeared for female subjects: increased weighted path length for higher PIQ, BD and MAT scores ($P$ <0.05); and a greater number of streamlines per connection on average for FSIQ, PIQ and BD, as well as for VOC ($P$ <0.05). For males, BD scores were positively correlated with weighted and unweighted clustering coefficient ($P$ <0.05), and small-worldness ($P$ <0.01).

Regarding spatial features in females, a larger convex hull volume was associated with greater PIQ ($P$ <0.05), while both a greater convex hull volume and Rentian exponent were associated with higher BD scores ($P$ <0.05). This correlation with the Rentian exponents indicates possible increased spatial complexity for females with greater age-adjusted BD scores. For males, the relative wiring length (calculated using the spatial arrangement of minimised and maximised networks) was lower (connectomes were more spatially optimised) for greater MAT scores ($P$ <0.05). Additionally for males, the total wiring length was shorter in cases of greater FSIQ ($P$ <0.05), PIQ ($P$ <0.01) and BD ($P$ <0.01) scorers, in addition to shorter streamline lengths in the connectomes of subjects with a greater BD score ($P$ <0.05).

When computing the EMD between the wiring length distributions of the original and minimal spatial arrangements over various bin sizes for each sex, we did not observe a significant correlation between any of the IQ scores and the EMD (Tables C.9 and C.10).

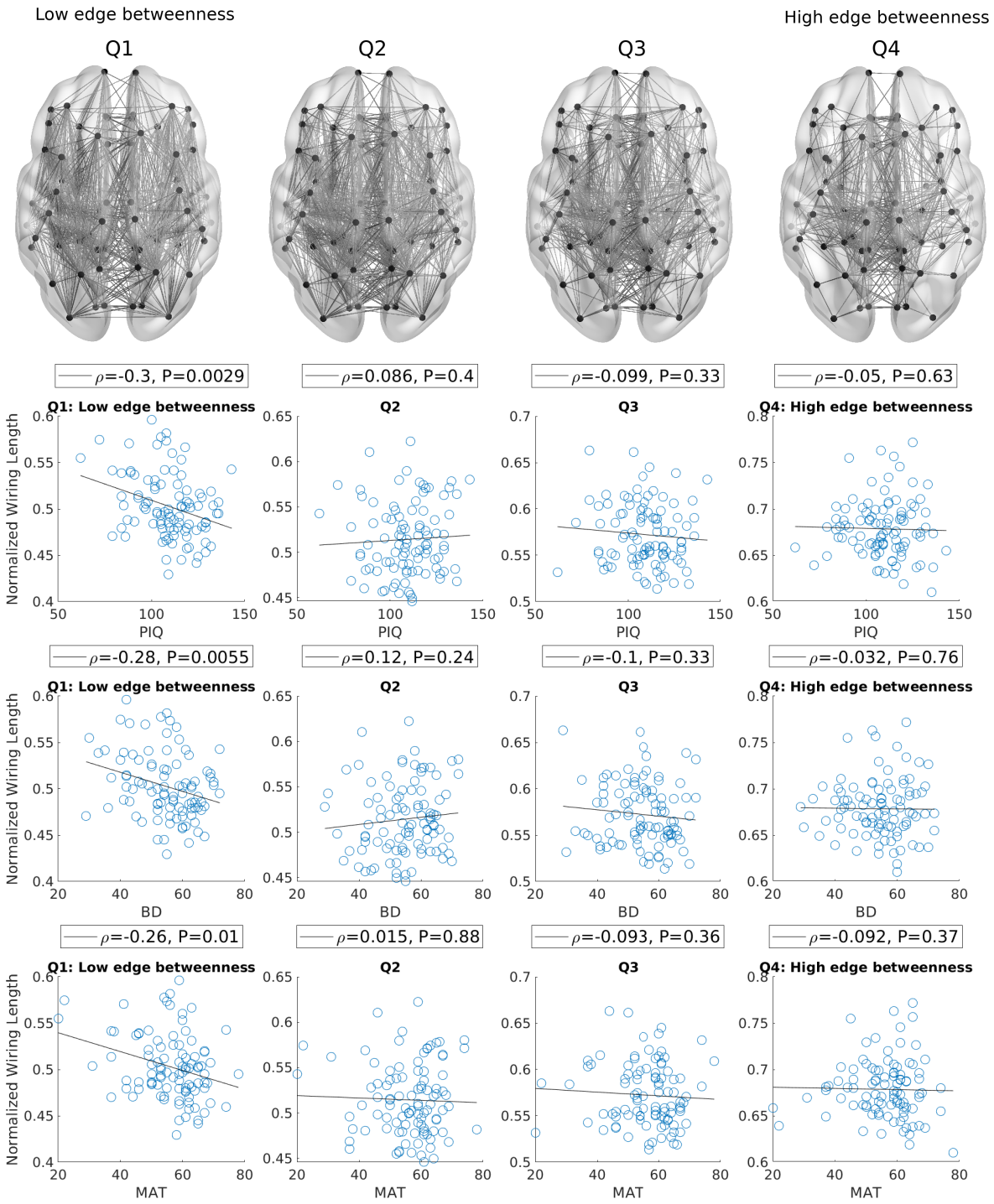


Figure 4.37: Spearman rank correlation between wiring length and fluid intelligence, grouped by edge betweenness. Edges were grouped into four categories: Q1 (low edge betweenness) to Q4 (high edge betweenness) for each subject, normalised against the wiring lengths of 100 randomly rewired networks. **Top row:** Axial view of the connectome showing the edges residing within each group, aggregated over all subjects. **Bottom rows:** Wiring length vs measures of fluid intelligence: performance IQ (PIQ), block design (BD) and matrix reasoning (MAT). Edges with low edge betweenness were shorter for higher fluid intelligence subjects (Spearman rank correlation, $P$ <0.05 corrected). Across all groups, no significant results were found when correlating with subject age ($P$ >0.05).

However, across all bin sizes, negative correlations were observed with age.

## 4.5 Differences In Relative Wiring Length Between Human Datasets

The relative wiring lengths varied across the three human connectome datasets (HCP: 0.45±0.03, schizophrenia: 0.14±0.01, NKI: 0.11±0.03). To investigate why this difference exists, we attempted to identify the network features affecting relative wiring length by using a simple linear model to predict the relative wiring length for all subjects across the datasets. We used as predictors 1) the edge density, 2) the mean and 3) the standard deviation of the normalised total wiring length before spatial rearrangement, and 4) the number of inter-hemispheric connections as a fraction of the total number of connections in the connectome. This latter feature was selected to explore the interaction between minimising the lengths of inter-hemispheric connections and preventing regions from moving between hemispheres during rearrangement (chosen to keep arrangements as biologically-plausible as possible); a greater number of hemispheric connections, as a fraction of the total connectome connections, may either hinder or enable greater reductions in wiring length during rearrangement. The four network features varied between the three datasets (Figure 4.38).

To gain an insight into the differences between the datasets, we constructed a multivariate linear model using the MATLAB `stepwiselm` function. This process iteratively adds each of the four network features to the linear model, preserving significant components ($P<0.05$). During model creation, we weighted each of the subjects such that each dataset contributed equally to the model prediction (the sum of weights within each dataset equalled one-third of the sum of all weights across all datasets). Results after concatenating these datasets and constructing the model are displayed in Table 4.5, and Figure 4.39.

When concatenating the three datasets together, several of the features were significant in predicting the relative wiring length within this linear regression model. Interaction effects contributed substantially, occurring between the fraction of inter-hemispheric connections and edge density/TW, as well as between TW and the standard deviation of TW; the effect of the fraction of inter-hemispheric connections on the relative wiring length depended on edge density and the initial wiring length, and a dependence also

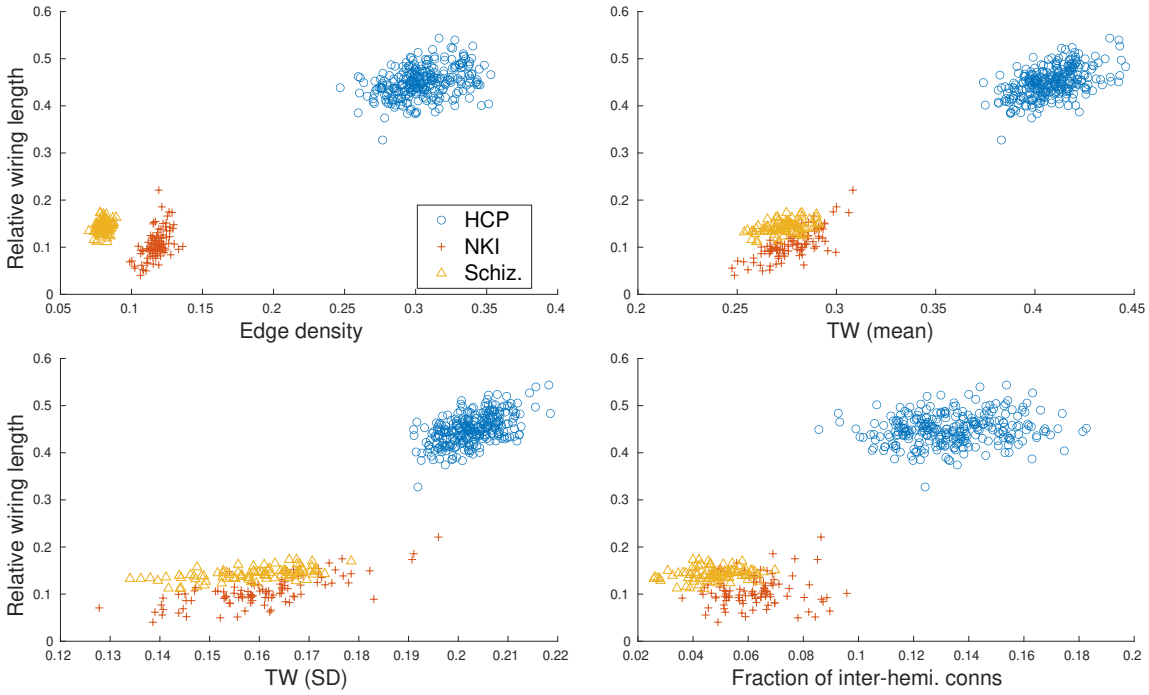


Figure 4.38: Relative wiring length versus network features across the three human connectome datasets. TW = Total wiring length (Euclidean, normalised against the maximum Euclidean distance between regions). SD = standard deviation.

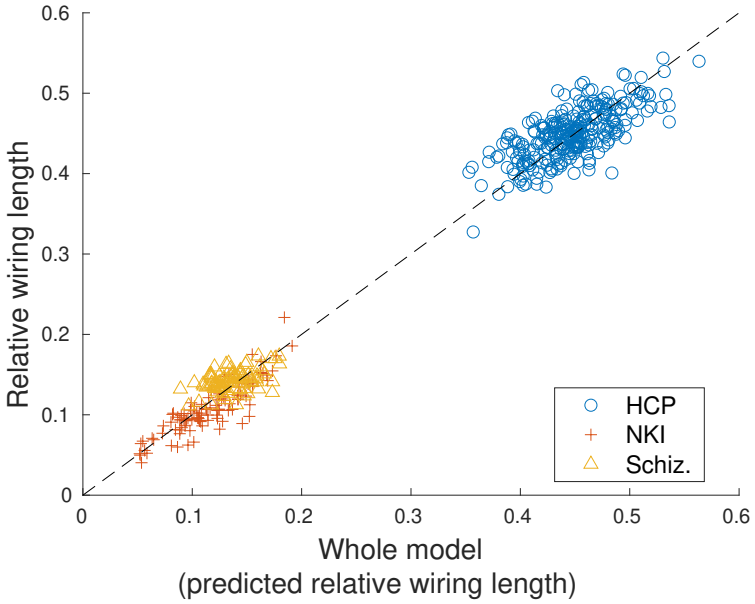


Figure 4.39: Relative wiring length versus the linear combination of network features using the combined three human connectome datasets.

Table 4.5: Model coefficients identified using step-wise regression of network features and the relative wiring length.

| Term | Estimate | SE | t stat | p value |
|---|---|---|---|---|
| (Intercept) | 0.12934 | 0.12441 | 1.0396 | 0.29906 |
| Edge density | -1.0744 | 0.15129 | -7.1019 | 4.7289e-12 |
| TW | 0.36996 | 0.45748 | 0.80871 | 0.4191 |
| TW (SD) | -5.7857 | 0.88094 | -6.5676 | 1.3902e-10 |
| Fraction of inter-hemi. conns. | 3.437 | 0.80397 | 4.275 | 2.3271e-05 |
| Edge density:Fraction of inter-hemi. conns. | 15.341 | 1.6743 | 9.1626 | 1.707e-18 |
| TW:TW (SD) | 23.151 | 3.0446 | 7.604 | 1.6413e-13 |
| TW:Fraction of inter-hemi. conns. | -24.438 | 3.1882 | -7.6651 | 1.0776e-13 |

*Note.* TW = total wiring length of all connections in a connectome (normalised between zero and one per connectome); TW (SD) = standard deviation of the initial wiring length of all connections in a connectome; SE = standard error.

existed between the mean and standard deviation of the initial wiring length. Fitting this model to the HCP, schizophrenia and NKI datasets individually explained 50%, 47% and 81% of the variance, respectively. For comparison, using TW alone explained 26%, 17% and 59%, respectively. While a more complex model may have explained more of the variance in the individual datasets, the simplicity of the model used here provides a simple perspective of the network features influencing the relative wiring length.

Greater values of all four connectome features contributed towards a larger relative wiring length in the HCP data; where relatively many connections existed, with many residing between hemispheres, and where the mean and standard deviation of their lengths were high, the rearrangement algorithm was able to reduce the wiring length by a greater amount, likely due to an increased number of long connections which can be leveraged for reduction. A greater number of edges is likely driving the increase in the other three features, with more edges reflecting the tendency for the tractography procedure to connect regions which are further away, and also those between hemispheres. A greater number of longer edges, many of which may be arranged close to parallel as they correspond to fibre bundles, may be providing opportunities for reducing the total wiring length in the HCP subjects.

Based on Figure 4.38, the cause of the difference in relative wiring length between the schizophrenia and NKI data is less obvious, however; the schizophrenia dataset displayed a greater relative wiring length compared with the NKI data (schizophrenia: 0.14±0.01, NKI: 0.11±0.03), while both had similar values of TW (schizophrenia: 0.274±0.009; NKI:

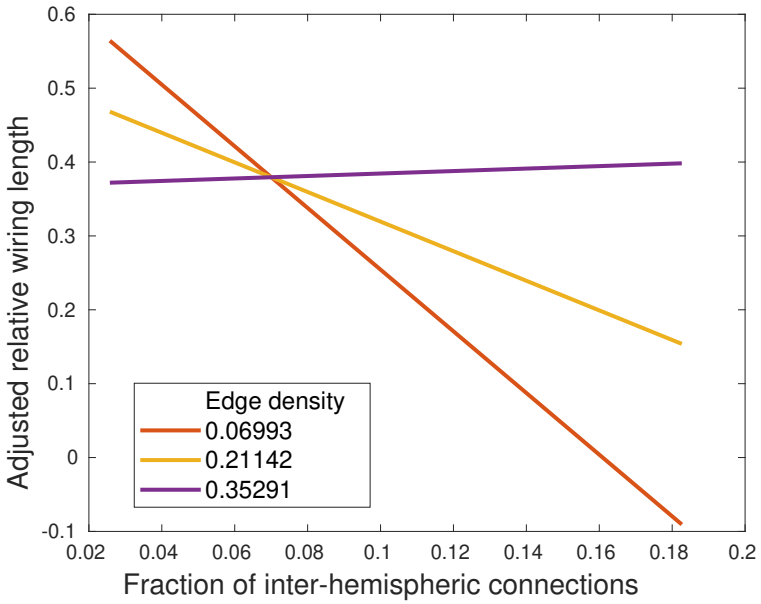


Figure 4.40: The interaction plot relating the effect of edge density and fraction of inter-hemispheric connections on relative wiring length. The fraction of inter-hemispheric connections has a negative effect on the relative wiring length for connectomes with a reduced edge density, becoming less negative for connectomes with more edges.

0.278±0.013). The interaction plot showing the effect of the fraction of inter-hemispheric connections alongside edge density explains this difference in relative wiring length (Figure 4.40). Compared with the schizophrenia data, the NKI dataset had a greater fraction of inter-hemispheric connections (schizophrenia: 0.048±0.0095; NKI: 0.062±0.012) and a greater edge density (schizophrenia: 0.080±0.004; NKI: 0.118±0.007). Considering that the edge densities for both datasets are relatively low compared with the HCP data, the interaction between edge density and the fraction of inter-hemispheric connections meant that an increase in the fraction of inter-hemispheric connections contributed towards a decrease in the relative wiring length in the NKI dataset (the algorithm struggled to find reductions); where, of the relatively few connections, fewer were intra-hemispheric, the rearrangement algorithm likely had to rely on reducing the wiring length of the usually much longer and more constrained inter-hemispheric connections. The constraint here manifested as fewer good options for placement for the end-points of inter-hemispheric edges — the reduction of the length of an inter-hemispheric connection required both end-points to move close to the centre of the connectome (due to the correction of inter-hemispheric connections through the centre of mass of the connectome), while for two end-points *within* a hemisphere they only need be close to one another to reduce the connection length, irrespective of their positions relative to the centre.

# Chapter 5. Discussion

In this study we explored the extent to which wiring in the connectome is optimised with respect to minimising the sum of connection lengths between all regions. For the macaque subjects, we found that the macaque connectome is sub-optimal in its spatial arrangement with respect to minimising the total wiring length. Also, we found evidence for the visual areas being particularly altered during rearrangement. Our results overall emphasise the presence of constraints in wiring configuration of the connectome, other than minimising the total wiring length.

Additionally, by analysing wiring length distributions and rearranging regions within the connectome, we provided evidence for the existence of a sub-optimal spatial placement of regions within the human connectome (identified in both the HCP and schizophrenia datasets). As noted in the HCP data, the presence of long-distance connections increased the total wiring length in the original networks, with spatially peripheral regions of the connectome being particularly sub-optimal in their positions. By simulating neural activity in the original and minimised arrangements, we identified differences in global dynamics between original and minimised arrangements; the presence of long-distance connections in the original connectomes, giving rise to sub-optimal spatial arrangements, significantly increases the levels of metastability within the brain. Using as a prerequisite the theory of communication through coherence as the mechanism for communication between regions (Fries 2015), the overarching result is that a sub-optimal arrangement may offer functional benefits by supporting bouts of integration and segregation, despite increasing the spatial and metabolic costs of the network.

Our observation of sub-optimal frontal lobe structure in schizophrenia subjects may be an underlying structural feature of the disease, disrupting functional integration with the rest of the network. This analysis provided a novel perspective into disorders of cognition and connectome structure, prompting further study.

When analysing connectome structure alongside intelligence, we identified several sig-

nificant, albeit weak, correlations between connectome structure and fluid intelligence scores. Many of these correlations were for spatial measures. Owing to this fact, this study emphasises the importance of considering *both* topological and spatial measurements when investigating the anatomical substrate of cognitive performance. It also highlights that fluid and crystallised intelligence are linked to connectivity in different ways: For some measures, a difference was observed only in performance IQ, block design and matrix reasoning scores, when considering all subjects. Between genders, the changes in correlations between fluid intelligence scores and spatial features suggests that males and females utilise alternative mechanisms of inter-region communication to solve novel problems. Overall, for this study, we have highlighted that higher fluid intelligence may be correlated with a brain region placement which is closer to optimal, and shorter wiring.

## 5.1 Spatial Arrangement of Regions Is Sub-Optimal In the Macaque Connectome

After performing a search over many possible spatial arrangements and maintaining the topology of the macaque connectome, we identified arrangements which reduced the total wiring length. In addition, the contribution to this reduction is not uniform across regions, with some regions displaying a greater wiring reduction than others. We then modelled the oscillatory activity in the connectome before and after rearrangement in an attempt to explore the implications of a spatially sub-optimal arrangement on dynamics. Our model suggests that metastability is affected by the spatial aspects of the connectome, although we were not able to conclude whether metastability increases or decreases under a spatially sub-optimal arrangement.

The macaque connectomes were found to have characteristic path lengths and clustering coefficients similar to that found for the CoCoMac data; short path lengths — in our subjects, fewer than two edges needed to be traversed to reach another region — enables swift communication between regions (Hagmann et al. 2008; Watts et al. 1998). As was also the case for the CoCoMac data, following rearrangement, we were able to reduce the total wiring length for all subjects. Longer connections contributed to the sub-optimal placement of regions, and may offer benefits in the form of allowing direct communication between regions, limiting the number of processing steps (Kaiser and Hilgetag 2006) and striking a balance between the maintenance of cellular material and delay of information

transmission (Budd and Kisvárday 2012). We found that the original wiring length of the macaque connectomes were closer to the minimised arrangements than the maximised arrangements (relative wiring lengths were less than 0.5), suggesting that, whilst being sub-optimal in their spatial arrangements, the wiring configuration of the connectome attempts, to some degree, to keep wiring lengths shorter rather than longer. The same conclusion was reached in (Kaiser and Hilgetag 2006) and in (Raj et al. 2011) for human connectomes.

The CoCoMac data is an aggregated dataset (based on more than 300 studies, representing the connectivity of over 300 monkeys), whereas our data are of individual connectomes. Our subjects displayed greater reductions in wiring length after spatial rearrangement compared with the CoCoMac data. This difference in wiring length may suggest that an aggregation of connectivity provides a less accurate representation of organisation — network features, present in the individual connectomes, could be missing after aggregating across many subjects. These differences may therefore emphasise the importance of analysing connectomes at the level of the individual, preserving the finer details of connectivity which may be lost when taking an average across many subjects. The shorter mean connection length in the CoCoMac dataset may have been a result of this aggregation process, biasing the preservation of shorter connections.

The mixture of wiring length changes across the connectome, with some regions showing a greater reduction than others, suggesting that spatial constraints on wiring may differ between regions. Visual areas experienced a substantial decrease in wiring length following minimisation, highlighting the sub-optimal placement of these regions in the connectome; the connectome contains direct connectivity from visual regions to distant areas of the brain, despite the increased spatial cost from long-distance connections. Visual areas are early to mature during development of the brain (J. Hill et al. 2010), and such an early maturation may prevent optimal connectivity to later developing regions, such as those in the frontal lobe. Prefrontal areas in the macaque also showed sub-optimal placement, albeit to a lesser extent that the visual areas. Long-distance connections from this area to other regions exist in the macaque connectome (Markov et al. 2013), and alongside visual areas, are sub-optimal in their positions with regards to the lengths of their connections to other regions.

Association fibres including the inferior longitudinal fasciculus and the optic radia-

tion consists of projections between the occipital lobe and more anterior portions of the brain (Takemura et al. 2017). Long-distance connections have been suggested to support information integration between distant regions (Markov et al. 2013). As was suggested by a substantial reduction in wiring length for visual areas following rearrangement, direct connectivity with anterior regions may be a priority for visual areas, supporting fast communication with regions such as the frontal eye field positioned in the middle frontal gyrus of the frontal lobe (Bullier et al. 1996; Schall et al. 1995). The frontal eye field is essential for controlling fast movements of the eye (saccades), allowing the image of an object to be brought to the fovea (Sharpe et al. 2005, p. 827). These saccades vary in speed and amplitude, ranging from 30–700 degrees/sec, and between 0.5° to 40° (Sharpe et al. 2005, p. 828), and may benefit from fast information transmission from posterior visual areas. Moreover, the connections leaving the parieto-occipital region and projecting to the dorsal premotor areas enables visual information to guide arm movements when grasping objects (Rizzolatti et al. 1990). Thus, fast information transmission between occipital and frontal areas may support timely attention of salient features in the environment, enabling fast corrections to arm movements when performing grasping tasks. These connections however were found to impart a high spatial cost on the network, emphasising their functional importance for the brain.

Regions closer to the centre of mass of the connectome were better positioned (showing reduced changes following rearrangement), suggesting that such regions make effective use of their central positions to connect to regions distributed throughout the brain. Such regions may rely on shorter connections to minimise communication delays, enabling faster information transmission and synchronisation through binding (Deco, Jirsa, et al. 2009; Fries 2015; von der Malsburg 1995). The increase in wiring length of some regions in the minimised arrangements implies that other regions were able to more effectively use these spatial position to reduce the total wiring length. The thalamus for example, connects to cortical regions in many different directions (Sherman 2006), the spatial location of which was often replaced with other regions which helped to contribute towards a total wiring length reduction (as shown by an increase in wiring length for regions PM and MDpc [mediodorsal nucleus]).

## 5.2 Spatial Arrangement of Regions Is Sub-Optimal In the Human Connectome

In addition to the macaque connectome, our work supports the findings of other studies (B. L. Chen et al. 2006; Kaiser and Hilgetag 2006; Raj et al. 2011) by suggesting that non-optimal component placement exists in the human connectome, in the HCP, schizophrenia and NKI datasets. As was also the case in our macaque analysis, we used the Euclidean distance between regions instead of real fibre tracts, which will not follow a straight line between regions. Again, our analysis did not account for alterations to the conduction velocity from changes in myelination, an aspect that future studies should consider (Budd and Kisvárday 2012). Nonetheless, long-distance connections contributed to the non-optimal wiring in the original placement, often attributed to connections between occipital/parietal and frontal regions (as was found in the macaque data). Long-range connections to frontal regions form part of the structural back-bone of the connectome, the so-called rich club, identified as a high-cost network in the brain (van den Heuvel, Kahn, et al. 2012), postulated to integrate information among regions (Senden et al. 2017). In both HCP and schizophrenia data, regions in the occipital lobe experienced the greatest reduction in wiring length. Thus, along with our previous analysis on the macaque data, our results for the human data lend support for a universal law of costly anterior-posterior connectivity across species, contrasting with suggestions of strictly minimised wiring in neural systems (Cherniak 1994). Our work makes progress towards understanding the extent to which wiring costs are minimised across species (Budd and Kisvárday 2012), suggesting that brains of vastly different sizes (humans, macaques, as well as *C. Elegans*) follow similar wiring principles in the sense that long-distance connections, while increasing metabolic and spatial costs, may be a fundamental component of connectome structure supporting uninterrupted communication between distant regions, avoiding processing steps (Kaiser and Hilgetag 2006). Building on the previous work exploring spatial structure of the macaque and *C. Elegans*, our findings for the human connectome provide further evidence for the existence of a universal 'blueprint' of connectome structure across animals.

In the minimised arrangements the connection lengths often decreased for most regions, suggesting an overall sub-optimal positioning of regions throughout the brain. This reduction however was dominated by connections emanating from spatially peripheral re-

gions, particularly from the lateral occipital, superior parietal and rostral middle frontal cortices. Maintaining direct connectivity to regions on the spatial periphery of the connectome appears to be a prominent feature present in the human connectome. In particular, the lengths of connections from the occipital lobe could be greatly reduced in the minimised spatial arrangements. This included anterior-directed projections, overlapping with the inferior/superior fronto-occipital fasciculus, the superior longitudinal fasciculus and the cingulum (Felten et al. 2015, pp. 342–344). This emphasises the deviation of these connections from the normal pattern of wiring, alongside other findings showing that anterior-directed long-range connections from the occipital lobe exhibit more streamlines than would be expected based on length alone (Roberts et al. 2016). The sub-optimal placement of the occipital lobe, given its connections, suggests a need for information to move uninterrupted to/from distant regions, despite the increased wiring costs. From an evolutionary perspective, the occipital lobe is comparatively old and may have to compensate for its position with the use of long-distance connections to regions that show greater changes during evolution such as the frontal lobe (J. Hill et al. 2010).

While reducing the length of connections may reduce the amount of resources needed for connection establishment and maintenance, the inclusion of longer connections could offer functional advantages by minimising the number of processing steps between regions (Kaiser and Hilgetag 2006). By reducing the number of processing steps, these long-range direct connections may support stronger integration (Samu et al. 2014), enable synchronous processing in near and distant connected regions (Fries 2015), avoid passing through regions with different function, and prevent information being altered when multiple intermediate regions are involved. Inclusion of long-range connections helps to reduce the path length, enabling small world topologies (Gong, He, et al. 2008) and reducing the energy required to transmit information throughout the connectome (Bassett and Bullmore 2006).

Our procedure of swapping the positions of regions is dependent on the parcellation used to divide the brain into regions. In our studies for the macaque and human, different cortical and subcortical parcellations were used. Structural differences, particularly the increased size of the frontal cortex in humans (consisting of 28.5% of the human cortex versus 11.3% in the macaque (Elston 2007, p. 218)), makes it difficult to justify using the same parcellation across species. Moreover, tractography procedures differed between

the two datasets, altering the connectivity represented in the adjacency matrices. The edge density in the HCP human subjects (≈0.30) was comparable to that of the macaque connectomes (≈0.28). However, the relative wiring lengths between the two species differed substantially (humans: 0.45±0.03, macaque: 0.25±0.02). Nonetheless, similarities occurred in the spatial arrangement of regions across the two species. Above all, both the human and macaque connectomes showed sub-optimal component placement — all subjects experienced a decrease in wiring length following rearrangement. In particular, visual areas in both species displayed sub-optimal spatial positioning, with connections emanating from visual regions towards the anterior parts of the brain being particularly costly. These connections ensure direct connectivity with frontal areas, and may support timely communication with the frontal eye fields, as mentioned previously.

For the schizophrenia and NKI datasets, we were able to rearrange brain regions to reduce the total wiring length for all subjects (the sum of all wiring lengths in the network). Findings for these datasets corroborates our previous findings, suggesting that the spatial arrangement of the human connectome is sub-optimal with respect to its wiring configuration. As shown in other species (Kaiser and Hilgetag 2006), long-distance connections contributed to the sub-optimal placement. Again, this wiring was closer to optimal than for the spatial placement which maximised the total wiring length (Figures 4.30, 4.34, B.7 and B.8). These findings suggest that the connectome attempts to keep the total wiring length low, aligning with our previous findings where the wiring length of the original arrangements was closer to that the of the minimised arrangements.

While the long-distance connections increase the wiring length, they reduce the number of intermediate steps on shortest paths (Kaiser and Hilgetag 2006) as suggested by an increase in the unweighted characteristic path length $L_u$ for the compact networks compared with the original networks (for the NKI dataset). When compared with the expanded and random networks, the relative similarity in the mean unweighted clustering coefficient $C_u$ for the compact and original networks (alongside a wiring length reduction of over 25% in the compact networks) suggests that the connectome reduces the number of intermediate steps on the shortest paths through long-range connections whilst maintaining clustered connectivity, features which define small-world networks (Humphries et al. 2008; Watts et al. 1998). This similarity in segregated connectivity suggests that the connectome encourages segregated processing among spatially localised regions, whilst

ensuring long-range connectivity promoting integration (Samu et al. 2014). Segregated connections ensure that communication occurs between functionally similar regions, enabling contextualised processing (such as within the context of visual processing), while longer connections promote timely sharing and processing in other contexts (such as moving visual information to regions like the frontal lobe that perform higher order processing, such as planning). As suggested in our previous studies, connectivity which supports this type of segregated and integrated connectivity may reduce the time taken to respond changes in the environment (Buckner et al. 2007; Deco, Jirsa, et al. 2009), with different connection lengths boosting metastable dynamics in the system. Pushing a system into a state of fluctuating activity levels may ensure sensitivity to external perturbations (e.g. being able to spot a hungry lion running towards you, out in the distance!) (Cavagna et al. 2010). Collectively, from our work, we reiterate here the importance of sub-optimal placement in encouraging advantageous brain dynamics from an evolutionary perspective.

## 5.3 Alterations In Metastability Between Spatial Arrangements for the Macaque Dataset

For the macaque dataset, we observed differences in the K/V parameter spaces between the original and minimised arrangements; similar metastability and synchrony was obtained at lower K/V values in the minimised spatial arrangements. Shorter connectivity reduces the conduction delay between regions, allowing for similar dynamics at slower speeds and strengths. This coincides with the reduced conduction velocity in animals with smaller brains (Swadlow et al. 2012). Between original and minimised arrangements, we were able to identify parameters which produced similar levels of synchrony between arrangements. However, when considering both frequencies (40 and 60Hz), our simulations provided inconclusive evidence for the effect of spatial layout on metastability. It may be possible that spatial properties have limited effect on dynamics, when compared to changes in topology (which was preserved for each subject in this study). Indeed, for humans, changes in the network topology by lesioning regions may alter metastable dynamics (Hellyer, Scott, et al. 2015; Váša et al. 2015), and a small-world organisation is thought to enable efficient information transmission throughout the brain (Bassett and Bullmore 2006). Relying on this dataset alone, it remains unclear the extent to which spatial factors influence dynamics, and subsequently, brain function.

The small sample size used in the macaque study limited the potential for conclusive results. Other limitations include approximating the lengths of connections based on the Euclidean distances, which is a clear departure from the real wiring length — the lengths of which will almost always be greater than that of a straight line — likely altering the influence of conduction speed in the model. Moreover, increased myelination might compensate for the length of long-distance connections and further reduce delays, features which were not considered in the model. Changes in the speed of transmission will almost certainly affect the changes in synchronisation between regions, and the extent to which the spatial positioning of regions influences bouts of integration and segregation. Future studies could therefore take into account differences in the level of myelination between fibres, axon diameter and the physical shape of each fibre tract to determine the presence of optimal wiring, and subsequently the extent to which the brain compensates for longer connections (Waxman 1977).

## 5.4 Alterations In Metastability Between Spatial Arrangements for the Human Dataset

For the human connectomes from the HCP dataset, the differences in metastability were more apparent between spatial arrangements when compared with the macaque subjects; we observed significant reductions in metastability in the Kuramoto model for the connectomes following spatial rearrangement. Previous studies have linked changes in delays between oscillators in the Kuramoto model with changes in metastability (Niebur et al. 1991; Shanahan 2010b). Wildie et al (2012) highlight an increase in global synchrony for smaller delays, and a peak in metastability at the boundary of high and low synchrony in the connectivity/delay parameter space. This peak in metastability was also noted in our parameter space, along with faster communication leading to greater global synchrony for a fixed coupling strength. In the same study, they noted the dependence on network structure and metastability, in particular the inclusion of both long- and short-range connections supporting complex metastable behaviour in their example models. Also making use of Kuramoto oscillators, Petkoski and Jirsa (2019) note the importance of heterogeneous time delays in shaping the functional dynamics within the connectome. Similarly, our model is a coarse-grained approximation of neural activation and communication, where a change in metastability following spatial rearrangement is likely influenced by homogenisation of the distribution of communication delays between

regions. In combination with previous findings, the inclusion of time-delay differences in the connectome appears to influence fluctuations in global synchrony. Not only do our results enrich previous studies which emphasise a causal relationship between network structure and dynamics, we also provide a novel link between the spatial organisation of empirically-obtained connectome structure with changes in oscillatory activity in the brain, highlighting that deviation from a spatially optimal configuration may promote fluctuations in synchrony reminiscent of healthy neural dynamics (Deco, Kringelbach, et al. 2017; Deco, Rolls, et al. 2009).

While reducing the length of connections may reduce the resources needed for connection establishment and maintenance, our model suggests that a spatially sub-optimal layout, one which includes long-range connectivity — in particular, emanating between frontal and occipital/parietal lobes — may offer functional advantages by supporting states of integration and segregation in the brain, features thought to be crucial for healthy brain function (Deco, Rolls, et al. 2009). These changing states of integration and segregation are represented by fluctuating periods of increased and decreased global synchrony in the system, a postulated mechanism of neural communication (Deco and Kringelbach 2016; Fries 2015). This interpretation about changes in metastability makes the assumption that synchronisation between neural populations is the mechanism by which groups of neurons communicate (Fries 2015). Under this assumption, and the finding that metastable dynamics enable phase-driven communication (Deco and Kringelbach 2016), we provide evidence to suggest that a sub-optimal arrangement enabling metastable dynamics facilitates communication between regions, enabling cognitive processes to interact.

Spatially sub-optimal connectivity between anterior and posterior regions could be driving much of the observed increase in metastability, aligning with the structural basis of the parieto-frontal integration theory (P-FIT) of intelligence (Richard J. Haier 2016, pp. 92–95). In this theory, structural and functional variables in the parietal and frontal lobes are coupled with intellectual performance, stating that communication between parietal and the frontal regions underlies problem solving, evaluation and hypothesis testing (Richard J. Haier and Rex E. Jung 2018, p. 221). In our analysis, connections between the rostral middle frontal and superior parietal regions disappeared in the minimised networks for almost all subjects, with the rostral middle frontal playing a vital

role in facilitating communication within the P-FIT network (Pineda-Pardo et al. 2016). Indeed, greater metastability is associated with greater performance on a range of cognitive tasks (Garrett et al. 2011; Hellyer, Scott, et al. 2015). As such, the long-range connections between anterior and posterior areas, those which are of a high spatial cost, may assist in problem solving by enabling activation fluctuations at a global level, aligning with structural and functional aspects described by the P-FIT framework.

At a more general level, the perceived effects of long-range connectivity coincides with the metastable dynamics of small-world networks which naturally consist of connections of different lengths (Watts et al. 1998; Wildie et al. 2012). This work also aligns with previous computational analyses which identify a reduction in functional diversity when long-distance connections are omitted from the connectome (Betzel et al. 2018). While other studies have highlighted the importance of network features such as clusters and hub nodes in supporting integrated and segregated activity (Sporns 2013), our results emphasise that spatial features may also contribute towards such dynamics (Fukushima et al. 2020; Seguin et al. 2018), and that minimising wiring length may actually be detrimental for healthy brain function. Metastable dynamics have been attributed to lateral regions of the connectome (Váša et al. 2015), not only aligning with our finding of the spatial influence on dynamics, but also with the sub-optimal placement of regions — those on the periphery of the connectome, further from the connectome's COM — increasing metastability. Indeed, regions on the edge of a network have the capacity to generate long-range connections to other regions. Perhaps activity on the spatial periphery of the connectome drives much of the metastable dynamics of the brain, as suggested by our findings.

The healthy brain operates as an unstable non-equilibrium system, moving through points of quasi-equilibrium in the phase space (Chialvo 2010), displaying peak levels of metastability (Deco, Kringelbach, et al. 2017). Heightened metastability reflects the outcome of two competing forces: independent versus dependent/coupled dynamics. In our simulations, however, the strongest correlation with empirical functional connectivity produced metastability levels far less than the maximum identified in the parameter space, conflicting with the theory that the brain operates at maximum metastability (Deco, Kringelbach, et al. 2017; Hellyer, Shanahan, et al. 2014). Our model is relatively simple compared to other more sophisticated and computationally demanding alternatives

(e.g. H. R. Wilson et al. 1972), and also makes several deviations from reality — such as approximating connection lengths as straight lines and applying the same underlying oscillation frequency to each region — which almost certainly would have affected the levels of metastability observed.

Nonetheless, by showing that a less spatially optimised arrangement displays greater metastability, we have provided evidence suggesting that the spatial arrangement of regions affects dynamics, and specifically, that a sub-optimal component placement may benefit dynamics by increasing global fluctuations, enabling processes such as task switching (Deco, Kringelbach, et al. 2017). From a survival perspective, it may then be advantageous for the connectome to have a spatially sub-optimal brain, in the sense of incorporating direct structural connections between distant regions, if such an arrangement enables flexible behaviour for operating in unpredictable environments that the animal is situated. In humans, more consistently correct and faster performers undergoing assessments of cognition displayed greater levels of metastability in their neural dynamics (Garrett et al. 2011), as well as in resting state networks during tasks that required fluid intelligence (Alderson et al. 2020).

In our model, heightened metastability may reflect model transitioning between states of segregated (independent) and integrated (dependent) processing, corresponding to moments of reduced and increased global synchrony, respectively. The global workspace theory of consciousness is a hypothesised high-level framework for how the brain processes information. The theory describes neural populations as processes, and bouts of competition between spatially distributed processes alongside moments of information being broadcast globally to all processes (Baars 2005). In this theory, the long-range connectivity observed in the connectomes may enable efficient broadcasting of information to distant regions, supporting integration. Such transitions between competition and broadcast may align with the notion of a metastable system — with competition reflecting a dynamic, partially synchronised state, and broadcast correlating with increased global synchronisation. This mechanism enables distributed processing and a collective response, a hypothesised core element of conscious processing (Shanahan 2008). Indeed, several theories of conscious processing refer to system transitions between integrated and segregated states, a prerequisite for maximising the system's information capacity (Oizumi et al. 2014; Tononi, Boly, et al. 2016). Increased metastability seen in sub-optimal compo-

nent placement may correspond to an increase in the range of unique patterns of activity, possibly representing an increase in the system's capacity to distribute and process information (Deco, Hagmann, et al. 2014).

Metastable dynamics can occur in systems which are undergoing phase transitions, on the boundary between order and disorder, also known as being in a 'critical' state. While systems displaying criticality are capable of exploring many different states — moving between metastable quasi-equilibria — it is important to emphasise that metastability can occur without a system being critical; metastability will be high in the trivial case where a system periodically moves between two states: complete synchronisation and complete desynchronisation, showing great variance in stability whilst being limited in its exploration of system states. However, such an extreme case is not observed in the brain, which instead consists of a diverse mix of transitions between segregated and integrated states over spatial and temporal timescales, coinciding with critical dynamics (Haldeman et al. 2005; Werner 2007). Thus, our finding that a spatially sub-optimal arrangement increases metastability may imply that such a network is better equipped to give rise to critical dynamics, displaying sensitivity to subtle perturbations in the environment and cascades of neural activation at many spatial scales, known as 'neural avalanches' (Beggs et al. 2003).

A final comment on metastability: Increased metastability in a spatially sub-optimal arrangement could represent an increased duration that information — in the form of bursts of neural activity — persists in the connectome: information is processed sooner by regions which are only a short distance away, whilst at the same time propagating — unprocessed — over long connections towards distant regions. Similar in nature to pipelining in semiconductor processors where initial and subsequent instructions are processed concurrently (J. P. Shen et al. 2013, Chapter 2), this temporal staggering of processing steps may increase the influence of a burst of activation throughout the connectome, promoting binding between distant regions (von der Malsburg 1995). Increasing the variety of information in the connectome at any given moment may support a broader exploration of system states, allowing the brain to reside in new functional configurations, possibly leading to greater fluctuations in dynamics and a more diverse repertoire of behaviours.

Regarding the development of the Kuramoto model, our efforts here to simulate global activity were made easier with the use of MATLAB MEX code to speed up the Kuramoto

model. Compared with the pure MATLAB implementation, a naive `for` loop implementation in MEX code required 70% less time to simulate the same biological duration. This speed up helped to reduce the time needed to explore the parameter space, involving many hundreds of simulations (especially so for the null-model). Figure A.9 depicts the differences in run times, as well as showing very similar mean synchrony between the two implementations, validating the MEX approach. The drawback with using MEX is the increased difficulty in building the model, relying on knowledge of the lower level language, C (Kernighan et al. 2006).

## 5.5 Wiring Optimisation In the Frontal Lobe Predicts Symptom Severity In Schizophrenia Patients

We identified reductions in edge density and streamline counts for subjects with schizophrenia, compared to controls. Reductions in the number of connections, and in the number of streamlines may have been caused by the enlargement of ventricles within the brain, reducing white matter volume (Steen et al. 2006). Despite evidence suggesting that subjects with schizophrenia have smaller total brain volumes (Steen et al. 2006), we did not observe a difference in brain size between groups as approximated by the convex hull of the connectome. The convex hull is only an approximation of total brain volume, as it does not account for concave areas of the brain caused by features such as the intersection between the anterior temporal lobe and the ventral frontal cortices. However, our observation that schizophrenia patients preserve a small-world organisation (as presented in Table 4.3, showing a small-worldness value greater than one, without a significant difference from controls) has also been reported in other studies (van den Heuvel, Mandl, et al. 2010). Some studies however have noted alterations in network efficiency in cases of the disease (Q. Wang et al. 2012), a difference not seen here; the influence of this particular choice of parcellation with a given spatial scale will likely affect our calculated small-worldness values Zalesky et al. 2010, and further analysis is needed, including making use of parcellations with a differing number of regions compared with the number used in our study.

In the schizophrenia patients, we found that subjects with less spatially optimised frontal lobe networks were more likely to have severe positive and negative symptoms. In these networks, changes in the spatially embedded topology partly explained symptoms

in patients. The similar mean wiring length across subjects (Figure B.11) suggests that the change in the relative wiring length (Figure 4.32) is less likely to be caused by additional long-range connections in cases of more severe symptoms, instead being driven by changes in connectivity to regions positioned at a similar distance away. The alterations in integration observed in other studies for subjects with positive symptoms may be explained by the presence of sub-optimal connectivity in the frontal lobe (Russell-Smith et al. 2010). Even though a trend of longer mean wiring existed for subjects with more severe positive symptoms ($P$ <0.1), no such trend was observed for negative symptoms which still presented spatially sub-optimal arrangements in more severe cases.

In light of our previous analysis on the HCP subjects, sub-optimal arrangements may increase activity fluctuations in the frontal lobe in subjects with more severe symptoms. While such a feature may be advantageous for *global* dynamics, it may instead hinder communication within or between other lobes if fluctuations are excessive *within* a localised cluster of regions. Excessive localised fluctuations may hinder binding with other areas of the brain (Fries 2015; Singer and C. M. Gray 1995), possibly leading to reduced functional integration globally (Lynall et al. 2010). Impairments in gamma power have been observed in the frontal lobe of schizophrenia patients (Minzenberg et al. 2010), suggesting functional dysconnection with other cortical areas. Reduced spatial optimisation within a localised part of the connectome may therefore disrupt information transmission with other areas, dysconnecting the frontal lobe from the rest of the brain. The frontal lobe is attributed to higher level cognitive processes and limiting its capacity to integrate with the rest of the brain may be a contributing factor of positive and negative symptoms, such as disorganised thought and a difficulty in forming abstractions. Unfortunately, functional connectivity was unavailable to assess this hypothesis, providing opportunities for future studies to simulate the changes in synchronisation between the frontal lobe and the rest of the network.

Our findings assume that metastability is beneficial for cognition, enabling task switching (Deco, Kringelbach, et al. 2017) and a timely response to external stimuli (Buckner et al. 2007; Deco, Jirsa, et al. 2009). It remains unclear whether excessive metastability at a more localised level within parts of the connectome (when compared with the level of metastability present in the network as a whole) has an undesirable effect on cognition. Such a state may disrupt synchronisation and thus communication between a cluster of

regions and the rest of the network (if one adopts the view that differences in the phase of neural oscillations underlies communication between neural populations (Fries 2015)). For instance, it is possible to imagine a situation where a cluster of regions is unwilling or too eager to leave its current attractor in the space of phase couplings, leading to impairment of synchronisation — and therefore integration — with the remainder of the network, or on the other hand disrupting local functional connectivity within the cluster resulting in hindrance to segregated processing, respectively. Thus, in addition to the mean global metastability occurring at any given time, the extent to which the brain is maintaining healthy cognitive processes may be a function of the variance in metastability within parts of the network consisting of several communication regions (corresponding, for instance, to entire lobes or their partitions). Further models of computational dynamics within and between clusters of regions may shed light on this question.

The increased relative wiring length in more severe cases of schizophrenia suggests a link between the disease and increased levels of metastability occurring in the frontal lobe. If parts of the network are not able to become functionally integrated with the rest of the connectome, binding of sensory information may be disrupted (Robertson 2003). Sub-optimal placement leading to excessive metastability may limit the duration of communication with other regions residing in other areas of the brain, interrupting information exchange by nudging dynamics from one attractor to another. These uncoordinated shifts in dynamics could make it difficult for different sensory modalities to bind together (von der Malsburg 1995). This dysfunctional mechanism could underpin hallucinations, with the brain unable to balance the level of metastability occurring globally and also at a more localised level within parts of the connectome (such as within lobes).

The *post-hoc* analysis involving spatial rearrangement of the frontal lobe was informed by known structural and functional alterations in the frontal lobe of schizophrenia patients (Minzenberg et al. 2010; Mubarik et al. 2016). However, as with any scientific study, the results must be treated with caution, especially so in this case as the data was altered (isolating part of the full connectome) before re-applying our statistical analysis. Nonetheless, this kind of analysis — observing the spatial arrangement of the connectome in the context of disease — may provide a new perspective on understanding disorders of the brain.

Regarding the spatial optimisation of connectivity of the entire connectome, we did

not see a difference between healthy controls and schizophrenia patients. Our results suggest that global changes in spatial optimisation are not an underlying feature of the disorder. The lack of difference between groups at the level of the entire connectome may suggest that structural abnormalities in schizophrenia are more localised, as suggested by our analysis of the frontal lobe. We did not observe a difference in the hub architecture between groups, contradicting the reported alterations in hub regions (Bassett, Bullmore, et al. 2008). However, these results will have been affected by the omission of the insula and thalamus from the connectome, and future work may involve the spatial analysis of the complete connectome. Additionally, accounting for aspects such as the duration and type of anti-psychotic mediation may alter our results (Ho et al. 2011), an approach which has been used when analysing structural and functional changes in schizophrenia (e.g. Minzenberg et al. 2010).

### 5.6 Shorter Wiring Lengths for Subjects With High Fluid Intelligence

Within the NKI cohort, concerning the application of the rearrangement algorithm and calculation of the relative wiring length, the spatially embedded topology of the network appears to enable a shorter total wiring length in subjects with higher age-adjusted fluid intelligence scores. Shorter connectivity was also identified in these subjects. Reductions in the total wiring length may reduce the delay of information transmission between regions (Innocenti et al. 2013), supporting faster reaction times (Penke et al. 2012) and synchronous processing facilitating binding (von der Malsburg 1995). Spatially optimised connectomes may enable efficient usage of brain resources in individuals which score highly in novel problem solving tasks (Richard J Haier, Siegel, et al. 1992). Reducing the communication delay between two regions may promote 0° relative phase synchronisation, a condition which has been associated with improved cognitive performance (Polanía et al. 2012). In our analysis of the HCP data, sub-optimal spatial arrangements were associated with increased levels of metastability. For the NKI data, component placements which were more spatially optimal were associated with greater fluid performance, with this kind of performance linked to *increased* metastability (Alderson et al. 2020). Perhaps there is a trade-off between maintaining reduced conduction delays between regions, whilst enabling metastable dynamics.

Despite the reduction in wiring length, we did not see a difference in the metric

characteristic path length $L_m$, $L_u$ or $C_u$ across fluid intelligence scores aligning with recent claims that for functional connectivity neither $C$ nor $L$ significantly correlate with general, fluid or crystallised intelligence (Kruschwitz et al. 2018). Altogether, this raises doubt whether small-world properties, whether for functional or structural connectivity, underpin intelligence. However, for male subjects, an association between higher BD scores and greater small-worldness was observed, suggesting a structural difference in fluid processing across sexes (Richard J Haier, Rex E Jung, et al. 2005; Ingalhalikar et al. 2014). Moreover, the greater volume of the convex hull in higher fluid scores aligns with other studies exploring brain size and intelligence (Pietschnig et al. 2015). And the increase in the weighted characteristic path length $L_w$ for high BD scorers suggests a greater number of streamlines within localised clusters of regions. This claim is supported by the mean weighted clustering coefficient $C_w$ showing the strongest correlation with BD ($\rho$=0.19, Table C.2). Alterations in streamlines counts (greater streamline counts for high PIQ and BD scorers) could be explained by increases in the white matter integrity *within* the right hemisphere for higher fluid intelligence (Kocevar et al. 2019).

Auxiliary connections were found to be shorter in higher PIQ/BD/MAT scorers, inferred from our edge betweenness analysis, reconciling the shorter wiring but unchanged metric characteristic path lengths 4.37. These shorter auxiliary connections may reduce communication delays within clusters of regions, supporting more efficient segregated processing. Segregated processing is thought to be a core component of performance in the BD test (Stewart et al. 2009), and our results suggest that this kind of supporting connectivity is a core component of fluid capacity.

We did not identify a correlation between the IQ scores and the mean wiring angle taken between all pairs of connections attached to a single region, nor when any single region was observed in isolation. This finding suggests that a given region on average connects with other regions that are similarly spatially distributed irrespective of intelligence. In turn, this may suggest that the extent to which communication can take place between these spatially dispersed regions, and subsequently the extent of information propagation between them — using direct connections which bypass intermediate processing steps — may not be a key determinant of intelligence within the human connectome.

In our analysis of spatial arrangement — and as was the case for the previous macaque and HCP studies — we do not consider the actual physical trajectory of white matter

connections between brain regions, instead modelling connections as straight lines. Physical fibre tracts, due to cortical folding, interfering tracts, and the space occupied by cortical and subcortical structures will often be longer. Differences in the size of brain regions when they are swapped was also ignored for this dataset. However, owing to the complexity needed to build a model which reshapes the 3D trajectory of fibre tracts as regions are moved, we used the current approximation as a starting point for analysing spatial features in the context of intelligence.

Many of the observed correlations were relatively weak, which, alongside the quantity of correlations performed, prompts the need for caution when drawing conclusions on the link between spatial/topological structure and intelligence. Given restrictions such as the use of a single parcellation, and a single collection of tractography parameters, our results could not refute the hypothesis that the significant correlations listed here are not associated with intellectual ability. Euclidean distances used as connection lengths undermine conclusions which refer to changes in wiring length following spatial rearrangement, as these are approximations of the real wiring length. Moreover, the limited variety of tests used to measure crystallised and fluid intelligence makes it difficult to find conclusive evidence which links fluid or crystallised intelligence generally to structural features. Naturally, the limited sample size, and the choice of imaging resolution places further restrictions on the robustness of the findings in this study. As emphasised by Haier (2016, p. xiv): no story about the brain is simple, no one study of the brain is definitive, and many studies are needed before a weight of evidence can be obtained on the truth about brain structure and function.

### 5.7 Connectome Differences Across Age and Sex

Between sexes in the HCP data, we observed significant differences in the edge density and mean wiring length (normalised by the maximum wiring length per subject) (Table 4.2). The difference was small, however, with females showing a 3% mean increase in edge density and a 1% mean increase in wiring length over males. Alterations to the tractography parameters will certainly have an effect on these results, and smaller brain sizes will likely make it easier for streamlines to terminate in grey rather than white matter. Nonetheless, our results coincide with observed differences in connectivity between sexes (Gong, Rosa-Neto, et al. 2009). The longer normalised connection lengths in females may be due

to reported increases in inter-hemispheric connectivity (Ingalhalikar et al. 2014).

Alongside the longer normalised connection lengths and increased connectivity in females, the lack of significant difference in the relative wiring length between sexes implies similar spatially sub-optimal connectivity between sexes, and where the additional connectivity in females does not support wiring configurations that are closer to optimal. Similar levels of optimisation were also found in both age groups, specifically that sub-optimal wiring persists across age, albeit across the rather limited age range used in this study.

For the NKI dataset, several network measures were found to significantly correlate with age. The observed decrease in edge density and streamline count in older subjects likely reflects a change in white matter volume, which tends to decrease into old age (Lim et al. 2013; Sullivan et al. 2006). Despite a reduction in the edge density in older subjects, the edges that remain are those which enable short paths between regions, indicated by reductions in $L_u$ and $L_m$. Moreover, the reduced relative wiring length and EMD in older subjects is likely caused by the lower edge density, enabling less restrictive optimised placement of regions (this correlation was also identified in the HCP dataset — Figure B.1).

While we identified correlations between spatial features of the connectome and fluid intelligence, our findings indicate that fluid intelligence may depend on different spatial structures of the connectome between sexes. Although many of the correlations were relatively weak for the NKI dataset, some stronger correlations existed for male subjects, in particular a greater small-worldness ($\rho$=0.38, P<0.01) and shorter wiring length ($\rho$=-0.43, P<0.01) in higher BD scorers. Interestingly, greater BD performance was linked to a greater weighted and unweighted clustering coefficient in males, emphasising the potential involvement of segregated processing whilst performing this test, as noted in cases of autism (Stewart et al. 2009). Differences in connectome structure and function have been observed between sexes (Chiêm et al. 2018; Gong, Rosa-Neto, et al. 2009; Jiang et al. 2019; Tomasi et al. 2012), and our findings indicate a tentative distinction between sexes in the mechanisms that underpin intelligence — the association of increased small-worldness values, shorter wiring lengths and clustered connectivity loosely implies a reliance on combined information integration and segregation when males solve novel problems. Males and females are thought to use their brains differently when addressing

problems, achieving similar levels of intellectual performance when doing so (Richard J Haier, Rex E Jung, et al. 2005; Richard J Haier, Siegel Jr, et al. 1988). Perhaps the structural elements with which females use to address fluid tasks are not captured by our course-grained connectomes. Indeed, DTI has numerous limitations (Jbabdi et al. 2011), and alternative parcellations and tractography parameters will subsequently change the structure of the connectomes and possibly downstream results.

It is also important to note the possibility of within-sex differences regarding how brains solve problems (Deary et al. 2010), and that our results could have been influenced by variations within the sexes. Also, our findings may change if we had used subjects from a different distribution of age or IQ scores — our sample had a greater number of younger subjects than older. Nonetheless, from an evolutionary standpoint, it seems plausible that differences in cognitive processing between males and females would be selected for, with each gender contributing a different perspective when both are faced with the same problem, widening the repertoire of skills needed to address novel challenges throughout our evolutionary past. Our findings prompt the need for further studies with larger numbers of male and female subjects, and a greater range of intelligence scores. Our results also emphasise that future studies should consider sex differences when attempting to identify structural correlates of intelligence (Richard J Haier, Rex E Jung, et al. 2005).

Taken together, spatial and topological correlates of intelligence may differ between sexes, a finding that will benefit from larger sample sizes and different imaging parameters producing alternative connectomes; these findings are far from decisive, and are highly dependent on the image processing parameters and methods used to build the connectomes. Our results in this aspect are not conclusive, and future work may elucidate any potential differences in connectome structure between age and sex.

## 5.8 Differences In the Relative Wiring Length Between Human Datasets

Using a linear model, we found dependencies between the relative wiring length and several connectome features (edge density, mean/SD of the total wiring length and the fraction of inter-hemispheric connections) which partly explained differences in the relative wiring length among the three human connectome datasets. In addition to the initial total wiring length, the interactions with the inter-hemispheric connections suggests that this

aspect of the connectome has a substantial effect on the performance of the rearrangement algorithm. Differences in the lengths of connections, including the proportion of inter-hemispheric connections, depend on image quality, and on the tractography parameters/techniques used to construct the connectomes. For example, reducing the maximum turning angle during streamline creation will likely reduce the length and number of connections. Using different imaging parameters and performing spatial arrangement using alternative high/low resolution parcellations may lead to changes in the relative wiring length. The calculation of a 'mean' relative wiring length for individual subjects might be possible in such a scenario, and may provide a better estimation of the actual spatial optimisation in the connectome. And of course, the parameters used in our simulated annealing algorithm will influence the resulting spatial arrangements. Nonetheless, by combining the three datasets and applying a linear model, we have attempted to identify patterns in the structural differences between datasets, partly explaining the contrasting relative wiring lengths. Moreover, either all (for the schizophrenia and NKI datasets) or the majority of subjects (94.6% of the HCP dataset) across the three datasets exhibited relative wiring lengths that were below 0.5, supporting the claim that the spatial arrangement of regions and their connections within the human connectome is closer to optimised compared with being maximally sub-optimised, despite their structural differences.

# Chapter 6. Conclusion

The relationship between the structure and the function of the brain is as on-going area of research. In this thesis, we contributed towards this endeavour by exploring the structure of the human and macaque connectomes. Using an algorithm to rearrange the spatial positions of connectome regions, a dynamical model of neural oscillations and several connectome datasets, we investigated how structure influences dynamic aspects of the brain, the link between connectome structure and intelligence, and how alterations in connectivity might explain symptom severity in schizophrenia. Here we consolidate the key findings, and mention avenues for further work.

Across the several datasets used in this study, we looked at the spatial arrangement of brain regions in the connectome. We applied computational search techniques to assess the extent to which the spatial layout of components in the connectome are optimised with respect to minimising the total wiring length. For the macaque and human connectome project data, we also constructed a dynamical model, capable of simulating inter-region communication, so as to gain an insight into the dynamics that manifest from the particular spatial arrangement of cortical and subcortical regions.

For the macaque dataset, our results reiterated previous findings showing that the macaque connectome is sub-optimal in its arrangement with respect to minimising the total wiring length (Kaiser and Hilgetag 2006). By swapping the positions of regions, we were able to reduce the total wiring length of the macaque connectome for all four of our subjects. Long distance connections contributed towards the sub-optimal placement of regions, and variations in wiring length reductions at the region level highlighted that visual areas are particularly sub-optimal in their positions with respect to minimising the wiring length. Areas on the spatial periphery also displayed sub-optimal placement — subcortical and auditory areas, which were particularly close to the centre of the connectome, showed minimal change between arrangements, highlighting their optimised wiring layout to other regions in the macaque connectome. Our modelling attempt showed

changes in the dynamics between arrangements, although further study is needed using larger sample sizes to draw meaningful conclusions with respect to this part of our analysis.

For the human connectome project data, we found that the arrangement of the human connectome does not minimise the total wiring length — for all human connectome project subjects, the locations of brain regions could be swapped to reduce the total wiring length. Instead, the connectome allows for specific long-distance connections, in particular fibre tracts connecting frontal and occipital/parietal regions. These connections, involved in non-optimal component placement, may increase integration and segregation within the connectome, increasing the spatial and temporal influence of information throughout the brain.

Our ability to identify a spatial arrangement of regions which is closer to optimal in the human dataset coincides with that of the macaque connectome, suggesting that a universal rule of spatial arrangement exists across mammalian species. This rule takes the form of incorporating long distance connections in the connectome to reduce the number of processing steps, ensuring direct connectivity with visual areas despite the increased spatial costs, areas which are older from an evolutionary standpoint. Our results with the large HCP sample contributes towards an understanding of the effect of spatial arrangement on the dynamics of the brain, stating that a sub-optimal component placement increases metastability in the brain system. Despite the increased wiring cost, a sub-optimal arrangement may be beneficial for maintaining activity which supports flexible communication between regions, and subsequently improved cognitive processing performance (Deco and Kringelbach 2016; Fries 2015; Hellyer, Scott, et al. 2015; von der Malsburg 1995). The connections implicated in the sub-optimal arrangement aligned with those that link regions within the P-FIT theory of intelligence, and may underpin cognitive ability by increasing flexible dynamics at a global level. Perhaps minimisation of the wiring length of the connectome is one aspect of our anatomy that evolution does not pursue, instead opting for the inclusion of longer connections to enable greater fluctuations in global neuronal activation, ultimately designing a brain that is more functionally flexible and adaptable at dealing with an unpredictable world.

Our finding that a sub-optimal spatial arrangement affects metastability informed the suggestion that sub-optimal functional connectivity between the frontal lobe and the rest of the connectome may explain symptoms seen in schizophrenia (Lynall et al. 2010;

Minzenberg et al. 2010). Specifically, our work suggests that excess metastability at a local level may hinder temporal binding with the rest of the connectome (von der Malsburg 1995), leading to frontal lobe dysconnection. Scope exists for future studies to simulate functional connectivity between frontal areas under different spatial organisations, assessing changes in metastability within the frontal lobe and the rest of the connectome.

Which structural features of the connectome are associated with greater cognitive performance? Using measurements of intelligence, we made several discoveries linking spatial and topological features of the human connectome with cognitive abilities. Regarding the analysis on connectome structure and intelligence, Figure 6.1 provides an overview of the spatial features which were found to correlate with measures of fluid intelligence across the NKI subjects. Our work contributes towards an understanding of the structural properties of the connectome and cognition. Measures involving wiring lengths were significantly correlated with fluid but not crystallised intelligence. These spatial measures were more informative than standard topological measures, giving rise to several significant correlations with IQ scores. For subjects with higher fluid intelligence, our results strongly suggest that structural connectivity allows faster information transmission through shorter wiring lengths, particularly within segregated clusters of regions (as suggested by the differences in wiring length changes across the edge betweenness categories). A spatial arrangement of regions which is closer to optimal in higher fluid intelligence provides evidence for efficient routing of information between processes. Moreover, we find several reasonably strong correlations for males when comparing spatial and topological features with intelligence (for higher performers — primarily in block design — a greater small-worldness, clustering coefficient, and shorter connectivity), correlations which suggest a difference in the connectome structure that underpins fluid processing between sexes (Stewart et al. 2009). This work provides a starting point to study the link between the spatial connectome organisation — influencing the delays for information propagation ('delayome') — and cognitive performance.

Overall, our results contribute towards our understanding of the spatial constraints imposed on wiring in the connectome, and the trade-off between wiring cost and the need for direct communication between regions.

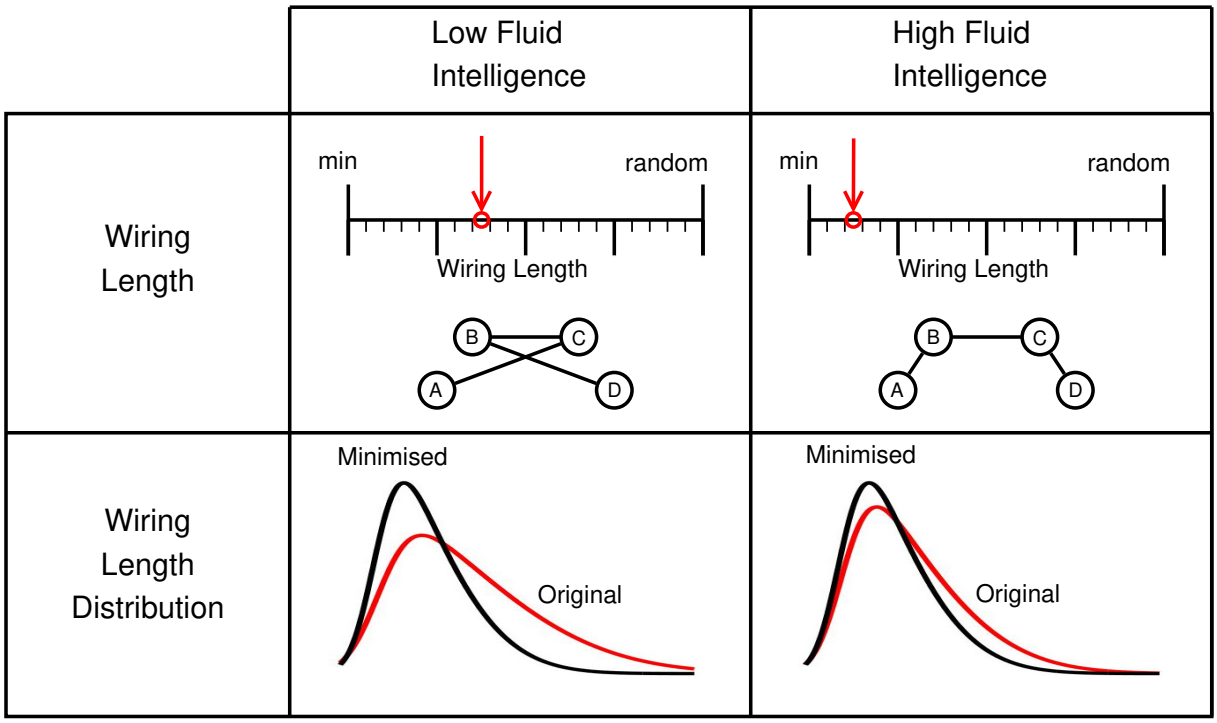


Figure 6.1: Summary of the spatial features which were found to correlate with measures of fluid intelligence. Compared with low fluid intelligence, our results suggest that for subjects with high fluid intelligence: the spatial embedding of the network topology supports a reduced total wiring length, and a closer match of the wiring length distribution between the original and minimised spatial arrangements, as suggested by the earth mover's distance metric.

**Spatially sub-optimal arrangements of the connectome across species**

Relying on a search heuristic allowed us to test the hypothesis that the spatial arrangement of regions in the brain is sub-optimal with respect to minimising its wiring length. Using a simulated annealing search routine provided a means to find spatial arrangements which reduced the total wiring length of both the human and macaque connectomes. This work supports the claims made by others regarding the spatial arrangement of the brain (Kaiser and Hilgetag 2006), and further emphasises the presence of other constraints on connectome structure, rather than minimising the wiring length (Cherniak 1990, 1994). Our findings align with the hypotheses that connectivity supports direct communication, reducing the number of intermediate processing steps between regions. This work provides a foundation for further work exploring the link between connectome spatial organisation and cognitive performance, emphasising the influence of conduction delays for information propagation — the "delayome" of the brain.

Diffusion imaging is not without its limitations (Jbabdi et al. 2011), including proper delineation of fibre tracts in the presence of branching and crossing fibres. Our work is very much reliant on the pipeline and parameters that we selected during the image processing stages. When processing the HCP dataset, we decided on a number of parameters primarily based on those used in the literature (Hutchings et al. 2015; Lim et al. 2013). Such parameters include the streamline angular cut-off, and the total number of streamlines generated per subject. The edge density of generated adjacency matrices is particularly sensitive to parameters used in the tractography process, which in our case was performed using DSI-Studio. A bias against identifying long fibre tracts also interferes with the creation of a representative connectome, one which accounts for short and long distance connections (Reveley, Seth, et al. 2015). The lack of directionality of the identified connections also limits modelling attempts, although major fibre bundles — particularly cortico-cortical — contain roughly equal numbers of connections in both directions (Schmahmann et al. 2009, pp. 420–460). Moreover, the presence of false positives — streamlines representing non-existent fibre tracts — is always of concern, although attempts have been made in this study to reduce these (Yeh, Panesar, et al. 2019). As a result, the inferences made based on connectivity obtained from streamline tractography must be treated with caution. Our conclusion that metastability is increased in the sub-optimal arrangement would greatly benefit from further studies making use of the

human connectome. Should time have permitted, additional analysis on our HCP dataset with alternative imaging parameters may have supported our findings (using a mixture of maximum turning angles for the streamlines, for example).

**Pressures of occipital lobe connectivity on spatial arrangement**

In both human and macaque datasets, we noticed that regions in the occipital lobe were positioned in a particularly sub-optimal location, when considering their connections to the rest of the brain. Many of these connections projected to the frontal areas, including prefrontal cortices. The ability for the occipital and frontal cortices to communicate with minimal delay appears to be an integral feature of the primate brain, possibly reducing the time for the eye to direct the fovea towards salient stimuli with the use of saccades, and also speeding up the guidance of grasping objects. These connections were particularly costly to the total wiring of the connectome, emphasising their functional importance. It seems logical that information from the eye should be delivered to higher level processes in a timely fashion, reducing the time needed for the animal to react to what it is seeing, or to gather more information by moving the eye. By identifying this costly connectivity between anterior and posterior regions, our results contribute towards a universal architecture for visual processing in the brain, as well as highlighting the extent to which this design is prioritised in the brain despite its spatial and metabolic costs. Later studies could analyse wiring in other primate species, investigating the extent to which occipito-frontal connectivity is maintained alongside the minimisation of wiring lengths. It would also be interesting to follow these results with a higher-resolution analysis of the mammalian connectome, where the end-points of these occipital-frontal projections can be more accurately identified and costed.

**The impact of spatial arrangement on dynamics**

Using a dynamical model of brain activation, we provided mechanistic reasoning for why brain regions are sub-optimal in their spatial arrangement (with respect minimising the wiring length). This reasoning came in the form changes to metastable dynamics — spatial sub-optimisation increased fluctuations in the level of global synchronisation in the system, a property associated with cognitive processing and healthy brain function (Deco and Kringelbach 2016). By linking structure with a computational model, we offer a novel

insight into the impact that spatial arrangement of regions and their connections has on global brain dynamics.

### Spatial analysis of the connectome as a means to understand schizophrenia

Our analysis of schizophrenia did not highlight differences in the spatial structure of the entire connectome, but did identify differences when the frontal lobe was analysed in isolation. The symptoms associated with schizophrenia are numerous and heterogeneous, often varying in their severity (Hubl et al. 2004; Rubinov et al. 2013; Steen et al. 2006; Tandon et al. 2008). It is therefore likely that no single structural principle may account for the symptoms observed, making it challenging to identify consistent changes in the connectome across schizophrenia subjects. Our work was also limited by lack of data on the specific symptoms that each subject experienced. Further studies may be able to distinguish spatial alterations given a more precise demarcation of symptoms, for instance, focusing on those that experienced a small subset of symptoms only, such as hallucinations. Furthermore, the PANSS scores for controls, despite being classed as non-schizophrenic, were also unavailable, a fact that limits the interpretation of our results as such data could have been used to exclude controls who may have displayed minor symptoms of schizophrenia. Importantly, our spatial analysis in the context of brain disorders offers new possibilities for future applications to other neurological conditions. For instance, structural changes in cases of autism, whose connectomes show fewer long distance connections (Barttfeld et al. 2011), may give rise to changes in the spatial optimisation of particular areas, helping to inform the cause of functional abnormalities.

### Spatial features of the connectome and intelligence

By representing the connectome as a network, we found that some network features correlated with measures of fluid intelligence. Our results concerning a greater spatial optimisation for connectomes with higher fluid intelligence highlights a possible avenue for further study. Some such routes may involve correlating IQ scores with spatial features *within* lobes, focusing on the frontal and parietal areas (Colom et al. 2009; Rex E Jung et al. 2007). Improvements were made to the CPO algorithm over the course of the research, in particular, correcting for the length of inter-hemispheric connections (by routing them through the centre of the network, and also by ensuring that regions do not move between

hemispheres). Future work could expand on this by including the physical position of the corpus callosum during this correction, potentially making the rearrangement more biologically plausible.

### Connectome differences alongside sex

Several of our findings identified changes between sexes, either in connectome structure, or when correlating with fluid intelligence scores. In particular, we found that spatial features and fluid intelligence may differ between males and females. Such findings suggest differences in the way information is processed between sexes, contributing towards observed changes in structure (Ingalhalikar et al. 2014) and function (Richard J Haier, Rex E Jung, et al. 2005). Nonetheless, when comparing sex, we did not see differences in the extent of spatial optimisation in the connectome, prompting the need for further work to reconcile structural with functional differences across sex.

### Demonstrating the usefulness of the Kuramoto model

This study highlights the usefulness of simulating brain activity at a global level. Using the Kuramoto model, we were able to provide evidence for the existence of a dependency between activity changes in the connectome (in terms of the fluctuations in the level of global synchronisation) and the spatial arrangement of its regions. While the Kuramoto model is a relatively basic tool to model dynamics, we were able to provide evidence for its usefulness in understanding dynamics at a global level. This relatively simple model also allowed us to explore a wider and more granular parameter search, easing the computational load. This was especially important for both the HCP and macaque datasets, with the former consisting of a large sample size, and the latter's connectomes comprising of many regions. By making use of optimisation techniques, including the high performance Rocket computing cluster at Newcastle University, and using MEX code to speed up MATLAB subroutines, we were further able to reduce the time needed to simulate dynamics. The thesis has an underlying result, namely that computers are powerful tools in the quest to understand biological systems.

### Using a spatial arrangement technique that dynamically reorganises regions and their connections

Future work may involve the use of more accurate ways of assessing the level of spatial optimisation in the brain. This could involve the use of more biologically plausible models of spatial rearrangement, ones which represent connections as flexible 'cables' which can bend around obstacles (subcortical regions, and ventricles in particular). Regions would be relocated on the native surface of the brain, extending the previous attempts by Raj et al. 2011, where regions were constrained to the surface of a sphere, using a separate, arbitrarily sized sphere for subcortical regions. A more realistic, 'elastic' model of the connectome may reposition neighbouring regions into a minimal energy state — one that reduces the wiring length — while accounting for the constraints of the skull and the surface area and volume of each region. In such a scenario, moving a single region may cause other neighbouring regions to reposition themselves dynamically, affecting the lengths of directly and indirectly connected regions. It may then be possible to identify arrangements which exceed the percentage reductions found using our current technique, providing a more accurate assessment of spatial organisation. The effects on conduction delays are more likely to be biologically feasible too, as wiring lengths will no longer based on Euclidean distances. Thus, simulating neuronal dynamics using a model of flexible wiring will likely provide a more accurate insight into dynamical changes between original and spatially minimised arrangements.

Inspiration for this kind of model may be drawn from the domain of protein folding, where models are used to alter the three-dimensional structure into a minimised energy state (Su et al. 2008); or from the techniques used to minimise the wiring lengths in electrical circuits (Kedem et al. 1984). In the latter case, electrical components on a circuit-board represent nodes in a graph, which can be positioned, likened to the 'block packing' visualisation in (Kedem et al. 1984, Fig. 9). The complexity of developing such a biologically realistic model, however, remains a significant challenge, one that could be addressed in future studies.

### Using alternative parcellations of the brain

For the human subjects, in this study, we used the Desikan–Killiany atlas and a Freesurfer subcortical segmentation for the parcellation of cortical and subcortical regions (Desikan

et al. 2006; Fischl, Salat, et al. 2002). It is however, a parcellation which uses structural landmarks — such as sulci and gyri — to define the boundaries between macroscopic regions. Geometric variability between subjects limits the accuracy of these methods (Van Essen, Drury, et al. 1998), with surface-based parcellation being argued as superior (Fischl, Sereno, et al. 1999). Additionally, other parcellations define the boundaries between regions based on the functional responsibilities of brain areas, mitigating some of the limitations of anatomic parcellations in segregating the brain into functionally distinct areas, often providing a finer level of detail over anatomical labelling (Van Essen, Glasser, et al. 2012). Because our study involved measurements which are likely to correlate with dynamics, using a functionally-derived parcellation of the brain may shed further light on the dependencies between spatial features of the connectome and cognition.

### Using alternative search methods to find optimal spatial arrangements

Regarding the simulated annealing algorithm relied upon in this study, greater reductions in wiring length may have been achieved through the use of other search techniques. In the case of genetic algorithms (Fraser 1957), each component placement could be treated as a 'gene', which may be combined to provide alternative spatial arrangements within a process of mutation, and selection based on fitness (the extent of wiring length reduction made possible by that arrangement). Although genetic algorithms are arguably more complex than the simulated annealing algorithm used here, they may be capable of finding spatial arrangements which reduce the wiring length by a greater extent. It would also be interesting to apply some of the more eclectic search techniques to this scenario, such as the one inspired by the foraging behaviour of honey bees (Karaboga et al. 2008).

### Simulating the effects of lesions on dynamics

Future studies may explore the changes in dynamics when regions are *removed* from the system, and subsequently the effects on wiring configuration, such as in cases of stroke patients or traumatic brain injury (Hellyer, Scott, et al. 2015). One approach taps into game theory, where an estimation can be made on the contribution of each region towards global synchronisation under various sub-optimal wiring configurations; estimating the Shapley value provides one way to estimate region contribution, treating brain regions as 'players' in a 'game' where the aim is to maintain global dynamics (such

as metastability) (Shapley 1988). The Shapley value can be estimated in cases where it is computationally intractable to compute the true contribution for each region (Keinan et al. 2004), and offers a more accurate calculation of region contribution by extending previous attempts which only consider the effects on dynamics when *single* regions are lesioned (Váša et al. 2015).

### Simulating macroscopic neural dynamics using other models

An additional avenue for further work may involve the use of different models of global dynamics. This may involve replicating the changes in dynamics observed in this study when a simpler model is used, such as the Greenberg-Hastings model (Greenberg et al. 1978). Or, perhaps a more biologically realistic model of brain dynamics could be used instead (H. R. Wilson et al. 1972). The Kuramoto model is regarded as a simple model on the spectrum of model complexity, as it does not account for aspects of neuron physiology such as inhibition or refractory periods, two key elements of activation regulation in the brain (Felten et al. 2015, pp. 20–24). Our dynamical model also omits noise — future models could consider the inclusion of normally distributed noise, reflecting extrinsic neural activation (Deco, Jirsa, et al. 2009). Further analyses using different oscillation frequencies will provide a more detailed picture of the relationship between spatial features and dynamics. Compared with the Kuramoto model, the Wilson-Cowan model is a more detailed choice for simulating neuronal dynamics, modelling both excitatory and inhibitory populations of neurons (H. R. Wilson et al. 1972). The use of alternative models which better reflect the biology will help to determine the validity of our results. Ultimately, any choice of model must find a balance between biological realism, and computational complexity. The Kuramoto model leans more towards computational savings, which was the primary reason for its use in this study. And above all, when relying on models it is crucial to remind ourselves that *"All models are wrong, but some are useful."* (Box 1976).

## *Closing statement…*

The brain is a wonderfully complex organ and many unanswered questions remain concerning its structure and function. Our work contributes towards an understanding of why the brain is wired the way it is, in both humans and macaques, and how a spatially sub-optimal connectome may benefit dynamics. We hope that further research

can continue to delve into the relationship between spatial features of the connectome and cognition. With computational methods and careful analysis, future progress can be made in the domain of computational neuroscience, helping us to unravel the mysteries of the mind.

# Appendix A. Macaque dataset/analyses

## A.1 Additional Tables and Figures

Table A.1: Region names and lobe mapping – Table 1

| Region abbreviation | Region full name | Lobe |
|---|---|---|
| V1 | visual area 1 (primary visual cortex) | Visual |
| V2 | visual area 2 | Visual |
| V3A | visual area V3A | Visual |
| V3v | visual area 3, ventral part | Visual |
| V4 | visual area 4 (dorsal part) | Visual |
| V6 | visual area 6 (or PO) | Visual |
| FST | floor of superior temporal area | Higher visual |
| MST | medial superior temporal area | Higher visual |
| MT | middle temporal area | Higher visual |
| TAa | area TAa (sts dorsal bank) | Higher visual |
| TEO | area TEO | Higher visual |
| TEa | area TEa (sts ventral bank) | Higher visual |
| TEad | dorsal subregion of anterior TE | Higher visual |
| TEm | area TEm (sts ventral bank) | Higher visual |
| TEpd | dorsal subregion of posterior TE | Higher visual |
| TFO | area TFO of the parahippocampal cortex | Higher visual |
| TGa | agranular part of the temporal pole | Higher visual |
| TGdd | dysgranular part of the dorsal temporal pole | Higher visual |
| TGdg | granular part of the dorsal temporal pole | Higher visual |
| TGsts | sts part of the temporal pole | Higher visual |
| TPO | area TPO (sts dorsal bank) | Higher visual |
| TTv | ventral tenia tectum | Higher visual |
| Tpt | temporo-parietal area | Higher visual |
| IPa | area IPa (sts fundus) | Higher visual |
| PGaM4 | area PGa | Higher visual |
| A1 | auditory area I, core region of the auditory cortex | Auditory |
| CL | caudal lateral, belt region of the auditory cortex | Auditory |
| CM | caudomedial, belt region of the auditory cortex | Auditory |
| CPB | caudal parabelt region of auditory cortex | Auditory |
| ML | middle lateral, belt region of the auditory cortex | Auditory |
| AL | anterior lateral, belt region of the auditory cortex | Auditory |
| R | rostral, core region of the auditory cortex | Auditory |
| RM | rostromedial, belt region of the auditory cortex | Auditory |
| RPB | rostral parabelt region of the auditory cortex | Auditory |
| RT | rostrotemporal, core region of the auditory cortex | Auditory |
| RTL | lateral rostrotemporal, belt region of the auditory cortex | Auditory |
| RTp | rostrotemporal, polar part | Auditory |
| Ri | retroinsula | Auditory |
| STGr | rostral superior temporal gyrus | Auditory |
| LIPd | lateral intraparietal area, dorsal subdivision | Parietal |
| LIPv | lateral intraparietal area, ventral subdivision | Parietal |
| LOP | lateral occipital parietal area | Parietal |
| MIPM4 | medial intraparietal area | Parietal |
| AIPM4 | anterior intraparietal area | Parietal |
| 5-(PE) | superior parietal lobule area (part of 5) | Parietal |

Table A.2: Region names and lobe mapping – Table 2

| Region abbreviation | Region full name | Lobe |
|---|---|---|
| 5-(PEa) | superior parietal lobule area, medial bank (part of 5) | Parietal |
| 5-(PEc) | superior parietal lobule area, dorsocaudal pole (part of 5) | Parietal |
| 7a-(Opt/PG) | visual area 7a (Opt/PG) | Parietal |
| 7b-(PFG/PF) | visual area 7b (PFG/PF) | Parietal |
| 7m | area 7m in the medial parietal cortex | Parietal |
| 7op | area 7op (parietal operculum) | Parietal |
| PEci | superior parietal lobule area (cingulate sulcus) | Parietal |
| PIP | posterior intraparietal area | Parietal |
| VIP | ventral intraparietal area | Parietal |
| 44 | area 44 | Premotor |
| 45a | area 45a | Premotor |
| 45b | area 45b | Premotor |
| 46d | area 46, dorsal subdivision | Premotor |
| 46f | area 46, | Premotor |
| 46v | area 46, ventral subdivision | Premotor |
| 8Ad | periarcuate area (or frontal eye field), dorsal subdivision | Premotor |
| 8Av | periarcuate area (or frontal eye field), ventral subdivision | Premotor |
| 8Bm | dorso-medial prefrontal area 8Bm | Premotor |
| 8Bs | dorso-lateral prefrontal area 8Bs, arcuate sulcus upper limb | Premotor |
| F5-(6Va/6Vb) | agranular frontal area F5 (6Va/6Vb) | Premotor |
| F1-(4) | agranular frontal area F1 (4) | Motor |
| F2-(6DR/6DC) | agranular frontal area F2 (6DR/6DC) | Motor |
| F3 | agranular frontal area F3 | Motor |
| F4 | agranular frontal area F4 | Motor |
| F6 | agranular frontal area F6 | Motor |
| PrCO | precentral opercular area | Prefrontal |
| 10mc | medial prefrontal area, caudal part | Prefrontal |
| 11l | orbital prefrontal area 11l | Prefrontal |
| 12l | ventro-lateral prefrontal area 12l | Prefrontal |
| 13a | orbital prefrontal area 13a | Prefrontal |
| 14c | orbito-medial prefrontal area 14c | Prefrontal |
| 25 | medial prefrontal area 25, subgenual cortex | Prefrontal |
| 32 | medial prefrontal area 32 | Prefrontal |
| 9m | dorso-medial prefrontal area 9m | Prefrontal |
| 23a | area 23a in posterior cingulate cortex | Prefrontal |
| 24ax | area 24a in anterior cingulate cortex | Prefrontal |
| 29 | area 29 in retrosplenial cortex | Prefrontal |
| 31 | area 31 in posterior cingulate gyrus | Prefrontal |
| Claustrum | Claustrum | Subcortical |
| LGNm | lateral geniculate nucleus, magnocellular | Subcortical |
| PI | parainsular area | Subcortical |
| PL | paralaminar nucleus in amygdala | Subcortical |
| PM | medial pulvinar | Subcortical |
| MDpc | mediodorsal nucleus, parvicellular division | Subcortical |
| SNr/c | substantia nigra pars reticulate or compacta | Subcortical |
| Striatum | Striatum | Subcortical |
| GPe/GPi | globus pallidus, external/internal segment | Subcortical |

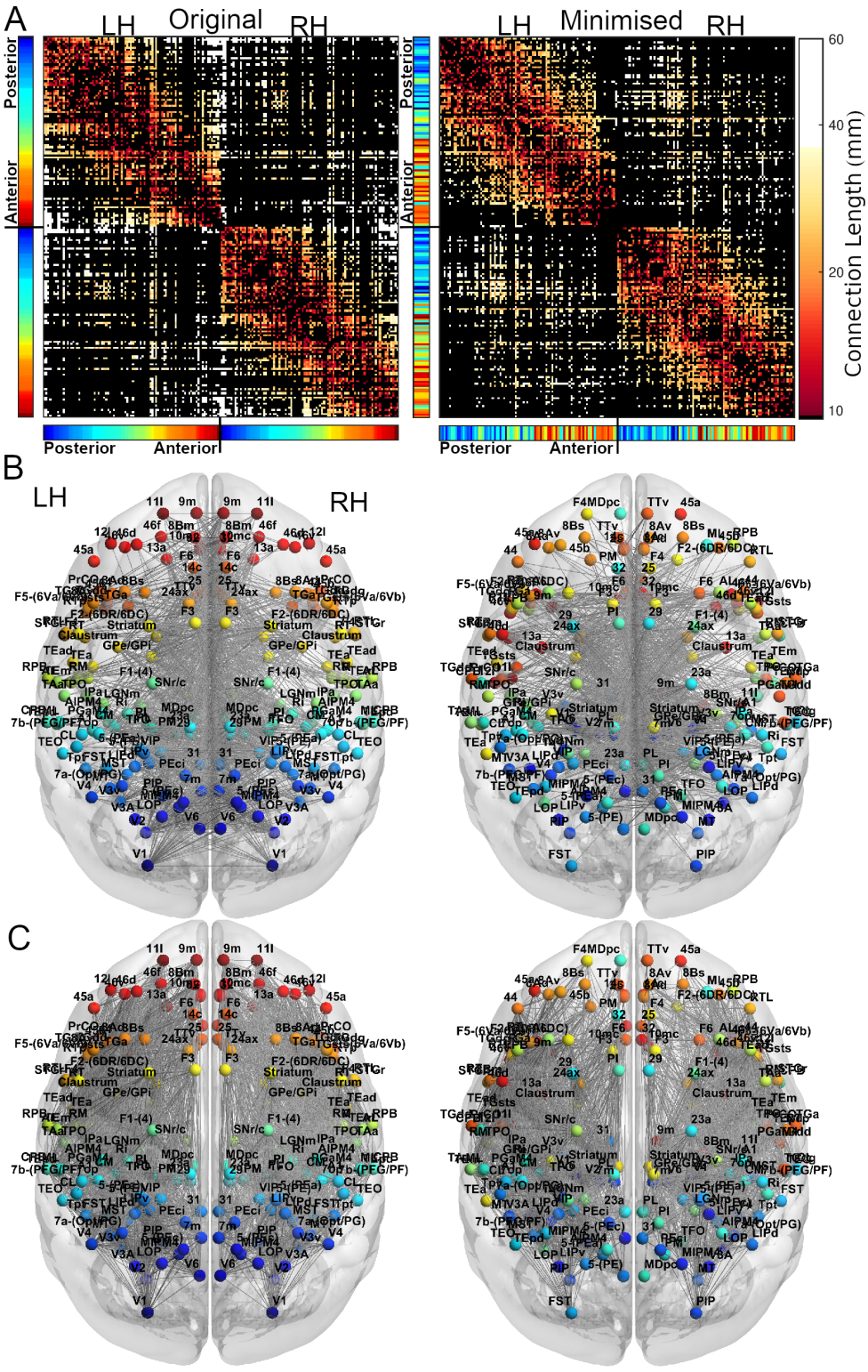


Figure A.1: For subject AL. Changes in connectome structure before and after rearrangement. **A:** Example adjacency matrices showing the connections between spatial locations for original and minimised spatial arrangements. Regions are coloured based on their anterior-posterior position in the original arrangement, displayed in the colour bars next to the adjacency matrices (red = anterior, blue = posterior). The topology of the connectome is preserved in both arrangements, but the positions of regions often differ. White connections in the adjacency matrices are those with lengths greater than 80% of connections in the original arrangement. **B/C:** Connections between hemispheres for connectomes, for the original arrangement **(left)** and the arrangement that minimises the total wiring length of the network **(right)**. For clarity, connectome connections are displayed separately for between and within hemispheres.

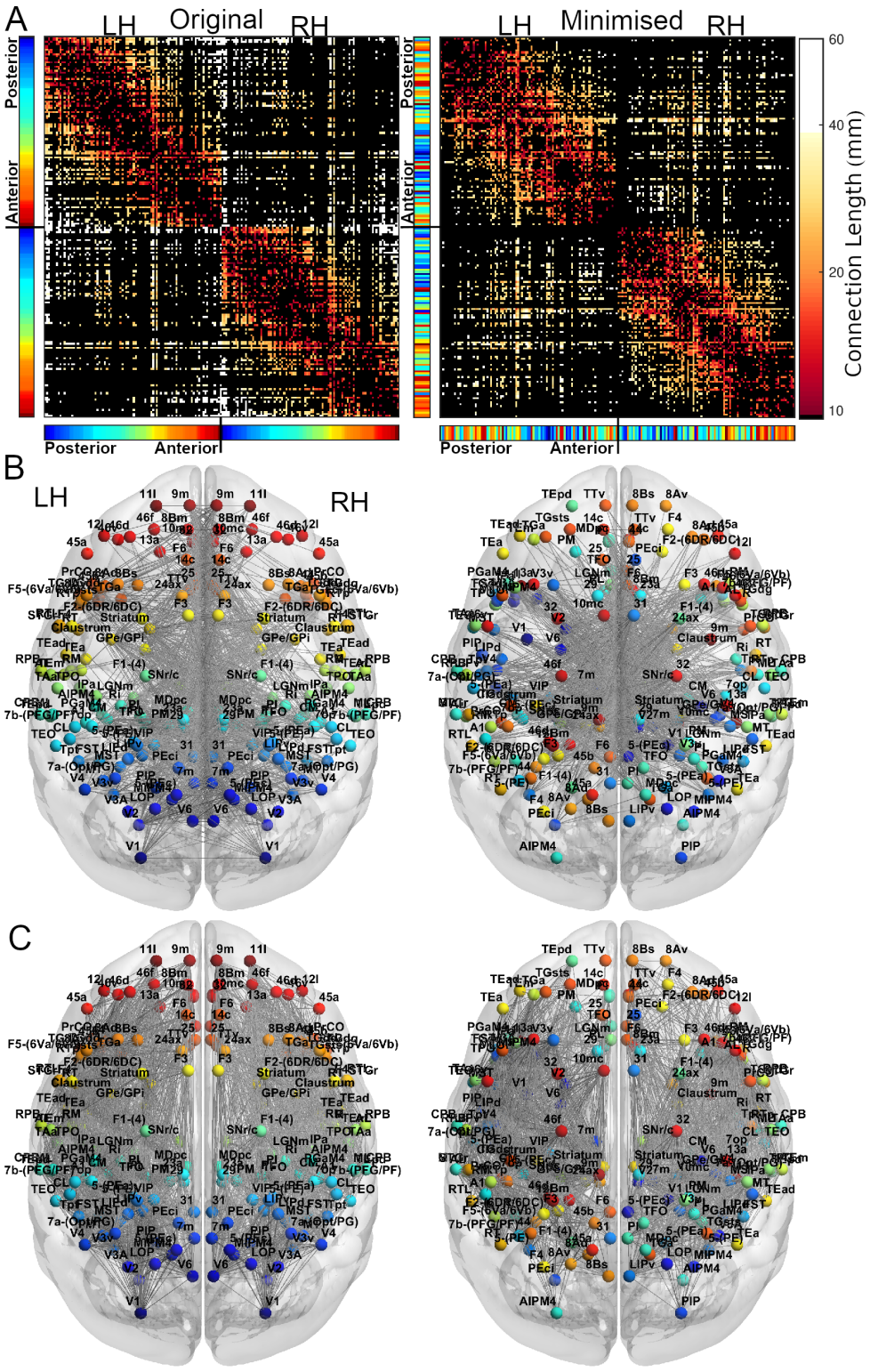


Figure A.2: For subject DP. Changes in connectome structure before and after rearrangement. **A:** Example adjacency matrices showing the connections between spatial locations for original and minimised spatial arrangements. Regions are coloured based on their anterior-posterior position in the original arrangement, displayed in the colour bars next to the adjacency matrices (red = anterior, blue = posterior). The topology of the connectome is preserved in both arrangements, but the positions of regions often differ. White connections in the adjacency matrices are those with lengths greater than 80% of connections in the original arrangement. **B/C:** Connections between hemispheres for connectomes, for the original arrangement **(left)** and the arrangement that minimises the total wiring length of the network **(right)**. For clarity, connectome connections are displayed separately for between and within hemispheres.

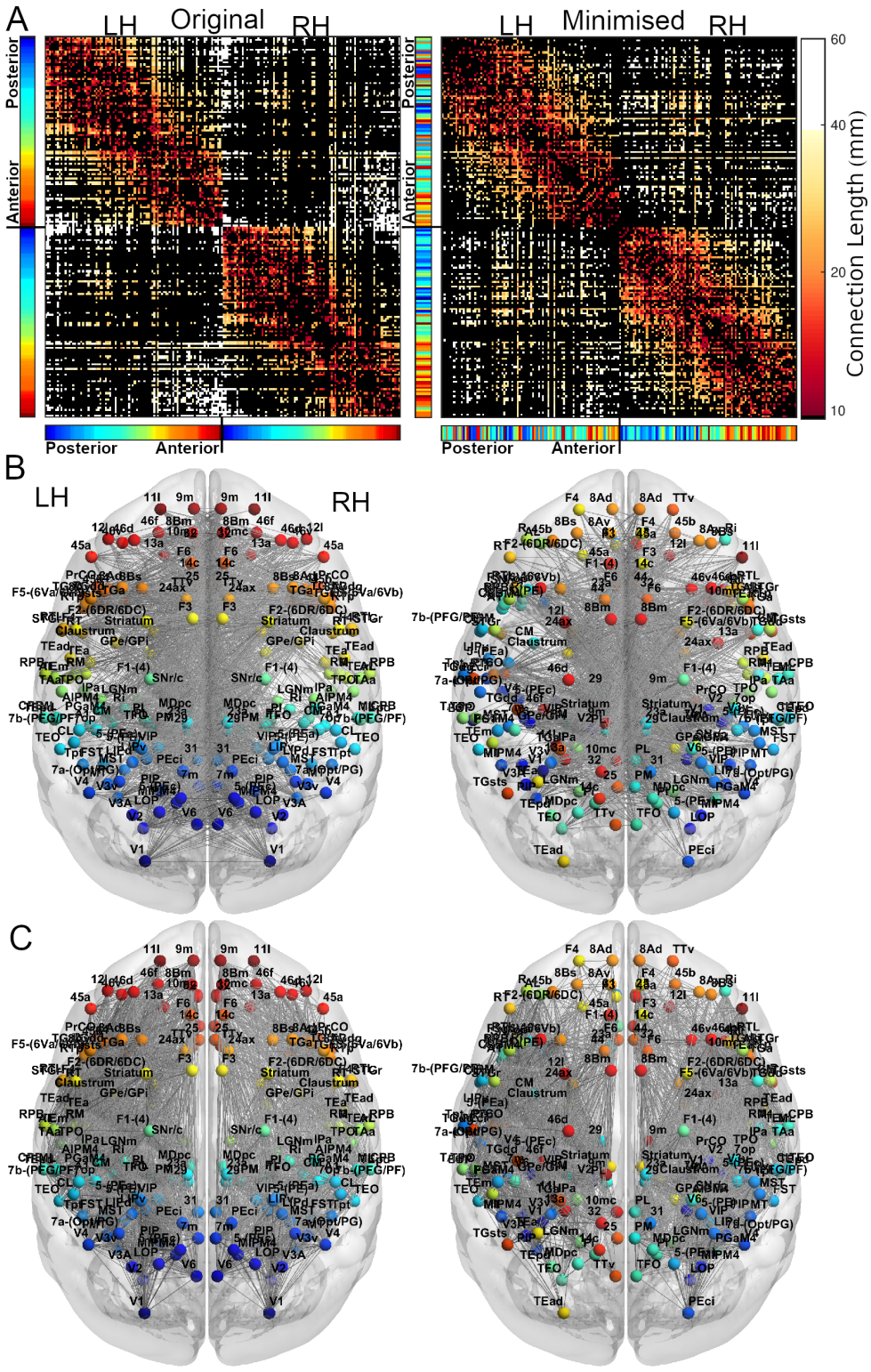


Figure A.3: For subject VL. Changes in connectome structure before and after rearrangement. **A:** Example adjacency matrices showing the connections between spatial locations for original and minimised spatial arrangements. Regions are coloured based on their anterior-posterior position in the original arrangement, displayed in the colour bars next to the adjacency matrices (red = anterior, blue = posterior). The topology of the connectome is preserved in both arrangements, but the positions of regions often differ. White connections in the adjacency matrices are those with lengths greater than 80% of connections in the original arrangement. **B/C:** Connections between hemispheres for connectomes, for the original arrangement **(left)** and the arrangement that minimises the total wiring length of the network **(right)**. For clarity, connectome connections are displayed separately for between and within hemispheres.

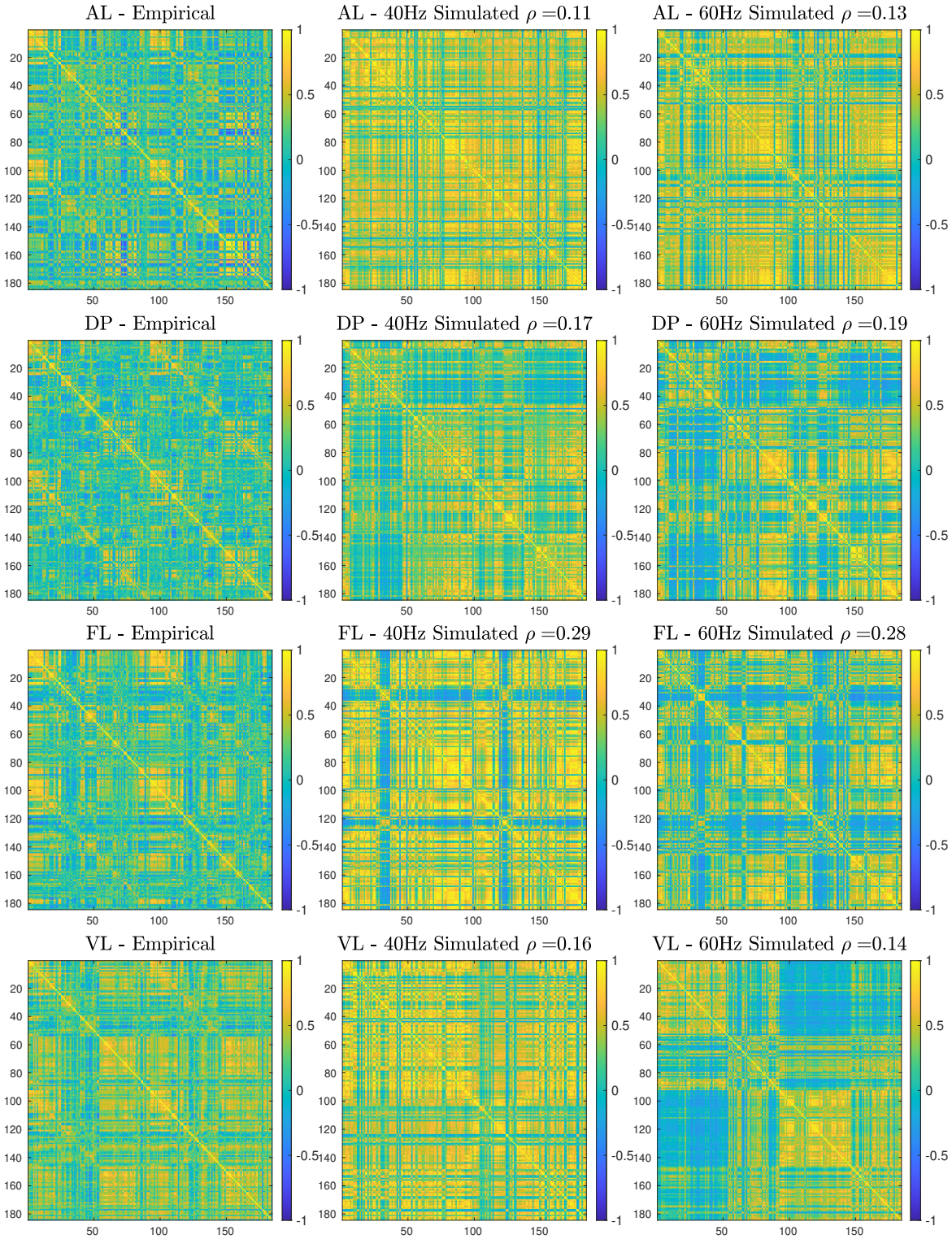


Figure A.4: For the four subjects, the empirical functional connectivity matrices and the corresponding simulated functional connectivity matrices showing the maximum correlation with the empirical data. Shown is the Pearson correlation between BOLD activation for all pairs of 184 regions. Spearman rank correlation coefficients, $\rho$, between empirical and simulated correlation matrices were 0.1090, 0.1679, 0.2888 and 0.1583 (40Hz); and 0.1293, 0.1932, 0.2774 and 0.1433 (60Hz); for AL, DP, FL and VL, respectively.

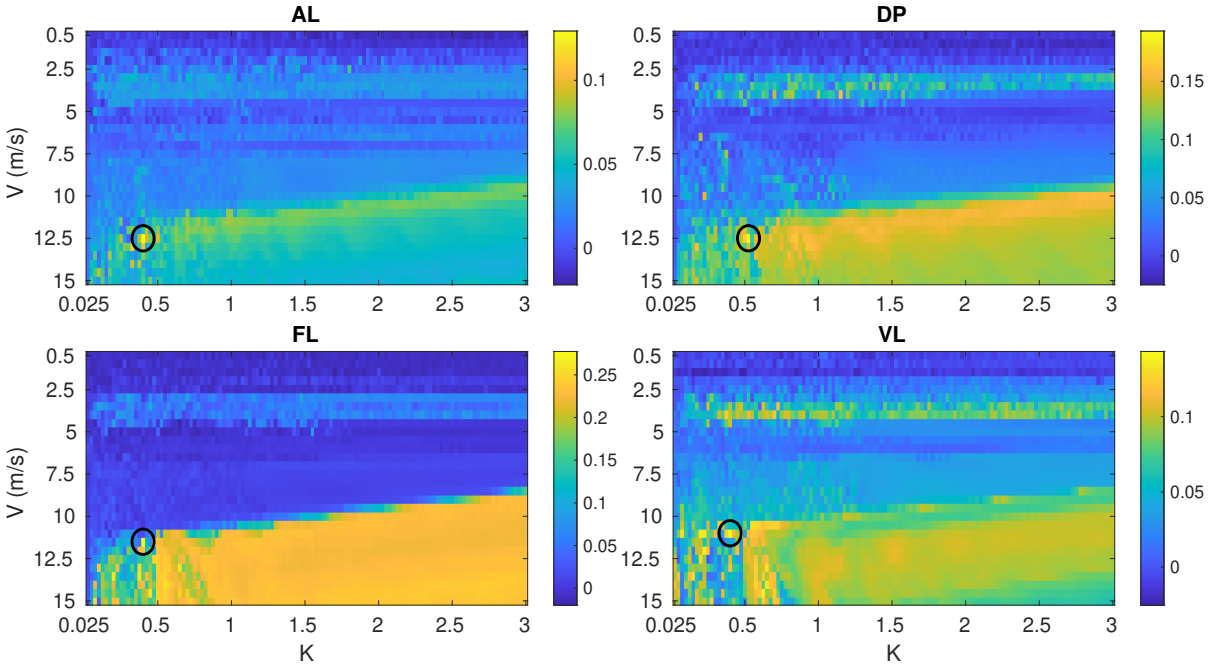


Figure A.5: For 60Hz: For the four subjects (AL, DP, FL, VL), the Spearman rank correlation coefficients between the empirical and simulated functional connectivity matrices over the parameter space of coupling strengths (K) and conduction velocities (V). Circled is the pair of parameters which maximise the correlation with the empirical functional connectivity.

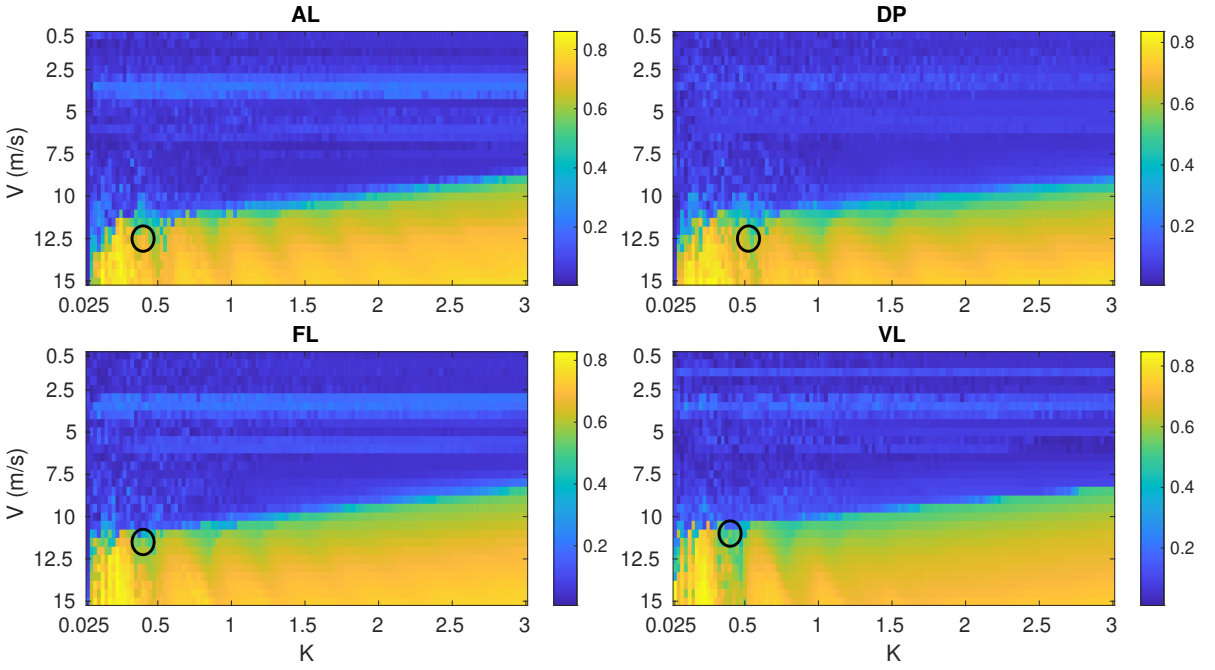


Figure A.6: For 60Hz: For the four subjects (AL, DP, FL, VL), the mean global synchrony between regions from the simulated neural activity over the parameter space of coupling strengths (K) and conduction velocities (V). Circled is the pair of parameters which maximise the correlation with the empirical functional connectivity.

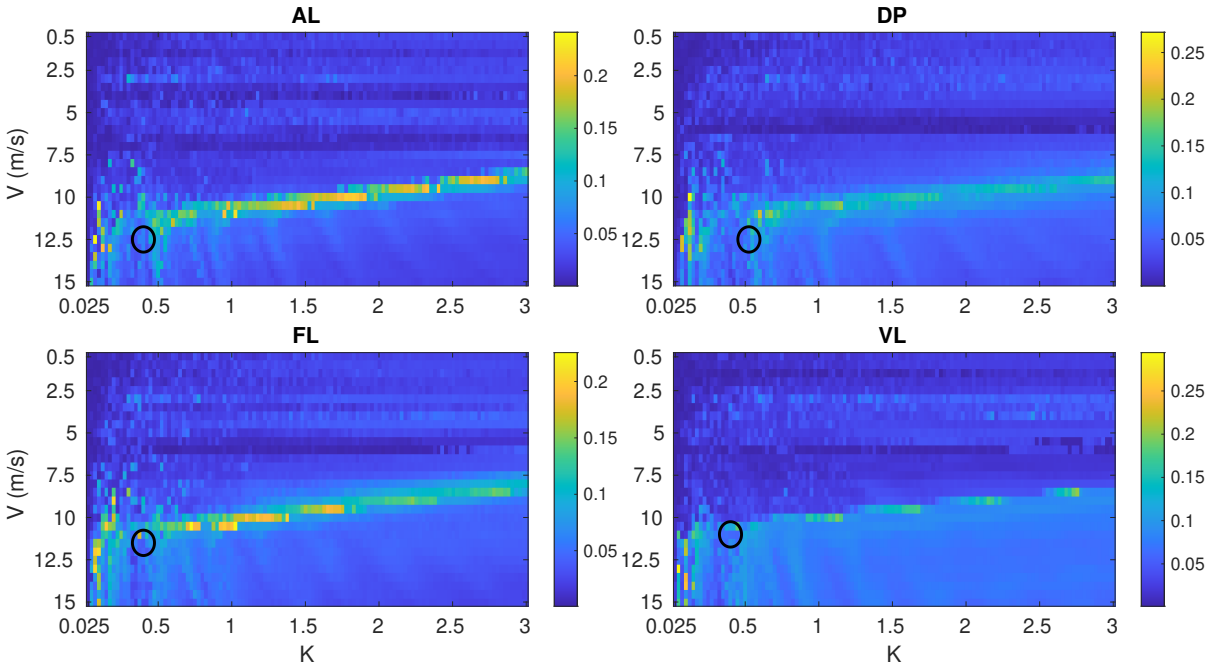


Figure A.7: For 60Hz: For the four subjects (AL, DP, FL, VL), the metastability from the simulated neural activity over the parameter space of coupling strengths (K) and conduction velocities (V). Circled is the pair of parameters which maximise the correlation with the empirical functional connectivity.

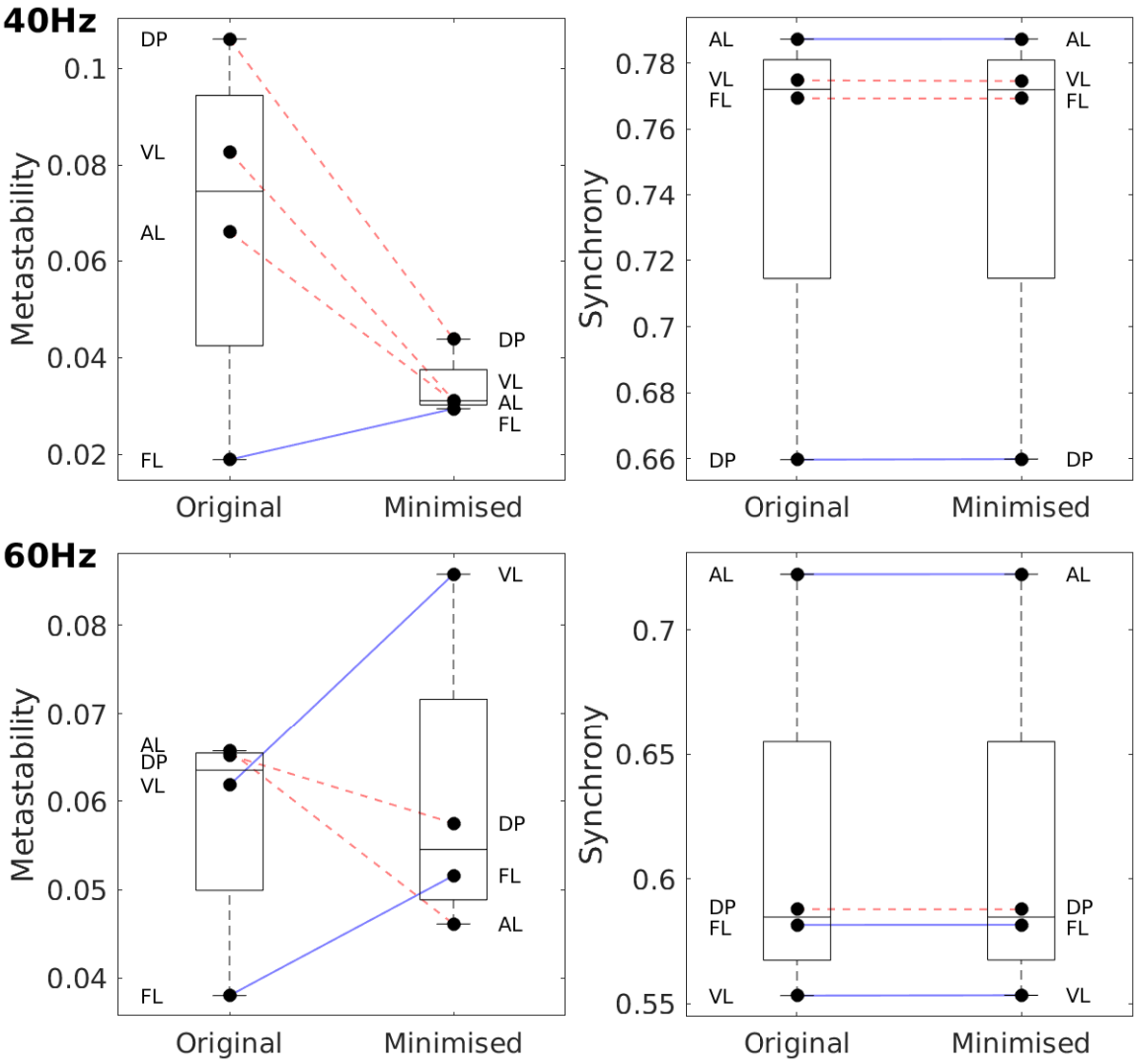


Figure A.8: Bi-partite plots showing the changes in metastability and synchrony between original and minimised arrangements when minimising the difference in synchrony by *simultaneously* searching over both the coupling strengths and conduction velocities in the parameter space. Subjects are labelled: AL, DP, FL, VL. At 40Hz: AL, DP, and VL showed reductions in metastability in the minimised spatial arrangement (denoted by dashed red lines). At 60Hz: Only AL and DP displayed reductions in metastability in the minimised arrangement.

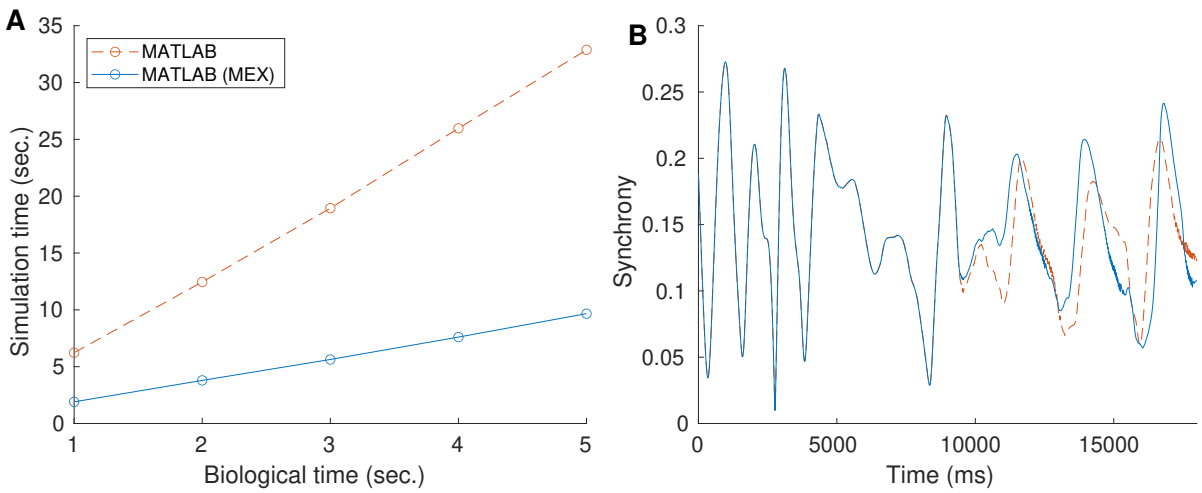


Figure A.9: Comparing Kuramoto model run times of pure MATLAB and MEX code implementations. **A:** Run times for a simulation of five seconds of biological time using an identical macaque connectome. The MEX implementation offers a substantial reduction in simulation run time. **B:** For a longer simulation, the mean synchrony over the course of the pure MATLAB version (dashed line), and that for the MEX implementation (solid line). Similar mean synchrony is displayed between simulations, with visible divergence occurring at later times (>9000 ms). We attribute this divergence to differences in the numerical precision used for pure MATLAB and MEX implementations — for the MEX code, several variables were defined as floats (single precision) to speed up the simulation, whereas for MATLAB, double precision was used.

# Appendix B. HCP and schizophrenia datasets/analyses

## B.1 Supporting Information for the HCP Dataset

Supplementary information for the Human Connectome Project and schizophrenia datasets.

### B.1.1 Scanning parameters

**For the structural and diffusion data**: All Human Connectome Project imaging data (Van Essen, Ugurbil, et al. 2012) were acquired on a Siemens Skyra 3T scanner with a customised SC72 gradient insert. T1w 3D MPRAGE were acquired with TR=2400ms, TE=2.14ms, TI=1000ms, flip angle=8°, FOV=224×224, 0.7mm isotropic voxel, bandwidth=210Hz/px, iPAT=2, Acquisition time=7:40(min:sec). Diffusion weighted images were acquired with Spin-echo EPI sequences (b-values=0, 1000, 2000, 3000 s/mm$^2$ in approximately 90 gradient directions, TR=5520 ms, TE=89.5 ms, flip angle=78°, refocusing flip angle=160°, FOV=210×180 (RO×PE) matrix=168×144 (RO×PE), slice thickness=1.25mm, 111 slices, 1.25mm isotropic voxels, Multiband factor=3, Echo spacing=0.78ms, BW=1488 Hz/Px, Phase partial Fourier 6/8.

**For the resting-state fMRI**: Sequence: Gradient-echo PLI, TR: 720ms, TE: 33.1ms, flip angle 52 deg, FOV: 208×180 mm (RO×PE), Matrix: 104×90 (RO×PE), Slice thickness: 2.0 mm; 72 slices; 2.0 mm isotropic voxels. Multiband factor: 8, Echo spacing: 0.58 ms, BW: 2290 Hz/Px. Resting state data produced 1200 frames per run (time points), of total duration: 14 minutes 33 seconds. For the oblique axial acquisitions, we used phase encoding in a left-to-right direction. Subjects were told to keep their eyes open with relaxed fixation on a projected bright cross-hair on a dark background. We used the ICA-FIX denoised rfMRI data, with spurious correlations removed from the BOLD signal, using a combination of MELODIC and FSL FIX. For further details, see (Smith, C. F. Beckmann, et al. 2013).

### B.1.2 Functional data processing

Resting state fMRI BOLD data was obtained from the Human Connectome Project, specifically from the S1200 resting state FIX-denoised release, consisting of 15 minutes of BOLD signal activity per subject (Glasser et al. 2013; Smith, C. F. Beckmann, et al. 2013). Using FSL fnirt, we performed a non-linear registration of each subject's structural parcellation (Freesurfer's aparc+aseg file) into the MNI space. For each region, we obtained a mask which consisted of the associated segmented cortical region, and its associated segmented white matter (also included in the Freesurfer parcellation data). Using this combined mask, we used FSL fslmeants to extract the 1200 BOLD signal time points, repeating this for the 68 cortical and 14 sub-cortical regions. Sub-cortical regions did not have an associated white matter parcellation. After extraction of the BOLD signal for each region, we applied a bandpass filter of between 0.01Hz and 0.2Hz to each region's BOLD signal. For each subject, the global mean signal was regressed out from the signals of each region. We obtained the simulated functional connectivity (FC) matrix by computing the Pearson correlation between all pairs of 82 time-series. FC matrices were used to validate our model of brain activation.

### B.1.3 Structural data processing and tractography

Structural and diffusion imaging data was obtained from the Human Connectome Project (S1200 release). We used pre-processed T1-weighted 3T MRI (download: <subjectID>_3T_Structural_preproc_extended) and pre-processed diffusion imaging data (download: <subjectID>_3T_Diffusion_preproc) (Glasser et al. 2013; Smith, C. F. Beckmann, et al. 2013). An additional bias field correction of the diffusion images was applied using FSL fast. After applying the nodif_brain_mask (supplied with the diffusion imaging data) to the mean b0 image for each subject, we registered the parcellated regions from Freesurfer to the mean b0 image using an automated boundary-based registration algorithm (Freesurfer's bbregister tool).

The registered Freesurfer regions (82 in total: 34 cortical and 7 subcortical per hemisphere, based on the Desikan atlas (Desikan et al. 2006)) were used as input into DSI-Studio for deterministic fibre tracking (DSI-Studio release Jul 2019) (Yeh, Wedeen, et al. 2010). Reconstruction of the diffusion images took place using generalised q-sampling

imaging reconstruction (Gangolli et al. 2017) with a diffusion sampling length ratio of 1.25. The Freesurfer `aparc+aseg` file was applied as a mask during the reconstruction step in DSI-Studio, ensuring that the streamlines remained within identified anatomical regions. Additionally, we used DSI-Studio to perform two iterations of erosion to the image boundary during reconstruction to further prevent escaping streamlines. DSI-studio was configured to use sub-voxel seeding, initially producing 1 million streamlines per subject, with a streamline maximum turning angle of 60 degrees and a step size of 0.625. Streamlines shorter than 10mm and longer than 300mm were discarded. Streamline tracking was terminated upon contact with ventricles. After tracking, one iteration of topology-informed pruning was applied to help remove false connections (Yeh, Panesar, et al. 2019). All other settings in DSI-Studio were set to their default values. The tractography process was carried out by Christopher Hayward and Xue Chen.

Output from tractography produced symmetric connectivity matrices, with entry $(i, j)$ containing the number of streamlines with endpoints in regions $i$ and $j$. For all subjects, all regions had at least one connection to another region, and that no single region was disconnected from its respective hemisphere. We did not use an arbitrary number of streamlines to threshold connections in the adjacency matrices — in the binary form, connections between regions were set to one if they were connected by at least one streamline, and zero otherwise. For the component placement analysis, we only considered the Euclidean distance between connected regions, independent of streamline counts.

### B.2 Additional Tables and Figures

Table B.1: For the Desikan-Killiany atlas and Freesurfer subcortical parcellation, brain region abbreviations and full names (34 cortical and 7 subcortical regions per hemisphere)

| Cortical | | | |
|---|---|---|---|
| BSTS | Bank SSTS | PARC | Paracentral |
| CAC | Caudal Anterior Cingulate | POPE | Pars Opercularis |
| CMF | Caudal Middle Frontal | PORB | Pars Orbitalis |
| CUN | Cuneus | PTRI | Pars Triangularis |
| ENT | Entorhinal | PCAL | Pericalcarine |
| FP | Frontal Pole | PSTC | Postcentral |
| FUS | Fusiform | PC | Posterior Cingulate |
| IP | Inferior Parietal | PREC | Precentral |
| IT | Inferior Temporal | PCUN | Precuneus |
| INS | Insula | RAC | Rostral Anterior Cingulate |
| ISTC | Isthmus Cingulate | RMF | Rostral Middle Frontal |
| LOCC | Lateral Occipital | SF | Superior Frontal |
| LOF | Lateral Orbitofrontal | SP | Superior Parietal |
| LING | Lingual | ST | Superior Temporal |
| MOF | Medial Orbitofrontal | SMAR | Supramarginal |
| MT | Middle Temporal | TP | Temporal Pole |
| PARH | Parahippocampal | TT | Transverse Temporal |
| Subcortical | | | |
| ACC | Nucleus Accumbens | PAL | Pallidum |
| AMYG | Amygdala | PUTA | Putamen |
| CAUD | Caudate | THAL | Thalamus |
| HIPP | Hippocampus | | |

Table B.2: Connections missing in the minimised arrangements in at least 80% of subjects — for connections which were present in all subjects prior to rearrangement.

| Endpoint 1 | Endpoint 2 | Missing % | Eucl. Wiring Length (mm) |
|---|---|---|---|
| rh.superiorparietal | rh.rostralmiddlefrontal | 99.3 | 110 |
| rh.lingual | rh.rostralmiddlefrontal | 99.3 | 113 |
| rh.lateraloccipital | rh.rostralmiddlefrontal | 98.9 | 128 |
| rh.precuneus | rh.superiorfrontal | 95 | 83 |
| lh.precuneus | lh.superiorfrontal | 95 | 82 |
| lh.paracentral | rh.precentral | 92.9 | 96 |
| lh.superiorparietal | rh.superiorparietal | 92.1 | 129 |
| lh.precuneus | lh.caudalanteriorcingulate | 92.1 | 75 |
| lh.precentral | rh.paracentral | 91.1 | 94 |
| lh.lateraloccipital | lh.superiorparietal | 88.9 | 48 |
| lh.precuneus | rh.superiorparietal | 88.2 | 117 |
| rh.lateraloccipital | rh.superiorparietal | 87.1 | 49 |
| lh.isthmuscingulate | lh.superiorfrontal | 86.4 | 73 |
| lh.superiorparietal | rh.precuneus | 86.1 | 116 |
| lh.lateraloccipital | lh.superiortemporal | 85 | 77 |
| lh.superiorfrontal | rh.superiorfrontal | 81.4 | 101 |
| rh.superiorparietal | rh.putamen | 80 | 77 |

Table B.3: Connections missing in the minimised arrangements in all subjects with that connection — for connections which were present in at least 50% of subjects prior to rearrangement.

| Endpoint 1 | Endpoint 2 | Missing % | Eucl. Wiring Length (mm) |
|---|---|---|---|
| rh.lingual | rh.frontalpole | 100 | 129 |
| rh.cuneus | rh.rostralmiddlefrontal | 100 | 124 |
| rh.pericalcarine | rh.rostralmiddlefrontal | 100 | 124 |
| rh.superiorparietal | rh.parsorbitalis | 100 | 115 |
| rh.cuneus | rh.parsorbitalis | 100 | 123 |
| rh.pericalcarine | rh.parsorbitalis | 100 | 121 |
| rh.pericalcarine | rh.lateralorbitofrontal | 100 | 111 |
| rh.lateraloccipital | rh.superiorfrontal | 100 | 117 |
| lh.lateraloccipital | rh.precuneus | 100 | 129 |
| lh.lateraloccipital | rh.lingual | 100 | 133 |
| lh.cuneus | lh.rostralmiddlefrontal | 100 | 124 |
| lh.pericalcarine | lh.rostralmiddlefrontal | 100 | 125 |
| lh.pericalcarine | lh.parsorbitalis | 100 | 122 |
| lh.superiorparietal | lh.medialorbitofrontal | 100 | 113 |
| lh.cuneus | lh.lateralorbitofrontal | 100 | 114 |
| lh.cuneus | lh.superiorfrontal | 100 | 106 |
| lh.lateraloccipital | lh.superiorfrontal | 100 | 118 |
| lh.cuneus | lh.temporalpole | 100 | 106 |

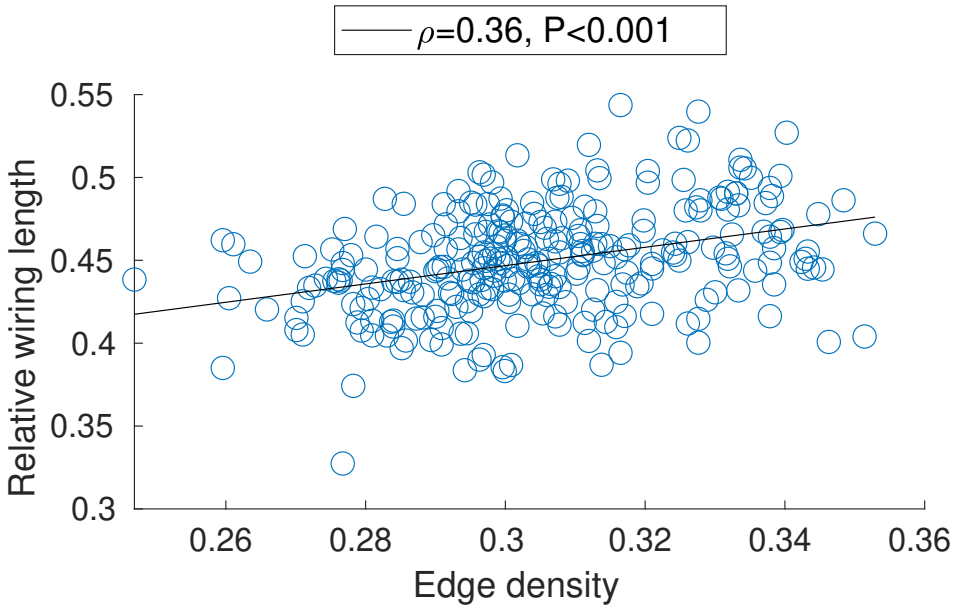


Figure B.1: Comparing relative wiring length and edge density. Networks with reduced relative wiring lengths generally had fewer connections ($\rho$ = Spearman rank correlation).

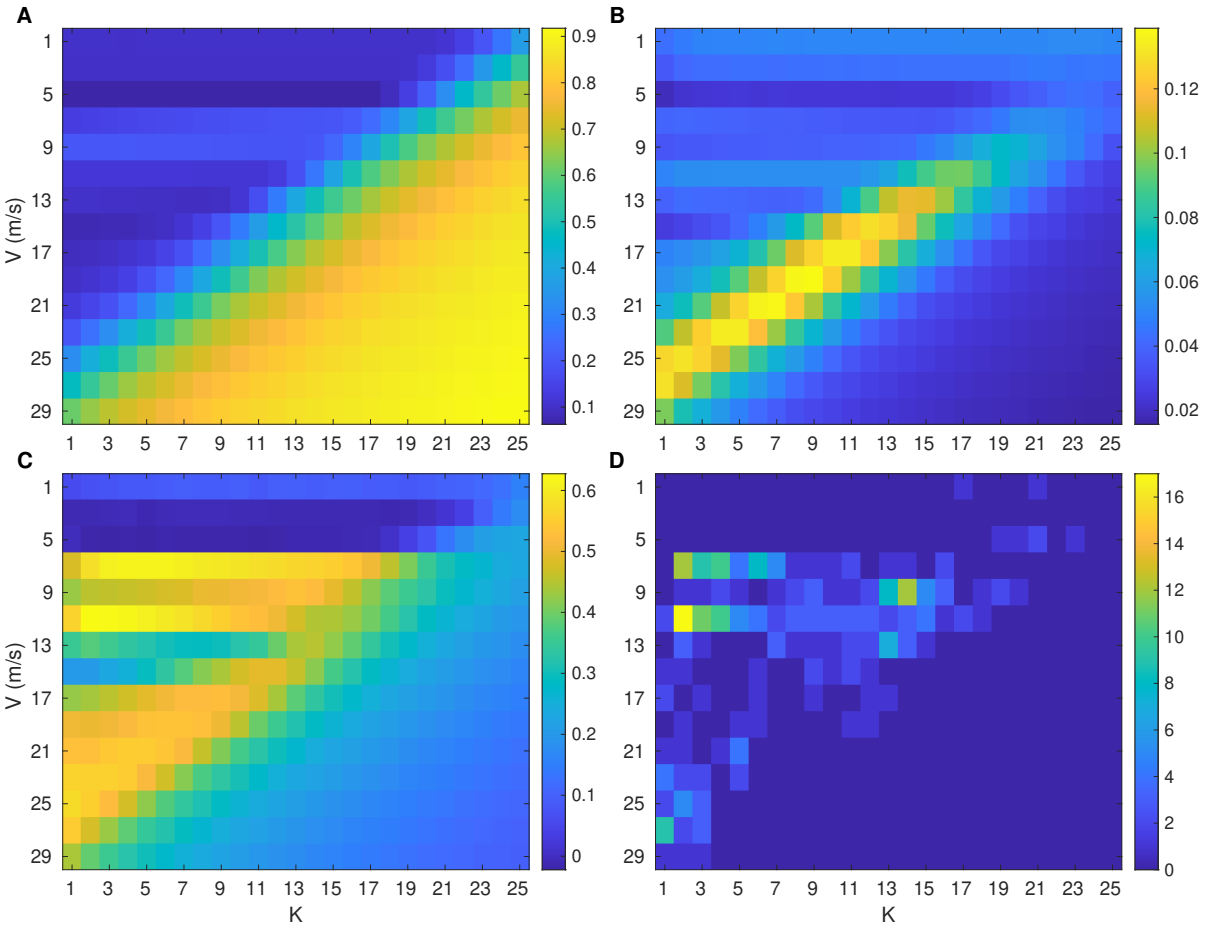


Figure B.2: The changes in dynamics over the parameter space of conduction velocities (V) and coupling strengths (K), for 60Hz. For all subjects and over all conduction velocities and coupling strengths, **A:** Mean synchrony, **B:** Mean metastability, **C:** Mean normalised Pearson correlation (maximum correlation set to 1, for each subject) with empirical rs-fMRI data, and **D:** The number of occurrences in the parameter space for which a pair of parameters provided the maximum correlation with empirical data.

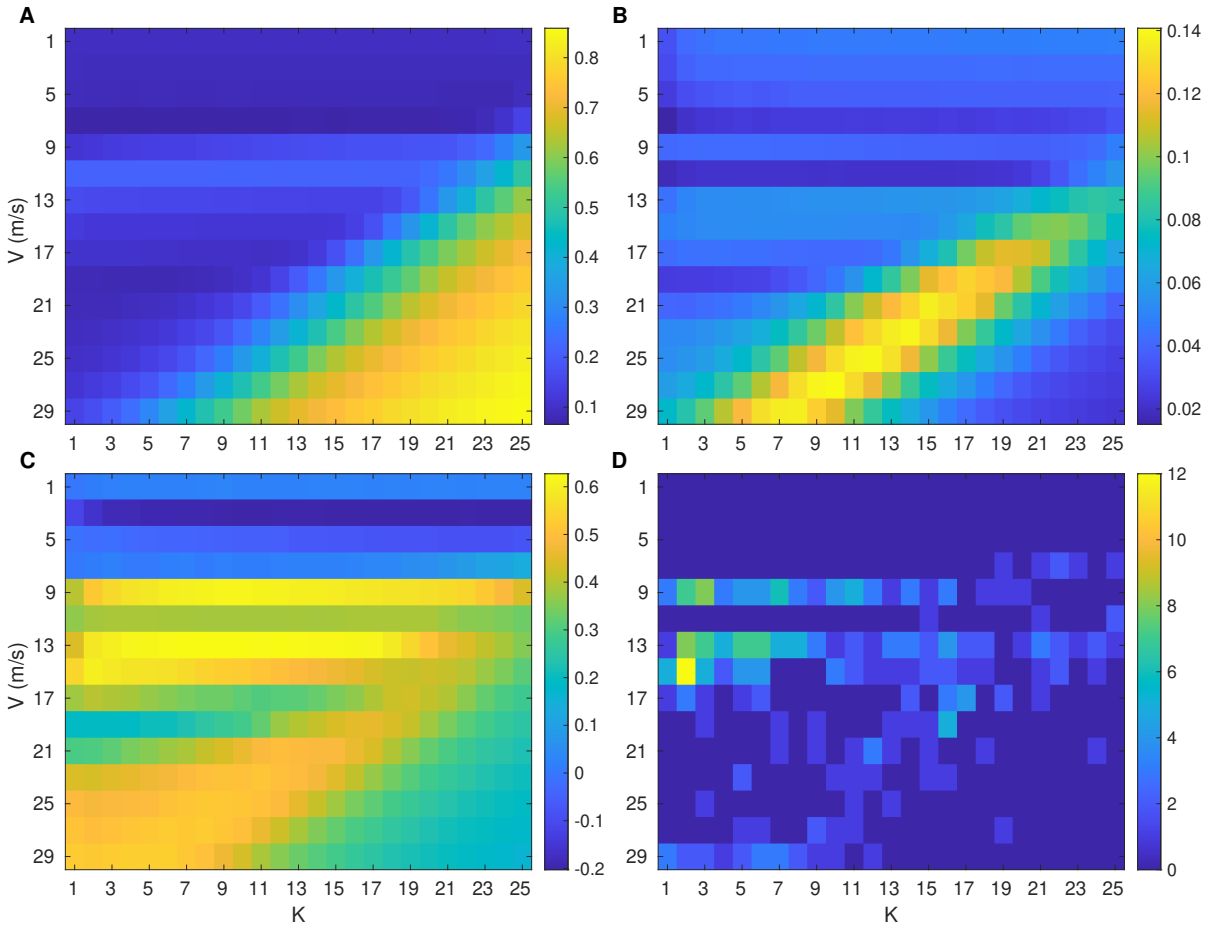


Figure B.3: The changes in dynamics over the parameter space of conduction velocities (V) and coupling strengths (K), for 80Hz. For all subjects and over all conduction velocities and coupling strengths, **A:** Mean synchrony, **B:** Mean metastability, **C:** Mean normalised Pearson correlation (maximum correlation set to 1, for each subject) with empirical rs-fMRI data, and **D:** The number of occurrences in the parameter space for which a pair of parameters provided the maximum correlation with empirical data.

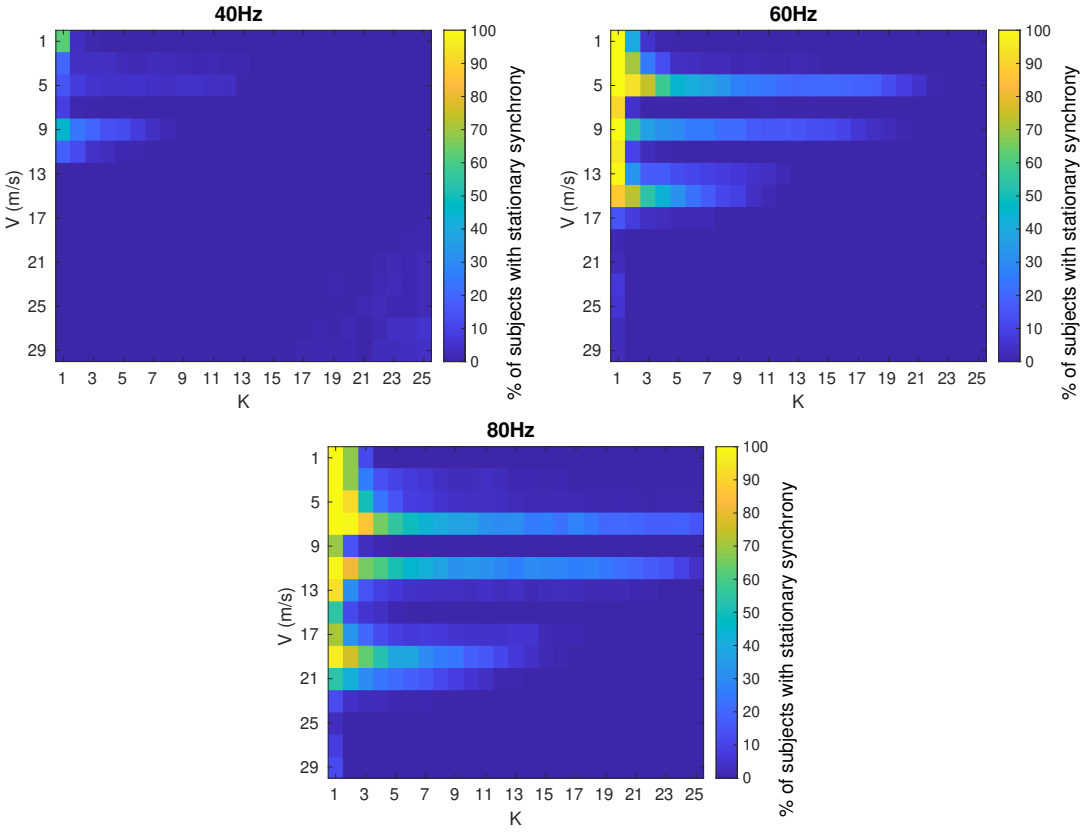


Figure B.4: Across the parameter space of coupling strengths (K) and conduction velocities (V), the mean percentage of subjects displaying stationary synchrony (where the standard deviation of the mean global synchrony falls below $10^{-7}$). Subsequently, across all subjects, (1±1)%, (7±2)% and (11±4)% of the parameter space was discarded for 40Hz, 60Hz and 80Hz, respectively. In our analyses, we considered both cases where stationary activity was either included or discarded.

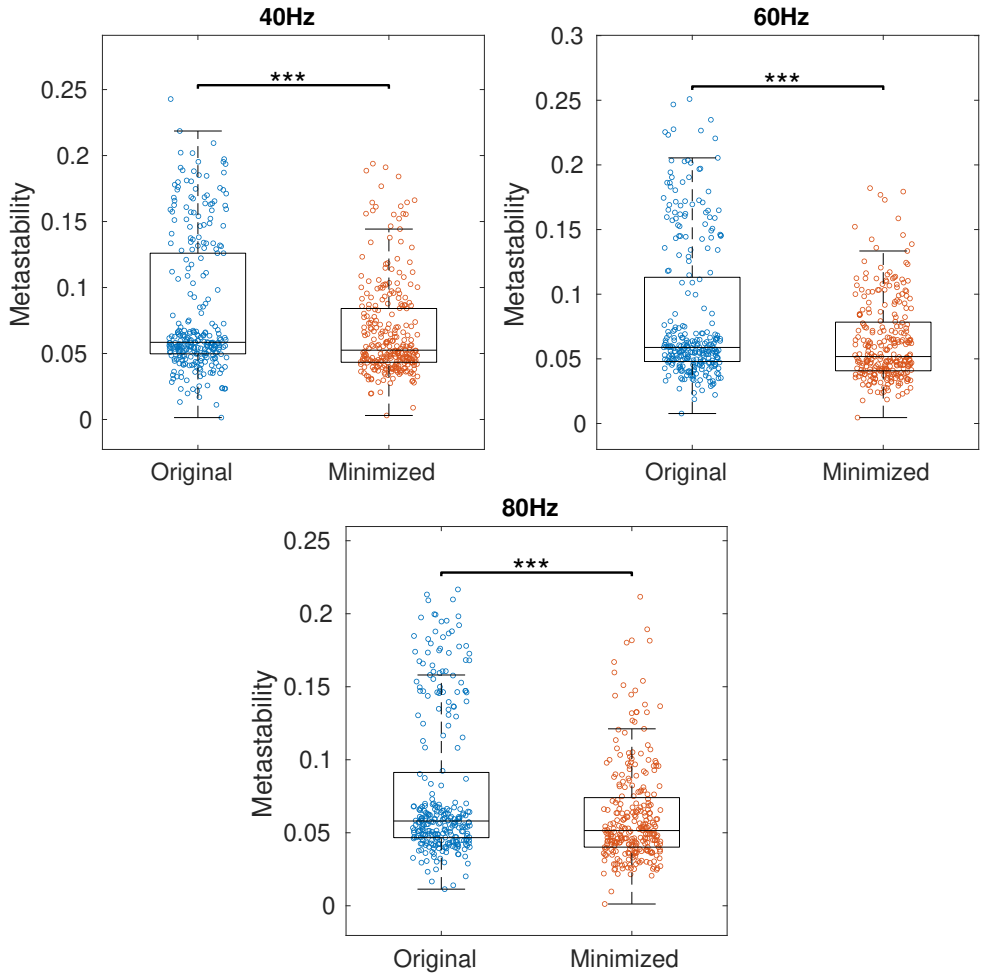


Figure B.5: **Including stationary synchrony.** In this case, we did not omit from the parameter space the pairs of parameters which resulted in a reduction in the standard deviation of the mean global synchrony to a value below $10^{-7}$. Across all subjects, metastability for the original and minimized arrangements for 40Hz, 60Hz and 80Hz. Metastability displayed significant reductions in the minimized arrangements ($P$ <0.001, Wilcoxon signed-rank test). Cohen's $d$: 0.36, 0.43, 0.39, for 40Hz, 60Hz and 80Hz, respectively. 69%, 67% and 67% of subjects experienced a reduction in metastability in the minimized arrangements, for 40Hz, 60Hz and 80Hz, respectively.

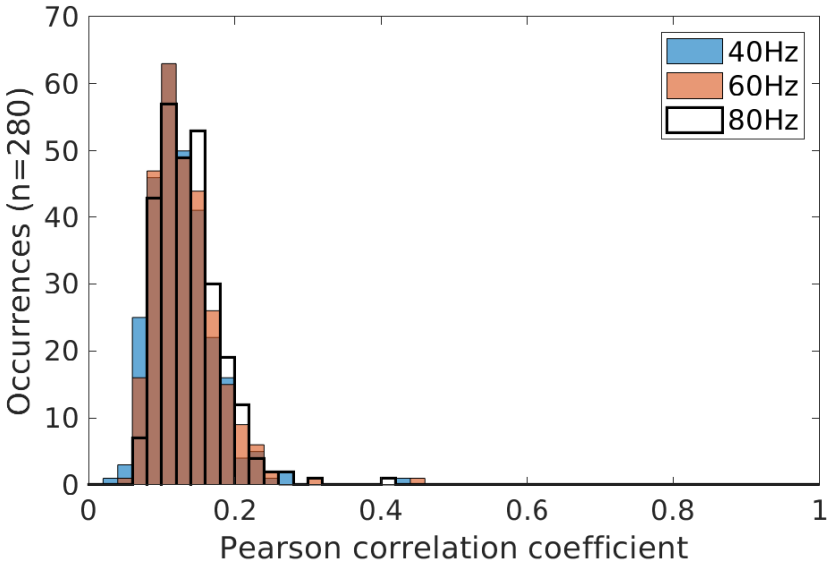


Figure B.6: For the Kuramoto model, the maximum Pearson correlation coefficient (r) across the parameter space between empirical and simulated functional connectivity for all subjects. These correlations correspond to that obtained when using the coupling strength and conduction velocity which maximised the correlation between simulated and empirical activity. r=0.13±0.04 (40Hz), 0.13±0.04 (60Hz) and 0.14±0.04 (80Hz).

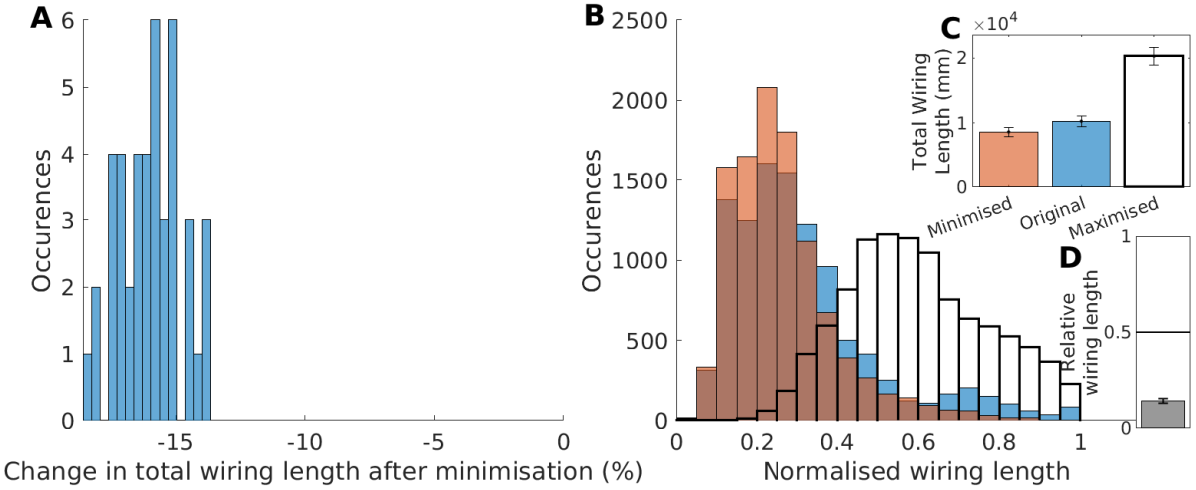


Figure B.7: For the schizophrenia dataset (healthy controls only) — changes in wiring length distributions for the original, minimised and maximised spatial arrangements. **A:** The percentage difference in wiring length between the original connectomes and the spatial arrangements which minimise the total wiring length (mean -16.0±1.2%). **B**: The distribution of wiring lengths for the original (orange), minimised (blue) and maximised (transparent, bold) spatial arrangements. **C:** The mean wiring lengths for the minimised, original and maximised arrangements. **D:** The mean relative wiring length across all subjects (0.141±0.011) — original lengths normalised against that of minimised and maximised arrangements (error bars = ±1 SD.).

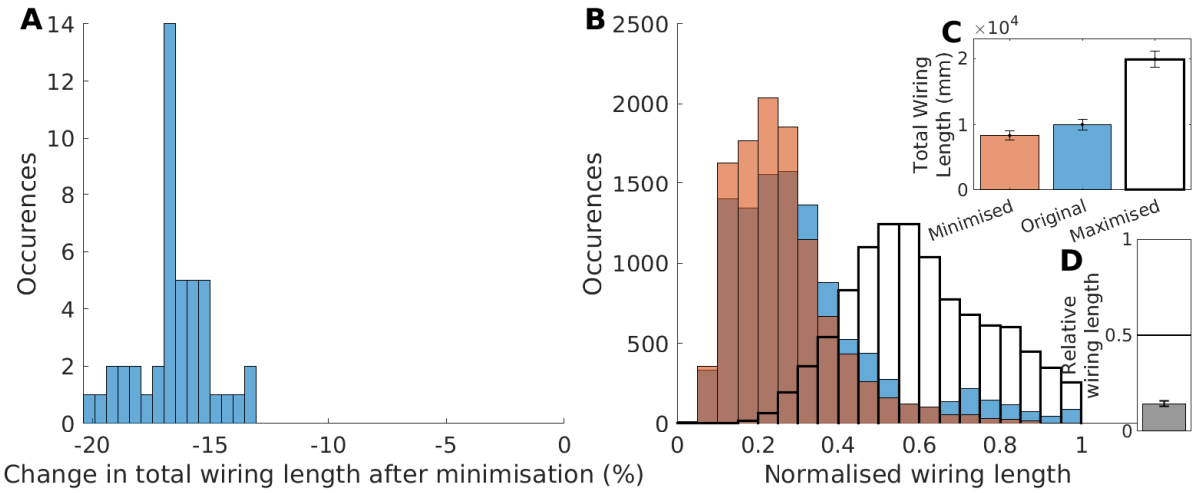


Figure B.8: For the schizophrenia dataset (schizophrenia subjects only) — changes in wiring length distributions for the original, minimised and maximised spatial arrangements. **A:** The percentage difference in wiring length between the original connectomes and the spatial arrangements which minimise the total wiring length (mean -16.5±1.6%). **B**: The distribution of wiring lengths for the original (orange), minimised (blue) and maximised (transparent, bold) spatial arrangements. **C:** The mean wiring lengths for the minimised, original and maximised arrangements. **D:** The mean relative wiring length across all subjects (0.144±0.015) — original lengths normalised against that of minimised and maximised arrangements (error bars = ±1 SD.).

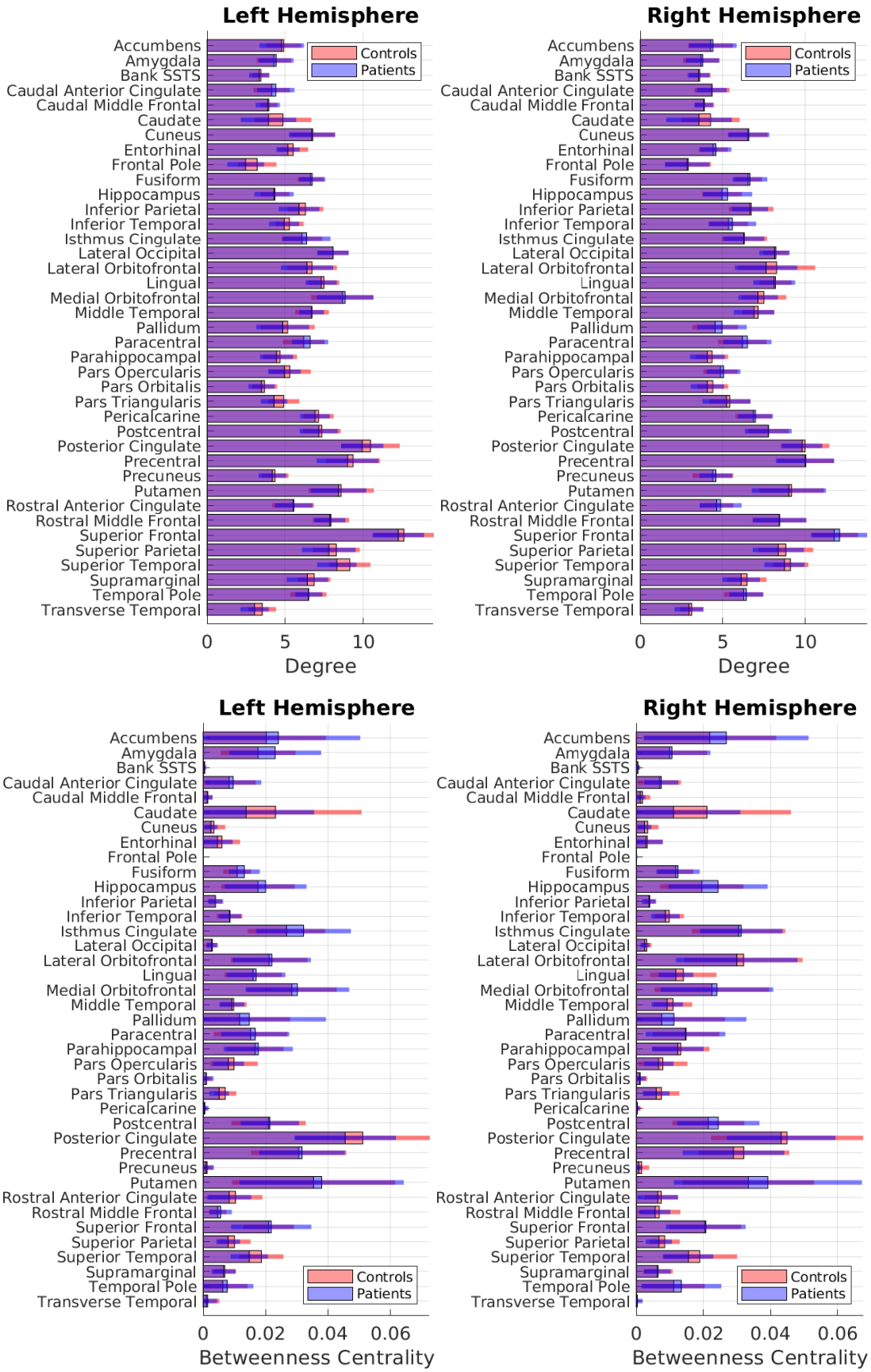


Figure B.9: Between controls and schizophrenia patients: Comparing region degree and betweenness centrality (the fraction of the total number of paths where a region exists on a shortest path between any two regions) — measures of 'hub-ness'. After FDR, we did not observe a significant difference between controls and patients for any region.

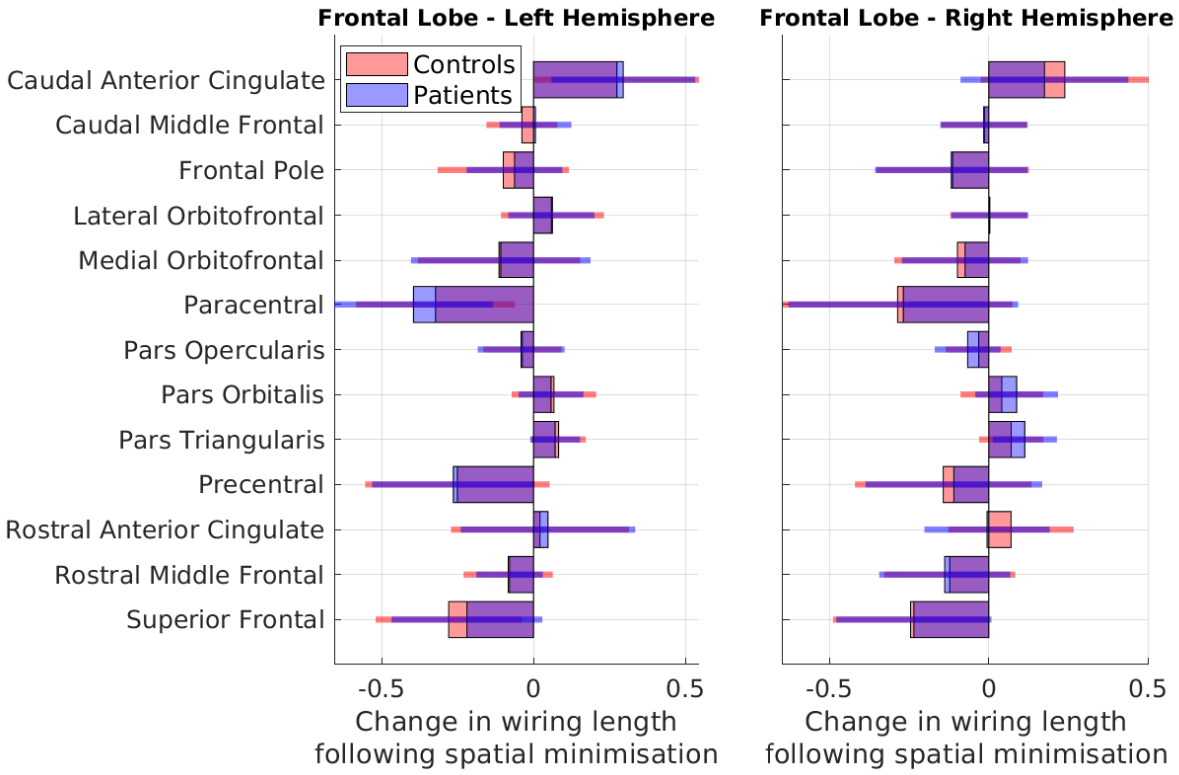


Figure B.10: For healthy controls and schizophrenia patients, the change in wiring length for individual regions in the isolated frontal network following spatial rearrangement. This is comparing the wiring length of regions in the original arrangement against that for the spatial arrangement minimising the total wiring length. Most regions displayed a reduction in wiring length following spatial minimisation. After FDR, we did not observe a significant difference between controls and patients for any region.

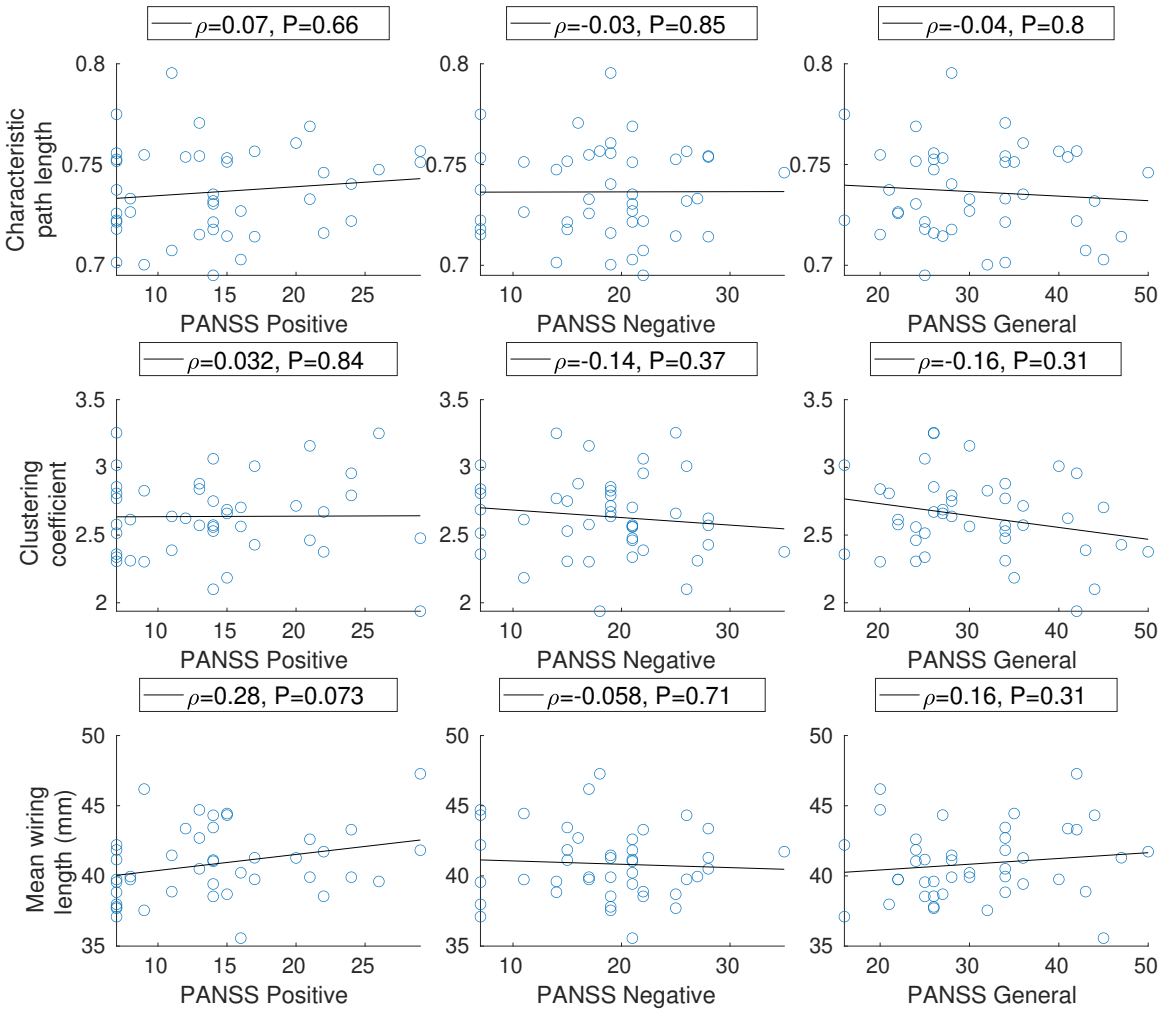


Figure B.11: Network characteristics for the isolated frontal lobe network in schizophrenia patients. The characteristic path length and clustering coefficient are normalised against that of 100 randomly rewired networks preserving the degree distribution. The path length and mean wiring length make use of the Euclidean distance between connected regions, and the clustering coefficient is based on binary connectivity. No significant correlation existed with these measures and the PANSS scores ($P$ >0.05, Spearman rank correlation coefficient).

# Appendix C. NKI dataset/analyses

## C.1 Additional Tables and Figures

Table C.1: Correlations between WASI scores and subject age

| | FSIQ | PIQ | BD | MAT | VIQ | SIM | VOC |
|---|---|---|---|---|---|---|---|
| PIQ | **0.9**$^{***}$ | - | - | - | - | - | - |
| BD | **0.81**$^{***}$ | **0.91**$^{***}$ | - | - | - | - | - |
| MAT | **0.83**$^{***}$ | **0.89**$^{***}$ | **0.65**$^{***}$ | - | - | - | - |
| VIQ | **0.84**$^{***}$ | **0.54**$^{***}$ | **0.47**$^{***}$ | **0.53**$^{***}$ | - | - | - |
| SIM | **0.76**$^{***}$ | **0.51**$^{***}$ | **0.44**$^{***}$ | **0.5**$^{***}$ | **0.87**$^{***}$ | - | - |
| VOC | **0.72**$^{***}$ | **0.45**$^{***}$ | **0.4**$^{***}$ | **0.45**$^{***}$ | **0.9**$^{***}$ | **0.58**$^{***}$ | - |
| Age | -0.049 | -0.048 | -0.17 | 0.11 | -0.038 | 0.041 | -0.11 |

*Note.* Values are Spearman rank correlations ($\rho$) $^{***} = P < 0.001$

Table C.2: For all subjects: Correlations between topological measures and WASI scores / subject age

| Measure | FSIQ (PIQ+VIQ) | PIQ (BD+MAT) | BD | MAT | VIQ (SIM+VOC) | SIM | VOC | Age |
|---|---|---|---|---|---|---|---|---|
| $C_u$ | 0.079 | 0.089 | 0.12 | 0.03 | 0.07 | 0.12 | 0.017 | 0.025 |
| $C_w$ | 0.12 | 0.16 | 0.19 | 0.099 | 0.054 | 0.069 | 0.054 | -0.025 |
| $L_u$ | 0.073 | -0.011 | -0.0056 | -0.036 | 0.18 | 0.18 | 0.14 | **-0.23**$^{*}$ |
| $L_w$ | 0.16 | 0.18 | **0.22**$^{*}$ | 0.091 | 0.1 | 0.056 | 0.075 | 0.049 |
| Edge Density | -0.1 | -0.15 | -0.14 | -0.14 | -0.046 | -0.12 | 0.041 | **-0.39**$^{***}$ |
| Small-Worldness | 0.089 | 0.12 | 0.15 | 0.07 | 0.037 | 0.1 | -0.017 | 0.11 |
| Streamline Count | 0.18 | **0.22**$^{*}$ | **0.24**$^{*}$ | 0.14 | 0.089 | -0.021 | 0.17 | **-0.47**$^{***}$ |

*Note.* Values are Spearman rank correlations ($\rho$) * = $P < 0.05$, ** = $P < 0.01$, *** = $P < 0.001$.
$L$ = characteristic path length, $C$ = mean clustering coefficient, $m/u/w$ = metric/unweighted/weighted.

Table C.3: For all subjects: Correlations between spatial measures and WASI scores / subject age

| Measure | FSIQ (PIQ+VIQ) | PIQ (BD+MAT) | BD | MAT | VIQ (SIM+VOC) | SIM | VOC | Age |
|---|---|---|---|---|---|---|---|---|
| $L_m$ | -0.0027 | -0.035 | -0.039 | -0.04 | -0.0082 | -0.026 | 0.021 | **-0.4**$^{***}$ |
| CPO: Earth Movers Distance | -0.14 | -0.18 | -0.15 | **-0.2**$^{*}$ | -0.097 | -0.097 | -0.094 | **-0.44**$^{***}$ |
| CPO: Relative Wiring Length | -0.18 | **-0.24**$^{*}$ | **-0.21**$^{*}$ | **-0.24**$^{*}$ | -0.12 | -0.14 | -0.075 | **-0.46**$^{***}$ |
| Convex Hull Volume | 0.11 | **0.2**$^{*}$ | **0.22**$^{*}$ | 0.11 | -0.02 | -0.085 | 0.033 | -0.033 |
| Rentian Exponent | -0.0055 | 0.042 | 0.082 | -0.0023 | -0.042 | -0.033 | -0.038 | -0.19 |
| TW (Euclidean) | **-0.2**$^{*}$ | **-0.25**$^{*}$ | **-0.23**$^{*}$ | **-0.22**$^{*}$ | -0.14 | -0.18 | -0.085 | -0.19 |
| TW (Streamline) | -0.19 | **-0.26**$^{*}$ | **-0.25**$^{*}$ | -0.16 | -0.1 | -0.051 | -0.13 | 0.11 |
| Wiring Angle | 0.052 | 0.0058 | -0.058 | 0.08 | 0.15 | 0.11 | 0.16 | 0.17 |

*Note.* Values are Spearman rank correlations ($\rho$) * = $P < 0.05$, ** = $P < 0.01$, *** = $P < 0.001$.
$L$ = characteristic path length, $m/u/w$ = metric/unweighted/weighted. TW=Total wiring length. CPO=Component Placement Optimisation.

Table C.4: For all subjects: Earth Mover's Distance — effect of wiring length bin-width on the correlation with WASI scores / age

| Bin width | FSIQ (PIQ+VIQ) | PIQ (BD+MAT) | BD | MAT | VIQ (SIM+VOC) | SIM | VOC | Age |
|---|---|---|---|---|---|---|---|---|
| 0.05 | -0.14 | -0.18 | -0.15 | **-0.21**$^{*}$ | -0.099 | -0.097 | -0.099 | **-0.45**$^{***}$ |
| 0.1 | -0.12 | -0.16 | -0.14 | -0.18 | -0.082 | -0.075 | -0.091 | **-0.46**$^{***}$ |
| 0.15 | -0.16 | **-0.22**$^{*}$ | -0.17 | **-0.24**$^{*}$ | -0.1 | -0.12 | -0.066 | **-0.47**$^{***}$ |
| 0.2 | -0.14 | -0.17 | -0.18 | -0.14 | -0.11 | -0.11 | -0.1 | **-0.34**$^{***}$ |
| 0.25 | -0.1 | -0.14 | -0.087 | -0.19 | -0.078 | -0.083 | -0.076 | **-0.4**$^{***}$ |

*Note.* Values are Spearman rank correlations ($\rho$) * = $P < 0.05$, ** = $P < 0.01$

Table C.5: For female subjects: Correlations between topological measures and WASI scores / subject age

| Measure | FSIQ (PIQ+VIQ) | PIQ (BD+MAT) | BD | MAT | VIQ (SIM+VOC) | SIM | VOC | Age |
|---|---|---|---|---|---|---|---|---|
| $C_u$ | -0.012 | 0.043 | -0.022 | 0.063 | -0.083 | 0.066 | -0.16 | 0.17 |
| $C_w$ | 0.071 | 0.2 | 0.12 | 0.19 | -0.11 | 0.0039 | -0.13 | 0.13 |
| $L_u$ | 0.094 | 0.075 | 0.038 | 0.08 | 0.098 | 0.18 | -0.0036 | -0.25 |
| $L_w$ | 0.28 | **0.35**$^{*}$ | **0.32**$^{*}$ | **0.32**$^{*}$ | 0.058 | -0.0091 | 0.086 | 0.077 |
| Edge Density | -0.08 | -0.12 | -0.033 | -0.18 | 0.0042 | -0.12 | 0.088 | **-0.45**$^{**}$ |
| Small-Worldness | -0.00046 | 0.067 | -0.0084 | 0.096 | -0.096 | 0.037 | -0.15 | 0.27 |
| Streamline Count | **0.32**$^{*}$ | **0.35**$^{*}$ | **0.32**$^{*}$ | 0.26 | 0.23 | 0.077 | **0.28**$^{*}$ | **-0.55**$^{***}$ |

Table C.6: For male subjects: Correlations between topological measures and WASI scores / subject age

| Measure | FSIQ (PIQ+VIQ) | PIQ (BD+MAT) | BD | MAT | VIQ (SIM+VOC) | SIM | VOC | Age |
|---|---|---|---|---|---|---|---|---|
| $C_u$ | 0.22 | 0.17 | **0.35**$^{*}$ | 0.0002 | 0.2 | 0.18 | 0.16 | -0.11 |
| $C_w$ | 0.2 | 0.13 | **0.3**$^{*}$ | -0.004 | 0.18 | 0.13 | 0.22 | -0.15 |
| $L_u$ | 0.099 | -0.045 | 0.018 | -0.12 | 0.22 | 0.16 | 0.23 | -0.22 |
| $L_w$ | 0.051 | -0.0082 | 0.13 | -0.15 | 0.13 | 0.089 | 0.076 | 0.015 |
| Edge Density | -0.14 | -0.17 | -0.23 | -0.069 | -0.083 | -0.12 | 0.0044 | **-0.35**$^{*}$ |
| Small-Worldness | 0.23 | 0.23 | **0.38**$^{**}$ | 0.058 | 0.16 | 0.16 | 0.12 | -0.035 |
| Streamline Count | 0.11 | 0.081 | 0.16 | -0.018 | 0.094 | -0.029 | 0.23 | **-0.58**$^{***}$ |

*Note.* Values are Spearman rank correlations ($\rho$) * = $P < 0.05$, ** = $P < 0.01$, *** = $P < 0.001$.
$L$ = characteristic path length, $C$ = mean clustering coefficient, $m/u/w$ = metric/unweighted/weighted.

Table C.7: For female subjects: Correlations between spatial measures and WASI scores / subject age

| Measure | FSIQ (PIQ+VIQ) | PIQ (BD+MAT) | BD | MAT | VIQ (SIM+VOC) | SIM | VOC | Age |
|---|---|---|---|---|---|---|---|---|
| $L_m$ | 0.033 | -0.0077 | 0.029 | -0.036 | 0.05 | 0.031 | 0.041 | **-0.44**$^{**}$ |
| CPO: Earth Movers Distance | -0.14 | -0.13 | -0.11 | -0.15 | -0.12 | -0.13 | -0.12 | **-0.4**$^{**}$ |
| CPO: Relative Wiring Length | -0.17 | -0.17 | -0.14 | -0.17 | -0.13 | -0.17 | -0.081 | **-0.42**$^{**}$ |
| Convex Hull Volume | 0.27 | **0.32**$^{*}$ | **0.34**$^{*}$ | 0.21 | 0.1 | -0.022 | 0.19 | -0.024 |
| Rentian Exponent | 0.21 | 0.26 | **0.3**$^{*}$ | 0.18 | 0.071 | 0.15 | 0.028 | **-0.37**$^{**}$ |
| TW (Euclidean) | -0.047 | -0.084 | 0.0085 | -0.14 | -0.056 | -0.087 | -0.0067 | -0.2 |
| TW (Streamline) | -0.11 | -0.23 | -0.18 | -0.2 | 0.0087 | 0.061 | -0.063 | 0.057 |
| Wiring Angle | -0.12 | -0.17 | -0.22 | -0.055 | 0.051 | -0.073 | 0.14 | 0.15 |

Table C.8: For male subjects: Correlations between spatial measures and WASI scores / subject age

| Measure | FSIQ (PIQ+VIQ) | PIQ (BD+MAT) | BD | MAT | VIQ (SIM+VOC) | SIM | VOC | Age |
|---|---|---|---|---|---|---|---|---|
| $L_m$ | -0.04 | -0.033 | -0.06 | -0.017 | -0.037 | -0.064 | 0.038 | **-0.39**$^{**}$ |
| CPO: Earth Movers Distance | -0.16 | -0.19 | -0.12 | -0.23 | -0.15 | -0.14 | -0.17 | **-0.56**$^{***}$ |
| CPO: Relative Wiring Length | -0.23 | -0.27 | -0.22 | **-0.28**$^{*}$ | -0.19 | -0.21 | -0.17 | **-0.57**$^{***}$ |
| Convex Hull Volume | -0.018 | 0.074 | 0.056 | -0.019 | -0.048 | -0.12 | 0.051 | -0.083 |
| Rentian Exponent | -0.21 | -0.16 | -0.089 | -0.19 | -0.15 | -0.17 | -0.086 | -0.054 |
| TW (Euclidean) | **-0.36**$^{*}$ | **-0.38**$^{**}$ | **-0.43**$^{**}$ | -0.26 | -0.25 | -0.27 | -0.21 | -0.17 |
| TW (Streamline) | -0.26 | -0.25 | **-0.3**$^{*}$ | -0.086 | -0.21 | -0.16 | -0.21 | 0.15 |
| Wiring Angle | 0.24 | 0.18 | 0.13 | 0.21 | 0.24 | 0.25 | 0.16 | 0.21 |

*Note.* Values are Spearman rank correlations ($\rho$) * = $P < 0.05$, ** = $P < 0.01$, *** = $P < 0.001$.
$L$ = characteristic path length, $m/u/w$ = metric/unweighted/weighted. TW=Total wiring length. CPO=Component Placement Optimisation.

Table C.9: For female subjects: Earth Mover's Distance — effect of wiring length bin-width on the correlation with WASI scores / age

| Bin width | FSIQ (PIQ+VIQ) | PIQ (BD+MAT) | BD | MAT | VIQ (SIM+VOC) | SIM | VOC | Age |
|---|---|---|---|---|---|---|---|---|
| 0.05 | -0.14 | -0.14 | -0.11 | -0.16 | -0.12 | -0.14 | -0.11 | **-0.4**$^{**}$ |
| 0.1 | -0.16 | -0.14 | -0.12 | -0.15 | -0.13 | -0.14 | -0.12 | **-0.42**$^{**}$ |
| 0.15 | -0.2 | -0.21 | -0.15 | -0.24 | -0.14 | -0.16 | -0.12 | **-0.44**$^{**}$ |
| 0.2 | -0.15 | -0.13 | -0.17 | -0.063 | -0.12 | -0.15 | -0.082 | **-0.29**$^{*}$ |
| 0.25 | -0.058 | -0.025 | 0.027 | -0.092 | -0.13 | -0.11 | -0.13 | **-0.36**$^{*}$ |

Table C.10: For male subjects: Earth Mover's Distance — effect of wiring length bin-width on the correlation with WASI scores / age

| Bin width | FSIQ (PIQ+VIQ) | PIQ (BD+MAT) | BD | MAT | VIQ (SIM+VOC) | SIM | VOC | Age |
|---|---|---|---|---|---|---|---|---|
| 0.05 | -0.15 | -0.19 | -0.11 | -0.24 | -0.14 | -0.11 | -0.18 | **-0.56**$^{***}$ |
| 0.1 | -0.099 | -0.14 | -0.07 | -0.19 | -0.096 | -0.078 | -0.13 | **-0.59**$^{***}$ |
| 0.15 | -0.15 | -0.21 | -0.13 | -0.24 | -0.16 | -0.2 | -0.11 | **-0.57**$^{***}$ |
| 0.2 | -0.17 | -0.17 | -0.12 | -0.2 | -0.16 | -0.15 | -0.19 | **-0.47**$^{***}$ |
| 0.25 | -0.17 | -0.22 | -0.15 | -0.25 | -0.091 | -0.12 | -0.099 | **-0.5**$^{***}$ |

*Note.* Values are Spearman rank correlations ($\rho$) * = $P < 0.05$, ** = $P < 0.01$, *** = $P < 0.001$

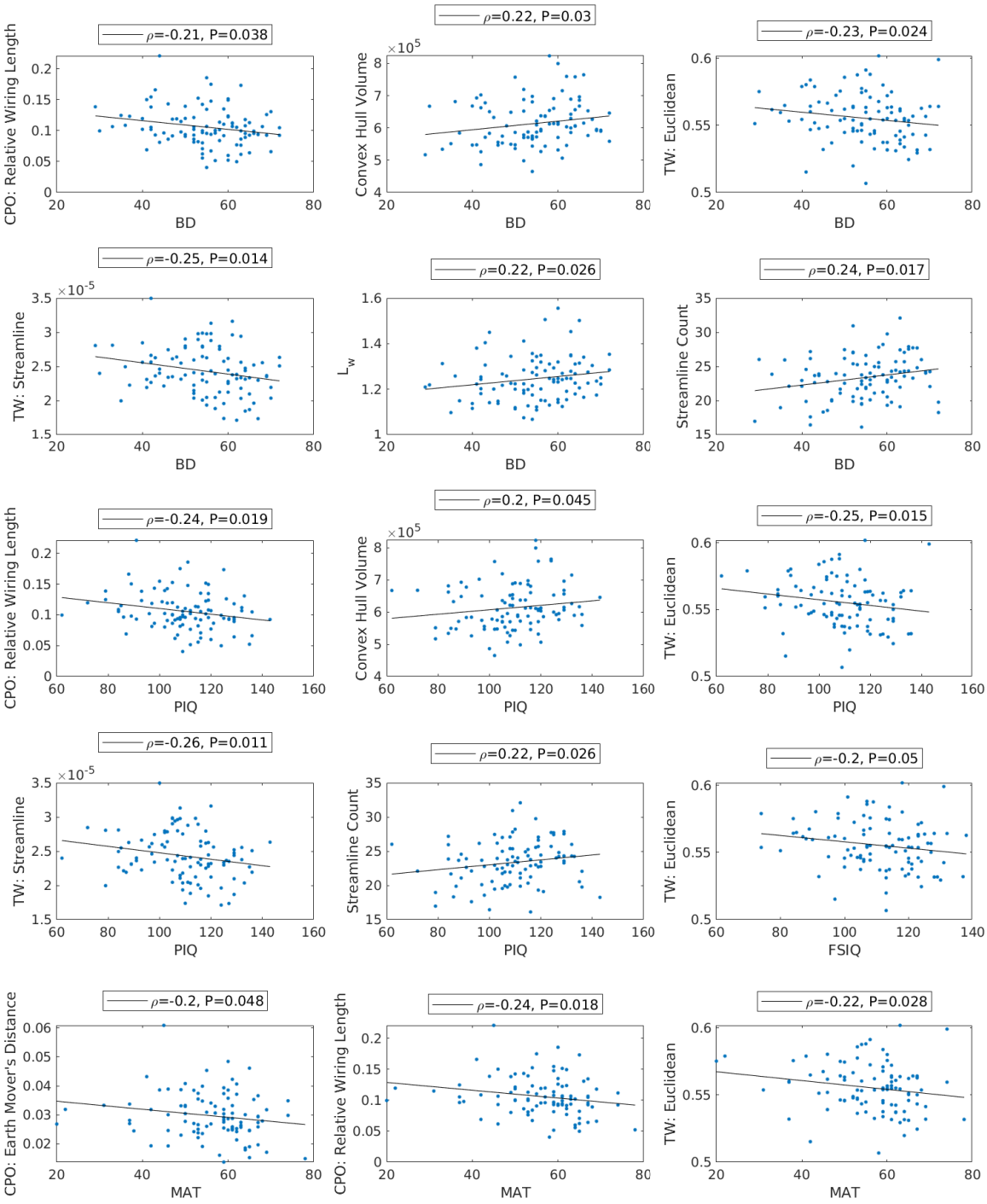


Figure C.1: Scatter plots of significant Spearman rank correlation ($\rho$) of WASI scores and spatial/topological network measures, as shown in Figure 4.33.

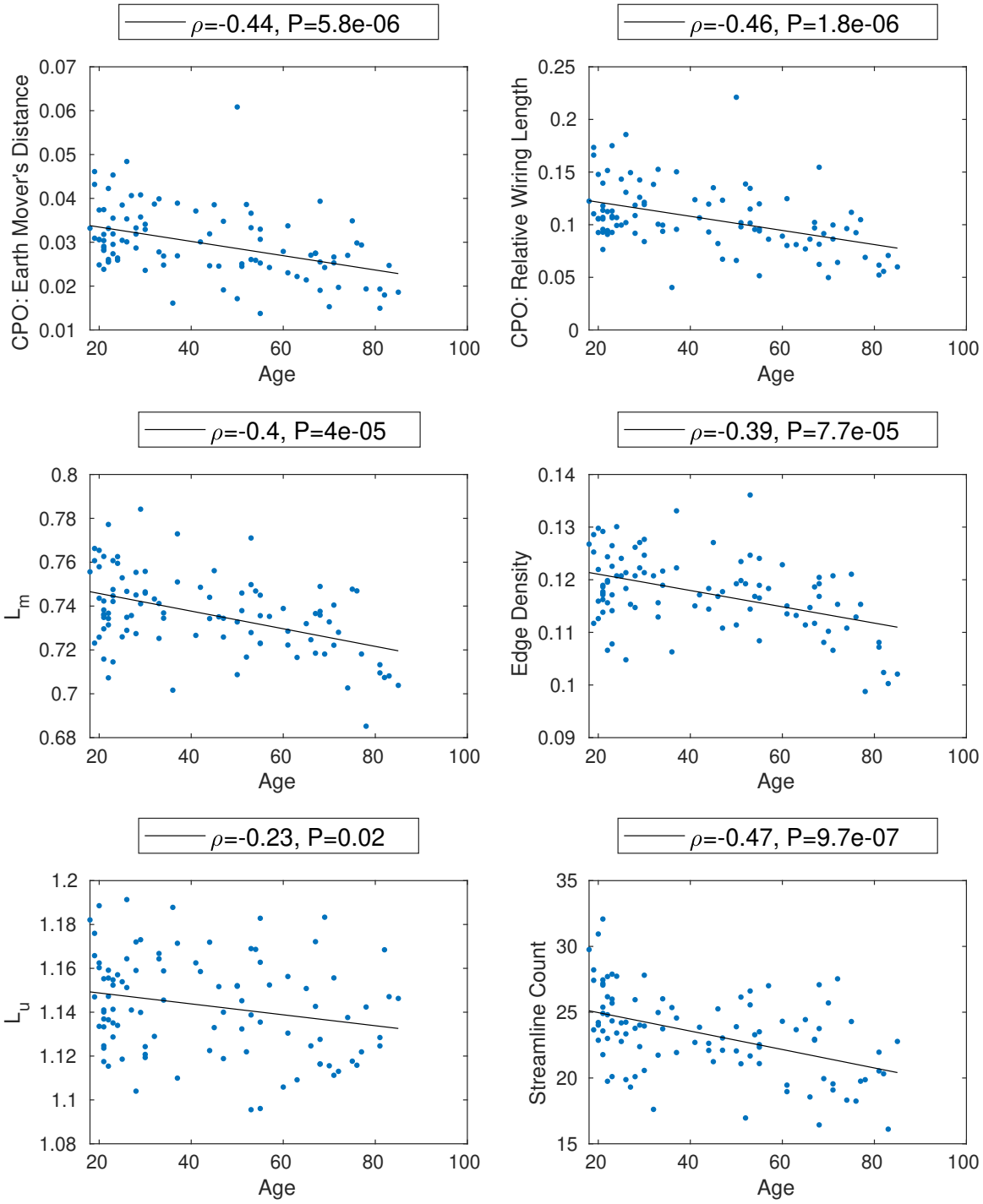


Figure C.2: Scatter plots of significant Spearman rank correlation ($\rho$) of age and spatial/topological network measures, as shown in Figure 4.33.

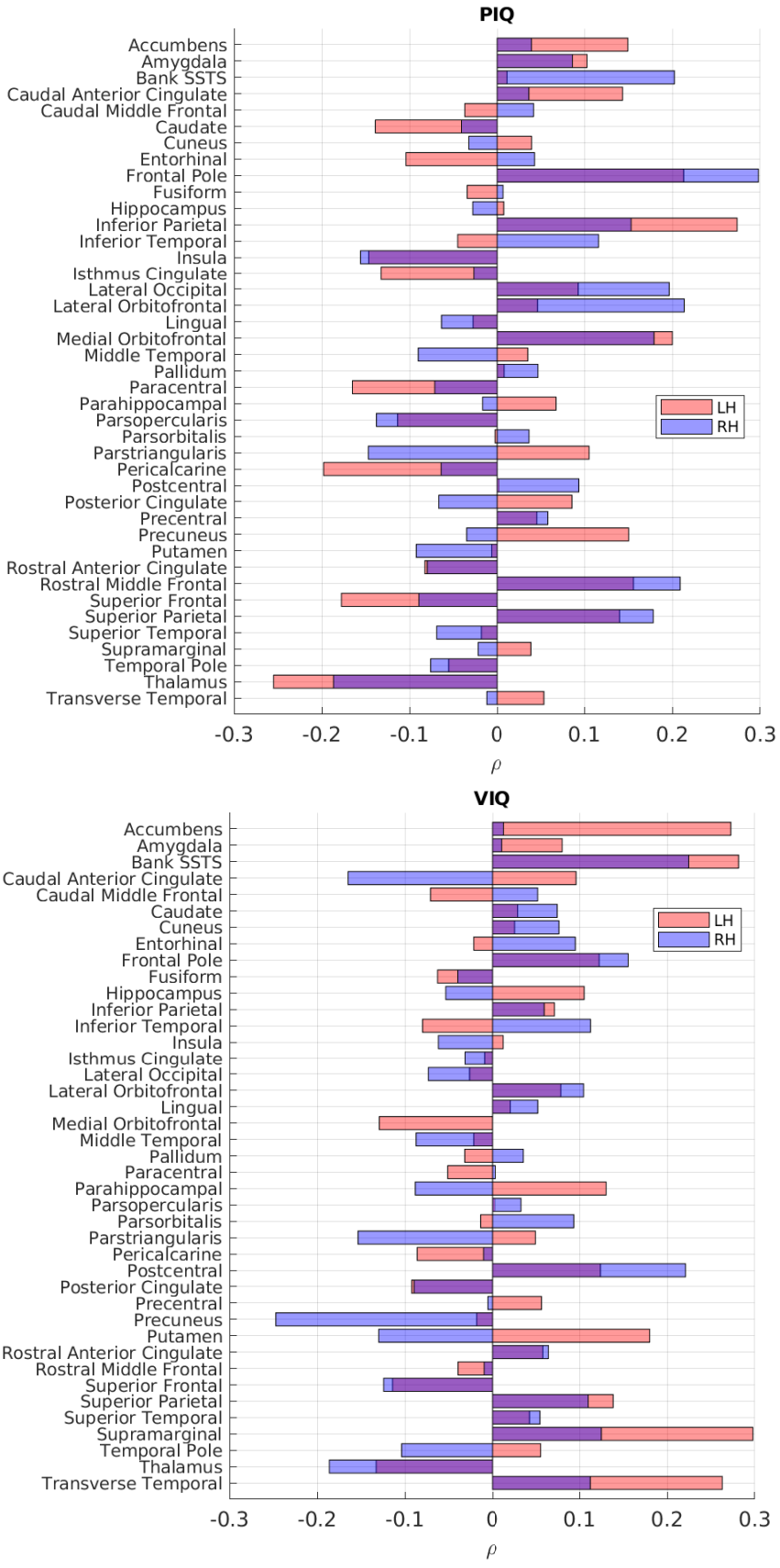


Figure C.3: For all subjects, the Spearman rank correlation coefficient ($\rho$) of performance IQ (PIQ) / verbal IQ (VIQ) and the mean wiring angle between all pairs of connections connected to that brain region. Positive correlations correspond to an increase in wiring angles for subjects with higher test scores. After correcting for multiple comparisons, no significant correlations exist. LH=Left Hemisphere, RH=Right Hemisphere.

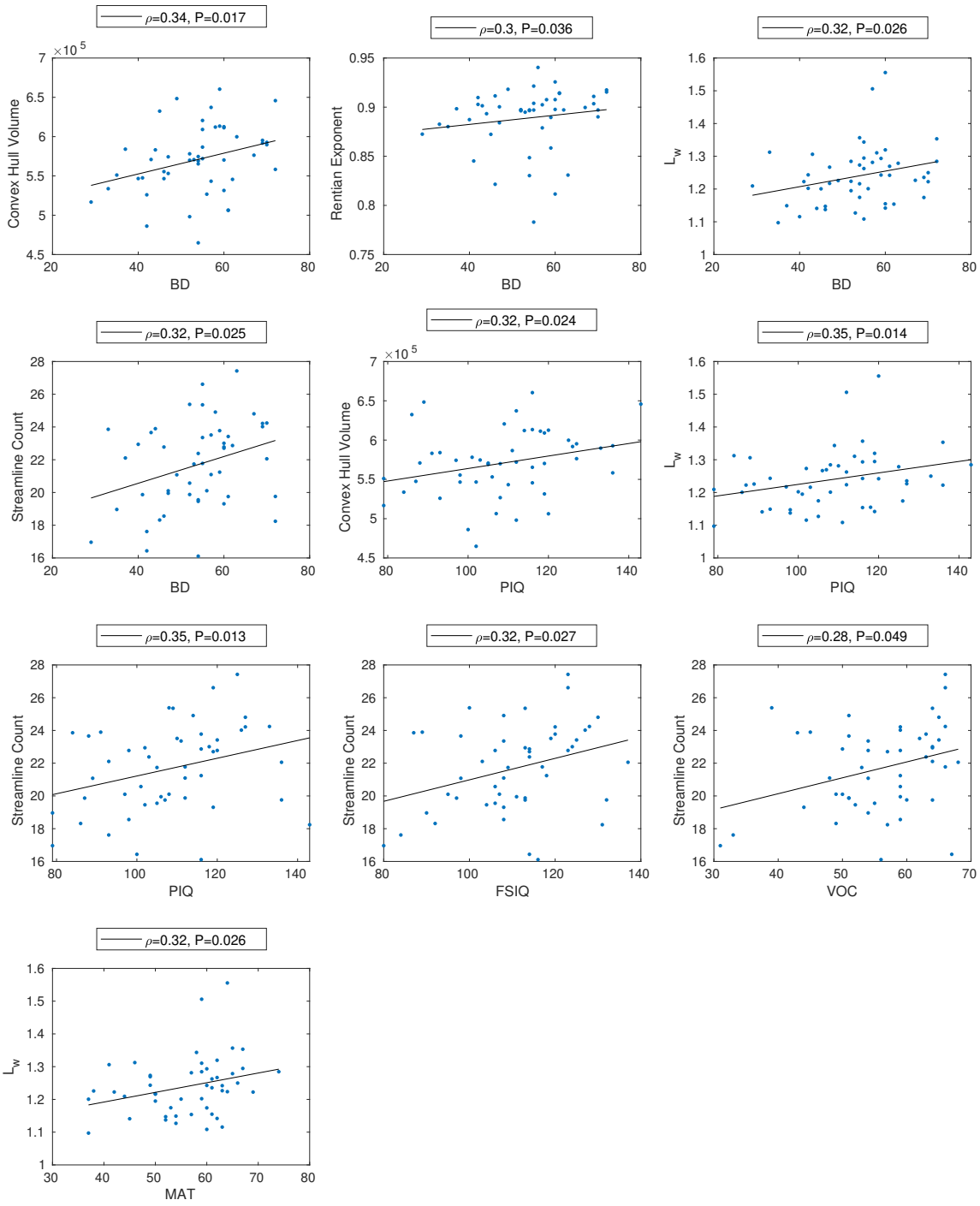


Figure C.4: For females, scatter plots of significant Spearman rank correlation ($\rho$) of WASI scores and spatial/topological network measures.

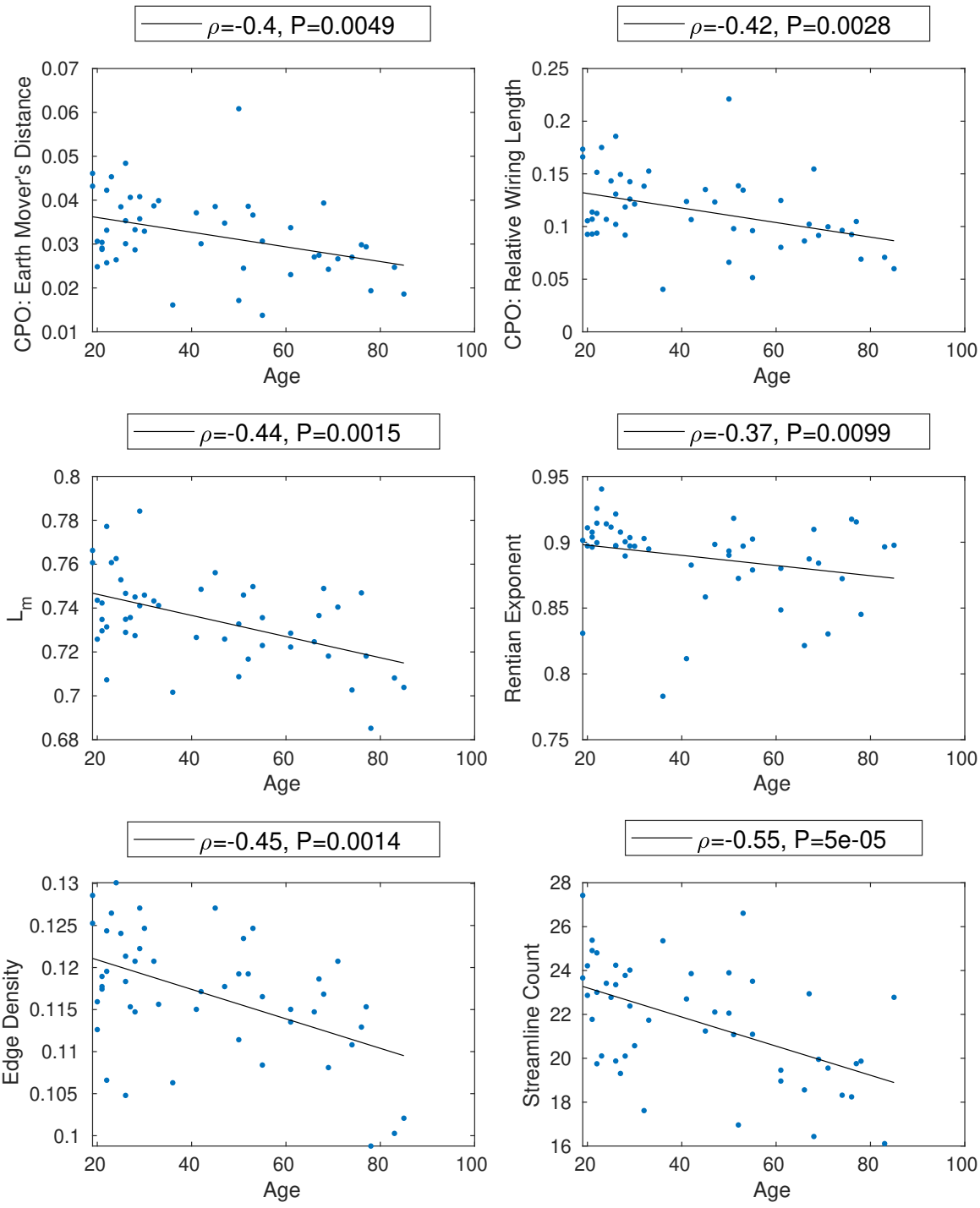


Figure C.5: For females, scatter plots of significant Spearman rank correlation ($\rho$) of age and spatial/topological network measures.

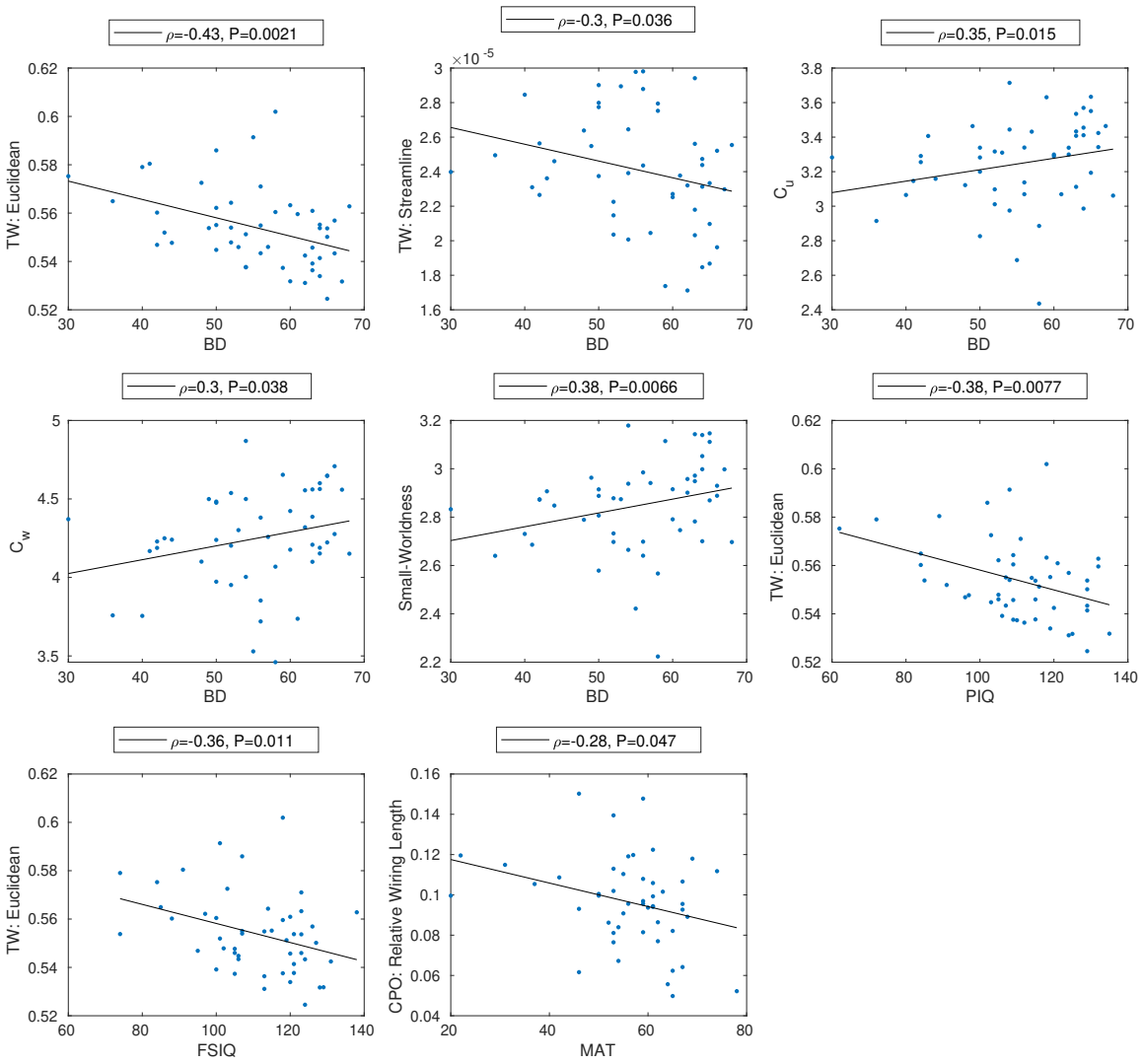


Figure C.6: For males, scatter plots of significant Spearman rank correlation ($\rho$) of WASI scores and spatial/topological network measures.

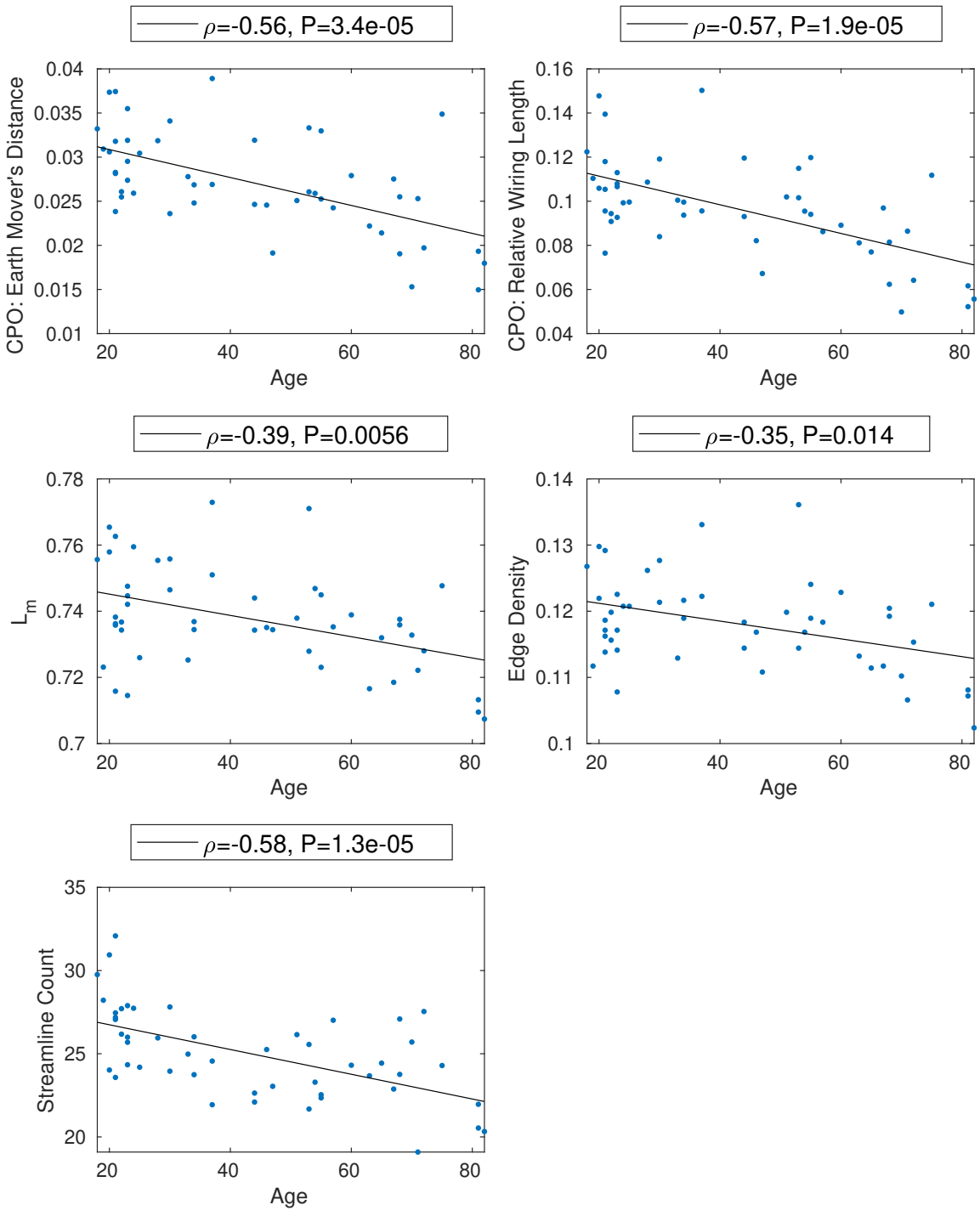


Figure C.7: For males, scatter plots of significant Spearman rank correlation ($\rho$) of age and spatial/topological network measures.

# Bibliography


Ackerman, Phillip L, Kristy R Bowen, et al. (2001). "Determinants of individual differences and gender differences in knowledge." In: *Journal of Educational Psychology* 93.4, p. 797.

Ackerman, Phillip L and David Z Hambrick (2020). "A primer on assessing intelligence in laboratory studies". In: *Intelligence* 80, p. 101440.

Aharonov, Ranit et al. (2003). "Localization of function via lesion analysis". In: *Neural Computation* 15.4, pp. 885–913.

Alderson, Thomas H et al. (2020). "Metastable neural dynamics underlies cognitive performance across multiple behavioural paradigms". In: *Human brain mapping* 41.12, pp. 3212–3234.

Allen, Colin (2017). "On (not) defining cognition". In: *Synthese* 194.11, pp. 4233–4249.

Atasoy, Selen, Gustavo Deco, and Morten L Kringelbach (2019). "Playing at the Edge of Criticality: Expanded Whole-Brain Repertoire of Connectome-Harmonics". In: *The Functional Role of Critical Dynamics in Neural Systems*. Springer, pp. 27–45.

Azevedo, Frederico A C et al. (2009). "Equal numbers of neuronal and nonneuronal cells make the human brain an isometrically scaled-up primate brain". In: *Journal of Comparative Neurology* 513.5, pp. 532–541.

Baars, Bernard J (2005). "Global workspace theory of consciousness: toward a cognitive neuroscience of human experience". In: *Progress in Brain Research* 150, pp. 45–53.

— (2007). "The global workspace theory of consciousness". In: *The Blackwell companion to consciousness*, pp. 227–242.

Bammer, Roland (2003). "Basic principles of diffusion-weighted imaging". In: *European journal of radiology* 45.3, pp. 169–184.

Barbey, Aron K et al. (2014). "Architecture of fluid intelligence and working memory revealed by lesion mapping". In: *Brain Structure and Function* 219.2, pp. 485–494.

Barta, Patrick and Paola Dazzan (2003). "Hemispheric surface area: sex, laterality and age effects". In: *Cerebral Cortex* 13.4, pp. 364–370.

Barttfeld, Pablo et al. (2011). "A big-world network in ASD: dynamical connectivity analysis reflects a deficit in long-range connections and an excess of short-range connections". In: *Neuropsychologia* 49.2, pp. 254–263.

Bassett, Danielle S and Edward T Bullmore (2006). "Small-world brain networks". In: *The neuroscientist* 12.6, pp. 512–523.

Bassett, Danielle S, Edward T Bullmore, et al. (2008). "Hierarchical organization of human cortical networks in health and schizophrenia". In: *Journal of Neuroscience* 28.37, pp. 9239–9248.

Bassett, Danielle S, Daniel L Greenfield, et al. (2010). "Efficient physical embedding of topologically complex information processing networks in brains and computer circuits". In: *PLoS Computational Biology* 6.4, e1000748.

Bastos, Andre M, Julien Vezoli, and Pascal Fries (2015). "Communication through coherence with inter-areal delays". In: *Current opinion in neurobiology* 31, pp. 173–180.

Beauducel, André and Martin Kersting (2002). "Fluid and crystallized intelligence and the Berlin Model of Intelligence Structure (BIS)." In: *European Journal of Psychological Assessment* 18.2, p. 97.

Beggs, John M and Dietmar Plenz (2003). "Neuronal avalanches in neocortical circuits". In: *Journal of neuroscience* 23.35, pp. 11167–11177.

Benjamini, Yoav and Yosef Hochberg (1995). "Controlling the false discovery rate: a practical and powerful approach to multiple testing". In: *Journal of the Royal Statistical Society: Series B (Methodological)* 57.1, pp. 289–300.

Betzel, Richard F. and Danielle S Bassett (2018). "Specificity and robustness of long-distance connections in weighted, interareal connectomes". In: *Proceedings of the National Academy of Sciences* 115.21, E4880–E4889.

Bird, Christopher David and Nathan John Emery (2009). "Rooks use stones to raise the water level to reach a floating worm". In: *Current Biology* 19.16, pp. 1410–1414.

Bishop, Sonia J et al. (2008). "COMT val158met genotype affects recruitment of neural mechanisms supporting fluid intelligence". In: *Cerebral Cortex* 18.9, pp. 2132–2140.

Blackmore, Susan (2017). *Consciousness: A very short introduction*. Oxford University Press.

Boly, Melanie et al. (2011). "Preserved feedforward but impaired top-down processes in the vegetative state". In: *Science* 332.6031, pp. 858–862.

Bonnefond, Mathilde, Sabine Kastner, and Ole Jensen (2017). "Communication between brain areas based on nested oscillations". In: *eneuro* 4.2.

Boring, Edwin G (1923). “Intelligence as the tests test it”. In: *New Republic* 35.6, pp. 35–37.

Boruvka, Otakar (1926). “O jistém problému minimálním (About a certain minimal problem)”. In: *Práce Mor. Prırodved. Spol. v Brne (Acta Societ. Scienc. Natur. Moravicae)* 3.3, pp. 37–58.

Bosman, Conrado A et al. (2012). “Attentional stimulus selection through selective synchronization between monkey visual areas”. In: *Neuron* 75.5, pp. 875–888.

Box, George EP (1976). “Science and statistics”. In: *Journal of the American Statistical Association* 71.356, pp. 791–799.

Braaten, Ellen B and Dennis Norman (2006). “Intelligence (IQ) testing”. In: *Pediatrics in review* 27.11, p. 403.

Braitenberg, Valentino (2007). “Brain”. In: *Scholarpedia* 2.11. revision #133105, p. 2918. DOI: 10.4249/scholarpedia.2918.

Braitenberg, Valentino and Almut Schüz (2013). *Cortex: statistics and geometry of neuronal connectivity*. Springer Science & Business Media.

Brandes, Ulrik (2005). *Network analysis: methodological foundations*. Vol. 3418. Springer Science & Business Media.

Brodmann, Korbinian (1909). *Vergleichende Lokalisationslehre der Grosshirnrinde in ihren Prinzipien dargestellt auf Grund des Zellenbaues*. Barth.

Buckner, Randy L and Justin L Vincent (2007). “Unrest at rest: default activity and spontaneous network correlations”. In: *Neuroimage* 37.4, pp. 1091–1096.

Budd, Julian M L and Zoltán F Kisvárday (2012). “Communication and wiring in the cortical connectome”. In: *Frontiers in neuroanatomy* 6, p. 42.

Budd, Julian M L, Krisztina Kovács, et al. (2010). “Neocortical axon arbors trade-off material and conduction delay conservation”. In: *PLoS computational biology* 6.3.

Buehner, Markus et al. (2006). “Cognitive abilities and their interplay: Reasoning, crystallized intelligence, working memory components, and sustained attention”. In: *Journal of Individual Differences* 27.2, pp. 57–72.

Bullier, Jean, Jeffrey D Schall, and Anne Morel (1996). “Functional streams in occipitofrontal connections in the monkey”. In: *Behavioural brain research* 76.1-2, pp. 89–97.

Bullmore, Edward T and Olaf Sporns (2009). “Complex brain networks: graph theoretical analysis of structural and functional systems”. In: *Nature Reviews Neuroscience* 10.3, p. 186.

Bullmore, Edward T and Olaf Sporns (2012). "The economy of brain network organization". In: *Nature Reviews Neuroscience* 13.5, p. 336.

Cabral, Joana et al. (2011). "Role of local network oscillations in resting-state functional connectivity". In: *Neuroimage* 57.1, pp. 130–139.

Calvo Garzón, Paco and Fred Keijzer (2011). "Plants: Adaptive behavior, root-brains, and minimal cognition". In: *Adaptive behavior* 19.3, pp. 155–171.

Carpenter, Patricia A, Marcel A Just, and Peter Shell (1990). "What one intelligence test measures: a theoretical account of the processing in the Raven Progressive Matrices Test." In: *Psychological review* 97.3, p. 404.

Carroll, John B et al. (1993). *Human cognitive abilities: A survey of factor-analytic studies*. Cambridge University Press.

Casarotto, Silvia et al. (2016). "Stratification of unresponsive patients by an independently validated index of brain complexity". In: *Annals of neurology* 80.5, pp. 718–729.

Cattell, Raymond B (1943). "The measurement of adult intelligence." In: *Psychological bulletin* 40.3, p. 153.

— (1963). "Theory of fluid and crystallized intelligence: A critical experiment." In: *Journal of Educational Psychology* 54.1, p. 1.

— (1987). "Intelligence: its structure, growth and action". In: *Advances in psychology* 35.

Cattell, Raymond B and John L Horn (1978). "A check on the theory of fluid and crystallized intelligence with description of new subtest designs". In: *Journal of Educational Measurement* 15.3, pp. 139–164.

Cavagna, Andrea et al. (2010). "Scale-free correlations in starling flocks". In: *Proceedings of the National Academy of Sciences* 107.26, pp. 11865–11870.

Cerullo, Michael A (2015). "The problem with phi: a critique of integrated information theory". In: *PLoS Comput Biol* 11.9, e1004286.

Chen, Beth L, David H Hall, and Dmitri B Chklovskii (2006). "Wiring optimization can relate neuronal structure and function". In: *Proceedings of the National Academy of Sciences* 103.12, pp. 4723–4728.

Cheng, Hu et al. (2020). "Segmentation of the brain using direction-averaged signal of DWI images". In: *Magnetic resonance imaging* 69, pp. 1–7.

Cherniak, Christopher (1990). "The bounded brain: toward quantitative neuroanatomy". In: *Journal of Cognitive Neuroscience* 2.1, pp. 58–68.

— (1994). "Component placement optimization in the brain". In: *Journal of Neuroscience* 14.4, pp. 2418–2427.

Cherniak, Christopher et al. (2004). "Global optimization of cerebral cortex layout". In: *Proceedings of the National Academy of Sciences* 101.4, pp. 1081–1086.

Chialvo, Dante R (2010). "Emergent complex neural dynamics". In: *Nature physics* 6.10, pp. 744–750.

Chiêm, Benjamin, Frédéric Crevecoeur, and Jean-Charles Delvenne (2018). "Supervised classification of structural brain networks reveals gender differences". In: *2018 19th IEEE Mediterranean Electrotechnical Conference (MELECON)*. IEEE, pp. 269–274.

Christie, Phillip and Dirk Stroobandt (2000). "The interpretation and application of Rent's rule". In: *IEEE Transactions on Very Large Scale Integration (VLSI) Systems* 8.6, pp. 639–648.

Christofides, Nicos (1976). *Worst-case analysis of a new heuristic for the travelling salesman problem*. Tech. rep. Carnegie-Mellon Univ Pittsburgh Pa Management Sciences Research Group.

Christoforou, Andrea et al. (2014). "GWAS-based pathway analysis differentiates between fluid and crystallized intelligence". In: *Genes, brain and behavior* 13.7, pp. 663–674.

Cohen, Jessica R and Mark D'Esposito (2016). "The segregation and integration of distinct brain networks and their relationship to cognition". In: *Journal of Neuroscience* 36.48, pp. 12083–12094.

Cole, Michael W, Takuya Ito, and Todd S Braver (2015). "Lateral prefrontal cortex contributes to fluid intelligence through multinetwork connectivity". In: *Brain Connectivity* 5.8, pp. 497–504.

Cole, Michael W, Tal Yarkoni, et al. (2012). "Global connectivity of prefrontal cortex predicts cognitive control and intelligence". In: *Journal of Neuroscience* 32.26, pp. 8988–8999.

Colom, Roberto et al. (2009). "Gray matter correlates of fluid, crystallized, and spatial intelligence: Testing the P-FIT model". In: *Intelligence* 37.2, pp. 124–135.

Cook, Stephen A (1971). "The complexity of theorem-proving procedures". In: *Proceedings of the third annual ACM symposium on Theory of computing*, pp. 151–158.

Creed, Jennifer A et al. (2011). "Concussive brain trauma in the mouse results in acute cognitive deficits and sustained impairment of axonal function". In: *Journal of neurotrauma* 28.4, pp. 547–563.

Crick, Francis C and Christof Koch (2005). "What is the function of the claustrum?" In: *Philosophical Transactions of the Royal Society B: Biological Sciences* 360.1458, pp. 1271–1279.

Crossley, Nicolas A et al. (2014). "The hubs of the human connectome are generally implicated in the anatomy of brain disorders". In: *Brain* 137.8, pp. 2382–2395.

Deary, Ian J, Lars Penke, and Wendy Johnson (2010). "The neuroscience of human intelligence differences". In: *Nature reviews neuroscience* 11.3, pp. 201–211.

Deco, Gustavo, Patric Hagmann, et al. (2014). "Modeling resting-state functional networks when the cortex falls asleep: local and global changes". In: *Cerebral cortex* 24.12, pp. 3180–3194.

Deco, Gustavo, Viktor Jirsa, et al. (2009). "Key role of coupling, delay, and noise in resting brain fluctuations". In: *Proceedings of the National Academy of Sciences* 106.25, pp. 10302–10307.

Deco, Gustavo and Morten L Kringelbach (2016). "Metastability and coherence: extending the communication through coherence hypothesis using a whole-brain computational perspective". In: *Trends in neurosciences* 39.3, pp. 125–135.

Deco, Gustavo, Morten L Kringelbach, et al. (2017). "The dynamics of resting fluctuations in the brain: metastability and its dynamical cortical core". In: *Scientific reports* 7.1, pp. 1–14.

Deco, Gustavo, Edmund T Rolls, and Ranulfo Romo (2009). "Stochastic dynamics as a principle of brain function". In: *Progress in neurobiology* 88.1, pp. 1–16.

Deco, Gustavo, Diego Vidaurre, and Morten L Kringelbach (2021). "Revisiting the Global Workspace orchestrating the hierarchical organization of the human brain". In: *Nature Human Behaviour*, pp. 1–15.

Dehaene, Stanislas, Michel Kerszberg, and Jean-Pierre Changeux (1998). "A neuronal model of a global workspace in effortful cognitive tasks". In: *Proceedings of the national Academy of Sciences* 95.24, pp. 14529–14534.

Dehaene, Stanislas and Lionel Naccache (2001). "Towards a cognitive neuroscience of consciousness: basic evidence and a workspace framework". In: *Cognition* 79.1-2, pp. 1–37.

Deming, W Edwards (1993). "The new economics for industry, government, education". In: *Cambridge: MIT Center for Advanced Engineering Study*.

Desikan, Rahul S et al. (2006). "An automated labeling system for subdividing the human cerebral cortex on MRI scans into gyral based regions of interest". In: *Neuroimage* 31.3, pp. 968–980.

Duncan, John, Paul Burgess, and Hazel Emslie (1995). "Fluid intelligence after frontal lobe lesions". In: *Neuropsychologia* 33.3, pp. 261–268.

Dykiert, Dominika, Catharine R Gale, and Ian J Deary (2009). "Are apparent sex differences in mean IQ scores created in part by sample restriction and increased male variance?" In: *Intelligence* 37.1, pp. 42–47.

Eickhoff, Simon B, B T Thomas Yeo, and Sarah Genon (2018). "Imaging-based parcellations of the human brain". In: *Nature Reviews Neuroscience* 19.11, pp. 672–686.

Elston, Guy N (2007). *Specialization of the Neocortical Pyramidal Cell during Primate Evolution*. Vol. 4. ISBN: 9780123708786.

Englot, Dario J and Hal Blumenfeld (2009). "Consciousness and epilepsy: why are complex-partial seizures complex?" In: *Progress in brain research* 177, pp. 147–170.

Euler, Leonhard (1845). *Institutionum calculi integralis*. Vol. 4. impensis Academiae imperialis scientiarum.

Fan, Lingzhong et al. (2016). "The human brainnetome atlas: a new brain atlas based on connectional architecture". In: *Cerebral cortex* 26.8, pp. 3508–3526.

Felleman, Daniel J and David C Van Essen (1991). "Distributed hierarchical processing in the primate cerebral cortex." In: *Cerebral Cortex (New York, NY: 1991)* 1.1, pp. 1–47.

Felten, David L, M Kerry O'Banion, and Mary E Maida (2015). *Netter's atlas of neuroscience*. Elsevier Health Sciences.

Fiorito, Graziano, Christoph von Planta, and Pietro Scotto (1990). "Problem solving ability of Octopus vulgaris lamarck (Mollusca, Cephalopoda)". In: *Behavioral and neural biology* 53.2, pp. 217–230.

Fischl, Bruce (2012). "FreeSurfer". In: *Neuroimage* 62.2, pp. 774–781.

Fischl, Bruce, David H Salat, et al. (2002). "Whole brain segmentation: automated labeling of neuroanatomical structures in the human brain". In: *Neuron* 33.3, pp. 341–355.

Fischl, Bruce, Martin I Sereno, et al. (1999). "High-resolution intersubject averaging and a coordinate system for the cortical surface". In: *Human brain mapping* 8.4, pp. 272–284.

Fornito, Alex, Andrew Zalesky, and Michael Breakspear (2013). "Graph analysis of the human connectome: promise, progress, and pitfalls". In: *Neuroimage* 80, pp. 426–444.

Fornito, Alex, Andrew Zalesky, and Edward T Bullmore (2016). *Fundamentals of brain network analysis*. Academic Press.

Fraser, Alex S (1957). "Simulation of genetic systems by automatic digital computers I. Introduction". In: *Australian Journal of Biological Sciences* 10.4, pp. 484–491.

Freeman, Linton C (1977). “A set of measures of centrality based on betweenness”. In: *Sociometry*, pp. 35–41.

Fries, Pascal (2005). “A mechanism for cognitive dynamics: neuronal communication through neuronal coherence”. In: *Trends in Cognitive Sciences* 9.10, pp. 474–480.

— (2015). “Rhythms for cognition: communication through coherence”. In: *Neuron* 88.1, pp. 220–235.

Friston, Karl J (1997). “Transients, metastability, and neuronal dynamics”. In: *Neuroimage* 5.2, pp. 164–171.

Fukushima, Makoto and Olaf Sporns (2020). “Structural determinants of dynamic fluctuations between segregation and integration on the human connectome”. In: *bioRxiv*.

Gangolli, Mihika et al. (2017). “Quantitative validation of a nonlinear histology-MRI coregistration method using generalized Q-sampling imaging in complex human cortical white matter”. In: *Neuroimage* 153, pp. 152–167.

Garey, Michael R and David S Johnson (1979). *Computers and intractability*. Vol. 174. freeman San Francisco.

Garrett, Douglas D et al. (2011). “The importance of being variable”. In: *Journal of Neuroscience* 31.12, pp. 4496–4503.

Gignac, Gilles E (2015). “Raven’s is not a pure measure of general intelligence: Implications for g factor theory and the brief measurement of g”. In: *Intelligence* 52, pp. 71–79.

Gläscher, Jan et al. (2010). “Distributed neural system for general intelligence revealed by lesion mapping”. In: *Proceedings of the National Academy of Sciences* 107.10, pp. 4705–4709.

Glasser, Matthew F et al. (2013). “The minimal preprocessing pipelines for the Human Connectome Project”. In: *Neuroimage* 80, pp. 105–124.

Gollo, Leonardo L et al. (2018). “Fragility and volatility of structural hubs in the human connectome”. In: *Nature neuroscience* 21.8, pp. 1107–1116.

Gong, Gaolang, Yong He, et al. (2008). “Mapping anatomical connectivity patterns of human cerebral cortex using in vivo diffusion tensor imaging tractography”. In: *Cerebral cortex* 19.3, pp. 524–536.

Gong, Gaolang, Pedro Rosa-Neto, et al. (2009). “Age-and gender-related differences in the cortical anatomical network”. In: *Journal of Neuroscience* 29.50, pp. 15684–15693.

Gordon, Evan M et al. (2017). “Individual variability of the system-level organization of the human brain”. In: *Cerebral cortex* 27.1, pp. 386–399.

Gottfredson, Linda S (1997). "Mainstream Science on Intelligence: An Editorial with 52 Signatories, History, and Bibliography." In: *Intelligence* 24.1, pp. 13–23.

Gray, Jeremy R, Christopher F Chabris, and Todd S Braver (2003). "Neural mechanisms of general fluid intelligence". In: *Nature Neuroscience* 6.3, p. 316.

Greenberg, James M and SP Hastings (1978). "Spatial patterns for discrete models of diffusion in excitable media". In: *SIAM Journal on Applied Mathematics* 34.3, pp. 515–523.

Greicius, Michael D et al. (2003). "Functional connectivity in the resting brain: a network analysis of the default mode hypothesis". In: *Proceedings of the National Academy of Sciences* 100.1, pp. 253–258.

Hagmann, Patric (2005). *From diffusion MRI to brain connectomics*. Tech. rep. EPFL.

Hagmann, Patric et al. (2008). "Mapping the structural core of human cerebral cortex". In: *PLoS Biology* 6.7, e159.

Haier, Richard J, Rex E Jung, et al. (2005). "The neuroanatomy of general intelligence: sex matters". In: *NeuroImage* 25.1, pp. 320–327.

Haier, Richard J, Benjamin Siegel, et al. (1992). "Intelligence and changes in regional cerebral glucose metabolic rate following learning". In: *Intelligence* 16.3-4, pp. 415–426.

Haier, Richard J, Benjamin V Siegel Jr, et al. (1988). "Cortical glucose metabolic rate correlates of abstract reasoning and attention studied with positron emission tomography". In: *Intelligence* 12.2, pp. 199–217.

Haier, Richard J. (2016). *The neuroscience of intelligence*. Cambridge University Press.

Haier, Richard J. and Rex E. Jung (2018). "The Parieto-Frontal Integration Theory". In: *Contemporary Intellectual Assessment: Theories, Tests, and Issues*.

Haimovici, Ariel et al. (2013). "Brain organization into resting state networks emerges at criticality on a model of the human connectome". In: *Physical review letters* 110.17, p. 178101.

Haldeman, Clayton and John M Beggs (2005). "Critical branching captures activity in living neural networks and maximizes the number of metastable states". In: *Physical review letters* 94.5, p. 058101.

Hebb, Donald O (1939a). "Intelligence in man after large removals of cerebral tissue: defects following right temporal lobectomy". In: *The Journal of General Psychology* 21.2, pp. 437–446.

Hebb, Donald O (1939b). "Intelligence in man after large removals of cerebral tissue: report of four left frontal lobe cases". In: *The Journal of General Psychology* 21.1, pp. 73–87.

Heimer, Lennart and Martine J Robards (2013). *Neuroanatomical tract-tracing methods*. Springer Science & Business Media.

Heinrichs, R Walter (2005). "The primacy of cognition in schizophrenia." In: *American Psychologist* 60.3, p. 229.

Hellyer, Peter J, Gregory Scott, et al. (2015). "Cognitive flexibility through metastable neural dynamics is disrupted by damage to the structural connectome". In: *Journal of Neuroscience* 35.24, pp. 9050–9063.

Hellyer, Peter J, Murray Shanahan, et al. (2014). "The control of global brain dynamics: opposing actions of frontoparietal control and default mode networks on attention". In: *Journal of Neuroscience* 34.2, pp. 451–461.

Herculano-Houzel, Suzana (2010). "Coordinated scaling of cortical and cerebellar numbers of neurons". In: *Frontiers in neuroanatomy* 4, p. 12.

Herrmann, Christoph S, Matthias HJ Munk, and Andreas K Engel (2004). "Cognitive functions of gamma-band activity: memory match and utilization". In: *Trends in cognitive sciences* 8.8, pp. 347–355.

Hess, Andreas et al. (2018). "On the usage of brain atlases in neuroimaging research". In: *Molecular Imaging and Biology* 20.5, pp. 742–749.

Hilgetag, Claus C and Marcus Kaiser (2004). "Clustered organization of cortical connectivity". In: *Neuroinformatics* 2.3, pp. 353–360.

Hill, Elisabeth L and Uta Frith (2003). "Understanding autism: insights from mind and brain". In: *Philosophical Transactions of the Royal Society of London. Series B: Biological Sciences* 358.1430, pp. 281–289.

Hill, Jason et al. (2010). "Similar patterns of cortical expansion during human development and evolution". In: *Proceedings of the National Academy of Sciences* 107.29, pp. 13135–13140.

Ho, Beng-Choon et al. (2011). "Long-term antipsychotic treatment and brain volumes: a longitudinal study of first-episode schizophrenia". In: *Archives of general psychiatry* 68.2, pp. 128–137.

Hodgkin, Alan L and Andrew F Huxley (Aug. 1952). "A quantitative description of membrane current and its application to conduction and excitation in nerve". In: *J. Physiol. (Lond.)* 117.4, pp. 500–544.

Hofman, Michel A (1988). “Size and shape of the cerebral cortex in mammals”. In: *Brain, behavior and evolution* 32.1, pp. 17–26.

Honey, Christopher J et al. (2007). “Network structure of cerebral cortex shapes functional connectivity on multiple time scales”. In: *Proceedings of the National Academy of Sciences* 104.24, pp. 10240–10245.

Hopfield, John J (1982). “Neural networks and physical systems with emergent collective computational abilities”. In: *Proceedings of the national academy of sciences* 79.8, pp. 2554–2558.

Horn, John L (1965). “Fluid and crystallized intelligence: a factor analytic study on the structure among primary mental abilities”. PhD thesis. University of Illinois at Urbana-Champaign.

Horvát, Szabolcs et al. (2016). “Spatial embedding and wiring cost constrain the functional layout of the cortical network of rodents and primates”. In: *PLoS biology* 14.7, e1002512.

Hubl, Daniela et al. (2004). “Pathways that make voices: white matter changes in auditory hallucinations”. In: *Archives of general psychiatry* 61.7, pp. 658–668.

Hummel, John E and Irving Biederman (1992). “Dynamic binding in a neural network for shape recognition.” In: *Psychological Review* 99.3, p. 480.

Humphries, Mark D and Kevin Gurney (2008). “Network ‘small-world-ness’: a quantitative method for determining canonical network equivalence”. In: *PloS one* 3.4.

Hunt, Earl (2000). “Let’s hear it for crystallized intelligence”. In: *Learning and Individual Differences* 1.12, pp. 123–129.

Hutchings, Frances et al. (2015). “Predicting surgery targets in temporal lobe epilepsy through structural connectome based simulations”. In: *PLoS computational biology* 11.12.

Ingalhalikar, Madhura et al. (2014). “Sex differences in the structural connectome of the human brain”. In: *Proceedings of the National Academy of Sciences* 111.2, pp. 823–828.

Innocenti, Giorgio M, Alessandro Vercelli, and Roberto Caminiti (2013). “The diameter of cortical axons depends both on the area of origin and target”. In: *Cerebral Cortex* 24.8, pp. 2178–2188.

Isingrini, Michel and Florence Vazou (1997). “Relation between fluid intelligence and frontal lobe functioning in older adults”. In: *The International Journal of Aging and Human Development* 45.2, pp. 99–109.

Izhikevich, Eugene M et al. (2003). "Simple model of spiking neurons". In: *IEEE Transactions on neural networks* 14.6, pp. 1569–1572.

Jaeggi, Susanne M et al. (2008). "Improving fluid intelligence with training on working memory". In: *Proceedings of the National Academy of Sciences* 105.19, pp. 6829–6833.

Jbabdi, Saad and Heidi Johansen-Berg (2011). "Tractography: where do we go from here?" In: *Brain Connectivity* 1.3, pp. 169–183.

Jensen, Ole and Ali Mazaheri (2010). "Shaping functional architecture by oscillatory alpha activity: gating by inhibition". In: *Frontiers in human neuroscience* 4, p. 186.

Jiang, Rongtao et al. (2019). "Gender differences in connectome-based predictions of individualized intelligence quotient and sub-domain scores". In: *Cerebral Cortex*.

Johnson-Laird, Philip N (1999). "Deductive reasoning". In: *Annual review of psychology* 50.1, pp. 109–135.

Jokisch, Daniel and Ole Jensen (2007). "Modulation of gamma and alpha activity during a working memory task engaging the dorsal or ventral stream". In: *Journal of Neuroscience* 27.12, pp. 3244–3251.

Jones, Derek K, Thomas R Knösche, and Robert Turner (2013). "White matter integrity, fiber count, and other fallacies: the do's and don'ts of diffusion MRI". In: *Neuroimage* 73, pp. 239–254.

Jung, Rex E and Richard J Haier (2007). "The Parieto-Frontal Integration Theory (P-FIT) of intelligence: converging neuroimaging evidence". In: *Behavioral and Brain Sciences* 30.2, pp. 135–154.

Kaiser, Marcus (2011). "A tutorial in connectome analysis: topological and spatial features of brain networks". In: *Neuroimage* 57.3, pp. 892–907.

— (2013). "The potential of the human connectome as a biomarker of brain disease". In: *Frontiers in human neuroscience* 7, p. 484.

Kaiser, Marcus and Claus C Hilgetag (2006). "Nonoptimal component placement, but short processing paths, due to long-distance projections in neural systems". In: *PLoS Computational Biology* 2.7, e95.

Kaiser, Marcus, Claus C Hilgetag, and Rolf Kötter (2010). "Hierarchy and dynamics of neural networks". In: *Frontiers in Neuroinformatics* 4, p. 112.

Kang, Xiaojian et al. (2015). "Hemispheric asymmetries in cortical and subcortical anatomy". In: *Laterality: Asymmetries of Body, Brain and Cognition* 20.6, pp. 658–684.

Karaboga, Dervis and Bahriye Basturk (2008). "On the performance of artificial bee colony (ABC) algorithm". In: *Applied soft computing* 8.1, pp. 687–697.

Kay, Stanley R, Abraham Fiszbein, and Lewis A Opler (1987). "The positive and negative syndrome scale (PANSS) for schizophrenia". In: *Schizophrenia bulletin* 13.2, pp. 261–276.

Kedem, Gershon and Hiroyuki Watanabe (1984). "Graph-optimization techniques for IC layout and compaction". In: *IEEE transactions on computer-aided design of integrated circuits and systems* 3.1, pp. 12–20.

Keefe, Richard SE and Philip D Harvey (2012). "Cognitive impairment in schizophrenia". In: *Novel antischizophrenia treatments*. Springer, pp. 11–37.

Keinan, Alon et al. (2004). "Fair attribution of functional contribution in artificial and biological networks". In: *Neural Computation* 16.9, pp. 1887–1915.

Kernighan, Brian W and Dennis M Ritchie (2006). *The C programming language*.

Kinouchi, Osame and Mauro Copelli (2006). "Optimal dynamical range of excitable networks at criticality". In: *Nature physics* 2.5, p. 348.

Kirchner, Wayne K (1958). "Age differences in short-term retention of rapidly changing information." In: *Journal of experimental psychology* 55.4, p. 352.

Kirkpatrick, Scott, C Daniel Gelatt, and Mario P Vecchi (1983). "Optimization by simulated annealing". In: *science* 220.4598, pp. 671–680.

Klimm, Florian et al. (2014). "Resolving structural variability in network models and the brain". In: *PLoS Computational Biology* 10.3, e1003491.

Knuth, Donald Ervin (1974). "Postscript about NP-hard problems". In: *ACM SIGACT News* 6.2, pp. 15–16.

Kocevar, Gabriel et al. (2019). "Brain structural connectivity correlates with fluid intelligence in children: A DTI graph analysis". In: *Intelligence* 72, pp. 67–75.

Kohs, Samuel C (1920). "The block-design tests." In: *Journal of Experimental Psychology* 3.5, p. 357.

Kötter, Rolf (2004). "Online retrieval, processing, and visualization of primate connectivity data from the CoCoMac database". In: *Neuroinformatics* 2.2, pp. 127–144.

Kovanda, Timothy J, R Shane Tubbs, and Aaron A Cohen-Gadol (2014). "Transsylvian selective amygdalohippocampectomy for treatment of medial temporal lobe epilepsy: Surgical technique and operative nuances to avoid complications". In: *Surgical neurology international* 5.

Kruschwitz, Johann Daniel et al. (2018). "General, crystallized and fluid intelligence are not associated with functional global network efficiency: a replication study with the human connectome project 1200 data set". In: *Neuroimage* 171, pp. 323–331.

Kruskal, Joseph B (1956). "On the shortest spanning subtree of a graph and the traveling salesman problem". In: *Proceedings of the American Mathematical society* 7.1, pp. 48–50.

Kumar, Sudhir and S Blair Hedges (1998). "A molecular timescale for vertebrate evolution". In: *Nature* 392.6679, pp. 917–920.

Kuramoto, Yoshiki (1975). "Self-entrainment of a population of coupled non-linear oscillators". In: *International symposium on mathematical problems in theoretical physics*. Springer, pp. 420–422.

Landman, Bernard S and Roy L Russo (1971). "On a pin versus block relationship for partitions of logic graphs". In: *IEEE Transactions on Computers* 100.12, pp. 1469–1479.

Langer, Nicolas et al. (2012). "Functional brain network efficiency predicts intelligence". In: *Human Brain Mapping* 33.6, pp. 1393–1406.

Lanzerotti, Mary Yvonne, Giovanni Fiorenza, and Rick A Rand (2005). "Microminiature packaging and integrated circuitry: The work of EF Rent, with an application to on-chip interconnection requirements". In: *IBM Journal of Research and Development* 49.4.5, pp. 777–803.

Laughlin, Simon B and Terrence J Sejnowski (2003). "Communication in neuronal networks". In: *Science* 301.5641, pp. 1870–1874.

Lee, Nancy Raitano et al. (2014). "Anatomical coupling among distributed cortical regions in youth varies as a function of individual differences in vocabulary abilities". In: *Human brain mapping* 35.5, pp. 1885–1895.

Lee, Won Hee, Edward T Bullmore, and Sophia Frangou (2017). "Quantitative evaluation of simulated functional brain networks in graph theoretical analysis". In: *Neuroimage* 146, pp. 724–733.

Lee, Won Hee, Gaelle E Doucet, et al. (2018). "Resting-state network connectivity and metastability predict clinical symptoms in schizophrenia". In: *Schizophrenia research* 201, pp. 208–216.

Li, Longchuan et al. (2013). "Mapping putative hubs in human, chimpanzee and rhesus macaque connectomes via diffusion tractography". In: *Neuroimage* 80, pp. 462–474.

Li, Yonghui et al. (2009). "Brain anatomical network and intelligence". In: *PLoS Computational Biology* 5.5, e1000395.

Lim, Sol et al. (2013). "Preferential detachment during human brain development: age- and sex-specific structural connectivity in diffusion tensor imaging (DTI) data". In: *Cerebral Cortex* 25.6, pp. 1477–1489.

Lohman, David F (2000). "Complex information processing and intelligence." In: *Handbook of intelligence*, pp. 285–340.

Lynall, Mary-Ellen et al. (2010). "Functional connectivity and brain networks in schizophrenia". In: *Journal of Neuroscience* 30.28, pp. 9477–9487.

Macnab, Robert M and Daniel E Koshland (1972). "The gradient-sensing mechanism in bacterial chemotaxis". In: *Proceedings of the National Academy of Sciences* 69.9, pp. 2509–2512.

Maier-Hein, Klaus H et al. (2017). "The challenge of mapping the human connectome based on diffusion tractography". In: *Nature Communications* 8.1, p. 1349.

Markov, Nikola T et al. (2013). "The role of long-range connections on the specificity of the macaque interareal cortical network". In: *Proceedings of the National Academy of Sciences* 110.13, pp. 5187–5192.

Martínez, Kenia et al. (2011). "Can fluid intelligence be reduced to 'simple'short-term storage?" In: *Intelligence* 39.6, pp. 473–480.

Mashour, George A et al. (2020). "Conscious processing and the global neuronal workspace hypothesis". In: *Neuron* 105.5, pp. 776–798.

Maslov, Sergei and Kim Sneppen (2002). "Specificity and stability in topology of protein networks". In: *Science* 296.5569, pp. 910–913.

Massobrio, Paolo et al. (2015). "Criticality as a signature of healthy neural systems". In: *Frontiers in systems neuroscience* 9, p. 22.

Matheson, Sandra and Robyn Langdon (2008). "Schizotypal traits impact upon executive working memory and aspects of IQ". In: *Psychiatry research* 159.1-2, pp. 207–214.

McGrew, Kevin S (2009). "CHC theory and the human cognitive abilities project: Standing on the shoulders of the giants of psychometric intelligence research". In: *Intelligence* 1.37, pp. 1–10.

Meller, Russell D and Yavuz A Bozer (1996). "A new simulated annealing algorithm for the facility layout problem". In: *International Journal of Production Research* 34.6, pp. 1675–1692.

Metropolis, Nicholas et al. (1953). "Equation of state calculations by fast computing machines". In: *The journal of chemical physics* 21.6, pp. 1087–1092.

Meunier, David et al. (2009). “Hierarchical modularity in human brain functional networks”. In: *Frontiers in Neuroinformatics* 3, p. 37.

Micheloyannis, Sifis et al. (2006). “Using graph theoretical analysis of multi channel EEG to evaluate the neural efficiency hypothesis”. In: *Neuroscience Letters* 402.3, pp. 273–277.

Minzenberg, Michael J et al. (2010). “Gamma oscillatory power is impaired during cognitive control independent of medication status in first-episode schizophrenia”. In: *Neuropsychopharmacology* 35.13, pp. 2590–2599.

Mubarik, Ateeq and Hassaan Tohid (2016). “Frontal lobe alterations in schizophrenia: a review”. In: *Trends in psychiatry and psychotherapy* 38.4, pp. 198–206.

Negrao, Bianca Lee and Margaretha Viljoen (2009). “Neural correlates of consciousness”. In: *African journal of psychiatry* 12.4, pp. 265–269.

Neisser, Ulric (1979). “The concept of intelligence”. In: *Intelligence* 3.3, pp. 217–227.

— (1998). “Introduction: Rising test scores and what they mean.” In: *U. Neisser (Ed.), The rising curve: Long-term gains in IQ and related measures*, pp. 3–22.

Nestor, Paul G et al. (2004). “Neuropsychological correlates of diffusion tensor imaging in schizophrenia.” In: *Neuropsychology* 18.4, p. 629.

Niebur, Ernst, Heinz G Schuster, and Daniel M Kammen (1991). “Collective frequencies and metastability in networks of limit-cycle oscillators with time delay”. In: *Physical review letters* 67.20, p. 2753.

Nooner, Kate Brody et al. (2012). “The NKI-Rockland sample: a model for accelerating the pace of discovery science in psychiatry”. In: *Frontiers in neuroscience* 6, p. 152.

Oizumi, Masafumi, Larissa Albantakis, and Giulio Tononi (2014). “From the phenomenology to the mechanisms of consciousness: integrated information theory 3.0”. In: *PLoS Computational Biology* 10.5, e1003588.

Ortiz-Rios, Michael et al. (2018). “Improved methods for MRI-compatible implants in nonhuman primates”. In: *Journal of neuroscience methods* 308, pp. 377–389.

Pakkenberg, Bente and Hans Jørgen G Gundersen (1997). “Neocortical neuron number in humans: effect of sex and age”. In: *Journal of comparative neurology* 384.2, pp. 312–320.

Pakkenberg, Bente, Dorte Pelvig, et al. (2003). “Aging and the human neocortex”. In: *Experimental gerontology* 38.1-2, pp. 95–99.

Palaniyappan, Lena et al. (2019). "Structural covariance and cortical reorganisation in schizophrenia: a MRI-based morphometric study". In: *Psychological medicine* 49.3, pp. 412–420.

Papadopoulos, Lia et al. (2016). "Embedding of bilogical distribution networks with differing environmental constraints". In: *arXiv preprint arXiv:1612.08058*.

Penfield, Wilder and Theodore Rasmussen (Dec. 1950). "The Cerebral Cortex of Man: A Clinical Study of Localization of Function". In: *Journal of the American Medical Association* 144.16, pp. 1412–1412. ISSN: 0002-9955. DOI: 10.1001/jama.1950.02920160086033.

Penke, Lars et al. (2012). "Brain white matter tract integrity as a neural foundation for general intelligence". In: *Molecular psychiatry* 17.10, p. 1026.

Pessoa, Luiz (2009). "Cognition and emotion". In: *Scholarpedia* 4.1. revision #91134, p. 4567. DOI: 10.4249/scholarpedia.4567.

Petkoski, Spase and Viktor K Jirsa (2019). "Transmission time delays organize the brain network synchronization". In: *Philosophical Transactions of the Royal Society A* 377.2153, p. 20180132.

Picchioni, Marco M and Robin Murray (2008). "Schizophrenia". In: *Scholarpedia* 3.4. revision #90760, p. 4132. DOI: 10.4249/scholarpedia.4132.

Pietschnig, Jakob et al. (2015). "Meta-analysis of associations between human brain volume and intelligence differences: How strong are they and what do they mean?" In: *Neuroscience & Biobehavioral Reviews* 57, pp. 411–432.

Pineda-Pardo, José Angel et al. (2016). "Structural efficiency within a parieto-frontal network and cognitive differences". In: *Intelligence* 54, pp. 105–116.

Polanía, Rafael et al. (2012). "The importance of timing in segregated theta phase-coupling for cognitive performance". In: *Current Biology* 22.14, pp. 1314–1318.

Press, William H et al. (1988). *Numerial Recipes in C*. Cambridge University Press.

Purves, Dale et al. (2004). "Neuroscience". In: *Sunderland, MA: Sinauer Associates* 773, pp. 16–18.

Raby, Caroline R et al. (2007). "Planning for the future by western scrub-jays". In: *Nature* 445.7130, pp. 919–921.

Raj, Ashish and Yu-hsien Chen (2011). "The wiring economy principle: connectivity determines anatomy in the human brain". In: *PloS one* 6.9.

Ramon y Cajal, S (1909). "Histology of the Nervous System of Man and Vertebrates.(English translation by N. Swanson and LW Swanson) Oxford Univ Press, NY. Originally pub-

lished: Histologie du systeme nerveux de l'homme et des vertebres". In: *Trans. L. Azoulay, Paris* 1911.

Reveley, Colin, Audrūnas Gruslys, et al. (2017). "Three-dimensional digital template atlas of the macaque brain". In: *Cerebral cortex* 27.9, pp. 4463–4477.

Reveley, Colin, Anil K Seth, et al. (2015). "Superficial white matter fiber systems impede detection of long-range cortical connections in diffusion MR tractography". In: *Proceedings of the National Academy of Sciences* 112.21, E2820–E2828.

Rizzolatti, Giacomo et al. (1990). "Neurons related to reaching-grasping arm movements in the rostral part of area 6 (area 6a$\beta$)". In: *Experimental brain research* 82.2, pp. 337–350.

Roberts, James A et al. (2016). "The contribution of geometry to the human connectome". In: *Neuroimage* 124, pp. 379–393.

Robertson, Lynn C (2003). "Binding, spatial attention and perceptual awareness". In: *Nature Reviews Neuroscience* 4.2, pp. 93–102.

Roca, María et al. (2009). "Executive function and fluid intelligence after frontal lobe lesions". In: *Brain* 133.1, pp. 234–247.

Rocca, Maria Assunta et al. (2019). "Cognitive reserve, cognition, and regional brain damage in MS: a 2-year longitudinal study". In: *Multiple Sclerosis Journal* 25.3, pp. 372–381.

Rolls, Edmund T et al. (2020). "Automated anatomical labelling atlas 3". In: *Neuroimage* 206, p. 116189.

Rubinov, Mikail et al. (2013). "Schizophrenia and abnormal brain network hubs". In: *Dialogues in clinical neuroscience* 15.3, p. 339.

Rubinov, Mikail and Olaf Sporns (2010). "Complex network measures of brain connectivity: uses and interpretations". In: *Neuroimage* 52.3, pp. 1059–1069.

Rubner, Yossi, Carlo Tomasi, and Leonidas J Guibas (2000). "The earth mover's distance as a metric for image retrieval". In: *International Journal of Computer Vision* 40.2, pp. 99–121.

Russell-Smith, Suzanna N, Murray T Maybery, and Donna M Bayliss (2010). "Are the autism and positive schizotypy spectra diametrically opposed in local versus global processing?" In: *Journal of autism and developmental disorders* 40.8, pp. 968–977.

Saleem, Kadharbatcha S and Nikos K Logothetis (2012). *A combined MRI and histology atlas of the rhesus monkey brain in stereotaxic coordinates*. Academic Press.

Samu, David, Anil K Seth, and Thomas Nowotny (2014). "Influence of wiring cost on the large-scale architecture of human cortical connectivity". In: *PLoS computational biology* 10.4.

Sastry, Kumara, David Goldberg, and Graham Kendall (2005). "Genetic algorithms". In: *Search methodologies*. Springer, pp. 97–125.

Schall, Jeffrey D et al. (1995). "Topography of visual cortex connections with frontal eye field in macaque: convergence and segregation of processing streams". In: *Journal of Neuroscience* 15.6, pp. 4464–4487.

Schmahmann, Jeremy D and Deepak Pandya (2009). *Fiber pathways of the brain*. OUP USA.

Seguin, Caio, Martijn P van den Heuvel, and Andrew Zalesky (2018). "Navigation of brain networks". In: *Proceedings of the National Academy of Sciences* 115.24, pp. 6297–6302.

Senden, Mario et al. (2017). "Cortical rich club regions can organize state-dependent functional network formation by engaging in oscillatory behavior". In: *NeuroImage* 146, pp. 561–574.

Sergent, Claire and Stanislas Dehaene (2004). "Neural processes underlying conscious perception: Experimental findings and a global neuronal workspace framework". In: *Journal of Physiology-Paris* 98.4–6, pp. 374–384.

Shah, Amitta and Uta Frith (1993). "Why do autistic individuals show superior performance on the block design task?" In: *Journal of Child Psychology and Psychiatry* 34.8, pp. 1351–1364.

Shanahan, Murray (2006). "A cognitive architecture that combines internal simulation with a global workspace". In: *Consciousness and cognition* 15.2, pp. 433–449.

— (2008). "A spiking neuron model of cortical broadcast and competition". In: *Consciousness and cognition* 17.1, pp. 288–303.

— (2010a). *Embodiment and the inner life: Cognition and Consciousness in the Space of Possible Minds*. Oxford University Press, USA. Chap. 6 - The inner life.

— (2010b). "Metastable chimera states in community-structured oscillator networks". In: *Chaos: An Interdisciplinary Journal of Nonlinear Science* 20.1, p. 013108.

— (2012). "The brain's connective core and its role in animal cognition". In: *Philosophical Transactions of the Royal Society B: Biological Sciences* 367.1603, pp. 2704–2714.

Shapley, Lloyd S (1988). "A value for n-person games". In: *The Shapley value*, pp. 31–40.

Sharpe, James and Agnes MF Wong (2005). "Anatomy and physiology of ocular motor systems". In: *Walsh and Hoyt's Clinical Neuro-Ophthalmology* 16, pp. 809–885.

Shen, John Paul and Mikko H Lipasti (2013). *Modern processor design: fundamentals of superscalar processors*. Waveland Press.

Shen, Kelly et al. (2019). "A macaque connectome for large-scale network simulations in TheVirtualBrain". In: *Scientific data* 6.1, pp. 1–12.

Sherman, S. Murray (2006). "Thalamus". In: *Scholarpedia* 1.9. revision #137867, p. 1583. DOI: 10.4249/scholarpedia.1583.

Shine, James M, Patrick G Bissett, et al. (2016). "The dynamics of functional brain networks: integrated network states during cognitive task performance". In: *Neuron* 92.2, pp. 544–554.

Shine, James M, Michael Breakspear, et al. (2019). "Human cognition involves the dynamic integration of neural activity and neuromodulatory systems". In: *Nature Neuroscience* 22.2, p. 289.

Simpson-Kent, Ivan L et al. (2020). "Neurocognitive reorganization between crystallized intelligence, fluid intelligence and white matter microstructure in two age-heterogeneous developmental cohorts". In: *Developmental cognitive neuroscience* 41, p. 100743.

Singer, Wolf (2000). "Phenomenal awareness and consciousness from a neurobiological perspective". In: *Neural correlates of consciousness: Empirical and conceptual questions*, pp. 121–137.

Singer, Wolf and Charles M Gray (1995). "Visual feature integration and the temporal correlation hypothesis". In: *Annual review of neuroscience* 18.1, pp. 555–586.

Smith, Stephen M., Peter R. Bannister, et al. (2001). "FSL: New tools for functional and structural brain image analysis". In: *NeuroImage* 13.6, p. 249.

Smith, Stephen M., Christian F. Beckmann, et al. (2013). "Resting-state fMRI in the human connectome project". In: *Neuroimage* 80, pp. 144–168.

Songthawornpong, Nicharatch et al. (2021). "Is There a Correlation Between the Number of Brain Cells and IQ?" In: *Cerebral Cortex* 31.1, pp. 650–657.

Spearman, Charles (1904). ""General Intelligence" objectively determined and measured". In: *The American Journal of Psychology* 15.2, pp. 201–292.

— (1923). *The nature of "intelligence" and the principles of cognition*. Macmillan.

Spencer, Robert J et al. (2016). "Incidental learning: A brief, valid measure of memory based on the WAIS–IV vocabulary and similarities subtests". In: *Cognitive and Behavioral Neurology* 29.4, pp. 206–211.

Sperry, Megan M et al. (2016). “Rentian scaling for the measurement of optimal embedding of complex networks into physical space”. In: *Journal of Complex Networks* 5.2, pp. 199–218.

Sporns, Olaf (2013). “Network attributes for segregation and integration in the human brain”. In: *Current Opinion in Neurobiology* 23.2, pp. 162–171.

Sporns, Olaf, Dante R Chialvo, et al. (2004). “Organization, development and function of complex brain networks”. In: *Trends in Cognitive Sciences* 8.9, pp. 418–425.

Sporns, Olaf, Giulio Tononi, and Rolf Kötter (2005). “The human connectome: a structural description of the human brain”. In: *PLoS Computational Biology* 1.4, e42.

Standring, Susan et al. (2005). “Gray’s anatomy: the anatomical basis of clinical practice”. In: *American Journal of Neuroradiology* 26.10, p. 2703.

Steen, R Grant et al. (2006). “Brain volume in first-episode schizophrenia: systematic review and meta-analysis of magnetic resonance imaging studies”. In: *The British Journal of Psychiatry* 188.6, pp. 510–518.

Stewart, Mary E et al. (2009). “Autistic traits predict performance on the block design”. In: *Autism* 13.2, pp. 133–142.

Stratton, Peter and Janet Wiles (2015). “Global segregation of cortical activity and metastable dynamics”. In: *Frontiers in systems neuroscience* 9, p. 119.

Stroop, J Ridley (1935). “Studies of interference in serial verbal reactions.” In: *Journal of experimental psychology* 18.6, p. 643.

Su, Ji Guo et al. (2008). “Protein unfolding behavior studied by elastic network model”. In: *Biophysical journal* 94.12, pp. 4586–4596.

Sullivan, Edith V and Adolf Pfefferbaum (2006). “Diffusion tensor imaging and aging”. In: *Neuroscience & Biobehavioral Reviews* 30.6, pp. 749–761.

Swadlow, Harvey A and Stephen G Waxman (2012). “Axonal conduction delays”. In: *Scholarpedia* 7.6. revision #125736, p. 1451. DOI: 10.4249/scholarpedia.1451.

Tadayon, Ehsan, Alvaro Pascual-Leone, and Emiliano Santarnecchi (2020). “Differential contribution of cortical thickness, surface area, and gyrification to fluid and crystallized intelligence”. In: *Cerebral Cortex* 30.1, pp. 215–225.

Tadel, François et al. (2011). “Brainstorm: a user-friendly application for MEG/EEG analysis”. In: *Computational intelligence and neuroscience* 2011, p. 8.

Tagliazucchi, Enzo (2017). “The signatures of conscious access and its phenomenology are consistent with large-scale brain communication at criticality”. In: *Consciousness and cognition* 55, pp. 136–147.

Tagliazucchi, Enzo, Marion Behrens, and Helmut Laufs (2013). "Sleep neuroimaging and models of consciousness". In: *Frontiers in psychology* 4, p. 256.

Tagliazucchi, Enzo, Dante R Chialvo, et al. (2016). "Large-scale signatures of unconsciousness are consistent with a departure from critical dynamics". In: *Journal of The Royal Society Interface* 13.114, p. 20151027.

Takahashi, Tsutomu et al. (2009). "Progressive gray matter reduction of the superior temporal gyrus during transition to psychosis". In: *Archives of general psychiatry* 66.4, pp. 366–376.

Takemura, Hiromasa et al. (2017). "Occipital white matter tracts in human and macaque". In: *Cerebral Cortex* 27.6, pp. 3346–3359.

Tandon, Rajiv, Matcheri S Keshavan, and Henry A Nasrallah (2008). "Schizophrenia, "just the facts" what we know in 2008. 2. Epidemiology and etiology". In: *Schizophrenia research* 102.1-3, pp. 1–18.

Thatcher, Robert W, Duane M North, and Carl J Biver (2008). "Intelligence and EEG phase reset: a two compartmental model of phase shift and lock". In: *NeuroImage* 42.4, pp. 1639–1653.

Tognoli, Emmanuelle and J A Scott Kelso (2014). "The metastable brain". In: *Neuron* 81.1, pp. 35–48.

Tomasi, Dardo and Nora D Volkow (2012). "Gender differences in brain functional connectivity density". In: *Human brain mapping* 33.4, pp. 849–860.

Tononi, Giulio (2005). "Consciousness, information integration, and the brain". In: *Progress in brain research* 150, pp. 109–126.

Tononi, Giulio, Melanie Boly, et al. (2016). "Integrated information theory: from consciousness to its physical substrate". In: *Nature Reviews Neuroscience* 17.7, p. 450.

Tononi, Giulio, Olaf Sporns, and Gerald M Edelman (1994). "A measure for brain complexity: relating functional segregation and integration in the nervous system". In: *Proceedings of the National Academy of Sciences* 91.11, pp. 5033–5037.

Tortora, Gerard J and Bryan H Derrickson (2018). *Principles of anatomy and physiology*. John Wiley & Sons.

Turner, Emily C et al. (2016). "Distributions of cells and neurons across the cortical sheet in old world macaques". In: *Brain, behavior and evolution* 88.1, pp. 1–13.

Vakhtin, Andrei A et al. (2014). "Functional brain networks contributing to the parieto-frontal integration theory of intelligence". In: *Neuroimage* 103, pp. 349–354.

van den Heuvel, Martijn P, René S Kahn, et al. (2012). "High-cost, high-capacity backbone for global brain communication". In: *Proceedings of the National Academy of Sciences* 109.28, pp. 11372–11377.

van den Heuvel, Martijn P, René CW Mandl, et al. (2010). "Aberrant frontal and temporal complex network structure in schizophrenia: a graph theoretical analysis". In: *Journal of Neuroscience* 30.47, pp. 15915–15926.

van den Heuvel, Martijn P and Hilleke E Hulshoff Pol (2010). "Exploring the brain network: a review on resting-state fMRI functional connectivity". In: *European neuropsychopharmacology* 20.8, pp. 519–534.

van den Heuvel, Martijn P, Marcel A de Reus, et al. (2015). "Comparison of diffusion tractography and tract-tracing measures of connectivity strength in rhesus macaque connectome". In: *Human brain mapping* 36.8, pp. 3064–3075.

van den Heuvel, Martijn P, Cornelis J Stam, et al. (2009). "Efficiency of functional brain networks and intellectual performance". In: *Journal of Neuroscience* 29.23, pp. 7619–7624.

Van Essen, David C (2002). "Windows on the brain: the emerging role of atlases and databases in neuroscience". In: *Current opinion in neurobiology* 12.5, pp. 574–579.

Van Essen, David C, Heather A Drury, et al. (1998). "Functional and structural mapping of human cerebral cortex: solutions are in the surfaces". In: *Proceedings of the National Academy of Sciences* 95.3, pp. 788–795.

Van Essen, David C, Matthew F Glasser, et al. (2012). "Parcellations and hemispheric asymmetries of human cerebral cortex analyzed on surface-based atlases". In: *Cerebral cortex* 22.10, pp. 2241–2262.

Van Essen, David C, Kamil Ugurbil, et al. (2012). "The Human Connectome Project: a data acquisition perspective". In: *Neuroimage* 62.4, pp. 2222–2231.

Varela, Francisco et al. (2001). "The brainweb: phase synchronization and large-scale integration". In: *Nature Reviews Neuroscience* 2.4, p. 229.

Váša, František et al. (2015). "Effects of lesions on synchrony and metastability in cortical networks". In: *Neuroimage* 118, pp. 456–467.

von der Malsburg, Christoph (1995). "Binding in models of perception and brain function". In: *Curr Opin Neurobiol* 5.4, pp. 520–6. ISSN: 0959-4388 (Print) 0959-4388 (Linking). URL: `https://www.ncbi.nlm.nih.gov/pubmed/7488855`.

Wang, Qifeng et al. (2012). "Anatomical insights into disrupted small-world networks in schizophrenia". In: *Neuroimage* 59.2, pp. 1085–1093.

Ward, Lawrence M (2011). "The thalamic dynamic core theory of conscious experience". In: *Consciousness and Cognition* 20.2, pp. 464–486.

Wasserman, Stanley, Katherine Faust, et al. (1994). *Social network analysis: Methods and applications*. Vol. 8. Cambridge university press.

Watts, Duncan J and Steven H Strogatz (1998). "Collective dynamics of 'small-world' networks". In: *Nature* 393.6684, p. 440.

Waxman, Stephen G (1977). "Conduction in myelinated, unmyelinated, and demyelinated fibers". In: *Archives of Neurology* 34.10, pp. 585–589.

— (2006). "Axonal conduction and injury in multiple sclerosis: the role of sodium channels". In: *Nature Reviews Neuroscience* 7.12, pp. 932–941.

Wechsler, David (1997). "Wechsler adult intelligence scale". In: *New York, NY: The Psychological Corporation*.

Wechsler, David et al. (1999). "Manual for the Wechsler abbreviated scale of intelligence". In: *San Antonio, TX: Psychological Corporation*.

Wechsler, David (2008). "Wechsler adult intelligence scale–Fourth Edition (WAIS–IV)". In: *San Antonio, TX: NCS Pearson* 22, p. 498.

Werner, Gerhard (2007). "Metastability, criticality and phase transitions in brain and its models". In: *Biosystems* 90.2, pp. 496–508.

Wertheimer, Max (1938). "Laws of organization in perceptual forms". In: *A source book of Gestalt Psychology*.

Whishaw, Ian Q (1990). "The decorticate rat." In: *The cerebral cortex of the rat*.

White, John G et al. (1986). "The structure of the nervous system of the nematode Caenorhabditis elegans". In: *Philos Trans R Soc Lond B Biol Sci* 314.1165, pp. 1–340.

Wildie, Mark and Murray Shanahan (2012). "Metastability and chimera states in modular delay and pulse-coupled oscillator networks". In: *Chaos: An Interdisciplinary Journal of Nonlinear Science* 22.4, p. 043131.

Wilson, Hugh R and Jack D Cowan (1972). "Excitatory and inhibitory interactions in localized populations of model neurons". In: *Biophysical journal* 12.1, pp. 1–24.

Winter, Taylor J and Elizabeth A Franz (2014). "Implication of the anterior commissure in the allocation of attention to action". In: *Frontiers in psychology* 5, p. 432.

Xia, Mingrui, Jinhui Wang, and Yong He (2013). "BrainNet Viewer: a network visualization tool for human brain connectomics". In: *PloS ONE* 8.7, e68910.

Yeh, Fang-Cheng, Sandip Panesar, et al. (2019). "Automatic removal of false connections in diffusion MRI Tractography using topology-informed pruning (TIP)". In: *Neurotherapeutics* 16.1, pp. 52–58.

Yeh, Fang-Cheng, Van Jay Wedeen, and Wen-Yih Isaac Tseng (2010). "Generalized q-sampling imaging". In: *IEEE transactions on medical imaging* 29.9, pp. 1626–1635.

Zalesky, Andrew et al. (2010). "Whole-brain anatomical networks: does the choice of nodes matter?" In: *Neuroimage* 50.3, pp. 970–983.

Zhang, Dongyang and Marcus E Raichle (2010). "Disease and the brain's dark energy". In: *Nature Reviews Neurology* 6.1, p. 15.

Zhang, Yuanchao et al. (2012). "Abnormal topological organization of structural brain networks in schizophrenia". In: *Schizophrenia research* 141.2-3, pp. 109–118.